## *The Impact of Climate Change upon the Snowmelt Hydrology of an Upland UK Catchment*

BAUGH, CALUM,ALEXANDER

# The Impact of Climate Change upon the Snowmelt Hydrology of an Upland UK Catchment

Calum Alexander Baugh

MSc by Research

Department of Geography

Durham University

May 2011

**The Impact of Climate Change upon the Snowmelt Hydrology of an Upland UK Catchment**

Calum Alexander Baugh

Snowmelt hydrology is important in the winter flow regime of upland catchments in the UK as it can attenuate the extremes of the river flow hydrograph. The sensitivity of snow accumulation and melt to changes in climate, in particular to increases in temperature, could impact upon the variability of the winter flow regime. The potential impacts of this change are increases in flood risk and decreases in low flows. Hence this project investigated the consequences of projected climatic change upon snowmelt hydrology of the Dacre Beck catchment in the English Lake District. A distributed snowmelt model was created which spatialised temperature and precipitation data across the catchment. The model accumulated snow when the temperature fell below 0°C and applied one of three temperature-index snowmelt equations to melt the accumulated snowpack. The model was driven using stochastic baseline and projected (2050s medium emissions) weather series calculated using the UKCP09 weather generator. The results showed a large future reduction in both winter snow accumulation and the magnitude of snowmelt hydrology. However, the limited hydrological process representation of the model meant it could not reliably forecast changes in the winter flow regime. Therefore the snow accumulation and melt equations were incorporated into the physically based Connectivity Runoff Model (CRUM). This improved model was calibrated to observed discharge data within a Generalised Likelihood Uncertainty Estimation (GLUE) framework before being run with a sample of baseline and projected UKCP09 weather generator series. The results showed that both high and low flows in the winter flow regime were likely to increase which contradicted previous expectations but it was unclear about the role of snowmelt hydrology in these changes. Further investigation using temperature perturbed weather series found that these changes in the winter flow regime were most likely caused by increases in rainfall which overrode the impact of changes in snowmelt hydrology.

**Table of Contents**

**Chapter 1: Snowmelt Hydrology in the UK ..... 1**

1.1 Introduction ..... 3

1.2 Snow Accumulation and Distribution ..... 3

1.3 Snowmelt Processes ..... 7

1.4 Runoff from Snowmelt ..... 10

1.5 Impact of Snowpack Accumulation and Snowmelt Runoff upon Hydrology ..... 11

1.6 Sensitivity of Snowmelt Hydrology to Projected Climatic Change ..... 15

1.7 UK Snowmelt Hydrology: Research Needs ..... 17

**Chapter 2: Study Catchment Context ..... 21**

2.1 General Context ..... 23

2.2 Elevation ..... 23

2.3 Climate ..... 25

2.4 Hydro-Climatology ..... 27

2.5 Catchment Hydrology ..... 31

2.5.1 Topography ..... 31

2.5.2 Land Cover ..... 34

2.5.3 Catchment Soils ..... 37

2.5.4 Catchment Geology ..... 39

2.5.5 Channel Network ..... 42

2.5.6 Anthropogenic Management and Intervention ..... 44

2.6 Ecology ..... 44

2.7 Study Catchment Overview ..... 45

**Chapter 3: Snowmelt Modelling ..... 47**

3.1 Snow Accumulation Modelling ..... 49

3.2 Snowmelt Modelling ..... 51

3.2.1 Energy Balance Modelling ..... 52

3.2.2 Temperature-Index Modelling ..... 55

3.3 Snowmelt Modelling Synthesis ..... 59

**Chapter 4: Distributed Snowmelt Model ..... 61**
4.1 Model Construction ..... 63
4.1.1 Input Data ..... 63
4.1.2 Spatial Discretisation and Process Implementation ..... 63
4.2 Model Verification ..... 67
4.2.1 Mass Balance Testing ..... 67
4.2.2 Sensitivity Analysis ..... 67
4.2.2.1 Parameter Identification ..... 68
4.2.2.2 Strategy ..... 70
4.2.2.3 Sampling of the Parameter Space ..... 70
4.2.2.4 Output Metric ..... 72
4.2.2.5 Sensitivity Assessment: Full Range Analysis ..... 72
4.2.2.6 Sensitivity Assessment: Response Comparison Analysis ..... 77
4.2.2.7 Sensitivity Assessment: Parameter Interactions ..... 80
4.2.3 Sensitivity Analysis Synthesis ..... 85
4.3 Conclusions ..... 85

**Chapter 5: Climate Change and Snowmelt Hydrology ..... 87**
5.1 Climate Change Modelling: UKCP09 ..... 89
5.1.1 UKCP09 Methodology ..... 89
5.1.2 UKCP09 Weather Generator ..... 93
5.2 Climate Change Modelling: Dacre Beck 2050s Medium Emissions ..... 96
5.2.1 Projections of Winter Temperature ..... 98
5.2.2 Projections of Winter Snow and Rain Accumulation ..... 99
5.2.3 Projections of Winter Solar Radiation ..... 101
5.2.4 Dacre Beck Weather Generator Conclusions ..... 102
5.3 Application of the Distributed Snowmelt Model ..... 102
5.4 Climate Change Modelling Conclusions ..... 107

**Chapter 6: Snowmelt within the Connectivity Runoff Model (CRUM) ..... 109**
6.1 Hydrological Model Selection ..... 111
6.2 Connectivity Runoff Model (CRUM) ..... 112
6.3 Incorporation of Snowmelt into CRUM ..... 115
6.4 Calibration, Uncertainty and Sensitivity Assessment ..... 117
6.4.1 Calibration and Optimisation ..... 117

6.4.2 Uncertainty Sources ..... 120
6.4.3 Uncertainty Assessment ..... 122
6.4.4 Implementation of the GLUE method ..... 127
6.4.5 Uncertainty Assessment Results: Structural Uncertainty ..... 130
6.4.6 Uncertainty Assessment Results: Parametric Uncertainty ..... 134
6.4.7 Uncertainty Assessment: Discussions ..... 143
6.5 Conclusions ..... 143

**Chapter 7: Hydrological Modelling of Climate Change Impacts upon Snowmelt Hydrology and the Winter Flow Regime ..... 145**
7.1 Selecting the Model Inputs ..... 147
7.2 Methodology ..... 149
7.3 Climate Change Impacts upon Snowmelt Hydrology and the Winter Flow Regime: Results ..... 150
7.4 Discussions and Conclusions ..... 161

**Chapter 8: Discussions and Conclusions ..... 163**
8.1 Introduction ..... 165
8.2 Research Questions: Key Findings and Discussions ..... 165
8.3 Recommendations for Future Work ..... 173
8.4 Snowmelt Hydrology and its Future Implications for the Winter Flow Regime: Concluding Remarks ..... 173

**Appendix 1: Sensitivity Analysis: Snowmelt Model Parameter Response Curves . 175**

**Appendix 2: Behavioural Hydrological Parameter Sets ..... 183**

**References ..... 187**

## List of Illustrations


| Figure Number | Figure Title | Page |
|---|---|---|
| | **Chapter 1** | |
| 1.1 | Snow accumulation and melt processes | 4 |
| 1.2 (a) | 1961-1990 UK average number of days of sleet/snow falling during the winter | 6 |
| 1.2 (b) | UK elevation | 6 |
| 1.3 | Areas of the UK which exceed the FEH 1 in 100 year snowmelt protection level | 14 |
| 1.4 | 1961-1990 UK mean winter temperature | 16 |
| | **Chapter 2** | |
| 2.1 | National and local context of the Dacre Beck catchment | 24 |
| 2.2 | Elevation and channel network of Dacre Beck | 25 |
| 2.3 | Dacre Bridge gauging station | 27 |
| 2.4 | Dacre Bridge observed daily discharge and observed daily precipitation from Hutton Green Close Farm gauge | 28 |
| 2.5 (a) | Dacre Beck topographic wetness index | 32 |
| 2.5 (b) | Dacre Beck slope derived from DEM | 32 |
| 2.6 | Dacre Beck land cover | 35 |
| 2.7 | Dacre Beck soils | 39 |
| 2.8 | Dacre Beck geology | 40 |
| 2.9 | Dacre Beck channel network | 43 |

**Chapter 3**


| | | |
|---|---|---|
| 3.1 | Decision chain used to invoke snow accumulation and melt modelling processes | 49 |


**Chapter 4**


| | | |
|---|---|---|
| 4.1 | Decision chain implemented by the distributed snowmelt model for each point in the landscape at each time step | 64 |
| 4.2 | Response surfaces from the sensitivity assessment for the degree-day/hour parameter for each snowmelt model | 74 |
| 4.3 | Sensitivity assessment comparison analysis response curves for each snowmelt model for the Q5 and Q50 output metrics | 79 |
| 4.4 | Response surface contours for snowmelt model 1 for the Q5 and Q50 output metrics | 82 |


**Chapter 5**


| | | |
|---|---|---|
| 5.1 | Probabilistic projections from the UKCP09 report of the mean winter temperature and precipitation for the Dacre Beck by the 2050s under a medium emissions scenario | 92 |
| 5.2 | Schematic representation of the Neyman-Scott Rectangular Pulses approach | 93 |
| 5.3 | Probabilistic estimates of means winter temperature in Dacre Beck for the baseline and scenario periods (a) across the entire catchment and (b) at the highest elevation | 98 |
| 5.4 | Projections of percentage change in winter snow and rain accumulation in Dacre Beck | 100 |
| 5.5 | Projections of change in the winter sum of total direct solar radiation and total sunshine hours in Dacre Beck | 101 |
| 5.6 | Projections of change in the winter Q5 of Dacre Beck from the snowmelt-only hydrograph and snowmelt and rainfall | 103 |

| | | |
|---|---|---|
| | hydrograph for all three snowmelt models | |
| 5.7 | Projections of change in the winter Q50 of Dacre Beck from the snowmelt-only hydrograph and snowmelt and rainfall hydrograph for all three snowmelt models | 105 |
| 5.8 | Projections of change in the number of winter precipitation days in Dacre Beck | 106 |
| | **Chapter 6** | |
| 6.1 | Point and landscape process representation of CRUM2D v3.1 before the incorporation of snowmelt processes | 113 |
| 6.2 | Point and landscape process representation of CRUM2D v3.1 after the incorporation of snowmelt processes | 116 |
| 6.3 | Conceptual response curve for a single model parameter | 120 |
| 6.4 | Dotty plot of the temperature lapse rate parameter with a subjectively defined objective function criterion | 126 |
| 6.5 | Modelled hydrograph and the associated hydrological parametric uncertainty plotted against the observed hydrograph and precipitation | 132 |
| 6.6 | Structural uncertainty from the snowmelt models | 133 |
| 6.7 | Snowmelt structural uncertainty | 134 |
| 6.8 | Probability Density Function curves of parametric uncertainty arising from the parameters within each snowmelt model and the hydrological parameters within CRUM for the (a) Q5 and (b) Q95 flows | 135 |
| 6.9 | Probability Density Function curves of parametric uncertainty arising through the combination of the snowmelt and hydrological parameters for the (a) Q5 and (b) Q95 flows | 137 |
| 6.10 | Non-behavioural and behavioural Cumulative Distribution Frequency curves for the parameters in snowmelt model one | 139 |

| | | |
|---|---|---|
| 6.11 | Non-behavioural and behavioural Cumulative Distribution Frequency curves for the parameters in snowmelt model two | 140 |
| 6.12 | Non-behavioural and behavioural Cumulative Distribution Frequency curves for the parameters in snowmelt model three | 142 |


**Chapter 7**


| | | |
|---|---|---|
| 7.1 | Combined Q5 and Q95 Cumulative Distribution Frequency curve used to sample three behavioural parameter sets for the first snowmelt model | 148 |
| 7.2 | Cumulative Distribution Frequency curve of mean winter temperature used to sample nine weather series | 149 |
| 7.3 | Projections of change in winter Q5 in Dacre Beck | 151 |
| 7.4 | Projections of change in winter Peak Over Threshold exceedence events using the (a) original FEH threshold value and (b) revised lower threshold value in Dacre Beck | 152 |
| 7.5 | Projections of change in winter Q95 in Dacre Beck | 153 |
| 7.6 | Projections of change in winter 7-day consecutive low flow in Dacre Beck | 154 |
| 7.7 | Cumulative Distribution Frequency curve of mean winter temperature change used to sample nine temperature perturbation change factors | 155 |
| 7.8 | Projections of change in winter Q5 in Dacre Beck using the temperature perturbation values | 157 |
| 7.9 | Projections of change in winter Peak Over Threshold exceedence events using the lower threshold value in Dacre Beck using the temperature perturbation values | 157 |
| 7.10 | Projections of change in the January 8$^{th}$ 2005 peak discharge using the temperature perturbation values | 158 |
| 7.11 | Projections of change in winter Q95 in Dacre Beck using the | 159 |

| | | |
|---|---|---|
| | temperature perturbation values | |
| 7.12 | Projections of change in winter 7-day consecutive low flow in Dacre Beck using the temperature perturbation values | 160 |


## List of Tables


| Table Number | Table Title | Page |
|---|---|---|
| | **Chapter 2** | |
| 2.1 | Dacre Beck hydro-climatic summary for six winter seasons | 30 |
| 2.2 | Land cover properties affecting evapotranspiration and infiltration-surface runoff partitioning in Dacre Beck | 37 |
| 2.3 | Hydraulic properties of the soils within Dacre Beck | 38 |
| 2.4 | Hydraulic properties of the bedrock within Dacre Beck | 41 |
| | **Chapter 3** | |
| 3.1 | Summary of Energy Balance snowmelt models | 53 |
| 3.2 | Summary of temperature-index snowmelt models | 58 |
| | **Chapter 4** | |
| 4.1 | Parameters within the distributed snowmelt model and their feasible ranges and base case values | 69 |
| | **Chapter 6** | |
| 6.1 | Hydrological parameters within CRUM and their feasible ranges | 119 |

| | | |
|---|---|---|
| 6.2 | Hydrological parameters within CRUM after the identification of narrower ranges | 129 |

**Chapter 7**

| | | |
|---|---|---|
| 7.1 | Mean winter temperature change factors selected from the mean winter temperature change Cumulative Distribution Frequency curve | 156 |

## List of Abbreviations

| Abbreviation | Definition |
|---|---|
| A1B | SRES medium emissions scenario |
| A1FI | SRES high emissions scenario |
| ALFA | Adaptive Land Use for Flood Alleviation |
| ANOVA | Analysis of Variance |
| B1 | SRES low emissions scenario |
| CEH | Centre for Ecology and Hydrology |
| $CO_2$ | Carbon Dioxide |
| CRUM | Connectivity Runoff Model |
| D8 | D8 Linear Flow Algorithm |
| DEM | Digital Elevation Model |
| EBM | Energy Balance Model |
| ERT | Eden Rivers Trust |
| ESRI ArcGIS | Environmental Systems Research Institute Arc Geographic Information System |
| FEH | Flood Estimation Handbook |

| | |
|---|---|
| FSR | Flood Studies Report |
| GCM | General Circulation Model |
| GLUE | Generalised Likelihood Uncertainty Evaluation |
| HadCM3 | Hadley Centre Coupled Model version 3 |
| HadSM3 | Hadley Centre Slab Model version 3 |
| HSY | Hornberger-Spear-Young |
| IPCC | Intergovernmental Panel on Climate Change |
| IVR | Inter-Variable Relationship |
| LAI | Leaf Area Index |
| $MODIS_{SCA}$ | Moderate Resolution Imaging Spectroradiometer instrument Snow Covered Area product |
| NLUD | National Land Use Database |
| NSRP | Neyman-Scott Rectangular Pulses |
| OAT | One-at-a-time |
| PDF | Probability Density Function |
| PDM | Probability Distributed Model |
| POT | Peaks Over Threshold |
| RCM | Regional Circulation Model |
| SCE | Shuffled Complex Evolution algorithm |
| SCS | United States Soil Conservation Service |
| SEPA | Scottish Environment Protection Agency |
| SHE | Systeme Hydrologique Europeén |
| SnowMIP | Snow Model Inter-comparison Project |
| SRES | IPCC Special Report on Emissions Scenarios |
| SWAT | Soil and Water Assessment Tool |

| | |
|---|---|
| SWE | Snow Water Equivalent |
| TopMODEL | Topography Model |
| TWI | Topographic Wetness Index |
| UKCP09 | United Kingdom Climate Projections 2009 |
| UKCIP98 | United Kingdom Climate Impact Projections 1998 |
| UK Met Office MIDAS | United Kingdom Meteorological Office Met Office Integrated Data Archive System |
| USACE | United States Army Corps of Engineers |

**List of Equation Terms**

| Equation Term | Definition | Units |
|---|---|---|
| $\acute{\alpha}$ | Cumulative upslope area draining through a point per unit contour length | $m^2$ |
| $\acute{\alpha}_c$ | Weather change factor | |
| $\acute{\alpha}_i$ | Error in an autoregressive data series | |
| $\acute{\alpha}_l$ | Albedo of snowpack | |
| $tan\beta$ | Slope angle | tan° |
| $\delta_t^*$ | Error model | |
| $\delta T/\delta z$ | Soil temperature gradient | °C $m^{-1}$ |
| $\Delta A_i$ | Fraction of the upslope area assigned to each downslope neighbouring cell | |
| $\acute{\varepsilon}_t$ | Residual model error | |
| $\acute{\eta}$ | Mean error | |

| | | |
|---|---|---|
| $\acute{\eta}_m$ | Mass concentration of blowing snow at height $z$ | |
| $\rho$ | Atmospheric vapour density | kg $m^{-3}$ |
| $\rho_s$ | Snowpack density | kg $m^{-3}$ |
| $\rho_w$ | Water density | kg $m^{-3}$ |
| $\sigma^2$ | Variance | |
| $\theta$ | Individual sampled parameter set | |
| $\Theta$ | Suite of sampled parameter sets | |
| $a_{snow}$ | Short wave solar radiation melt | W $m^{-2}$ mm hour$^{-1}$ °$C^{-1}$ |
| $A$ | Slope aspect | ° |
| $A'$ | Albedo from the previous day | |
| $A_u$ | Total upslope area | $m^2$ |
| $A_x$ | Maximum albedo | |
| $A_z$ | Azimuth angle of the slope | radians |
| $B$ | Thermal quality of the snowpack | |
| $c$ | Snow unloading coefficient | |
| $c_i$ | Ratio of saltation velocity to friction velocity | |
| $C_c$ | Canopy density | Proportional coverage |
| $C_p$ | Specific heat of rain | J °$C^{-1}$ |
| $D$ | Solar declination | Radians |
| $D_a$ | Day angle | Radians |
| $D_e$ | Bulk transfer coefficient for latent heat | W $m^{-2}$ $K^{-1}$ |
| $D_h$ | Bulk transfer coefficient for sensible heat | W $m^{-2}$ $K^{-1}$ |
| $D_p$ | Pipe diameter | m |

| | | |
|---|---|---|
| $e$ | Efficiency of saltation | $1/ms^{-1}$ |
| $e_a$ | Atmospheric vapour pressure | Pa |
| $e_s$ | Snow surface vapour pressure | Pa |
| $f$ | Friction factor | |
| $F$ | Error between observations and model predictions | |
| $F_o$ | Observed variance | |
| $F_{salt}$ | Redistribution of snow by wind saltation | $kg\ m^{-1}\ s^{-1}$ |
| $F_{susp}$ | Redistribution of snow by wind suspension | $kg\ m^{-1}\ s^{-1}$ |
| $g$ | Gravitational acceleration | $ms^{-2}$ |
| $G_s$ | Amount of solar radiation reaching the surface | $W\ m^{-2}$ |
| $h^*$ | Coefficient affecting time available for vertical diffusion of wind particles | |
| $H_a$ | Hour angle | radians |
| $H_l$ | Pressure head loss | m |
| $I$ | Snow interception | $kg\ m^{-2}$ |
| $I^*$ | Difference of current snow load with maximum snow load | $kg\ m^{-2}$ |
| $I_o$ | Initial snow load | $kg\ m^{-2}$ |
| $k$ | Soil thermal conductivity | $W\ K^{-1}\ m^{-1}$ |
| $k_v$ | von Kármán's constant | |
| $K$ | Degree-Day parameter | $mm\ °C^{-1}\ Day^{-1}$ |
| $K_{rain}$ | Rain-on-snow factor | $mm\ mm^{-1}\ Day^{-1}$ |
| $L$ | Slope length | m |
| $L_R$ | Temperature or precipitation lapse rate | $°C\ or\ mm\ m^{-1}$ |

| | | |
|---|---|---|
| $L(Y\|\theta)$ | Likelihood function | |
| *Lat* | Latitude | radians |
| *Long* | Longitude | ° |
| *M* | Snowmelt runoff | mm |
| $M_r$ | Rank | |
| *n* | Number of data points | |
| *NS* | Nash-Sutcliffe efficiency criterion | |
| $O_e$ | Orbital eccentricity | |
| $P_i$ | Exponential function of snowfall | kg $m^{-2}$ unit $time^{-1}$ |
| $P_r$ | Rainfall amount | mm |
| $P(\theta)$ | Prior distribution | |
| $P(\theta\|Y)$ | Posterior distribution | |
| *q* | Observed data (discharge) | $m^3$ $s^{-1}$ |
| $q^-$ | Mean of observed data (discharge) | $m^3$ $s^{-1}$ |
| *q'* | Modelled data (discharge) | $m^3$ $s^{-1}$ |
| $Q_a$ | Advective energy flux | W $m^{-2}$ unit $time^{-1}$ |
| $Q_e$ | Latent heat of condensation energy flux | W $m^{-2}$ unit $time^{-1}$ |
| $Q_g$ | Ground heat energy flux | W $m^{-2}$ unit $time^{-1}$ |
| $Q_h$ | Advective energy flux | W $m^{-2}$ unit $time^{-1}$ |
| $Q_{ln}$ | Net long wave radiation energy flux | W $m^{-2}$ unit $time^{-1}$ |

| | | |
|---|---|---|
| $Q_m$ | Total energy balance | W $m^{-2}$ unit $time^{-1}$ |
| $Q_n$ | Net radiation energy flux | W $m^{-2}$ unit $time^{-1}$ |
| $Q_{sn}$ | Net short wave radiation energy flux | W $m^{-2}$ unit $time^{-1}$ |
| $Q_t$ | Turbulent transfer energy flux | W $m^{-2}$ unit $time^{-1}$ |
| $R_i$ | Daily air temperature range | °C |
| *RMAE* | Relative Mean Absolute Error | |
| $R_p$ | Water equivalent depth of snow | mm |
| $S$ | Clear sky short wave solar radiation | W $m^{-2}$ |
| $S_c$ | Solar constant | W $m^{-2}$ |
| *SI* | Sensitivity indices | |
| $S_l$ | Slope angle | radians |
| $S_p$ | Tree species coefficient | kg $m^{-2}$ |
| $S_t$ | Solar time | hours |
| $T$ | Time | hours |
| $T_a$ | Air temperature | °C |
| $T_o$ | Threshold melt temperature | °C |
| $T_r$ | Rain temperature | °C |
| $T_s$ | Snowpack temperature | °C |
| $u^*$ | Atmospheric friction velocity | $ms^{-1}$ |
| $u_n^*$ | Portion of u* applied to non-erodible roughness elements | |
| $u_t^*$ | Portion of u* applied to non-erodible roughness elements | |
| $u_z$ | Wind velocity | $ms^{-1}$ |

| | | |
|---|---|---|
| $V$ | Flow velocity | $ms^{-1}$ |
| $V_i$ | Elementary effect of parameter $x_i$ | |
| $V_j$ | Elementary effect of parameter $x_j$ | |
| $V_{i,j}$ | Secondary effects between parameters $x_i$ and $x_j$ | |
| $V(Y)$ | Total model variance | |
| $x_i$ | Model parameter | |
| $x_j$ | Model parameter | |
| $Y$ | Model function | |
| $z$ | Height above snow surface | m |
| $z_h$ | Factor affected by time available for vertical diffusion of snow particles | |
| $z_o$ | Aerodynamic roughness height | m |
| $Z_{(i,j)}$ | Elevation difference between gauging station and landscape point *i,j* | m |

**Acknowledgements**

The author would like to express thanks to Dr Sim Reaney and Dr Rich Hardy who supervised this project and helped the author to climb what was a very steep learning curve. Dr Nick Odoni of Durham University whose valuable advice helped to calibrate the physically-based hydrological model in a more efficient manner. Ian Pattison formerly of Durham University (now at Southampton University) who provided information from his research about which parameters to focus upon in the uncertainty evaluation. Professor Chris Kilsby of Newcastle University who advised the author on the suitability of perturbing the temperature series produced by the stochastic weather generator. Helen DiGiorgio of the Environment Agency North West Division for providing the observed discharge data from the gauge at Dacre Bridge. Finally, the author wishes to express thanks to friends and family, especially the postgraduates in the Geography department and Van Mildert college, who helped maintain some form of work-life balance.

# Chapter 1
# Snowmelt Hydrology in the UK

## 1.1 Introduction

Snowmelt hydrology attenuates the variability of the winter hydrograph of a catchment (SEPA, 2008) by reducing peak flows and supplementing low flows. Peak flows are reduced during periods of snow accumulation by storing water on the hill slopes thus reducing the amount of water that reaches the outlet. After a snowpack accumulates it is subjected to number of different energy fluxes (**Figure 1.1**) which can raise its temperature to the point where it begins to release melt water. If this release occurs during long periods devoid of precipitation it can supplement low river flows (Dunn *et al.,* 2001) which are important for in-stream ecological conditions. However, if a large pulse of melt water release coincides with a high rainfall event then peak flows at the catchment outlet can be exacerbated leading to downstream flooding such as the January 1993 River Tay floods which inundated 780 homes in Perth causing £10 million of damage (Black and Anderson, 1993). Previous analysis of monthly trends in winter flows in Scottish catchments which were affected by snowmelt showed that flow variability increased over the last 40 years, high flows increased up to 46% and low flows decreased by up to 13% (SEPA, 2008). These trends were attributed to an increase in air temperatures associated with an increase in the number of Atlantic frontal weather systems which occurred each winter. Projections of future climate suggest that this warming trend will continue (Murphy *et al.,* 2009) hence it is likely that winter flow variability will increase further. This thesis aims to extend the previous research by coupling projections of future climate to a hydrological model that deals with snow accumulation and melt. This methodology will then be used to assess future changes in the snowmelt hydrology of an upland catchment in the English Lake District.

In this chapter the fundamental physical processes behind snow accumulation and melt (**Figure 1.1**) will be explained before outlining their importance in the winter flow regime of upland catchments in the UK. The sensitivity of these processes to climatic changes will then be outlined allowing the identification of research needs in snowmelt hydrology. Finally, from these research needs, the aims of this project will be formulated.

## 1.2 Snow Accumulation and Distribution

Snow is the solid state of precipitation which forms in the atmosphere in the presence of water vapour, ice nuclei and an air temperature at or below $0^0$C (Gray and Prowse, 1993). Ice nuclei are often initiated by dust particles around which ice can form eventually

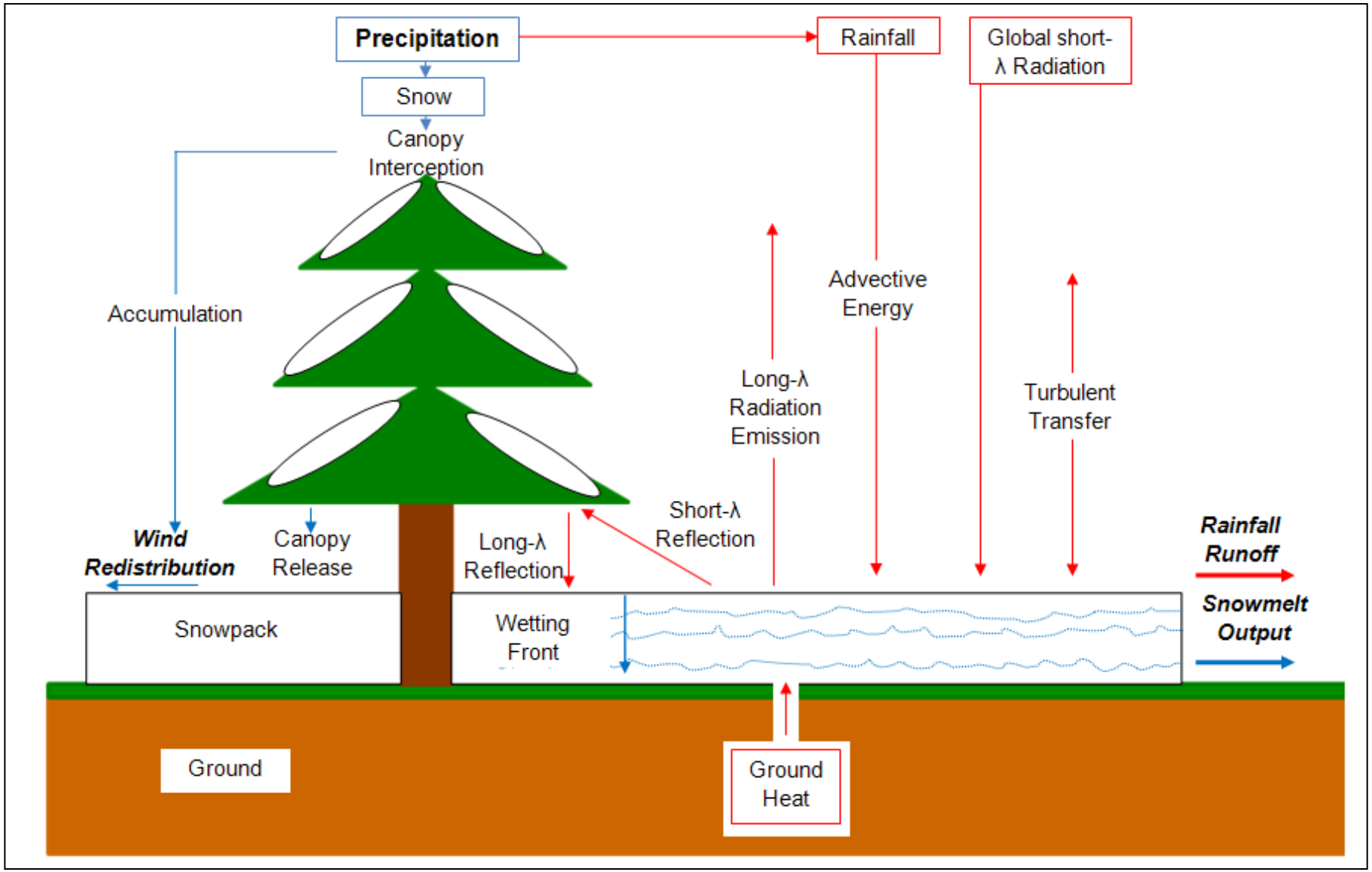


**Figure 1.1** Snow accumulation (blue) and melt (red) processes within a catchment. The precipitation input is shown in bold and the outputs are shown in bold italics.

growing into snow crystals (Gray and Prowse, 1993). In order for these snow crystals to reach the ground in their solid state the underlying air layers through which they fall must also be at or below 0°C. In the UK these meteorological conditions are most common during the winter months (December to February). The incidence of UK snowfall during the winter months has a positive relationship with elevation (**Figure 1.2** (**a**) & (**b**)) where areas above 500 m have the greatest amount of snowfall (Jackson, 1978a). This is caused by adiabatic processes (no energy enters or exits an air parcel) which create a temperature lapse rate with increasing elevation. When an air parcel rises it expands (Danielson *et al.,* 2003) which reduces the internal energy thus lowering the temperature (McIlveen, 1992). The temperature lapse rate within the UK is reported as 8.5°C $km^{-1}$ (Lawler, 1987; de Jong *et al*., 2009). A positive relationship between precipitation amount and elevation also exists due to orographic forcing where moist air is forced upwards causing it to cool and freeze (Birkeland and Mock, 1996). The rate of increase of annual precipitation with elevation in the UK is reported as 2.8 mm $km^{-1}$ (de Jong *et al*., 2009). Snowfall amount is therefore enhanced at higher elevations (Barry, 1992), above 500 m in the UK (**Figure 1.2** (**b**)), due to a combination of colder temperatures and increased precipitation delivery (Gurtz *et al.,* 2005).

Some of this snow may be intercepted by vegetation before it is able to reach the ground. In boreal forests interception can store up to 60% of cumulative snowfall by midwinter (Pomeroy *et al.,* 1998). Vegetative properties including branch strength, flexure, needle configuration and orientation, mass and surface area (Gray and Prowse, 1993) influence interception magnitude as does the vegetation type (see Chapter 3 *Eqs. 3.1* and *3.2*). Deciduous trees intercept much less due to losing their leaves in the winter. Scottish Spruce canopies can hold in excess of 20 mm of snow water equivalent (SWE), (Ward and Robinson, 2000) which is the equivalent amount of liquid water stored in the snowpack. During a snowfall event, the canopy gap fraction decreases due to the interception of snow flakes in the narrower gaps. This builds up small bridges between the gaps decreasing the gap fraction of the vegetation which positively feeds back to increase the amount of interception (Gray and Prowse, 1993). The maximum interceptive capacity of the vegetation is reached when the amount of snow falling to the ground is balanced by the amount that is intercepted.

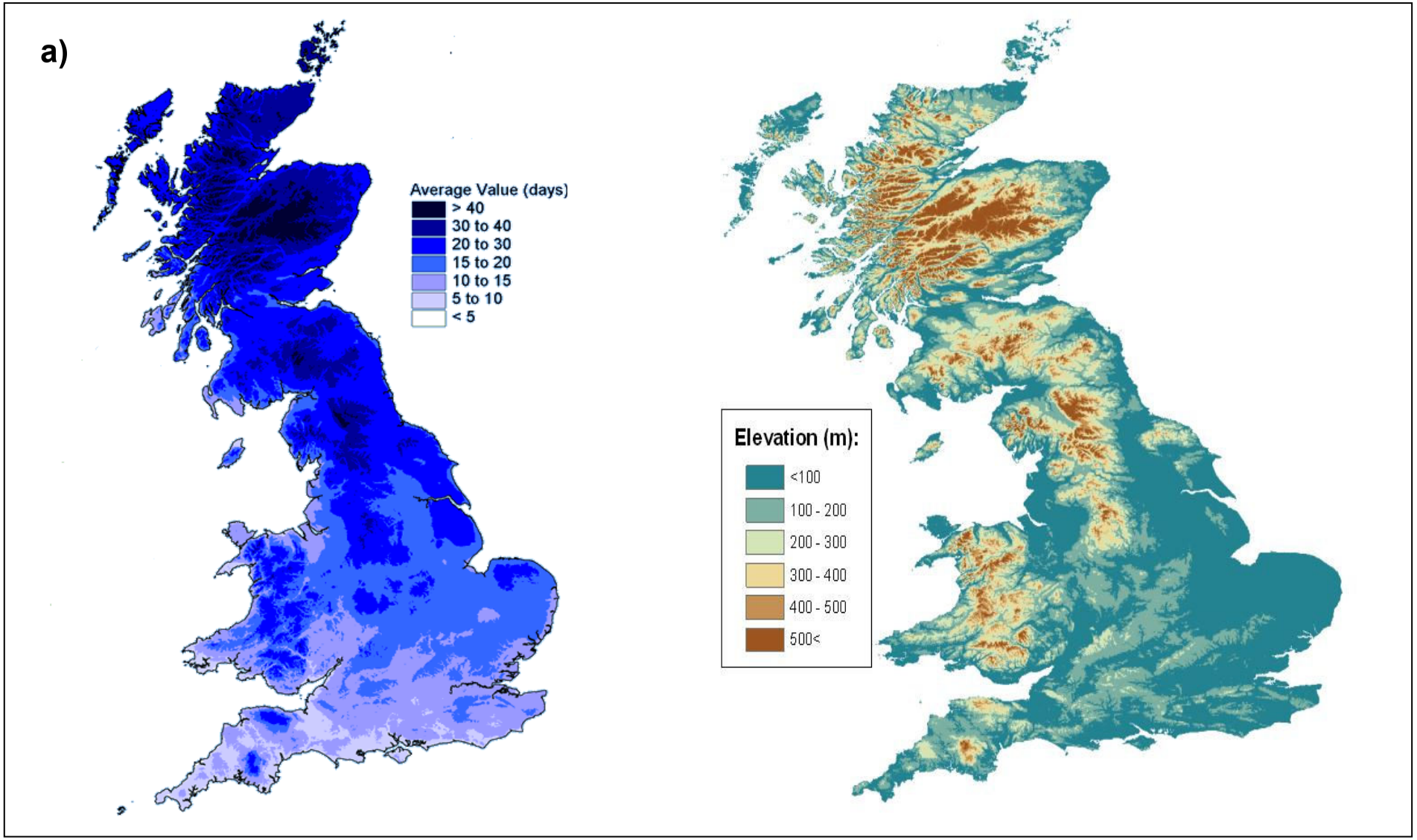


**Figure 1.2** (**a**) 1961-1990 average number of days of sleet/snow falling during the winter (December to February). Adapted from Jackson 1978(b), from: (http://www.metoffice.gov.uk/climate/uk/averages/ukmapavge.html#). (**b**) UK elevation from SRTM data re-sampled to 1 km resolution from: (http://srtm.csi.cgiar.org/)

Snow cover distribution displays areal variability across three spatial scales: macro- ($10^6 km^2$), meso- (linear distance 100 m-1 km) and micro- (linear distance 10-100 m) scales (Gray and Prowse, 1993). Variations at the macro-scale are due to dynamic meteorological effects e.g. standing waves in the atmosphere which lead to regional differences. Redistribution along relief and vegetative features due to wind affects the meso-scale whilst variations in airflow and transport patterns affect the micro-scale.

Redistribution by wind processes affects these last two scales through three mechanisms: creep, saltation and suspension (Gray and Prowse, 1993). The latter two are the most significant where snow particles are bounced along the surface and held in the air by turbulent diffusion respectively (MacDonald *et al.,* 2009). Consequently snow can be transported until it reaches an area where the energy available for transport by wind decreases, such as a topographic hollow, leading to deposition and hence spatially variable snow accumulation (Ward and Robinson, 2000).Wind transport can also induce snow loss through sublimation where snow changes from a solid phase into water vapour and enters the atmosphere (MacDonald *et al.,* 2009).

Each of the snow accumulation and redistribution processes lead to a complex spatial distribution of snow depth across the catchment (Ward and Robinson, 2000). This in turn can affect the spatial distribution of snowmelt, wind redistribution for example can lead to deep snow accumulations within topographic hollows which can release melt water for long periods of time (Dunn *et al.,* 2001). Hence, the next section explains how an accumulated snow can begin to produce snowmelt.

### 1.3 Snowmelt Processes

Once a snowpack has accumulated it is subjected to a range of energy fluxes (**Figure 1.1**) including net radiation $Q_n$, turbulent transfer $Q_t$, advective energy $Q_a$ and ground heat $Q_g$. These first three occur at the surface of the snowpack and the fourth at it base i.e. the snowpack interfaces with the atmosphere and the ground. The total input from all these fluxes is the total energy flux available to melt the snowpack $Q_m$ (Hock, 2005):

$$Q_m = Q_n + Q_t + Q_a + Q_g \qquad \text{(Eq. 1.1)}$$

Net radiation is the sum of net short- $Q_{sn}$ and long- $Q_{ln}$ wave radiation fluxes:

$$Q_n = Q_{sn} - Q_{ln} \quad \text{(Eq. 1.2)}$$

Short-wave radiation is electro-magnetic solar radiation between wavelengths of 0.2-4μm. The amount received at the top of the atmosphere is referred to as potential clear-sky direct solar radiation (Hock, 1999). On average however only 47% of this energy reaches the earth's surface (Gray and Prowse, 1993) as it is attenuated by reflection off clouds, scattered by air molecules and absorbed by molecular structures (United States Army Corps of Engineers (USACE), 1998). Global radiation is the amount of short-wave radiation which reaches the surface and can be calculated as a function of cloud cover, slope, aspect and exposure (Fu and Rich, 2002). The reflectivity of the snowpack (albedo) however, means that a percentage of the global radiation incident at the snowpack surface is reflected back into the atmosphere. The magnitude of reflection depends on snowpack properties such as wetness, impurities, particle size and density (Gray and Prowse, 1993). Such properties vary spatially as well as temporally (USACE, 1998) due to variable rates of snowpack metamorphosis (Pomeroy *et al.,* 1998, see section 1.3 for an explanation of metamorphosis) which are caused by variable receipts of each energy flux. Hence the impact of short-wave radiation receipt upon snowmelt production is highly variable across the snowpack.

Long-wave radiation occurs from reflection of short-wave radiation off the atmosphere and forest cover as well as emission from the Earth's surface (USACE, 1998). Some of the short-wave radiation absorbed by the snowpack can be radiated back into the atmosphere as long-wave radiation since snow is a near-perfect blackbody emitter (USACE, 1998). Consequently long-wave radiation often represents a loss of energy from the snowpack hence its negative sign in *Eq. 1.4*. Where there is a significantly dense forest canopy however, the emitted long-wave radiation from the snowpack can be reflected off the canopy and re-enter the snowpack thus contributing towards the total energy balance.

Turbulent transfer is the exchange of energy between the atmosphere and the snowpack due to sensible heat advection and latent heat of condensation (USACE, 1998). Sensible heat advection $Q_h$, is affected by the local temperature gradient above the snow surface $T_a$-$T_s$ (the difference between air and snowpack temperature respectively), and the corresponding wind speed $u_z$:

$$Q_h = D_h\, u_z(T_a - T_s) \quad \text{(Eq. 1.3)}$$

Where $D_h$ is the bulk transfer coefficient for sensible heat which can be assumed equal to $D_e$ (bulk transfer coefficient for latent heat, Suzuki *et al.,* 1999), its value lies at an order of magnitude of $x10^{-3}$. Latent heat of condensation $Q_e$ meanwhile is affected by the atmospheric $e_a$, and snow surface $e_s$, vapour pressure and the corresponding wind speed:

$$Q_e = D_e \, u_z(e_a - e_s) \quad \text{(Eq. 1.4)}$$

Where $D_e$ is the bulk transfer coefficient for latent heat which represents the evaporation rate from the snow surface, it can be calculated from the slope of the regression between evaporation and the bulk formulae, typical values range between 0.0021 to 0.0004 depending on vegetation canopy coverage (Suzuki *et al.,* 1999).

Heat conduction from the ground is a very small component of the overall energy budget and is deemed to be insignificant over periods shorter than one week, but over an entire melt season it can produce a large amount of melt (USACE, 1998). Its contribution is estimated using soil temperature gradients *dT/dz*, measured near the surface in an equation for steady-state, one-dimensional heat flow by conduction (USACE, 1998):

$$Q_g = k\left(\frac{dT}{dz}\right) \quad \text{(Eq. 1.5)}$$

Where $k$ is the thermal conductivity of the soil ($W\ K^{-1}\ m^{-1}$) which represents its ability to conduct heat. Typical values range from 0.15 to 1.5 $W\ K^{-1}\ m^{-1}$.

A key source for advective melt energy is from rain that falls directly on the snowpack. Rain has a positive temperature as it occurs on positive degree-days (USACE, 1998) hence when it enters a snowpack it transfers this positive energy to the snow crystals. For a snowpack which is already melting the magnitude of melt will increase due to the additional input of energy. In the case of a snowpack whose temperature is below zero rain water will enter and refreeze releasing its latent heat of fusion raising the snowpack's temperature increasing its vulnerability to melting (Gray and Prowse, 1993). The energy input from rain on snow can be estimated as a function of the rainfall amount $P_r$(mm), and rainfall temperature $T_r$ (°C) which is assumed to be equal to the air temperature (USACE, 1998):

$$Q_a = C_p \, \rho_w \, P_r(T_r - T_s) \quad \text{(Eq. 1.6)}$$

Where $C_p$ is the specific heat of rain, $\rho_w$ is the density of water and $T_s$ is the snow temperature (°C).

The relative importance of each flux varies as a function of spatial and temporal components. Differences in land use can lead to spatial variations, for example forest canopies dampen turbulent fluxes (Ward and Robinson, 2000) since they shelter snowpacks from high wind velocities. The relative importance of each energy flux can vary diurnally; at night for example the receipt of short-wave radiation is greatly reduced. Variations can also occur between days due to changing weather conditions, during windy conditions for example the turbulent transfer of latent and sensible heat are the most important energy fluxes. In the UK it has been shown that the main source of energy for melt in the UK is the turbulent transfer of latent and sensible heat (Ward and Robinson, 2000) which occur during the mild and windy conditions often associated with Atlantic frontal weather systems (SEPA, 2008).

The sum of all these energy fluxes can be converted into a melt water amount *M*, through (USACE, 1998):

$$M = \frac{Q_m}{(334.9\rho_w B)} \quad \text{(Eq. 1.7)}$$

Where *334.9* is the latent heat of fusion of ice which is the heat absorbed when it changes phase from liquid to solid, *B* is the thermal quality of the snow which depends on the amount of free-water contained within the snowpack (Singh and Singh, 2001), values range between 0.8 to 1.1 (USACE, 1956).

### 1.4 Runoff from Snowmelt

In order for the snowpack to produce melt water which can be converted into runoff both the cold-content, which refers to snowpack temperature, and liquid-water-holding capacity, which refers to snowpack liquid water saturation, conditions must be met. To meet the cold-content condition the snow temperature must be raised to 0°C. This occurs through the process of metamorphosis (ripening) which commences when there is a net input of energy into the snowpack. This process transforms the snow from being loose, dry and subfreezing to coarse, granular and moist at 0°C (USACE, 1998). Once the snow reaches these conditions it has satisfied the cold-content condition and is said to be *ripe*

(Gray and Prowse, 1993). Any additional energy input into *ripe* snow means that melt water can be produced. This melt water will not however begin to percolate through the snowpack until the second condition, the maximum liquid-water-holding capacity, is exceeded. The matrix of the snow crystals is able to hold a certain amount of water against gravity. When this amount is reached the liquid-water-holding capacity condition is met and any additional input of water is able to percolate through the snow matrix. These conditions are first met at the surface of the snowpack where the energy fluxes outlined above are at their greatest. Since these fluxes have a greatly reduced direct influence on the underlying snow layers the melt water produced at the surface must percolate downwards and release its energy so that the two conditions are met for the entire snowpack profile.

Melt water produced at the surface percolates downwards under gravity into the colder snow immediately below it and refreezes releasing its latent heat of fusion. Eventually the temperature of the snow immediately below the surface will become isothermal at 0°C. It will then receive melt water from above as well as producing its own which will be held within the snow matrix. Once the maximum liquid-water-holding capacity is exceeded melt water can then percolate to next cold layer of snow immediately below. The process is repeated until the two conditions are met for the entire snowpack making it able to produce runoff.

The process above is referred to as the advance of a wetting-front which separates the upper layers which can produce runoff from those beneath which cannot (Prowse and Gray, 1993). Irregularities in the advance occur due to the presence of ice layers within the snowpack which deflect flow leading to concentrated flow-fingers (USACE, 1998). Spatial variability in melt water production therefore exists within a snow pack.

### 1.5 Impact of Snowpack Accumulation and Snowmelt Runoff upon Hydrology

In the UK, snowpack accumulation and melt can decrease the variability of the hydrograph at the catchment outlet (SEPA, 2008). When precipitation enters a catchment as rain it immediately begins to route towards the outlet (although some may be lost through evapo-transpiration, Chapter 6). During periods when the amount of rainfall exceeds the catchment's soil moisture capacity large amounts of runoff are produced which reach the outlet in large quantities over a short period of time leading to extreme

flows. However, when a snowpack accumulates, it provides a storage zone preventing the precipitation which fell as snow from routing towards the outlet. During this time less water reaches the catchment outlet reducing the magnitude of the outlet hydrograph. Soulsby *et al.,* (1997) observed a reduction in the hydrograph of a Feshie sub-catchment during a prolonged period of snow accumulation in January 1994. The peak flow during this month was 10 mm $day^{-1}$ which was lower than the peak flow of 30 mm $day^{-1}$ in the milder January of 1993 (Soulsby *et al.,* 1997).

Once a snowpack begins to melt, it releases runoff gradually which supplements low flows during prolonged periods devoid of precipitation (SEPA, 2008). When a cycle of melt coincides with a dry spell it supplements the water delivered to the outlet by baseflow thus reducing the severity of low flows. Dunn *et al.,* (2001) found that this process contributed up to an average of 10 $m^3s^{-1}$ to stream flow in Mar Lodge (a sub-catchment of the river Dee, 293 $km^2$). They found that this effect was greater after winters of high snow accumulation and could still contribute to river flows in the following July (Dunn *et al.,* 2001). Low flows can impact negatively upon the in-stream ecological conditions, for example they can reduce the dilution of nitrates (Whitehead *et al.,* 2009). Consequently snowmelt supplementation of low flows can improve the ecological condition of the river channel within a catchment (Chapter 2 section 2.6).

Melt water release can also instigate temporal fluctuations in the outlet hydrograph as was observed in the diurnal hydrograph oscillations in a Feshie sub-catchment (Ferguson, 1984). These oscillations were synchronised to diurnal air temperature fluctuations which some have hypothesised to be linked to diurnal short-wave solar radiation receipt (Harding, 1986). Since solar radiation receipt is at a maximum at midday and minimum at midnight the release magnitude of melt water follows a similar temporal oscillation. However hourly modelling studies in the Monchyle Burn and Trout Beck catchments found the solar radiation budget to be negligible (Moore *et al.,* 1999). Instead they found that sensible heat exchange and latent heat of condensation were the most important fluxes. Both of these, in part, are related to air temperature which is in turn related to diurnal short-wave solar radiation receipt.

However, in extreme cases large pulses of melt water release which coincide with periods of intense rainfall can exacerbate extreme high flows. On these occasions more water is

routed to the outlet which can exceed the river's bankfull capacity resulting in flooding (Reed and Field, 1992). For example flooding on the River Tay in January 1993 was caused by a large input of rainfall coinciding with snowmelt (Black and Anderson, 1993). A large snowpack had accumulated over the previous six days which was followed overnight by a large input of rainfall (56.8 mm recorded in the Earn catchment) and a temperature increase of 4-6°C. This resulted in a peak flow of 2269 $m^3s^{-1}$ at the Ballathie gauging station (Black and Anderson, 1993). The occurrence of these events is rare due to small probability of extreme snowmelt and extreme rainfall occurring simultaneously.

Despite their rarity, the damaging consequences of floods resulting from extreme snowmelt and extreme rainfall prompted the Flood Studies Report (1975) and subsequent Flood Estimation Handbook (1999) to incorporate snowmelt into its calculation of the 1 in 100 year return period flood protection level. The reports took the median annual snow depth from 100 meteorological stations from 1946-1964 and multiplied the data by 7.5 to obtain the 100 year maximum snow depth. Assuming the density of snow was ~0.13 g $cm^{-3}$ enabled snow depth to be converted into SWE. A statistical relationship between the changes in daily snow depth and maximum air temperature was then developed. This relationship informed that a maximum snow melt rate of 42 mm $day^{-1}$ was possible (Houghton-Carr, 1999). It was found that the 100 year SWE figures could sustain this melt rate for five days hence this information is included when calculating the protection levels for a 1 in 100 year flood event.

However this protection level has been questioned since it was based on data from stations mostly at lower altitudes (Archer, 1981). Hough and Hollis (1997) found that this protection level was only adequate for a 10 year return period at Pennine and Scottish sites but suitable for a 1000 year event at low altitudes in England. **Figure 1.3** reinforces the first conclusion of Hough and Hollis (1997) showing that upland areas (defined in **Figure 1.2** (**b**)) are capable of producing melt rates which exceed this protection level. Therefore, the contribution of snowmelt to flood risk varies across the UK depending on the magnitude of the accumulated snowpack in accordance with local meteorological and physical conditions.

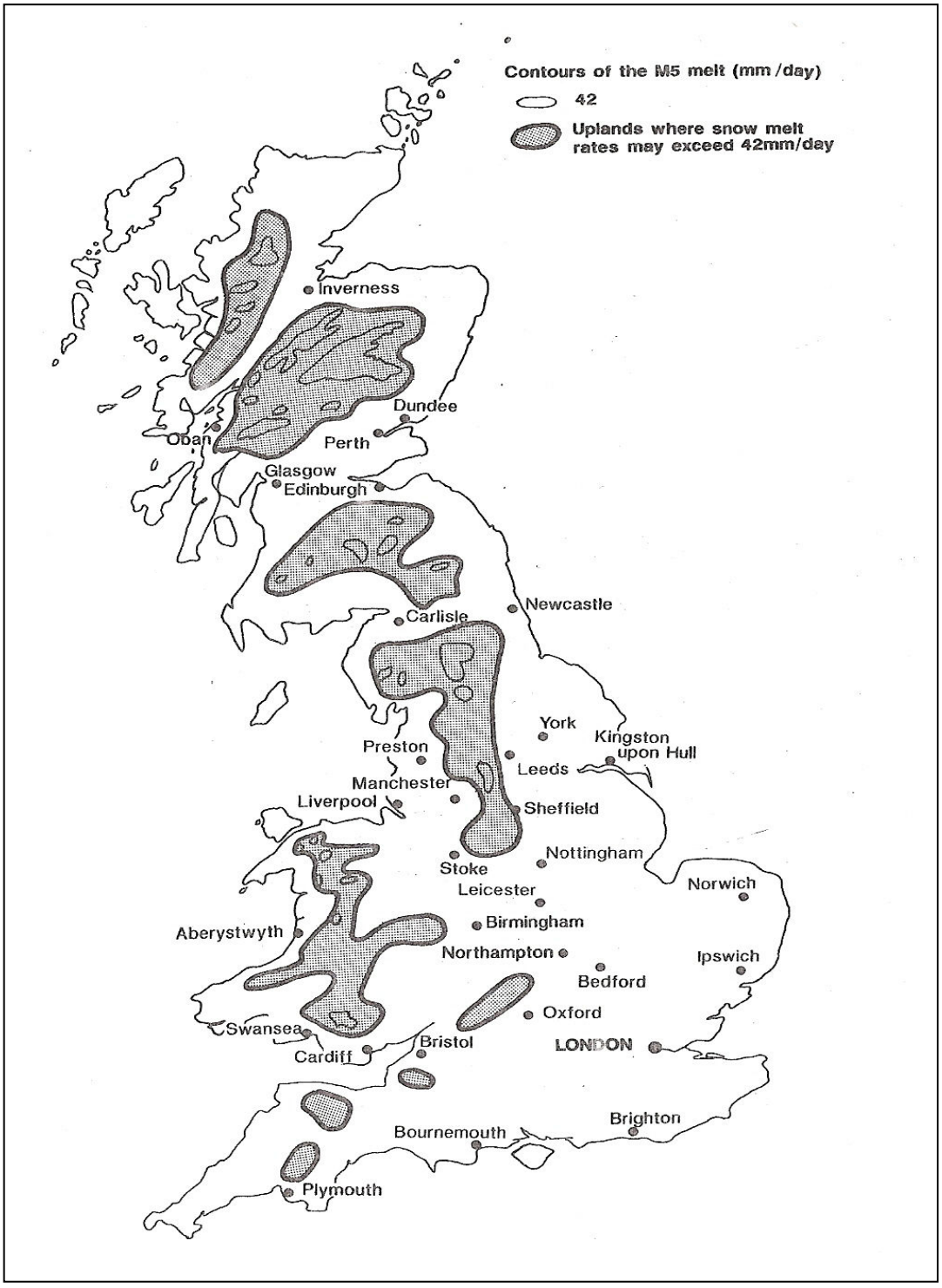


**Figure 1.3** Areas of the UK which exceed the FEH 1 in 100 year snowmelt protection level. Adapted from the Institute of Civil Engineers (1996)

The impact of snowmelt hydrology in the UK is most pronounced in upland areas (**Figure 1.2** (**b**)) where temperatures are colder (**Figure 1.4**) and precipitation is higher (section 1.3, de Jong *et al.,* 2009) allowing greater winter snowfall (**Figure 1.2** (**a**)) and hence snowpack accumulation. Since a larger snowpack has a greater influence on the winter flow regime (Soulsby *et al.,* 1997) this means that the signal of snowmelt hydrology is more distinguishable in upland catchments. Lower elevations have warmer winter temperatures (**Figure 1.4**) meaning that less precipitation falls as snow, instead it falls as

rain. Consequently the winter flow regime at low elevations is dominated by a rainfall signal meaning catchments at these elevations will display greater winter flow variability than upland ones.

### 1.6 Sensitivity of Snowmelt Hydrology to Projected Climatic Change

As explained above, the role of snowmelt hydrology is related to temperature and precipitation (Kingston *et al.,* 2009) meaning that it is sensitive to changes in these variables. Temperature controls the partitioning of precipitation between rain and snow where warmer temperatures will reduce the amount that falls as snow. The greatest sensitivity to temperature change has been shown to occur in areas with a mean winter temperature between $0^0$C to $5^0$C (Mote *et al.,* 2008) due to their close proximity to the freezing temperature. Consequently small changes in temperature in these areas can have a large impact on the number of negative degree days and hence the number of snowfall days. As **Figure 1.4** shows, much of the UK falls between these isotherms during the winter with most of the upland areas having a mean winter temperature very close to $0^0$C. Winter temperatures of upland UK areas are projected by the UKCP09 (Murphy *et al.,* 2009; see Chapter 4) to increase between 2-$4^0$C by the 2050s. The greatest impact of this in Scotland was found to be above altitudes of 400 m (Harrison *et al.,* 2001). The smaller snowpacks that accumulate in warmer temperatures would then be subjected to an increase in energy fluxes such as sensible and latent heat, for example, which are related to air temperature (Hock, 1999). The consequence of this is that the smaller snowpacks would melt faster which would increase the rate of decay from the initial melt release as they are depleted in a shorter time. Future increases in winter temperature therefore would be expected to reduce the magnitude of snowpack accumulation and increase the rate of snowpack depletion due to melting with these changes being most pronounced in upland areas.

Changes in winter precipitation have a secondary impact upon snowpack accumulation and snowmelt hydrology as they are controlled by changes in temperature. Winter precipitation in upland areas is likely to increase between 0-10% (Murphy *et al.,* 2009) so more snow may fall during an individual snowfall day. However, the increase in temperature means that more of this precipitation would actually be partitioned as rain thus reducing the impact of precipitation change upon snowpack accumulation. The increase in rainfall could increase the advective energy flux (*Eq. 1.6*) and hence increase

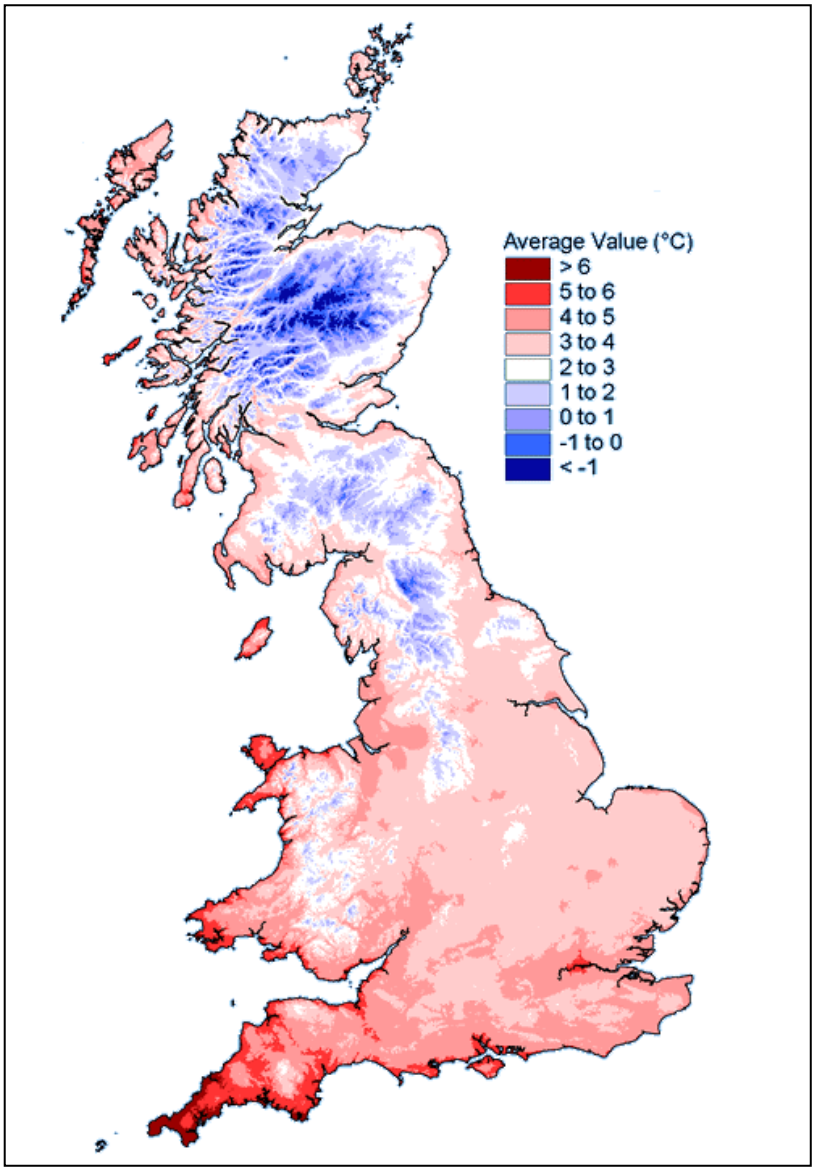


**Figure 1.4** UK Mean winter temperature between 1961-1990. Adapted from the UK Met Office website, from: (http://www.metoffice.gov.uk/climate/uk/averages/ukmapavge.html#)

melt but, as mentioned above, sensible and latent heat have been shown to be the most important energy fluxes in UK snowmelt hydrology (Ward and Robinson, 2000). Therefore changes snowmelt hydrology from precipitation changes may be small and therefore difficult to detect. Instead, changes in precipitation are most likely to affect changes in the overall winter flow regime as discussed below.

The contribution of snowmelt hydrology to the winter flow regime in light of climate change is likely to decrease (Arnell and Reynard, 1996) as smaller snowpacks will release less melt water. Changes in the winter flow regime therefore are likely to be affected by increases in the amount of precipitation partitioned as rainfall and increases in the overall amount of precipitation. This would be expected to increase the variability of the winter

flow regime as the attenuating role of snowpacks is reduced. Observations of monthly winter stream flow trends in Scottish catchments affected by snowmelt hydrology between 1961 to 2008 found that the flow regime became more variable (SEPA, 2008). In three upland Scottish catchments high flows (denoted by the 5$^{th}$ percentile of the flow duration curve (Q5)) increased between 16% to 46% and low flows (denoted by the 95$^{th}$ percentile of the flow duration curve (Q95)) decreased between 5% to 13% (SEPA, 2008). Consequently, climate change could see the winter flow regime of upland UK catchments become dominated by rainfall as the contribution of snowmelt hydrology declines.

### 1.7 UK Snowmelt Hydrology: Research Needs

The impacts of climate change upon UK snowmelt hydrology are already well conceptualised as outlined above. Previous research however has focussed upon trends in observed data and changes in future snow accumulation. To date there have been limited studies which have extrapolated these changes to assess future changes in snowmelt hydrology and the implications for the winter flow regime. Therefore it is the overall aim of this project to:

**Investigate the impacts of climate change upon snowmelt hydrology and their consequences for the winter flow regime of an upland UK catchment**

It was decided to focus upon a single catchment rather than a general region so that a modelling approach could be used to calculate the impact of future climate scenarios upon the winter snowmelt and general flow hydrology. The modelling approach was split into three research questions so that changes in snow accumulation, snowmelt hydrology and the winter flow regime could be dealt with explicitly:

1) *How will snow accumulation change in the future climate in comparison to present conditions?*

This question will aim to assess the changes in the amount of snow fall in the catchment during the winter since this governs the size of the accumulated snow pack. Snow accumulation then in turn affects how much snow is available to melt and thus contribute towards snowmelt hydrology. Previous research showed that warming winter temperature

trends from 1961 to 2004 led to a 30% reduction in number of days of snow lying in the winter (Barnett *et al.,* 2006). It is unclear however, whether changes in precipitation magnitude will compensate for some of the reduction in snowfall. Additionally it will look at how the proportion of snow to rain changes as this could be used to infer possible changes in the winter flow regime. It will achieve this by spatially distributing present and future weather series across the study catchment and modelling the amount of snow and rain that falls in each series.

2) *How will changes in climate affect snowmelt hydrology?*

The second question aims to assess how changes in snow accumulation combine with changes in climate to affect the snowmelt hydrology of the study catchment. Warmer temperatures are likely to decrease the magnitude of snowpack accumulation and increase the magnitude of the energy fluxes. Therefore, it is likely that the nature of snowmelt hydrology will change. Smaller snowpacks may decrease the amount melt water released into the catchment but the increase in the energy fluxes may override this by releasing larger pulses of melt water in initial melt events. Therefore changes in the nature of snowmelt hydrology will be assessed by comparing high and low flow statistics from present and future climate conditions of hydrographs composed solely from snowmelt. If the high flow statistics show a declining trend then this would mean that the increase in the energy fluxes is unable to compensate for the accumulation of smaller snowpacks. The snowmelt hydrographs will be generated from a hydrological model that will be developed to accumulate and melt snow.

3) *What are the implications of changes in climate and snowmelt hydrology for the winter flow regime?*

The final research question will address how changes in snowmelt hydrology in conjunction with climatological changes affect the winter flow regime of the study catchment. The winter flow regime of many upland UK catchments is affected by snowmelt hydrology hence future changes in climate are likely to instigate changes in the outlet hydrograph. Analysis of observed data has shown an increase in hydrograph variability due to warming temperature trends. It is likely therefore that this trend of winter flow regime change would continue in light of UK climate change projections. Changes in high flows will be assessed by comparing the Q5 and number of peak-over-threshold (POT) exceedence events for the winter hydrographs from present and future climate

conditions. Low flows meanwhile will be assessed by undertaking the same type of analysis for the high flows but for the Q95 and 7 day consecutive low flow statistics (Novotny and Stefan, 2007). The hydrographs used to derive the flow statistics from each weather series will be generated by developing upon the hydrological model in the second research question to deal with rainfall-runoff processes. This will enable it model the hydrograph that results from both snowmelt and rainfall.

The rest of this thesis describes how the overall aim of this project was achieved by investigating each of the three research questions outlined above. The next chapter explains which catchment was selected for this project and how it was affected at present by snowmelt hydrology. In preparation for the development of a hydrological model that can deal with snowmelt, Chapter 3 reviews the existing modelling approaches before selecting one that was appropriate for this project. Chapter 4 then describes the development of a model that could spatialise a given weather series before a hydrological routine was added to it using three snowmelt models from the approach selected in Chapter 3. Present and future weather series were then generated in Chapter 5 and applied to the model developed in the previous chapters. The results from this enabled an analysis of changes in snow accumulation and snowmelt hydrology thus beginning to answer the first two research questions. A rainfall component was then also added to this model in order to answer the third research question. The discussion of the model's results however found significant process deficiencies so Chapter 6 explained the incorporation of each snowmelt model into an existing physically-based hydrological model. Chapter 7 then applied this model, within an uncertainty framework, to the same weather series to assess changes in the winter flow regime of the study catchment and the role of snowmelt hydrology in these changes thus providing an answer to the third research question. Chapter 8 then presented the findings for each research question whilst simultaneously explaining the limitations of the approaches used in this project.

# Chapter 2

# Study Catchment Context

## 2.1 General Context

It was explained in Chapter 1 that this project would focus upon the changing role of snowmelt hydrology in an upland UK catchment. Therefore it was important to select a study catchment that displayed a clear snowmelt signal during the winter. However, it was also important to select a catchment that was suitable for the application of a hydrological model as this would be used to assess the changes both in snowmelt hydrology and the winter flow regime. The Dacre Beck catchment, Cumbria, UK, was selected as the study site for this project. This chapter firstly describes the characteristics of the catchment that affect snow accumulation, its subsequent melt and its impact upon the winter flow regime (sections 2.1 to 2.4). Then it outlines the hydrological characteristics of the site (land use and management, soils, geology and channel network (see section 2.5)) which make it an ideal location for the application of a hydrological model.

The Dacre Beck is situated in the north-west of England in the Cumbrian Lake District national park (**Figure 2.1**). It is situated 8km south-west of Penrith and 16km east of Keswick, the A66 which bisects it east-west providing direct access to both settlements. The catchment covers 36 $km^2$ upstream of the village of Dacre (**Figure 2.1**) and is a sub-catchment of the river Eden which exits into the Solway Firth 10 km north-west of Carlisle. The region in which it is located receives between 10 to 20 days more snowfall per winter season than the majority of the UK (Chapter 1 **Figure 1.2**(**a**), UK Met Office). This greater initial snow accumulation therefore would be expected to enhance the role of snowmelt hydrology in the catchment making changes easier to detect.

## 2.2 Elevation

Dacre Beck has an elevation range of 371 m, the lowest elevation is 163 m near the outlet at Dacre (**Figure 2.1**) and the highest is 534 m at the summit of Great Mell Fell (**Figure 2.2**). The relief of the catchment is relatively shallow near the outlet and rose gently towards the north-west but is much steeper in the south-west corner due to within-catchment geological variations (**Figure 2.10**).

Higher altitudes are be cooler than the rest of catchment due to the adiabatic temperature lapse rate (Chapter 1 section 1.1) meaning more snow is likely to accumulate here. The steeper relief is likely to decrease the catchment's response time from receiving rainfall to it reaching the channel network. Typically, steeper gradients mean shallower overlying soil

profiles which reach saturation quicker than deeper profiles. Hence they begin producing runoff earlier which increases catchment connectivity. In turn, this delivers larger quantities of water over a shorter period of time increasing hydrograph

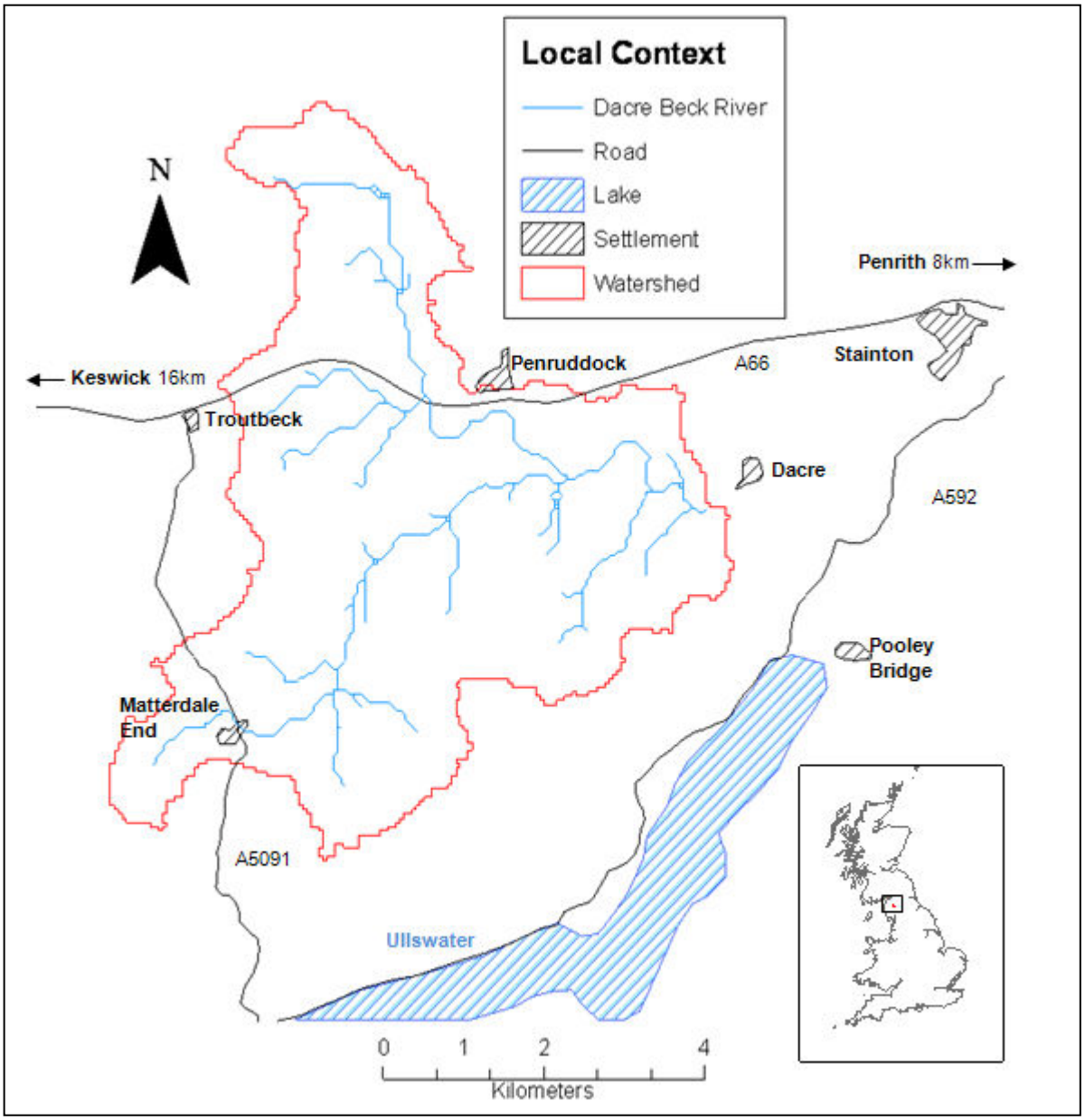


**Figure 2.1** UK (inset, from Edina Digimap (http://edina.ac.uk/digimap/), Crown Copyright for UK outline) and local context of the Dacre Beck catchment

variability. The high elevation of Dacre Beck therefore, is likely to enhance snow accumulation and its steep relief would be expected to enhance the variability of the hydrological response. Many of the slopes at the higher elevations have a north-east aspect. Being located in the northern hemisphere means these slopes are shaded from a large quantity of the solar radiation energy flux. Consequently snowpacks on these slopes

melt more slowly which may be important in the supplementation of low flows (Dunn *et al.,* 2001).

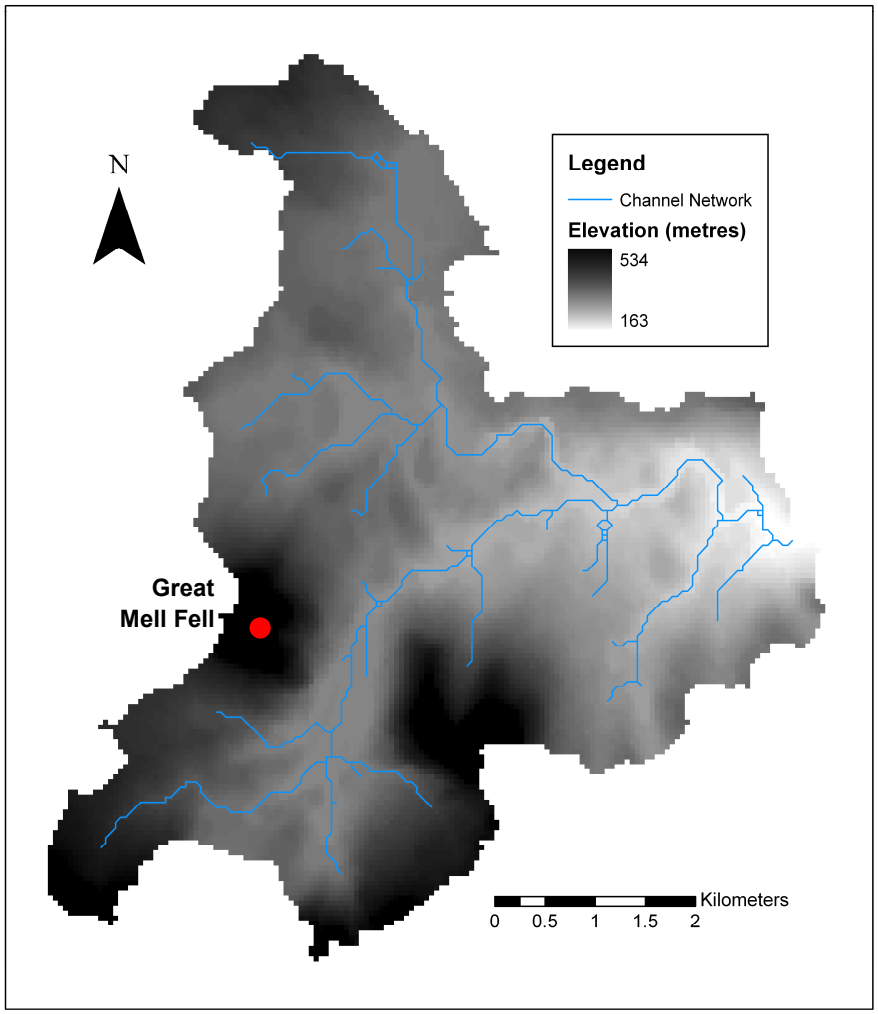


**Figure 2.2** Dacre Beck elevation and channel network (blue line). Data from Edina Digimap (http://edina.ac.uk/digimap/) and resampled to the 50 m resolution at which the hydrological model was applied

## 2.3 Climate

The catchment annual average temperature over the period 1971-2000 is 8.3°C and the average winter (December to Febraury) temperature over the same period is 3.5°C, with January being the coldest month (data from the Newton Rigg gauge 8 km north-east of the site at 169 m elevation). Within the north-west England region the catchment is colder than areas at lower altitudes or nearer the coast (annual average temperature between 9 to 10°C). It is however, warmer than areas at greater elevation e.g. central Lake District (annual average temperature between 3 to 6.5°C).

During some winters the mean winter temperature can drop much closer to 0°C. For example during the 2009/2010 winter the mean temperature was 0.9°C. Furthermore, the application of the temperature lapse rate (Chapter 1 section 1.1) showed that mean winter temperature over 1971-2000 at the summit of Great Mell Fell was 0.4°C and was -2.2°C for the 2009/2010 winter. Therefore snow is likely to feature regularly at the higher altitudes of the catchment and throughout all elevations during cold periods.

Annually the catchment receives an average of 1074 mm of precipitation (data from the Hutton Green Close Farm gauge within the catchment at 169 m elevation covering the period from 2000 to present), 30% of this falls during the winter (December to February). Most winter precipitation comes from frontal air masses coming off the Atlantic from the south-west. These deliver precipitation at a constant rate and often in sufficient quantities to bring soil conditions close to saturation. If a frontal system is immediately followed by another one which delivers its precipitation on the already saturated catchment then large quantities of surface runoff can be produced. In extreme cases this leads to flooding such as the November 2009 floods at Cockermouth. In this example, two large frontal systems reached the study catchment in quick succession, the latter of them delivered 314 mm of rainfall in 24 hours. This resulted in a peak discharge of 26 $m^3s^{-1}$ on the 19$^{th}$ November recorded at the Dacre Bridge gauging station (section 2.4).

Since most winter precipitation in Dacre Beck falls in frontal systems it is expected that the role of snowpacks in dampening hydrograph variability will be heightened. In milder years, for example, more precipitation will fall as rain which will then be delivered to the catchment outlet over a shorter period of time in greater quantities (section 1.4). Hence it is possible that in the years when the snowpack accumulation was lower than average the risk of downstream peak flows may have been heightened, this possibility is explored in the next section.

Dacre Beck received an annual average between 30 to 45 days of snow falling over the 1961-1990 period (UK Met Office) which increased by 5 days for every 100 m increase in elevation. Therefore, by applying this altitudinal increase to the altitude of the Hutton Green Close Farm rain gauge (169 m), it was found that the summit of Great Mell Fell should have received an annual average of between 47 to 62 days of snow falling. Of this annual total between 30% to 55% of the snowfall days were observed to occur during the

winter period (UK Met Office). Once snow had fallen UK Meteorological Office observations found that it lay on the ground in Dacre Beck for an annual average of between 30 to 50 days and a winter average between 20 to 30 days.

## 2.4 Hydro-Climatology

Observed measurements of catchment outlet discharge were available at a daily resolution from the Dacre Bridge gauge (National River Flow Authority ref. 76811, **Figure 2.3**) from the 22nd August 2000 to the 22nd April 2010. This data was collected and supplied by the Environment Agency. The Dacre Bridge gauging station is an open channel site which obtains discharge from a rating curve which converts measurements of river stage to discharge. Measurements of high flows can be distorted by flow diversion when a river goes out of bank. However at this gauge there is a bridge just downstream of the station which acts as a topographical funnelling feature ensuring that none of the flow is diverted.

**Figure 2.3** Dacre Bridge gauging station.

The daily discharge hydrograph across the time series (**Figure 2.4**) showed distinct seasonality where flows intensified in the winter and declined in the summer in response to precipitation trends. For example the 2006/2007 winter saw many consecutive days of precipitation exceeding 10 mm which brought the catchment to saturation (as described in section 2.3). On December 3rd 2006 36 mm of precipitation fell on the already saturated catchment so most of this was converted into surface runoff. This quickly routed

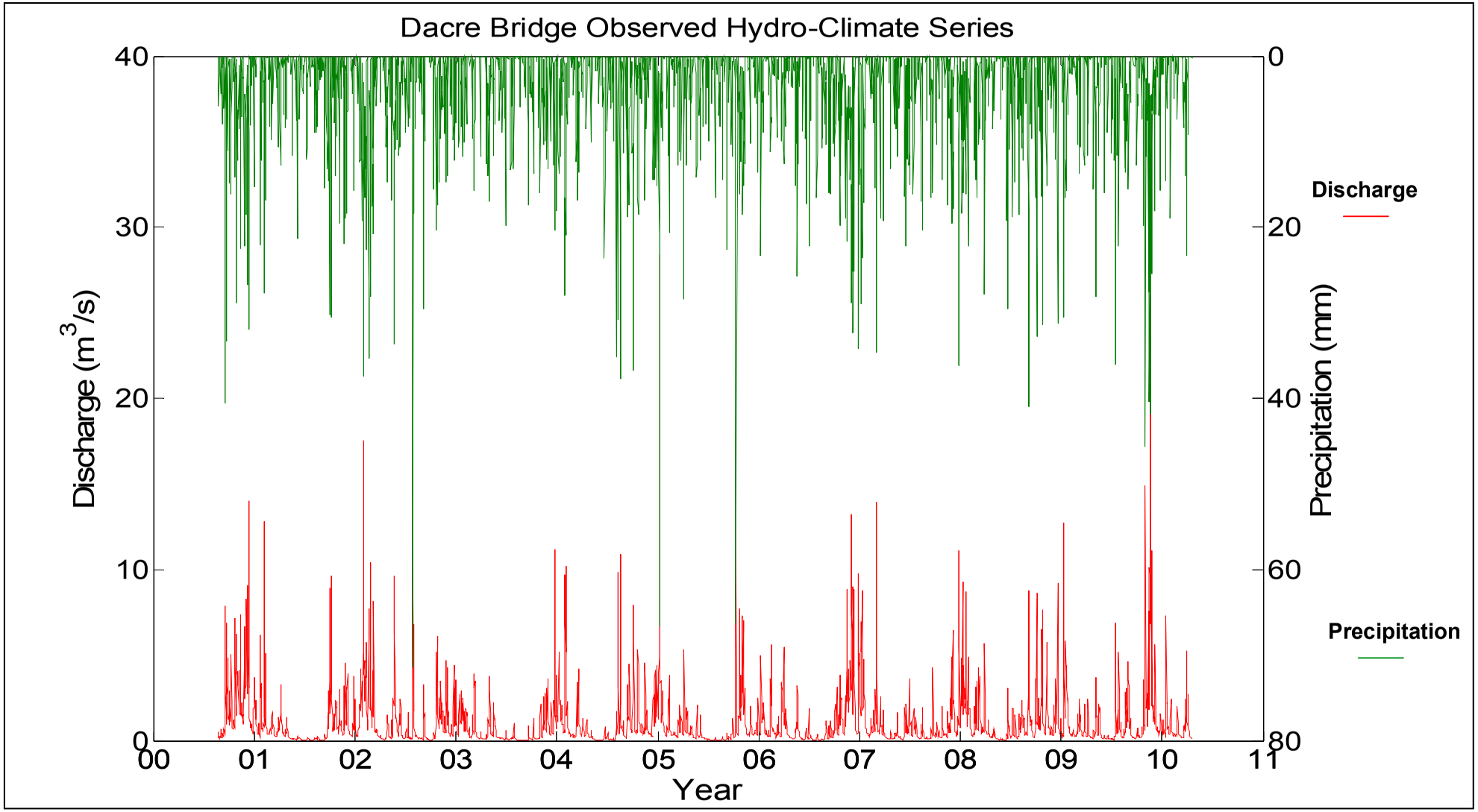


**Figure 2.4** Observed daily discharge from the gauge at Dacre Bridge (red line) and observed daily precipitation from the gauge at Hutton Green Close Farm (green line).

to the catchment outlet thus producing a peak discharge of 15$m^3s^{-1}$; the second largest flow of the season.

The observed discharge series (**Figure 2.4**) showed that winter flows intensified, this also meant that winter flows were more variable as there was a greater difference between the high and low flows. This variability can be demonstrated by comparing the flows from exceedence probabilities obtained from a flow duration curve that represents high and low flows. The flow duration curve shows the exceedence probability for a given flow in the observed discharge series, low flows for example have a high exceedence probability. This probability for each flow measurement can be calculated by ranking all of the discharge values in descending order, assigning each a rank to each (1 for the largest), $M_r$ before calculating the exceedence probability $P_o$:

$$P_o = 100 * \left(\frac{M_r}{n+1}\right) \quad \text{(Eq. 2.1)}$$

Where *n* is the number of records.

The exceedence probabilities that represent high and low flows are 5% (Q5) and 95% (Q95) respectively. Therefore the variability of winter flows were assessed relative to the variability of summer flows by finding the Q5 and Q95 flows for each season. The high flows were 5.6 $m^3s^{-1}$ for winter and 1.6 $m^3s^{-1}$ for summer whilst the low flows were 0.3$m^3s^{-1}$ and 0.03 $m^3s^{-1}$ for winter and summer respectively. The difference between the high and low flows were greatest for the winter season thus showing that observed flows were most variable during this season.

As was discussed in the first chapter (section 1.4), the high and low flows during the winter should be impacted by snowmelt (SEPA, 2008). Therefore comparing these two percentiles for six winter seasons was expected to demonstrate the impact of snowmelt hydrology upon the observed winter flow regime. It was expected that for seasons which featured a large amount of snowfall the Q5 would be smaller and the Q95 would be greater than seasons which did not have as much snow.

The results of this analysis (**Table 2.1**) appeared to affirm the expectation for the Q5. The 2006/2007 season had the least amount of snowfall and the greatest Q5 whilst the

2008/2009 season had the greatest amount of snowfall and a lower Q5. However the latter's Q5 value was not the lowest when compared to other seasons as was expected. When the 2008/2009 season was analysed in more detail it was found that high rainfall events had occurred throughout the season which resulted in high outlet discharges. For example 35.5 mm of rainfall fell on January 12th 2009 which led to a high discharge at the outlet (10.1 $m^3s^{-1}$). Consequently the Q5 from this season was higher than other seasons that experienced fewer high rainfall events relative to the amount of snowfall.

A link between snow fall amount and Q95 was however, much harder to distinguish since the difference between each Q95 value was much smaller. The 2006/2007 season had the smallest value however the value for the 2008/2009 season was only 0.04 $m^3s^{-1}$ greater. The latter season had the largest total snow fall so it was expected that the Q95 value would have been one of the highest. Further analysis found however that towards the end of the season there was a prolonged period devoid of both a snowpack and precipitation. Therefore there was a reduction in the amount of water being routed to the outlet which led to a decline in the river discharge. Consequently, like Q5, trends in Q95 were found to be affected by other factors in addition to snowmelt hydrology.

| Season | Total Precipitation (mm) | Mean Temperature (°C) | Total Snowfall (mm) | Q5 ($m^3s^{-1}$) | Q95 ($m^3s^{-1}$) |
|---|---|---|---|---|---|
| **2003/2004** | 302.7 | 4.1 | 32.3 | 3.65 | 0.21 |
| **2004/2005** | 298.3 | 4.8 | 24.6 | 3.87 | 0.27 |
| **2005/2006** | 148.0 | 3.3 | 11.0 | 3.96 | 0.23 |
| **2006/2007** | 520.8 | 4.9 | 5.6 | 7.78 | 0.14 |
| **2007/2008** | 439.9 | 4.5 | 20.0 | 4.82 | 0.25 |
| **2008/2009** | 261.2 | 2.8 | 49.1 | 4.17 | 0.18 |

**Table 2.1** Dacre Beck hydro-climatic summary over six winter seasons (December to February) within the discharge hydrograph series

A snowmelt signal therefore could be detected in the hydro-climatic summary of the observed winter flow regime (**Table 2.1**) however its clarity was not as great as was

conceptually expected. Instead, as explained above, the signal's clarity was influenced by rainfall events which occur during the season. Therefore the snowmelt hydrology of the Dacre Beck was dominated by a rainfall-snowmelt signal where processes from both combined to create a hydrograph which was not as variable as a rainfall-only signal and not as dampened as a snowmelt-only signal.

## 2.5 Catchment Hydrology

The previous sections in this chapter showed that the winter flow regime of Dacre Beck is currently impacted by snowmelt hydrology making it an ideal study catchment for this project. The next stage in confirming the catchment's suitability was to then assess the factors which affected its general hydrology. These factors included topography, land use and management, soils, geology and the stream network. Each of these factors affected the role of physical factors in transferring water from the landscape into the channel network before exiting at the outlet. Consequently they could affect how the catchment could be represented by a hydrological model. Therefore the subsequent sections assessed each factor and whether its role in Dacre Beck meant hydrological modelling of the catchment was appropriate.

### 2.5.1 Topography

Topography affected how water moved downhill under gravity towards the channel network. For example, where the slope was steeper it was expected that water would have rapidly moved towards areas of gentler relief e.g. the valley floor. Water would have then collected in these gentler reliefs and when a threshold of water accumulation was exceeded a channel network would be initiated. The topographic wetness index, *TWI* could be used to show the spatial distribution of these processes of topographically induced water accumulation. It showed the tendency of water to accumulate at any point in the catchment (Beven and Kirkby, 1979; Quinn *et al.,* 1991) and could be calculated by:

$$TWI = \ln\left(\frac{\alpha}{\tan\beta}\right) \quad \text{(Eq. 2.2)}$$

Where *α* was the cumulative upslope area draining through a point per unit contour length and *tanβ* was the slope angle at that point (Quinn *et al.,* 1991). In order to calculate the former this project conducted an analysis of flow pathways within the catchment was undertaken using the Multiple Flow Direction Algorithm (Freeman, 1991; Quinn *et al.,* 1991). Conceptually, the algorithm calculated the upslope area for each point in the

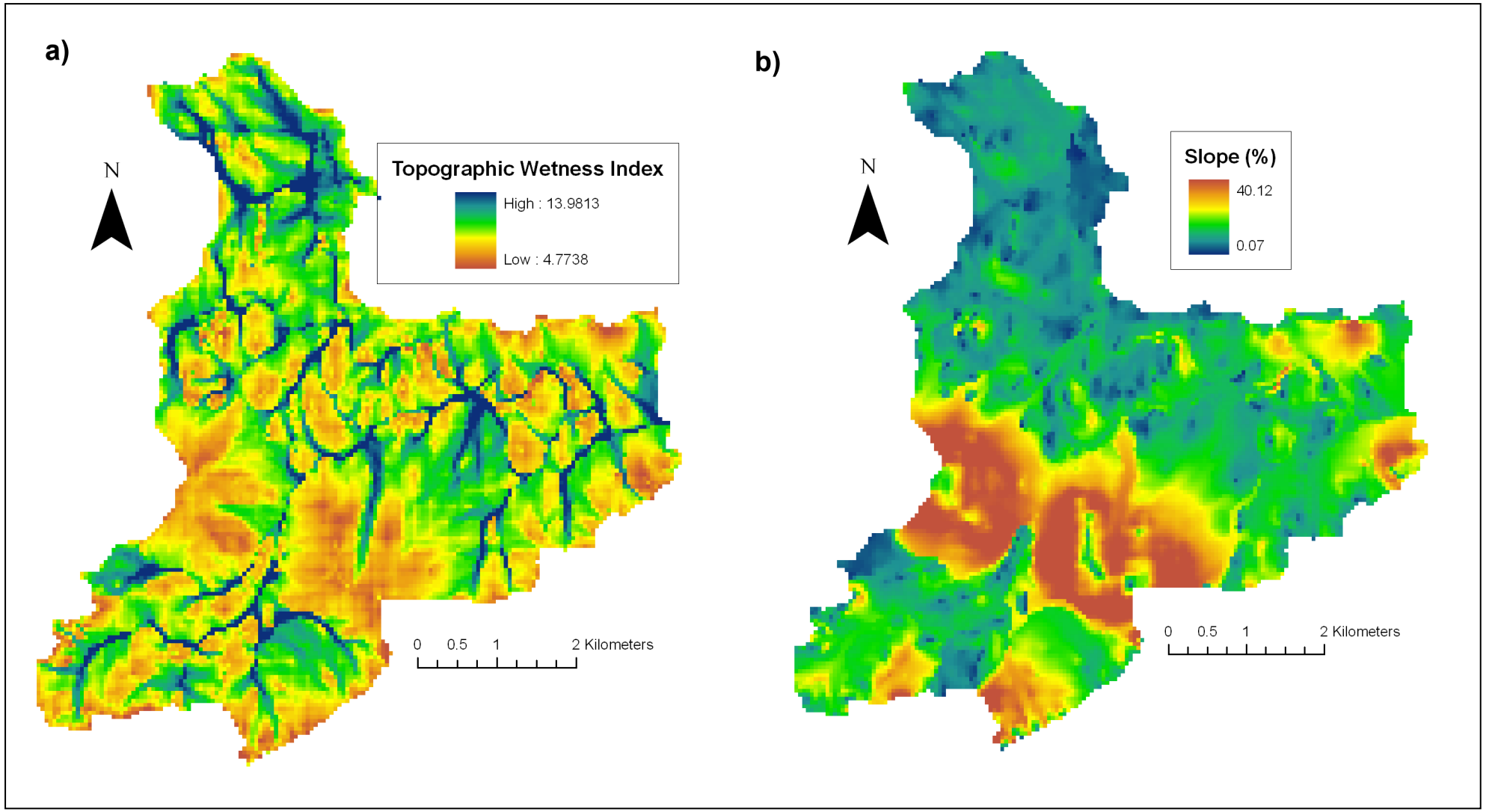


**Figure 2.5 a)** Dacre Beck Topographic Wetness Index and **b)** slope calculated using the technique described in section 2.5.1, 10 m DEM elevation data was obtained from Edina Digimap (http://edina.ac.uk/digimap/) and re-sampled to 50 m.

catchment and then distributed this amongst all of the neighbouring cells of a lower elevation. The fraction of upslope area assigned to each downslope neighbour, $\Delta A_i$ was a function of the downhill gradient where steeper gradients received a greater fraction:

$$\Delta A_i = \frac{A_u(\tan \beta_i L_i)}{\sum(\tan \beta_j L_j)} \quad \text{(Eq. 2.3)}$$

Where $A_u$ was the total upslope area, $tan\beta_i$ and $L_i$ were the slope angle and contour length of the *ith* neighbour and $\sum tan\beta_j L_j$ was the sum of the slope angle and contour length for all downslope neighbours. This allowed the upslope area of one point in the catchment to be distributed amongst all of its neighbours which lay below it.

This project initiated a channel network when the upslope area for a cell exceeded a threshold value which was proportional to the amount of water that accumulated in a cell. Beyond this threshold, flow pathways were calculated using the D8 Linear Flow Algorithm (O'Callaghan and Mark, 1984) which assumed that flow was only routed to the lowest neighbouring cell. The value of the linear flow threshold was selected by running the flow pathway algorithms with a range of threshold values. Each run produced an output of cells for which the D8 algorithm was applied which can be interpreted as a channel network. For the run whose pattern of cells most closely represented the observed channel network (**Figure 2.1**), the linear flow threshold value associated with it was selected to be used in the final calculation of the distributed $\alpha$ values.

The results above were then combined with distributed slope data (**Figure 2.5** (**b**)) which was calculated from a DEM of the catchment to calculate the *TWI* (**Figure 2.5** (**a**)). It showed that water accumulated in the valley floors beneath the slopes. For example at Great- and Little- Mell Fell (**Figure 2.2**) the steep slopes meant very little water could accumulate there. Instead the water moved downslope to the valley floor where the gentler slope meant it could accumulate due to the reduction in gravitationally induced runoff velocity. The close proximity of the steep slopes to the valley floor also had implications for runoff generation and hillslope-channel connectivity as was discussed in the subsequent channel network section.

### 2.5.2 Land Cover

Land cover affects the amount of precipitation that was intercepted and then lost through evapotranspiration. Additionally the depth and structure of the roots could have affected how much water could infiltrate into the soil matrix and hence the runoff production potential. Modification of land cover by anthropogenic management practices can alter the natural land cover hydrology. Naturally the Dacre Beck was entirely forested but clearances in the middle ages for agriculture left a lasting legacy upon the catchment. Using the National Land Use Database (NLUD, 2006) land cover classification scheme it was found that three land cover types dominated the catchment: improved grassland, coniferous forest and unimproved grass/moor (**Figure 2.6**). The properties which affect evapo-transpiration and infiltration-surface runoff partitioning for each are outlined below and summarised in **Table 2.2**.

Improved grassland occurs throughout the majority of the catchment especially at lower altitudes and on the gentler slopes. It reflects the area where the unimproved grass/moor observed elsewhere in the catchment has been modified in order to be suitable for hill-sheep farming and silage production. Vegetation in this land cover consists mostly of short, meadow grass (**Figure 2.6** (**b**)) which is kept at a maximum height between 15 cm to 20 cm through a combination of grazing and harvesting. Short grass typically loses less water through transpiration than other land covers due to its lower stomatal conductance which is directly proportional to the leaf area index which in turn is proportional to vegetation height (Shuttleworth, 1993). Improved grass cover also lost less water through evaporation than other land covers because it had a greater albedo (~0.25 (Markvart and Castaner, 2003)). Consequently it absorbs less incident solar radiation so less energy is available to evaporate the intercepted precipitation on the canopy. As a result this land cover loses less water through evapotranspiration so more is available to be partitioned between infiltration and overland flow. According to the United States Department of Agriculture Soil Conservation Service (SCS, 1986) this land cover will produce a moderate amount of overland flow. Their suggested curve number (which ranged from 30 to 100 where lower values mean a lower propensity to produce surface runoff) for pasture grassland in ‘good’ condition for hydrologic soil groups B and C (whose hydrologic properties were most similar to the soils which underlay this land cover in Dacre Beck as was described later in this section) lay between 60 to 70. This means that

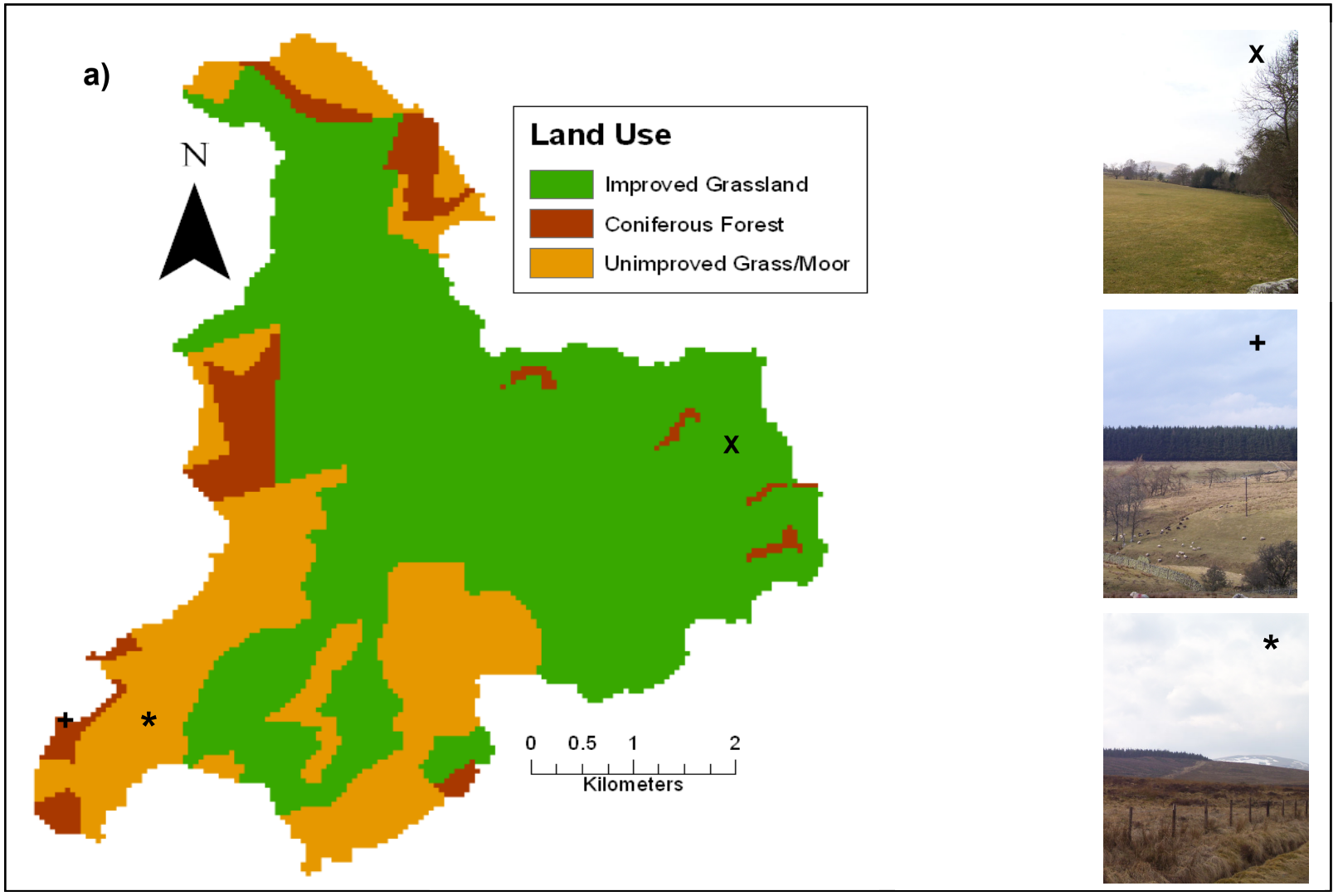


**Figure 2.6 a)** Land cover classification after National Land Use Database (NLUD 2006) for the Dacre Beck. **b)** to **d)** show examples of improved grassland, coniferous forest and unimproved grass/moor respectively as observed in the catchment. The symbols in the top-right corner of **b)** to **d)** correspond to the symbols in **a)** showing where in the catchment each photograph was taken

improved grass will produce a slightly greater amount of overland flow than infiltration which was mostly explained by soil compaction by livestock.

Small pockets of managed coniferous forest plantations are present in the catchment, for example Greystoke Moor plantation near Penruddock. The tree canopy in these plantations has a much greater leaf area index than the other two land covers due to the greater canopy height. Furthermore it has a much reduced albedo value of approximately 0.09 (Barry and Chorley, 1992) thus this land cover can intercept, and hence evapotranspire, much greater amounts of precipitation. The denser canopy is also able to intercept large amounts of snowfall (Chapter 1 section 1.1) and withhold it from impacting upon the hydrological processes below. The winter hydrology of this land cover therefore, can have had a much diminished snowmelt signal. The initial management practices in forestry plantations can enhance the amount of surface runoff and sediment that is delivered to the channel network. However the plantations in Dacre Beck are well matured enabling the development of an extensive root network which creates macropores that enhance infiltration. Furthermore the extensive nature of the root network means it takes up more water than other land covers. Consequently more water is able to infiltrate over the same period of time. The SCS curve number for this land cover is approximately 55 although the original report did not explicitly deal with coniferous forest. However, this land cover only accounts for only 5.3% of the catchment area. As such, it is likely that the effects described above will be negligible upon the hydrology of the entire catchment.

Unimproved grass/moor occurs mostly on the steeper slopes and hill summits of the catchment where the soils are too waterlogged or thin to sustain improved grass. Vegetation type ranges from long grass to bracken, both of which have a greater canopy height than improved grass. Hence the leaf area index is greater and so are evapotranspirative losses. The albedo value is expected to lie in between the values for the other two land covers at 0.15. The more extensive root networks associated with this land cover as opposed to improved grass are likely to enhance infiltration into the soil. However, the waterlogged properties of the underlying soil associated with this land cover in the catchment are likely to override this effect.

| Land Cover | Dominant Vegetation | Vegetation Height (m) | Albedo | Soil Conservation Service Curve Number |
|---|---|---|---|---|
| Improved Grassland | Grasses | 0.15 - 0.20 | 0.25 | 60 - 70 |
| Coniferous Forest | Conifer | 10 | 0.09 | 55 |
| Unimproved Grass/Moor | Coarse Grasses, Bracken | <1 | 0.15 | 60 |

**Table 2.2** Land cover properties affecting evapotranspiration and infiltration-surface runoff partitioning

### 2.5.3 Catchment Soils

The soils which underlie the land cover affect how much water can infiltrate and how quickly it can percolate away from the surface thus allowing further infiltration. For example, a profile with small infiltration capacity and a slow percolation rate only allows a small amount of surface water to enter. As a result, the majority of the water at the surface will become overland flow. Soil properties which affect this include the hydraulic conductivity (the ability of the soil to transmit water (Rawls *et al.,* 1993)), porosity (relative volume of pore spaces (Kutílek and Nielsen, 1994)) and the profile depth.

A combination of wet winter conditions and the hydraulic soil properties mean the soils in Dacre Beck (**Figure 2.7**) are seasonally waterlogged leading to saturated conditions and runoff generation. For example the Winter Hill class, which underlies most of the improved grass land cover, has a much lower hydraulic conductivity than the root layer (**Table 2.3**). Consequently water can infiltrate into the root layer and percolate relatively quickly but slows once it reaches the lower layers impeding any water that infiltrates subsequently. Conversely the soil classes at the higher altitudes are well drained. For example the Manod class found on the summits of Great- and Little- Mell Fell (**Figure 2.2**) has a much faster hydraulic conductivity but it is also much shallower reducing the amount of water that the soil can store. The underlying bedrock on these hills has a much slower

| Soil Class | Root Layer Hydraulic Conductivity ($ms^{-1}$) | Hydraulic Conductivity ($ms^{-1}$) | Hydraulic Conductivity Decay with Depth ($ms^{-1}$ $m^{-1}$) | Porosity (0:1) | Root Layer Depth (m) | Soil Depth Slopes (m) | Soil Depth Channels (m) | Soil Depth Ridges (m) |
|---|---|---|---|---|---|---|---|---|
| **Winter Hill** | $8x10^{-5}$ | $8x10^{-8}$ | -1 | 0.1 | 0.4 | 1.2 | 1.2 | 1.5 |
| **Clifton** | $1.8x10^{-6}$ | $1.8x10^{-5}$ | -1 | 0.5 | 0.1 | 0.8 | 0.8 | 1.0 |
| **Brickfield** | $1.8x10^{-7}$ | $1.8x10^{-6}$ | -1 | 0.6 | 0.2 | 0.8 | 0.8 | 1.0 |
| **Manod** | $1x10^{-5}$ | $1x10^{-4}$ | -1 | 0.6 | 0.3 | 0.5 | 0.5 | 0.6 |
| **Newbiggin** | $1x10^{-4}$ | $1x10^{-4}$ | -1 | 0.7 | 0.3 | 0.9 | 0.9 | 1.0 |
| **Malvern** | $1x10^{-4}$ | $1x10^{-4}$ | -1 | 0.7 | 0.1 | 1.0 | 1.0 | 1.2 |
| **Bangor** | $1x10^{-7}$ | $1x10^{-7}$ | -1 | 0.2 | 0.3 | 0.3 | 0.3 | 0.4 |

**Table 2.3** Hydraulic properties of the soil classes found within Dacre Beck. Data from the Soil Survey of England and Wales (Carroll *et al.,* 1979; Jarvis *et al.,*1984).

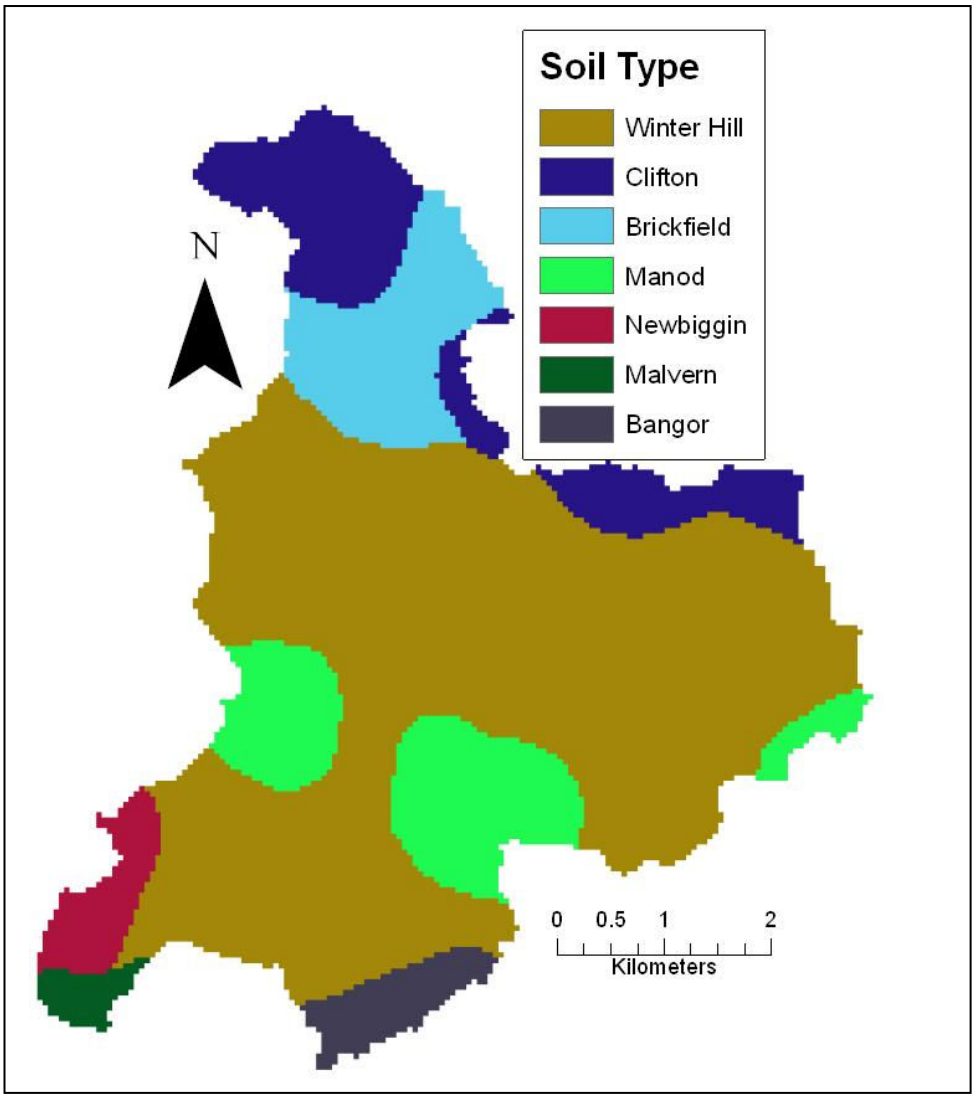


**Figure 2.7** Dacre Beck soil classification after the Soil Survey of Northern England (1976)

hydraulic conductivity so infiltrated water will accumulate at the soil-bedrock interface thus saturating the surrounding soil. More water then infiltrates into the soil and percolates down to the saturated area causing the upward migration of the saturated area. Since the soil profiles are so shallow it takes a minimal amount of time before the saturated area reaches the surface. Beyond this point, any water which reaches the soil surface will become overland flow.

### 2.5.4 Catchment Geology

The nature of the bedrock beneath the catchment affects how much water is lost to recharge. In this process soil water percolates downwards to replenish groundwater in an unconfined aquifer. Usually this water re-emerges into the channel network at an aquifer but none are present in the Dacre Beck catchment. Therefore it can be assumed that

groundwater aquifer contribution to stream flow is nil or negligible hence the amount of recharge can be assumed as a loss of water. The magnitude of recharge depends upon the porosity, hydraulic conductivity and permeability of the bedrock (Smith and Wheatcraft, 1993) which is related to whether the bedrock is a fluvial deposit, sedimentary, carbonate or igneous or metamorphic rock (Freeze and Cherry, 1979).

Basal Conglomerate covers the majority of the catchment (**Figure 2.8**) with the rest covered by volcanic terrain, a lava flow, metamorphosed rock and carboniferous limestone. The conglomerate represents a shallow marine transgression where sediment was deposited at the shoreline and then cemented together above an unconformity. The

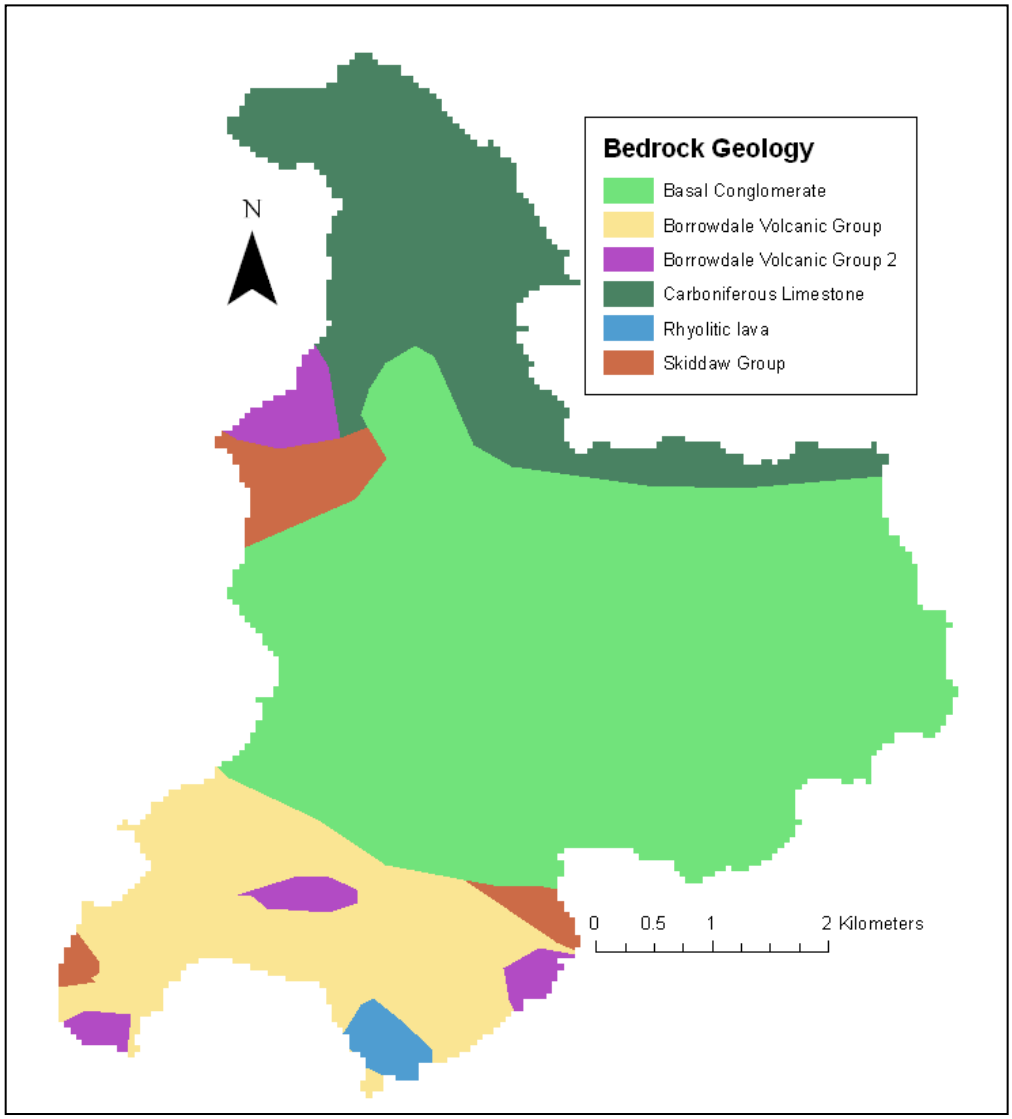


**Figure 2.8** Bedrock geology within Dacre Beck. Data from the British Geological Society, accessed through Edina Geology Digimap (http://edina.ac.uk/digimap/).

hydraulic properties of this rock type (**Table 2.4**) are very similar to that of sedimentary sandstone with porosities as low as 1% and hydraulic conductivity at a $x10^{-10}$ $ms^{-1}$ order of magnitude (Freeze and Cherry, 1979). The south-west corner of the catchment is dominated by the volcanic terrain of the Borrowdale volcanic groups formed by an Ordovician volcanic island arc. Their hydraulic properties are affected by the mode of extrusion, where permeability is greatest in the direction of basalt movement, and geologic controls on fracture development (Smith and Wheatcraft, 1993). The latter affects the formation of tuffs and agglomerates and whether or not these are welded. The porosity of a welded tuff is 15% and 30% for a non-welded tuff (Smith and Wheatcraft, 1993). These controls also affect the amount of fracturing which occur due to shear stress. Fractures can increase permeability and hydraulic conductivity since water will flow through them much faster than through the crystal lattice of the rocks. An unfractured volcanic bedrock has a hydraulic conductivity four orders of magnitude slower than fractured volcanic bedrock (Smith and Wheatcraft, 1993). The Rhyolitic lava flow may represent a volcanic eruption late in the Ordovician period which was not incorporated into Borrowdale volcanic group. Nevertheless its hydraulic properties and those of the metamorphosed sand- and silt-stones of the Skiddaw group are very similar due to the important role of shear stress fracturing in determining hydraulic conductivity and permeability. The carboniferous limestone in the north-west corner of the catchment was formed from calcite deposits in a warm tropical sea during the Carboniferous period. It has a relatively large porosity of 20% for coarse, blocky limestone (Freeze and Cherry, 1979) but its brittle nature meant it fractured easily under shear stress resulting in secondary permeability which increased the hydraulic conductivity by a few orders of magnitude.

| Bedrock Name | Porosity (%) | Hydraulic Conductivity ($ms^{-1}$) | Permeability ($m^2$) |
|---|---|---|---|
| **Basal Conglomerate** | 1:5 | $10^{-7}$:$10^{-10}$ | $10^{-14}$:$10^{-17}$ |
| **Borrowdale Volcanic Groups** | 0.1:10 | $10^{-6}$:$10^{-14}$ | $10^{-13}$:$10^{-21}$ |
| **Carboniferous Limestone** | 20:35 | $10^{-5}$:$10^{-9}$ | $10^{-21}$:$10^{-16}$ |
| **Rhyolitic Lava** | 0.1:10 | $10^{-6}$:$10^{-14}$ | $10^{-13}$:$10^{-21}$ |
| **Skiddaw Group** | 0.1:10 | $10^{-6}$:$10^{-14}$ | $10^{-13}$:$10^{-21}$ |

**Table 2.4** Bedrock hydraulic properties value ranges

The bedrock that underlies the Dacre Beck catchment drains very slowly meaning that relatively little should be lost to recharge. Instead it would be expected that water would accumulate at the soil-bedrock interface leading to saturated soil conditions.

### 2.5.5 Channel Network

The channel network affects the level of connection between water on the hill slopes and the outlet. An extensive network for example would enhance the amount of connection thus delivering greater amounts of water to the outlet in a shorter period of time. In Dacre Beck the channel network (**Figure 2.9** (**a**)) is mostly confined to the valley floors although its headwaters extend onto the hillslopes of the south- and north-west corners. The headwaters are very narrow and are fed mostly by overland flow; their course follows the path of steepest descent down to the valley floor. The extent of the headwater network varies temporally with expansion occurring during high precipitation events especially during the winter when these events are more frequent. Multiple headwater channels then converge at the valley floor forming a single channel which routes towards the outlet. At Great Mell Fell, for example, three headwater tributaries converge near Matterdale End. The resulting channel is wider and deeper and is confined to a narrow valley floor between the hills of Great- and Little- Mell Fell (**Figure 2.9** (**e**)). As the channel routes towards the outlet, following the path of steepest descent, it collects more water and becomes wider and deeper. There are two main tributaries in the catchment draining the south- and north-west corners which converge near Hutton. Beyond this point the discharge of the river increases and the channel is less confined by the topography hence it begins to meander. This flattening also allows the river to go out of bank during high discharge events as shown by the presence of deposited sediments on the river bank (**Figure 2.9** (**d**)). Since the river is able to expand laterally, its width increases with downstream distance more than depth (**Figure 2.9** (**b**)). Consequently the river depth can become very shallow during low discharge events.

The nature of the channel network within Dacre Beck impacts upon both flood risk downstream in the Eden valley and in-stream ecology. For example, on the 8$^{th}$ of January 2005 the Dacre Bridge gauge recorded its highest reading of 22 $m^3s^{-1}$. The associated storm hydrograph passed downstream and converged with the storm hydrographs of the other Eden sub-catchments which led to extensive flooding of the River Eden at Carlisle. In Dacre Beck the close proximity of steep slopes, which are often saturated during storm events, to the channel network enhances overland flow connectivity. This delivers more water to the channel network over a shorter period of time giving the catchment a flashy response to storm events. Since the channel is confined within a narrow valley it cannot go overbank during storm events hence most of the water is routed directly to the outlet in a very short period of time enhancing flood risk downstream. As mentioned above,

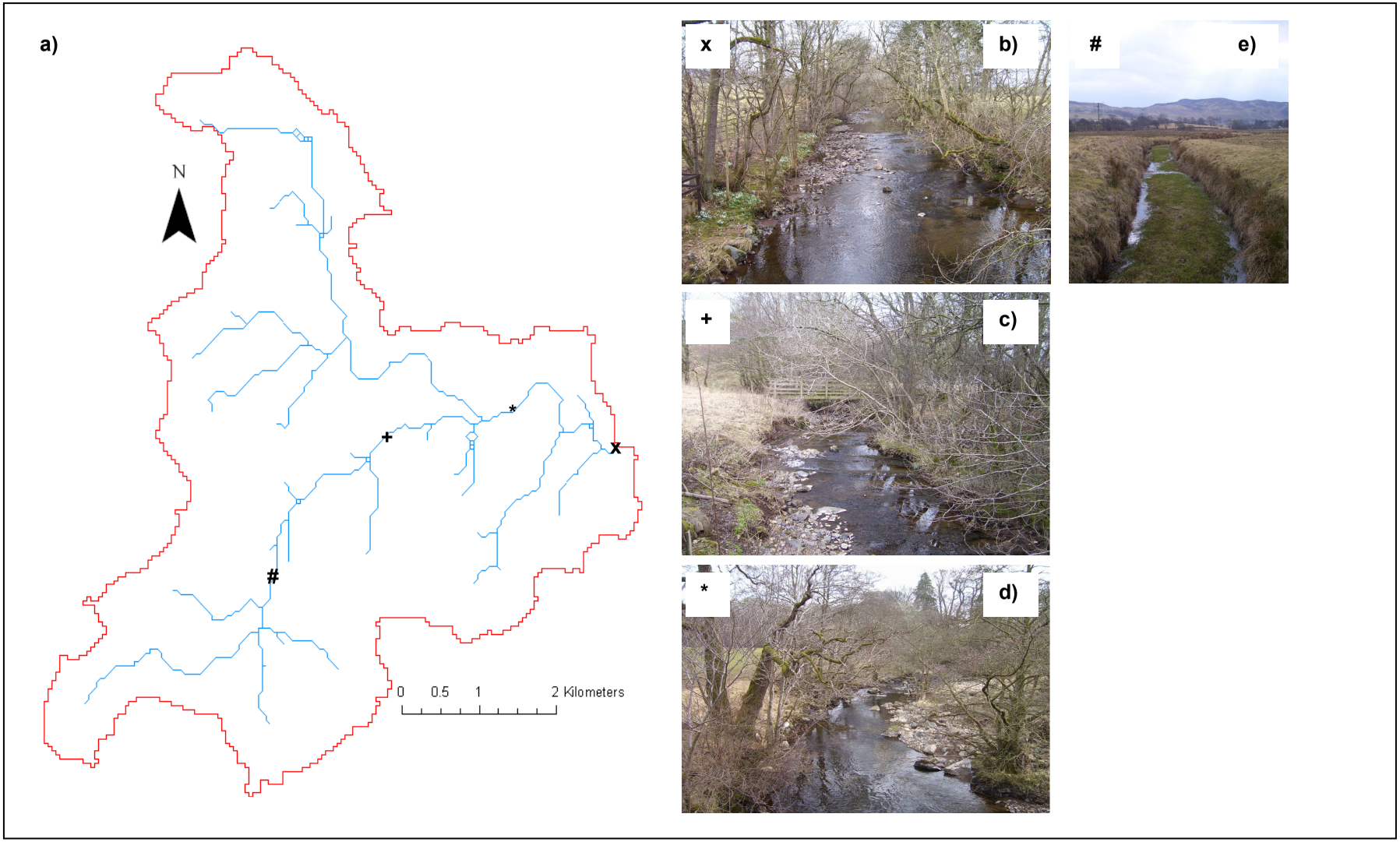


**Figure 2.9 a)** Dacre Beck channel network, **b)** to **e)** photographs along the network. The symbols show the location of each picture within the catchment.

the catchment consists of two main sub-catchments (one draining the south-west corner and the other the north-west). If the peak discharge from the storm hydrographs of each sub-catchment simultaneously reaches the confluence at Hutton the storm hydrograph at the outlet will be amplified hence increasing downstream flood risk.

### 2.5.6 Anthropogenic Management and Intervention

Human activity within the catchment is mostly centred round hill sheep farming which has led to widespread deforestation centuries ago. The improved grassland land cover provides perennial grazing land for livestock hence it is subjected to compaction and the use of fertilisers. The former decreases the hydraulic conductivity of the upper soil layer hence it produces more overland flow. If an excessive amount of fertilisers are used then the remaining nutrients will be taken up by the increased overland flow. This will then be inputted directly into the channel network impacting upon its physical habitat quality. Elsewhere afforestation has taken place in plantations such as Greystoke Moor. Initially these can increase overland flow and suspended sediment concentrations in the channel network but in mature plantations (such as those in the Dacre Beck catchment) these issues revert and the land cover actually reduces the amount of overland flow produced.

The channel network in the valley between Great- and Little- Mell Fell has been modified through straightening and the construction of a similar parallel channel. This increases the amount of water delivered to the outlet over a given period of time hence increasing downstream flood risk.

Land use management and river channel restoration both in the catchment, and across the Eden, has become a high priority for the Eden Rivers Trust (ERT) and the associated Adaptive Land Use for Flood Alleviation (ALFA) project. Both of these use the catchment as a study site to investigate new techniques in order to reduce downstream flood risk and improve in-stream ecology.

## 2.6 Ecology

In-stream ecology in the Dacre Beck and across the Eden catchment have gained increased interest since 1996 with the formation of the ERT. This organisation undertook

annual fry-density electro-fishing surveys since 2000 within Dacre Beck to establish the habitat quality for Salmon and Trout. Results in 2009 (ERT, 2010) for the former species found that fry-density was poor or altogether absent throughout the catchment. However the results from 2002-2008 found that fry density for this species was excellent. Meanwhile the 2009 results for Trout found excellent fry-density in the south-west corner showing an improvement upon the 2002-2008 results, however, they were absent from other areas of the catchment unlike the 2002-2008 surveys. The results of the surveys and their inter-annual variability may be in part due to inter-species competition but catchment and channel network factors are also likely to provide an explanation. For example, fry-density for both species was either poor or absent throughout the entire survey period in the north-west corner of the catchment. Afforestation in this area can produce high amounts of eroded sediments which are carried in the channel and cause silting of spawning gravels. The maturity of the plantations however made this scenario unlikely, instead the alkaline nature of the bedrock and hence the soils may affect all water that entered the channel hence altering the pH beyond tolerable limits for both species. The hydro-climatology of the discharge series also affected in-stream ecology as it controlled the physical habitat variables such as velocity, depth and width. Salmon and Trout redds (nests) are vulnerable to these during the winter, if low flows are prolonged then depth declines and the redds can be exposed to freezing air temperatures. A prolonged low flow period could also reduce velocity and channel width which reduces the level of in-stream dissolved oxygen (Whitehead *et al.,* 2009) and the availability of areas with suitable conditions for a particular species (Walsh and Kilsby, 2007). The attenuating role of snowmelt hydrology could therefore ensure that in-channel conditions, particularly velocity and width, remained within suitable ranges for the native species.

## 2.7 Study Catchment Overview

The Dacre Beck is an ideal study-site for a project focused upon snowmelt hydrology as it is situated in a region of high winter precipitation which combine with low winter temperatures to produce large amounts of snowfall. A snowmelt signal from these accumulated snowpacks is detectable in the present winter flow regime thus increasing the clarity of any future changes in snowmelt hydrology. High flows feature regularly in the winter hydrograph due to the thin, slowly-draining soils in combination with the wet winter climate frequently causing saturated conditions and hence a flashy hydrological response. It was shown that these winter high flows were attenuated by snowmelt hydrological processes. Low flows are also important in this catchment for in-stream ecology due to the presence of spawning species, however the role of snowmelt hydrology in attenuating

these is unclear. The bedrock consists of slowly draining rock types and there are no aquifers present in the catchment which simplifies computer model representation of the hydrological processes (explained in Chapters 4 and 6). Anthropogenic intervention in the catchment is largely through agricultural land management. There are no areas of water abstraction and urban land cover is negligible as there are no large settlements within the catchment. Consequently natural hydrological processes dominate and are only impacted in a manner that can be dealt with during the parameterisation process of the selected hydrological model (see Chapters 4 and 6). Therefore this chapter has selected a study catchment that is ideal for highlighting changes in snowmelt hydrology and their impacts upon the winter flow regime. The subsequent chapters focus upon developing a hydrological model for this catchment that represents snowmelt processes before modelling the impacts of climate change.

# Chapter 3

# Snowmelt Modelling

## 3.1 Snow Accumulation Modelling

In order to achieve both of the project's aims (Chapter 1, section 1.6) it is necessary to model the processes of snow accumulation and melt where the output from the latter can be fed into a conventional hydrological model (**Figure 3.1**). Fundamentally snow accumulation and melt modelling must achieve three operations at each timestep: extrapolate existing meteorological data to snowpack, calculate rates of snowmelt at different points and then integrate snowmelt over the current snowpack area in order to estimate the volume of new meltwater (Ferguson, 1999). This chapter will firstly review the existing methods of modelling snow accumulation (section 3.1) and melt (section 3.2) and select those that are most suitable for this project. Then it will outline the construction of a distributed snow accumulation and melt model (section 3.3) which will be applied to the Dacre Beck in subsequent chapters.

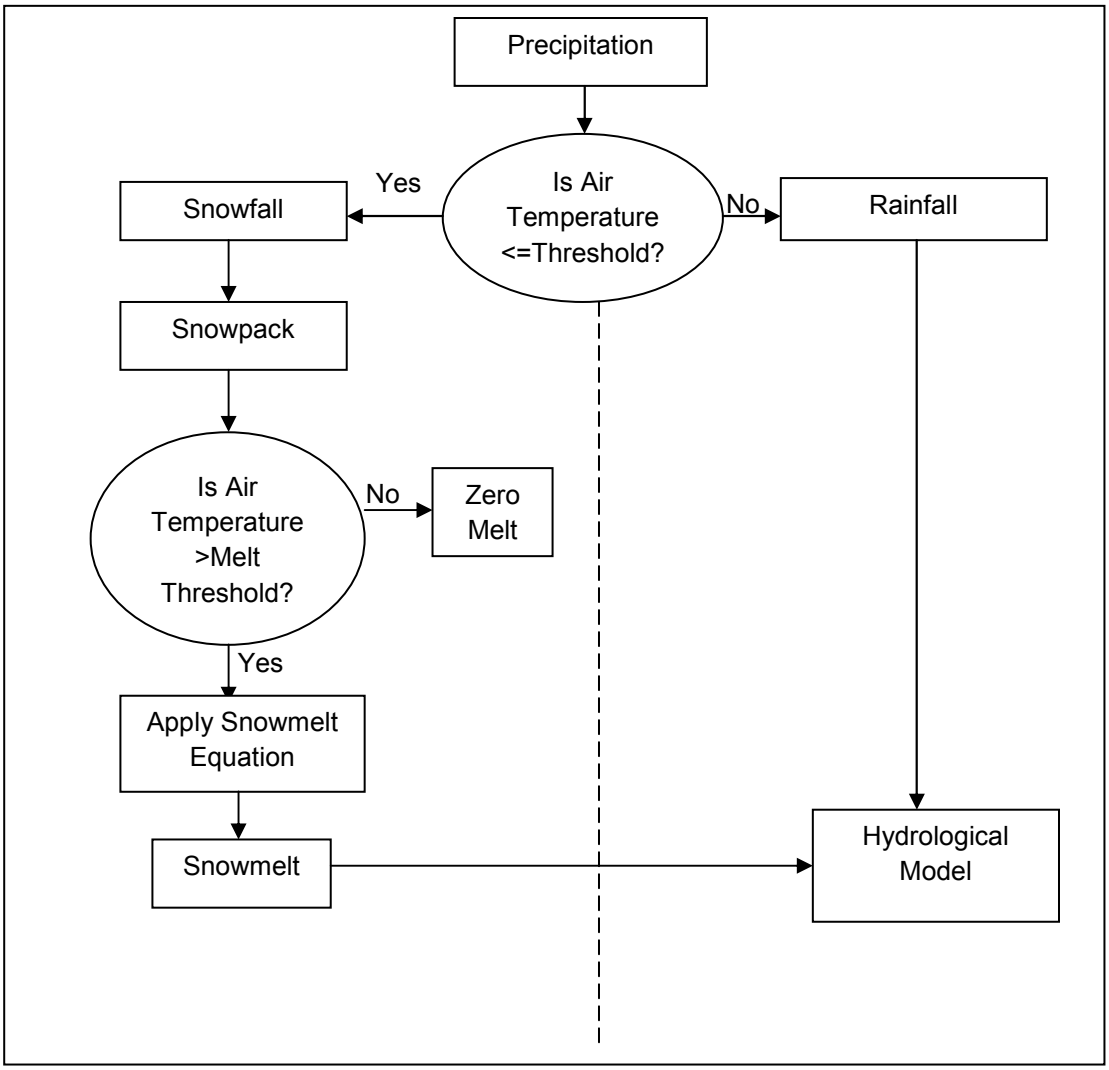


**Figure 3.1** Decision chain used to invoke snow accumulation and melt modelling processes

As explained in Chapter 1 (section 1.1) snow crystals can form in the atmosphere but in order for these to fall as snow on the ground the air temperature must not exceed the threshold temperature beyond which precipitation falls as rain (**Figure 3.1**). The value of this threshold temperature is not necessarily the same as the threshold melt temperature applied to the snowpack as it can remain frozen up to $5^0$C due to evaporative cooling (Ferguson, 1999). Typically the value of threshold precipitation temperature is around $0^0$C with some studies putting it at $0.01^0$C (the triple point of water) (Lòpez-Moreno *et al.,* 2009). For simplicity, this project will assume that the threshold precipitation temperature value is $0^0$C. Therefore the snow accumulation model in this project will assume that precipitation will fall as snow if the temperature is equal to or less than $0^0$C.

It was also mentioned in Chapter 1 that processes of interception and wind redistribution affect the accumulation of snow within a catchment. Interception, $I$ (kg m$^{-2}$) can be modelled as a function of snowfall and vegetation canopy properties (Pomeroy *et al.,* 1998):

$$I = c(I^* - I_o)\left(1 - e^{C_c \frac{P_i}{I^*}}\right) \quad \text{(Eq 3.1)}$$

Where $c$ = snow unloading coefficient (~0.7 for hourly time steps), $I_o$ = initial snow load (kg m$^{-2}$), $P_i$ = exponential function of snowfall (kg m$^{-2}$ unit time$^{-1}$), $C_c$ = canopy density (proportional coverage, and $I^*$ = difference of maximum snow load:

$$I^* = Sp\ LAI\ \left(0.27 + \frac{46}{\rho s}\right) \quad \text{(Eq 3.2)}$$

Where $Sp$ = tree species coefficient (kg m$^{-2}$) [~6.6 for pine, ~5.9 for spruce], $LAI$ = leaf area index (m$^2$ m$^{-2}$), and $\rho s$ = fresh snow density (kg m$^{-3}$).

However the above equations are only applicable to forested parts of a catchment. Since only 5.3% of the Dacre Beck catchment is forested (Chapter 2, section 2.5.2) it would be expected that interception plays a minimal role in the catchment's snowmelt hydrology. Hence it can omitted from processes which are included in this project's distributed snow accumulation and melt model.

Redistribution by wind saltation can be modelled as in MacDonald *et al.* ( 2009):

$$F_{salt} = \frac{c_i\, e\, \rho\, u_t^*}{g}(u^{*2} - u_n^{*2} - u_t^{*2}) \quad \text{(Eq. 3.3)}$$

Where *ci* = ratio of saltation velocity to friction velocity (~2.8), *e* = efficiency of saltation (1/4.2 u*), *ρ* = atmospheric density, *g* = gravitational acceleration (9.81 $ms^{-2}$), *u** = atmospheric friction velocity and $u^*_n$ and $u^*_t$ are portions of *u** applied to non-erodible roughness elements such as vegetation.

Redistribution by wind suspension can also be modelled (MacDonald *et al.,* 2009):

$$F_{susp} = \frac{u^*}{k_v}\int_{h^*}^{z_b} \eta_m(z) ln\left(\frac{z}{z_o}\right) dz \quad \text{(Eq. 3.4)}$$

Where $k_v$ = von Karmen's constant (0.41), $z_b$ = affected by the time available for the vertical diffusion of snow particles from *h** calculated from turbulent diffusion theory and logarithmic wind profile, $\eta_m$ = mass concentration of blowing snow at height *z* and *zo* = aerodynamic roughness height.

Many of the terms in *Eq. 3.3* and *Eq. 3.4* however, are calculated from vegetation data such as stalk density which is not available in Dacre Beck so it is not possible to apply these equations in this study. However the geographical and topographical context of the catchment means it is reasonable to expect that wind redistribution of snow is minimal. It is located in the north-west corner of the Lake District and its slopes are mostly oriented in a west to north-west direction hence it is sheltered from the prevailing south-westerly winds of the region. Furthermore its steep topography means it is much more sheltered than the topography of plains catchments where wind redistribution is observed to be significant (Gray and Prowse, 1993).

### 3.2 Snowmelt Modelling

Once a snowpack accumulates it can begin to receive energy from the surrounding physical fluxes, outlined in Chapter 1 (section 1.2), and eventually produce melt water runoff. There are two types of snowmelt model in common use: Energy Balance Models (EBMs) and temperature-index models (Hock, 2005). The former approach is physically-based as it accounts for the underlying physics of snowpack energy fluxes whereas

temperature-index modelling is empirical since it assumes a linear relationship between ablation and positive air temperature (Hock, 1999). The following sub-sections (3.2.1 and 3.2.2) review both approaches giving examples of models from each in order to assess their suitability for this project. Suitability will be judged by assessing models from each approach according to their process representation and data requirements. As shown above, some processes such as interception are unimportant in the Dacre Beck, so if a model accounts for additional, and otherwise unnecessary, processes it will only serve to add to output uncertainty (see Chapter 6) rather than data quality. The meteorological observations available to drive a snow melt model in Dacre Beck are: minimum and maximum daily air temperature and daily precipitation. Therefore, if a snow melt model's data requirements exceed this, it is highly likely that it will be non-applicable in the Dacre Beck. A synthesis of both approaches will be given in section 3.3 allowing a suitable snowmelt modelling approach to be selected.

### 3.2.1 Energy Balance Modelling

Many different EBMs are in existence (a review of some EBMs is given in **Table 3.1**) with a wide range of complexity. The SnowMIP investigation (Etchevers *et a.,* 2002; 2004) compared 26 and 23 EBMs respectively and found four bands of complexity; very simple (1 layer and simple energy budget), simple (1 layer and detailed energy budget), complex (2 or more snow layers) and very complex (include internal processes of snowpack).

Complex and very complex EBMs account for multiple layers within the snowpack in order to account for non-linear heat exchange close to the surface and internal energy transfer processes. An example of a complex EBM is given in Koivasulo (*et al.,* 2001) who use the SNTHERM.89 and UEB models to represent a 2 layer snowpack. This added complexity was found to improve the results of snow heat balance and liquid water content in comparison to simpler models, but only had minor effects for calculated bulk SWE and snow melt (Koivasulo *et al.,* 2001). Since this project only requires modelling of snow melt production it unnecessary for it to use a model from these classes of EBM complexity as results of a similar quality can be obtained from much simpler models.

Simpler EBMs treat the snowpack as a single layer such as that outlined in Lòpez-Moreno (*et al.,* 2009). In this model the energy budget considers the energy change associated with the melting of frozen soil moisture and snow, the snowpack is treated as an evolving

one-layer pack characterised by; temperature, mass and density. At each time step, radiative and turbulent fluxes are calculated followed by heat storage in the snowpack allowing the calculation of snowmelt. Atmospheric data including; screen air temperature, dew point temperature, anemometer-level wind magnitude, precipitation, surface pressure and incident solar radiation are inputted at an hourly resolution (data can be downscaled from an RCM using a cosine function, Lòpez-Moreno *et al.,* 2009). The results of SnowMIP (Etchevers *et al.,* 2004) show that models of this relative simplicity can adequately represent snow melt production over a range of snow cover climates. However it is not possible to obtain all the data required to drive the model as data downscaled from an RCM can only be used after the model has been calibrated using observed data.

An attempt was made by Walter (*et al.,* 2005) to build an EBM which has minimal data requirements. The model also treats the snowpack as a single layer which is subject to the same radiative and turbulent fluxes. Approximations are used instead of input data to calculate the magnitude of each energy flux thus reducing the data requirements to daily minimum and maximum air temperature and daily precipitation. However this introduces uncertainty into model results as the approximations mean the precise magnitude of each flux cannot be determined. For example in calculating the sensible heat exchange instead of using wind speed measurements from the site a constant windspeed equal to the geometric mean of the nearest measurements is used. Additionally, in calculating the heat form convective vapour exchange the vapour density of air is assumed to be equal to the saturation vapour density at the minimum daily air temperature. Whilst these assumptions may be physically reasonable they may not suffice as precise replacements. Consequently this introduces uncertainty into the results which reduces their quality to a level that may be achievable through even simpler temperature-index modelling.

| Reference | Model Type/ Name | Description | Data Input | Complexity |
|---|---|---|---|---|
| Zeinivand and De Smedt, 2009 | EBM | Calculates energy balance of snowpack before converting to snowmelt | Minimum, maximum and mean daily air temperature, windspeed | 2 |

**Table 3.1** Summary of the EBMs consulted reviewed by this project. Complexity ranges from 1-4. 1 is very simple, 4 being very complex (see Etchevers *et al.* 2004 for a full definition). A comparison of more EBMs can be found in *Table 2* Etchevers *et al.* 2004.

| | | | | |
|---|---|---|---|---|
| Jost *et al.,* 2009 | EBM | Looks at role of forest canopy in snowmelt, 2 layer canopy model | Air temperature, wind speed, vapour pressure, precipitation, longwave and shortwave radiation | 3 |
| Lòpez-Moreno *et al.,* 2009 | EBM | Snow modelled as evolving 1-layer pack characterised by temperature, mass and density. Changes in albedo over time and cloudiness are parameterised. | Screen air temperature, dew point temperature, anemometer-level wind magnitude, precipitation, surface pressure and incident solar radiation | 2 |
| Walter *et al.,* 2005 | EBM | Calculates change in SWE by accounting for all energy fluxes, many assumptions about values of input coefficients | Daily maximum and minimum temperature, day of the year, geographic latitude | 2 |
| Debele *et al.,* 2010 | EBM | Sum of heat fluxes to calculate change in heat content of snowpack, lump catchments into altitudinal HRUs | Precipitation, temperature, solar radiation, relative humidity | 2 |
| Debele *et al,.* 2010 | EBM – SWIFT algorithm | As above cell but use of algorithm to calculate snowmelt for individual pixels | Same as above and elevation, slope and aspect for each pixel (extracted from DEM) | 2 |
| Koivusalo *et al,.* 2001 | EBM-SNTHERM.89 | 2-layer treatment of snowpack to calculate internal processes, water treated in 3 phases | Net shortwave radiation, downward longwave radiation, air temperature, relative humidity, wind speed, precipitation | 3 |
| Koivusalo *et al.,* 2001 | EBM- UEB | 2-layer treatment of snowpack processes- soil and snow layer | Same as above | 3 |

**Table 3.1 cont.** Summary of the EBMs consulted reviewed by this project. Complexity ranges from 1-4. 1 is very simple, 4 being very complex (see Etchevers *et al.* 2004 for a full definition). A comparison of more EBMs can be found in *Table 2* Etchevers *et al.* 2004.

### 3.2.2 Temperature-Index Modelling

This form of model has been commonly used for modelling snow melt due to the wide availability of air temperature data, its computational simplicity and its generally good performance relative to physically-based EBMs (Hock, 2003). There are three levels of complexity in this approach: basic, improved and enhanced, **Table 3.2** provides a summary of different models from each.

The most basic approach of temperature-index modelling involves deriving the gradient of the linear relationship between observations of daily air temperature, *T* and snow melt runoff, *M* (Johnson, 1966), the value of this is called the degree-day melt factor, *K*. The resulting factor can then be used in a temperature-index equation as follows*:*

$$M = K(T - T_o) \quad \text{(Eq. 3.5)}$$

Where $T_o$ = threshold melt temperature hence $(T\text{-}T_o)$ represents the amount of positive degree energy available to melt the snowpack. This approach was successfully used by Johnson and Archer (1972) to calculate snow melt production during a flood event in the UK. The success of this approach is due to its high correlation with energy balance components such as long-wave radiation and sensible heat flux which account for 75% of the energy balance available for melt (Hock, 2003).

Improved temperature-index models were developed to increase the percentage of the energy balance represented in the temperature-index equations. Some have included the heat flux from rain-on-snow which was found to empirically relate to snow melt by (USACE, 1956):

$$M = 0.0126(T\,P_r) \quad \text{(Eq. 3.6)}$$

Where $T$ = Temperature of rainfall assumed to be equal to the air temperature and $P_r$ = amount of precipitation falling as rain. The value of 0.0126 is similar to the degree-day factor in *Eq.3.5* and derived in a similar manner but relates rainfall amount and temperature to melt water. An example of this inclusion into a temperature-index model can be found in Zeinivand and de Smedt (2009):

$$M = \left(K + (K_{rain} * P_r)\right) * (T - T_o) \quad \text{(Eq. 3.7)}$$

Where $K_{rain}$ = is the rain-on-snow factor which is 0.0126 in *Eq. 3.6*.

The above however were derived at a daily resolution hence they cannot account for sub-daily energy fluxes which have been shown to affect diurnal melt water production (Ferguson, 1984). Further improvements therefore were made by incorporating clear-sky short-wave solar radiation into temperature-index models. Clear-sky direct short-wave radiation, *S* can be calculated as follows:

$$S = S_C O_e(\sin Lat \cos S_l - \cos Lat \sin S_l \cos A_z \sin D + \cos Lat \cos S_l + \sin Lat \sin S_l \cos A_z \cos D \cos H_a + \cos D \sin S_l \sin A_z \sin H_a) \quad \text{(Eq. 3.8)}$$

Where $S_c$ = solar constant (1367 $Wm^{-2}$), $O_e$ = orbital eccentricity given by:

$$O_e = 1 + 0.033 \cos\left(\frac{2\pi Day}{365}\right) \quad \text{(Eq. 3.9)}$$

*Day* is given according to the day of the year. Referring back to *Eq. 3.6*, *Lat* = latitude of the study site (Radians), $S_l$ = slope angle (radians), $A_z$ = azimuth angle of the slope which is the slope aspect in degrees, *A* converted to radians by:

$$A_z = 180 - A\left(\frac{\pi}{180}\right) \quad \text{(Eq. 3.10)}$$

Back to *Eq. 3.8*, *D* = declination which is calculated using day angle, $D_a$:

$$D = 0.006918 - 0.399912 \cos D_a + 0.070257 \sin D_a - 0.006758 \cos(2D_a) + 0.000907 \sin(2D_a) - 0.002697 \cos(3D_a) + 0.00148 \sin(3D_a) \quad \text{(Eq. 3.11)}$$

Where $D_a$ is calculated by:

$$D_a = \frac{2\pi(Day-1)}{365} \quad \text{(Eq. 3.12)}$$

Back to *Eq. 3.8*, $H_a$ = hour angle which enables the process to represent sub-daily melt processes, it is calculated as a function of solar time, $S_t$:

$$H_a = \left(15\left(\frac{1200-(S_t-50)}{100}\right)\right)\left(\frac{\pi}{180}\right) \quad \text{(Eq. 3.13)}$$

Where $S_t$ is calculated from the time, $T$ in hours, longitude, $Long$ in degrees and the day angle, $D_a$:

$$S_t = T + (4\,Long) + \{0.000075 + (0.001868\,\cos D_a) - 0.032077\sin D_a - 0.014615\cos(2D_a) - 0.04089\sin(2D_a)\}229.18 \quad \text{(Eq. 3.14)}$$

Hock (1999) included $S$ into a temperature-index model as follows:

$$M = \left(\frac{1}{n}K + a_{snow}\,S\right)T_a \quad \text{(Eq. 3.15)}$$

Where $n$ = number of time steps per day (24 if modelling at an hourly resolution) and $a_{snow}$ = radiation factor empirically relating $S$ to $M$.

However the manner in which solar-radiation has been incorporated into temperature-index modelling in improved approaches fails to account for cloud cover and snow pack reflectivity or albedo. Enhanced temperature-index models such as Hock (1999) and Pellicciotti *et al.,* (2005) incorporate these effects. The former accounts for cloud cover through a ratio of clear-sky solar radiation, $S$ to the amount reaching the surface, $G_s$:

$$M = \left(\frac{1}{n}\,K + a_{snow}\,S\left(\frac{G_s}{S}\right)\right)T_a \quad \text{(Eq. 3.16)}$$

The latter meanwhile accounts for the effects of albedo, $\acute{\alpha}_l$ and the amount of solar radiation reaching the surface:

$$M = K\,T_a + a_{snow}(1-\alpha_l)G_s \quad \text{(Eq. 3.17)}$$

Albedo of new snow can be calculated as a function of its density (Walter *et al.,* 2005):

$$\alpha_l = A_x - (A_x - A')\,exp\left[-\left(\frac{4R_p\rho_s}{0.12}\right)\right] \quad \text{(Eq. 3.18)}$$

Where $A_x$ = maximum albedo (~0.95), $A'$ = albedo from the previous day, $R_p$ = water equivalent depth of snow and $\rho_s$ = density of new snow calculated as a function of solar radiation and air temperature. If no new snow falls, the albedo of the existing snow pack decays as a function of the time step:

$$\alpha_l = 0.35 - (0.35 - A_x) * exp\left[-\left(0.177 + ln\left(\frac{A_x - 0.35}{A' - 0.35}\right)^{2.16}\right)\right]^{0.46}$$ (Eq. 3.19)

Measurements of solar radiation at the surface however are not available for the study site meaning that it is not possible to implement enhanced temperature-index approaches. However the use of the other two approaches may be suitable for this project as they account for the most significant energy fluxes in UK snowmelt hydrology. Furthermore there is no literature proving that enhanced approaches perform significantly better than the others.

| Reference | Model Type | Process Representation | Data Input | Parameters |
|---|---|---|---|---|
| Johnson and Archer, 1972; Moore *et al.,* 1999; Beven, 2002; Fontaine *et al.,* 2002; Kayastha *et al.,* 2005 | Basic | Positive Daily Air Temperature | Daily Air Temperature | Degree-Day |
| Debele *et al.,* 2010 | Basic | Daily Positive Air Temperature and Snow pack Temperature | Daily Air Temperature | Degree-Day computed as a sinusoidal function of day of year |
| Hock, 1999 | Basic | Daily Positive Air Temperature Disaggregated to Hourly Resolution | Daily Air Temperature, Time Steps per Day | Degree-Day |
| Zeinivand and De Smedt, 2009 | Improved | Positive Daily Air Temperature and Precipitation | Daily Air Temperature and Precipitation | Degree-day and Rain-on-Snow |
| Jackson, 1978a; Reed and Field, 1992 | Improved | Positive Daily Air Temperature and Wind Speed | Daily Air Temperature and Wind Speed | Degree-Day and Wind Speed |
| Hock, 1999; 2003 | Improved | Positive Hourly Air Temperature and Clear-sky Solar Radiation | Hourly Air Temperature and Clear-sky Solar Radiation | Degree-Hour and Solar Radiation |

**Table 3.2** Summary of different Temperature-Index models reviewed for this project.

| | | | | |
|---|---|---|---|---|
| Moore *et al.,* 1999 | Improved | Positive Hourly Air Temperature, Wind Speed and Precipitation | Hourly Air Temperature, Wind Speed and Precipitation | Degree-Hour and Wind Speed |
| Hock, 1999 | Enhanced | Hourly Positive Air Temperature and Short Wave Solar Radiation at Surface | Hourly Air Temperature and Solar Radiation at Surface | Degree-Hour and Solar Radiation |
| Pellicciotti *et al.,* 2005 | Enhanced | Hourly Positive Air Temperature, Short Wave Surface Solar Radiation and Albedo | Hourly Air Temperature and Surface Solar Radiation | Degree-Hour and Solar Radiation |
| Bengtsson, 1986; Martinec, 1989 | Enhanced | Hourly Positive Air Temperature, Short Wave Surface Solar Radiation and Albedo | Hourly Air Temperature and Surface Solar Radiation | Degree-Hour, Solar Radiation and Albedo |
| Li and Williams, 2008 | Enhanced | Hourly Positive Air Temperature, Short Wave Surface Solar Radiation and Albedo | Hourly Air Temperature, Surface Solar Radiation | Degree-Hour, Solar Radiation and Latent Heat of Fusion |

**Table 3.2 cont.** Summary of different Temperature-Index models reviewed for this project.

### 3.3 Snow Melt Modelling Synthesis

As described in sub-section 3.2.1, EBMs provide a physically based approach to snow melt modelling. Multi-layer EBMs provide an unnecessary dimension of complexity as it was shown that they do not improve the modelling of snow melt production especially in shallow snow packs such as those in the UK (Etchevers *et al.,* 2002; 2004). However the extensive data requirements of all EBM types goes beyond the observational data available in the Dacre Beck. The use of physically reasonable assumptions may enable their implementation but it is likely that the uncertainty this introduces would be to the detriment of their quality in comparison to temperature-index approaches. Hence the decision was made not to use EBMs in this project and instead focus on implementing a temperature-index method.

Three levels of temperature-index process representation have been assessed in the second sub-section. Basic and improved approaches attempt to account for the most significant snow melt energy fluxes through empirically derived relationships. Enhanced approaches attempt to improve the physical basis of these through the inclusion of effects such as albedo and cloud cover. Insufficient data however is available in Dacre Beck to drive enhanced temperature-index models. It may be possible to make physically reasonable assumptions in order to implement them but it then it would be more appropriate to use the assumptive EBM of Walter *et al.,* (2005) due to its greater physical basis. It was decided therefore that this project would implement either a basic or improved temperature-index model.

None of the literature cited by this project however, showed that either the basic or improved approach outperformed the other when modelling snow melt production. The decision was made to implement three different temperature-index models each accounting for a different magnitude of process representation. Firstly a basic equation such as *Eq. 3.5* would be implemented followed by the inclusion of rain-on-snow processes such as in *Eq. 3.7* (Zeinivand and de Smedt, 2009). Thirdly a sub-daily equation accounting for clear-sky short-wave radiation such as *Eq. 3.15* (Hock, 1999) was chosen. The empirical rain-on-snow equation of *Eq. 3.6* (USACE, 1956) was added to the third equation in improve upon process representation beyond the other two. The next chapter describes the implementation of each selected temperature-index equation within a distributed snow accumulation and melt model of the Dacre Beck.

# Chapter 4

# Distributed Snowmelt Model

## 4.1 Model Construction

This chapter describes the construction and verification of a distributed snowmelt model which represents processes of snow accumulation and melt across the altitudinal range of the study catchment. Snow melt is modelled using three equations from the temperature-index approach reviewed in Chapter 3. The model then routes all snow melt and rainfall at each point in the catchment to the outlet enabling the production of an outlet hydrograph. The first section of this chapter (4.1) describes the construction of the model including its input data requirements, spatial discretisation and process implementation. Secondly in section 4.2, the model's behaviour is tested to ensure it behaves realistically by checking that mass is conserved and that it responds in a realistic manner to changes in its parameters (sensitivity analysis).

### 4.1.1 Input Data

The distributed snowmelt model constructed in this chapter requires gridded elevation data in the form of a Digital Elevation Model (DEM) and temperature and precipitation data. Raw DEM data were obtained from the Ordnance Survey Profile Digital Terrain Model dataset at a 10 m resolution however it was resampled to 50 m. This reduces the model run time, due to the reduced number of computation points. However, it still allows the model to represent hill slope scale processes as the average hill slope length was over 100m. The study catchment was delineated from the DEM using the Watershed Delineation Toolbox in ESRI ArcGIS 9.2. The delineated DEM was then used to calculate slope and aspect which form inputs into the solar radiation calculation of the Hock (1999) equation discussed in the previous chapter (*Eq. 3.15*). The temperature and precipitation data used in this study was obtained from the UK Met Office MIDAS database. It could also be generated from the UKCP09 Weather Generator (Jones *et al.,* 2009) so that the model could be used to predict the impacts of climate change scenarios.

### 4.1.2 Spatial Discretisation and Process Implementation

The temperature, $T_a$ and precipitation, $P_r$ data are obtained in point form hence they need to be spatially distributed across the catchment DEM. This is calculated using the lapse rate equation where either the temperature, $T_{a(i,j)}$ or precipitation, $P_{r(i,j)}$ for a point in the catchment DEM is given by:

$$T_{a(i,j)}\ or\ P_{r(i,j)} = \left(Z_{(i,j)}L_R\right) + [T_a\ or\ P_r] \qquad \text{(Eq. 4.1)}$$

Where $Z_{(i,j)}$ = elevation difference between gauge elevation and elevation at point *(i,j)* and $L_R$ = temperature or precipitation lapse rate ($^0$C or mm m$^{-1}$). The physical explanation and suggested values for both the temperature and precipitation lapse rates are outlined in Chapter 1 (section 1.1). After this spatial discretisation, the model is then able to implement the following set of decisions for each point in the catchment at each time step (**Figure 4.1**):

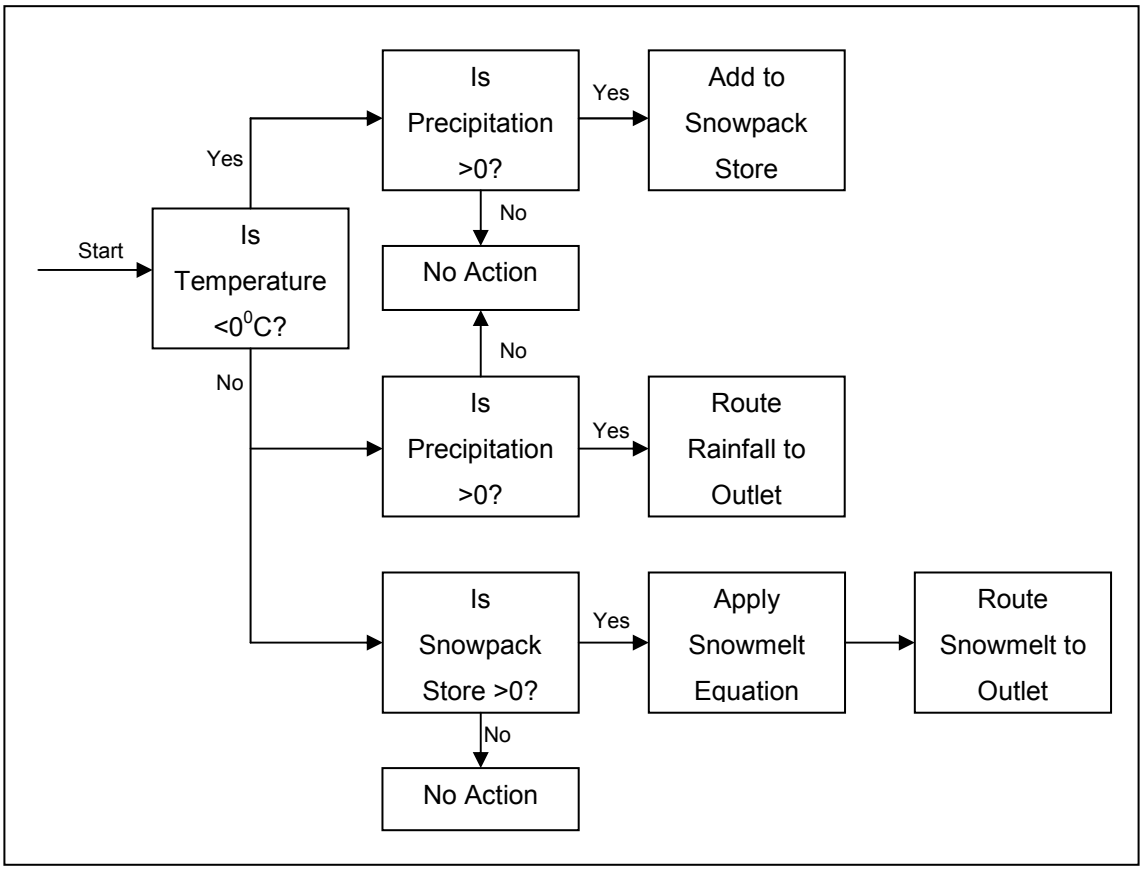


**Figure 4.1** Decision chain implemented by the model for each point in the catchment DEM for each timestep.

A point in the landscape is assumed to accumulate snow when the temperature is below a given threshold (0$^0$C) and the precipitation falling at that point and timestep is greater than 0mm. If however, the temperature at a point is greater than the threshold temperature (the threshold melt and accumulation temperatures are assumed to be the same) and a snowpack is also present, one of the three snowmelt equations chosen in Chapter 3 (section 3.2.3) is implemented.

The first snowmelt equation (*Snowmelt Model 1*) is a degree-day approach widely cited in the snowmelt literature (see Chapter 3 Table 3.2):

$$M = K(T_a - T_o) \quad \text{(Eq. 4.2)}$$

Where $M$ = amount of snowmelt produced (mm day$^{-1}$), $T_a$ = air temperature ($^0$C), $K$ and $T_o$ are parameters of the degree-day factor (mm $^0$C$^{-1}$ day$^{-1}$) and threshold melt temperature ($^0$C).

The second snowmelt equation (*Snowmelt Model 2*) is from Zeinivand and de Smedt (2009) which includes the effects of air temperature and precipitation:

$$M = \left(K + (K_{rain} * P)\right) * (T_a - T_o) \quad \text{(Eq. 4.3)}$$

The parameters in this approach are $K$, $T_o$ and $K_{rain}$ (mm mm$^{-1}$ day$^{-1}$) is a rain-on-snow factor relating a daily amount of precipitation to the amount of melt water it produces.

The third snowmelt equation (*Snowmelt Model 3*) is a combination of the hourly equation from Hock (1999) and the rain-on-snow equation from USACE (1956) which enables greater process representation:

$$M = \left\{\left(\frac{1}{n}K + a_{snow}S\right)T_a\right\} + \{K_{rain}(T_a * P)\} \quad \text{(Eq. 4.4)}$$

Where $n$ = number of time steps per day and $S$ = clear-sky short-wave solar radiation (W m$^{-2}$) calculated using the aspect and slope grids described above and the method in Chapter 3 (*Eqs 3.8* to *3.14*). The parameters are $K_{rain}$ and $a_{snow}$ (W m$^{-2}$ mm$^{-1}$ hour$^{-1}$ $^0$C$^{-1}$), the latter is a radiation factor linking short-wave solar radiation to the amount of melt water produced. Hock (1999) found the left-hand side of *Eq. 4.4* to work best when the threshold melt temperature was held at 0$^0$C hence $T_o$ will not be considered as a parameter in this equation.

Any precipitation falling at a point in the catchment when the temperature is above the threshold is treated as rainfall. It, along with any snow melt produced at the same point at that time step is routed by the model to the catchment outlet (see Chapter 2 **Figure 2.1**) as overland flow. The outlet hydrograph is constructed as a function of the concentration time for each point in the catchment. For example, if a point in the catchment takes eight hours to reach the outlet then the amount of runoff at that point is added to the hydrograph eight hours later. The time taken for each point in the catchment to reach the outlet is

calculated firstly by working out the distance between it and the outlet using the Multiple Flow Direction algorithm (Freeman, 1991; Quinn *et al.,* 1991) for hill slopes and the D8 Linear Flow Algorithm (O'Callaghan and Mark, 1984) for channels (see Chapter 2 section 2.5.1). It was then possible to work out the time taken for each point in the catchment to reach the outlet using the distance at each point and assuming a constant flow velocity of 0.2 $m^3s^{-1}$. This value was chosen by applying the Darcy-Weisbach head-loss equation of a fluid through a pipe re-arranged to solve for flow velocity *V* to the slope of Great Mell Fell (Chapter 2 **Figure 2.2**):

$$V = \sqrt{\frac{2H_l D_p g}{fL}} \qquad \text{(Eq. 4.5)}$$

Where $H_l$ is the head loss due to a reduction in pressure caused by friction, a value of 130 was chosen based upon the maximum value of the head loss coefficient in Hazen-Williams equation which is applicable to fluids up to $15.5^0$C. The maximum value was chosen as this represented a high magnitude of head loss which is feasible on a rough and steep hill slope. $D_p$ is the diameter of the pipe which in this case was chosen to be 3 m as this had been used in previous hydrological modelling (Lane *et al.,* 2009). Gravitational acceleration *g* was calculated from the vector of vertical gravitational acceleration (9.81 $ms^{-2}$) along the slope at Great Mell Fell, the resultant value was 3.93 $ms^{-2}$. A value of 75 was chosen for the friction factor *f* which represents roughness along the slope as this had again been used in previous hydrological modelling (Lane *et al.,* 2009). Finally, the slope length *L* of Great Mell Fell was calculated from the DEM to give a value of 500 m. A constant velocity had to be used as it was not possible to represent the dynamic relationship between velocity and depth as concentration time calculation was based upon average flow conditions for each point within the catchment.

The maximum time taken was 17 hours and 40 minutes hence the model was run at no greater than an hourly resolution in order to capture the hill slope processes. *Snowmelt Model 1* and *2* can only be applied at a daily resolution since this was the resolution upon which field studies derived them. Therefore these models are aggregated to a daily resolution after running the model for hourly time steps, the results from *Snowmelt Model 3* would be left at an hourly time step. The hydrograph can be composed either solely from snowmelt runoff or both rainfall- and snowmelt-runoff.

## 4.2 Model Verification

### 4.2.1 Mass Balance Testing

Ensuring that the model solves the above equations correctly can be achieved by checking that water mass is conserved where the output of water is equal to the amount inputted. For each point in the catchment at each time step, *t* the following mass balance ratio was implemented:

$$Rain + Snowfall + Snowpack_{(t-1)} = Rain + Snowmelt + Snowpack_{(t)}$$

(Eq. 4.6)

The left-hand side of *Eq. 4.6* refers to the inputs and the right-hand side represents the outputs. Mass conservation would be achieved when the value from *Eq. 4.6* was equal to zero, values greater than zero would mean water was being created and values smaller than zero would mean water is being lost.

To check mass balance the model firstly was set up using hourly temperature and precipitation data from the gauge at Keswick (situated 16km west of the catchment) for the December 2009-February 2010 period with November 2009 acting as a warm up month. Then *Eq. 4.6* was implemented at each time step, the results confirmed that the model was conserving mass.

### 4.2.2 Sensitivity Analysis

Sensitivity analysis is an intermediary process connecting both model verification and calibration (see chapter 6) since its results can be used to inform both (Trucano *et al.,* 2006). Firstly, it acts as a check on the robustness of the model's logic (Wainwright and Mulligan, 2004) ensuring a physically realistic response to alterations in the model parameters. Secondly it quantifies the amount that each parameter contributes to output variability (Saltelli, 2000) i.e. its sensitivity, and thus which parameters contribute to output uncertainty. A sensitive parameter therefore will constitute a relatively large amount of output variability and hence uncertainty.

#### 4.2.2.1 Parameter Identification

In designing a sensitivity analysis experiment the first step identifies the parameters that require analysis (Saltelli, 2000). These are inputs into the model equations which cannot be confidently constrained to a precise value due to spatial and temporal variability (Kirkby *et al.,* 1992). For example temporal variations in the UK precipitation lapse rates have been attributed to air mass movements where frontal rainfall during the winter strengthens the relationship between rainfall and altitude (Lawler, 1987). The lack of a precise constraining value propagates through to model output uncertainty and variability hence the need for the sensitivity analysis to focus upon this these parameters. The parameters that will be studied in this section are outlined in **Table 4.1**.

Upon identifying the parameters, the sensitivity analysis must focus within a range of physically realistic values. Each value range defines the parameter's space and the range of realistic values reflecting its uncertainty bounds due to it not representing sub-grid processes (Beven, 2002) such as temporal and spatial variations. It is important that the range is physically realistic as the results will be used to inform the calibration and uncertainty evaluations (Chapter 6). These will sample the same parameter ranges hence if the range is unrealistic there is a possibility that the final model results will be physically unrealistic.

Parameter ranges can be identified by reviewing existing literature which have undertaken detailed fieldwork at locations similar to the study site. Providing the previous research that is consulted undertook fieldwork in similar environments to the Dacre Beck their parameter ranges should be applicable. The ranges for each model parameter are outlined in **Table 4.1**. A slightly wider range than that identified from the literature was used in order to verify that the model behaved unrealistically when using unrealistic parameter values. In the case of the rain-on-snow and threshold melt temperature parameters no literature could be found to inform realistic ranges. Instead *base case* values were identified from previous studies and a range was based around them.

| Parameter (units) [Model] | Range (Source) | Range Used | *Base Case* (Source) |
|---|---|---|---|
| Temperature Lapse Rate ($^0$C m$^{-1}$) | -0.0045 : -0.0125 (Harding, 1979) | 0:-0.02 | -0.0085 (de Jong *et al.,* 2009) |
| Precipitation Lapse Rate (mm m$^{-1}$) | 0.000151 : 0.000531 (Lawler, 1987) | 0 : 0.001 | 0.00032 (Lawler, 1987) |
| Degree-Hour (mm Hour$^{-1}$ $^0$C$^{-1}$) [Hock, 1999] | 0.5 : 2.5 (Hock, 1999) | 0 : 3 | 1.8 (Hock, 1999) |
| Radiation Coefficient (W m$^{-2}$ mm hour$^{-1}$ $^0$C$^{-1}$) [Hock, 1999] | 0.0001 : 0.006 (Hock, 1999) | 0 : 0.01 | 0.0006 (Hock, 1999) |
| Rain-on-Snow (mm mm$^{-1}$) [Hock, 1999; Johnson and Archer, 1972] | No Source Found | 0 : 1 | 0.0126 (USACE, 1956) |
| Degree-Day (mm day$^{-1}$ $^0$C$^{-1}$) [Zeinivand and de Smedt, 2009; Johnson and Archer, 1972] | 0.029 : 0.383 (Singh and Singh, 2001) | 0 : 0.383 | 0.17 (Singh and Singh, 2001) |
| Rainfall Melt Rate (mm day-$^{1}$ $^0$C$^{-1}$) [Zeinivand and de Smedt, 2009] | 0.0005 : 0.01 (Zeinivand and de Smedt, 2009) | 0.0005 : 0.01 | 0.0032 (Zeinivand and de Smedt, 2009) |
| Threshold Melt Temperature ($^0$C) [Zeinivand and de Smedt, 2009; Johnson and Archer, 1972] | No Source Found | 0 : 1 | 0.000002 (Zeinivand and de Smedt, 2009) |

**Table 4.1** The parameters contained within the distributed snowmelt model and their ranges and *base case* values identified from previous literature.

#### 4.2.2.2 Strategy

A strategy was required that enabled the identification of output variability within each of the input parameters. The simplest way of achieving this is through the identification of the elementary effect of each parameter (Campolongo *et al.,* 2007). One-at-a-time (OAT) (Morris, 1991) is widely used (Hamby, 1994) to identify these elementary effects where each parameter is independently varied whilst holding all others constant. It is also a very economical method as it only samples the local parameter space. The effects of varying each parameter are quantified by replacing the model output with an objective function. Then the partial derivatives of the output objective function are computed with respect to the input factors (Campolongo *et al.,* 2000) thus quantifying the elementary sensitivities of each parameter.

The OAT strategy was implemented in this sensitivity analysis for each snowmelt equation within the distributed model. Each parameter within each snowmelt model would be analysed individually by sampling within the prescribed range, whilst holding all others at a *base case* value. The model would then be run for each sampled value within the parameter's space, the output variability would be assessed after each run by using an output metric. It was decided to use the output hydrograph composed solely from snowmelt-runoff as this was the key process of this project.

#### 4.2.2.3 Sampling of the Parameter Space

Each parameter range identified in **Table 4.1** required sampling in order to produce a suite of different input realisations for which the model was run. The sampling needed to sufficiently represent the entire parameter space whilst simultaneously being mindful of computational feasibility. Random (Monte Carlo) and stratified (Latin Hypercube) sampling techniques are commonly used to generate input parameter suites however their suitability required assessment of their design and computational cost.

Monte Carlo sampling, used in the Formal Bayesian and GLUE (Beven and Binley, 1992) uncertainty evaluations (Jin *et al.,* 2010), was developed to deal with physical problems containing a moderate number of parts (Metropolis and Ulam, 1949). In this method random processes select values from a predefined range informed by a posterior probability distribution (von Neumann and Ulam, 1945) representing the likelihood of

occurrence of a particular value within a predefined range. Fieldwork data collected at the study location is often used to inform this distribution (Kirkby *et al.,* 1992) but was not available for this project. Consequently a uniform distribution whereby every value within the range has an equal likelihood of occurrence must be assumed for the ranges in **Table 4.1**. For the Monte Carlo method this may mean that many samples must be taken before it can confidently be assumed that the entire parameter space has been adequately represented thus reducing computational economy. It is possible to update the probability distribution using the Bayes equation as more runs are undertaken (Beven and Binley, 1992) but other sampling strategies may prove to be more useful before this option needs to be considered.

Latin Hypercube stratified sampling splits a range into equi-probable strata based upon the cumulative distribution of the data and randomly samples one value from within each (McKay *et al.,* 1979). This approach has been described as a compromise procedure whereby it incorporates desirable features from both random and stratified sampling (Helton and Davis, 2003). It requires fewer runs than the Monte Carlo method (van Griensven 2005) since it subdivides the data distribution leading to more representative random sampling of the overall space. McKay *et al., (*1979) showed that it outperformed Monte Carlo random sampling under certain conditions of monotonicity (where a function is preserved) and if only a few parameters dominate (Campolongo *et al.,* 2000). However a lack of a prior probability distribution in this sensitivity analysis for the parameter ranges means a uniform distribution would have to be assumed for the cumulative distribution. Therefore the form of Latin Hypercube sampling that would be used in this project would have more in common with conventional stratified sampling. In this case, a range is split into bins of equal width and a value is randomly sampled from within each. Alternatively systematic sampling could be implemented where samples are taken at regular increments. This however risks decreasing computational economy since small increment values are required in order to prevent the sampling systematically missing trends in the data. Therefore stratified Latin Hypercube was felt to be the most suitable sampling strategy as it was the most effective at balancing the trade-off between accurately representing the data range and maximising computational economy. For each parameter twenty samples were generated from within the predefined range and the model was run for each.

#### 4.2.2.4 Output Metric

An output metric enables the quantification of elementary sensitivities by condensing the model output into a single statistic which can be compared against the statistics from other parameter realisations. In hydrology the Nash-Sutcliffe metric (Nash and Sutcliffe, 1970) which calculates the goodness of fit between the observed and simulated hydrographs is often used. However comparisons between the two hydrographs over the 2009-2010 winter found the model simulated the observed hydrograph extremely poorly since it only routes water as runoff i.e. it ignores base- and subsurface-flow. No attempt was made to calibrate the model, this would be undertaken after the snowmelt models were incorporated into a physically-based hydrological model (see Chapter 6). Instead, a different output metric was selected that demonstrated the model response to changes in the input parameters but did not require calibration.

The selected metric needed to capture the flow variability which has been highlighted as an important feature of UK snowmelt hydrology (SEPA, 2008 (see chapter 1 section 1.4 of this thesis)). No single metric is able to confidently represent both high and low flows for which snowmelt plays an important regulatory role (Black and Anderson, 1993; Novotny and Stefan, 2007). For example the Nash-Sutcliffe metric (Nash and Sutcliffe, 1970) biases towards high flows since it squares the residuals before summing them. Therefore two metrics, the $5^{th}$ percentile of probability exceedence (Q5) from the flow duration curve (see Chapter 2 section 2.4) to capture high flows and the $95^{th}$ percentile (Q95) for low flows were used to assess the model's parametric sensitivity. However in testing the latter, it was found that the flow duration curve became 0 $m^3s^{-1}$ from the $55^{th}$ percentile upwards so the Q95 would remain permanently at 0 $m^3s^{-1}$. This was especially true when the simulated hydrograph was composed solely from snowmelt. It is caused by the discontinuous nature of snowmelt in the UK meaning that there are significant periods of zero snowmelt runoff during the winter period either when a snowpack is present and not melting or altogether absent. Instead, it was decided to use the $50^{th}$ percentile as a metric of low flows as this represented some of the lowest flows in the simulated hydrographs.

#### 4.2.2.5 Sensitivity Assessment: Full Range Analysis

Firstly, for every parameter sample from all the parameters in all three snowmelt models, both output metrics were calculated. After the model had been run for every sample within a parameter's space, a suite of output metrics from each run was produced. The

sensitivity of the model output to each change in each parameter was then be assessed by comparing each metric to those of a *base case* model run. The *base case* run used values for each parameter which previous literature cited as producing the best results. The metric from each model run from each parameter sample was compared to the *base case* run by calculating the percentage difference. After this was done for all the samples from each parameter for each metric a graph of parameter sample value (*x-axis*) against the output metric percentage difference (*y-axis*) was plotted for each metric. This showed how changes in the parameter value impacted the output value allowing a judgement about whether the model behaved as was expected to be made.

The results of this analysis for each snowmelt model can be found in **Appendix 1**. One of the main observations from these response curves was the similarity and dissimilarity between the output metric responses for some of the parameters between each of the three models. For example the degree-day responses of *Snowmelt Model 1* and *2* are identical but that of *Snowmelt Model 3* is different (**Figure 4.2**).

This may be because the degree-day parameter in the first two snowmelt models (**Figure 4.2** (**a**) and (**b**)) was varied over a much wider range relative to the *base case* than the parameter in the third snowmelt model (**Figure 4.2** (**c**)). In the first two it was varied between -100% and +135% of the *base case* whilst in the third it was varied between -100% and +67% in accordance with previous literature (**Table 4.1**). Therefore the response curves from *Snowmelt Model 3* may only represent a small section of the response curves from the other two snowmelt models. There was no justification however in extending the range of this parameter in *Snowmelt Model 3* as this was the range that the original literature found to be physically realistic (Hock, 1999). The similar shape of all the response curves from all three provides evidence to support this explanation. Overall, the shape of the third snowmelt model degree-day response curves appear to approximately match the shape of the first two-thirds of the response curves of the other two snowmelt model. For example, the Q5 response surface of *Snowmelt Model 3* (**Figure 4.2** (**c**; **i**)) has a similar gradient and shape to the Q5 response curves for the first and second snowmelt models (**Figure 4.2** (**a** and **b**; **i**)) above the value of 0.25 mm $Day^{-1}$ $^{0}C^{-1}$.

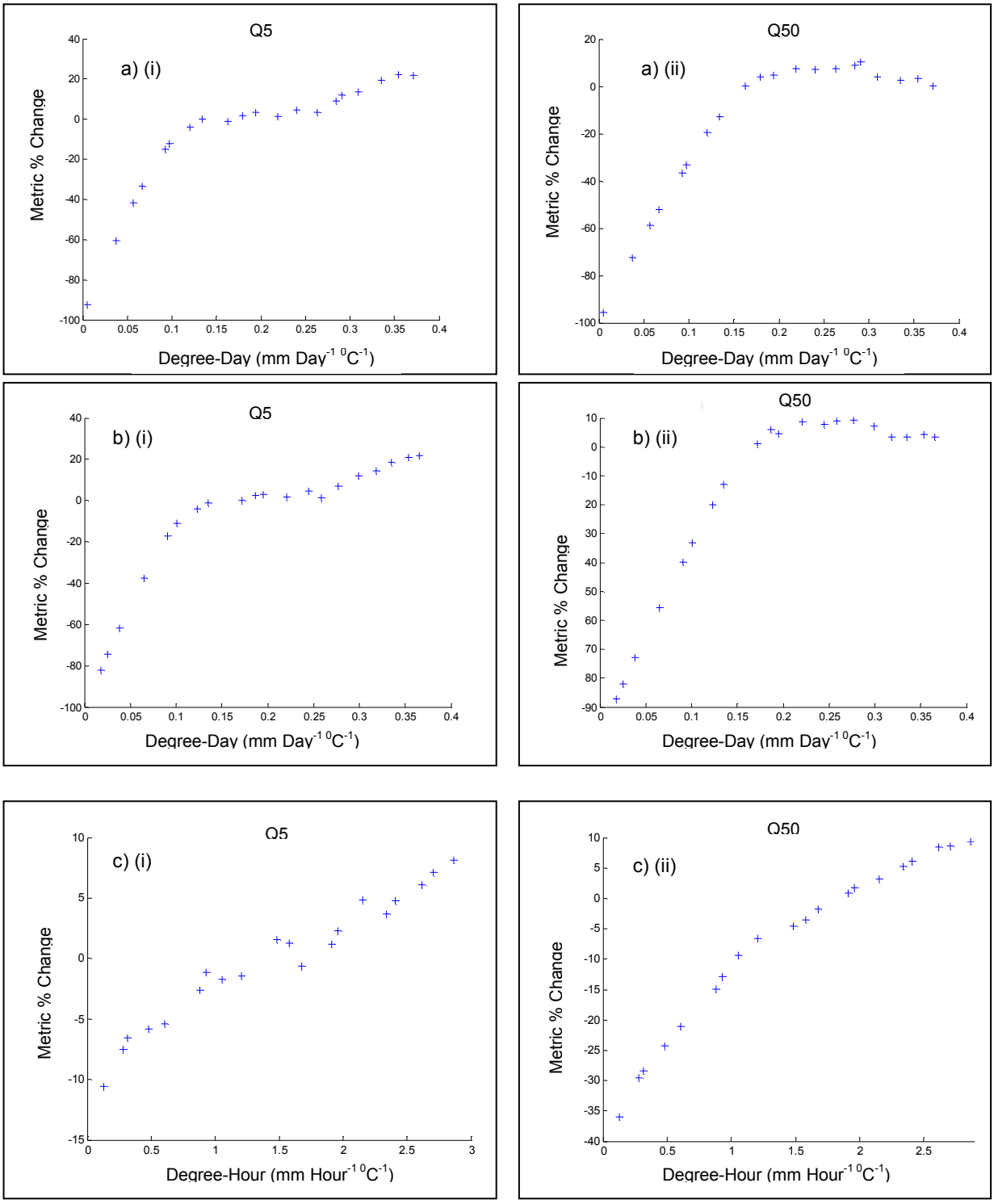


**Figure 4.2** Response surfaces from the sensitivity analysis for the degree-day/hour parameters for the (**a**) first, (**b**) second and (**c**) third snowmelt models for the (**i**) Q5 and (**ii**) Q50 output metrics.

The shape of the degree-day parameter response curves for both metrics in all three snowmelt models show an approximately non-linear increase with an increasing parameter value. This positive response is conceptually realistic for the Q5 metric (**Figure 4.2** (**i**)) since greater parameter values mean more melt is released per positive degree air

temperature leading to an increase in the overall magnitude of average and extreme melt releases. However it would be expected that the Q50 metric (**Figure 4.2** (**ii**)) would see a decreasing response as more snowmelt would be produced at the first time step at which melt occurs. Hence subsequent time steps would inherit smaller snowpacks which produce less snowmelt. This could be explained by the non-linear nature of the response curve where initially there is a very steep gradient which gradually flattens when the *base case* value is approached. Some of the initial steep gradient represents an area of the parameter range regarded as unrealistic by previous literature. The extension of this gradient into what is otherwise regarded by previous research as realistic parameter space may signify that these values are unrealistic for the context in which this study is applying the models. When the gradient begins to level out it may be that a threshold is passed where the parameter values are more realistic. In this case, if only the levelled-out part of the curve is analysed it becomes evident that the response negatively decreases by approximately 10%. No such decrease is observed in the Q50 response of *Snowmelt Model 3* if a similar analysis is undertaken however this may relate to the smaller range over which the parameter is varied as discussed above.

The response curves of both metrics for the rain-on-snow parameter in the second and third snowmelt models differ but have similar trends. They differ because they use different rain-on-snow equations and sample the same parameter over different ranges. The parameter in the second snowmelt model is sampled over a narrower range than the third snowmelt model for example. The Q5 metric, for both snowmelt models, shows a positive relationship with the parameter value which is conceptually realistic since greater parameter values increase the vulnerability of snowpacks to melt from rainfall events. Conversely, the Q50 metric for both snowmelt models shows a negative response as more snow is melted during initial rainfall events for higher parameter values so less snow if subsequently available to melt.

All temperature lapse rate metric response curves for all three snowmelt models are identical with each displaying an initial rising limb followed by a decline. Initially increasing the temperature lapse rate from zero increases the area within the catchment where snow can accumulate and hence the possible source areas of melt. When no temperature lapse rate was applied the majority of precipitation would have fallen as rain and hence not contributed to the snowmelt hydrograph. The decrease in melt output shown in all objective functions may be caused when the lapse rate enables temperatures at high

altitudes to prevent snowmelt. There may be insufficient snowfall at lower altitudes to compensate for the loss of melt input leading to an overall decline in the snowmelt hydrograph series and all associated objective functions.

Each of the precipitation lapse rate response curves responds positively to an increase in the parameter's value. The increased lapse rate means more precipitation is inputted to the catchment so larger snowpacks can accumulate. When these larger snowpacks melt they contribute more melt to the hydrograph series increasing its overall magnitude as well as extreme high and low flow events. Hydrograph variability also increases because the difference between conditions of maximum and no snow pack presence increases. The nonlinear responses of *Snowmelt Model 2* differ from the linear responses of the other two snowmelt models. The different responses of the second and third snowmelt models may be explained due to their differing representations of snowmelt from rain-on-snow. However the similarity of the response curves in the first snowmelt model, which does not represent this process, and the third either nullifies the previous explanation or indicates that the inclusion of the USACE (1956) equation makes little difference to the model output in this context.

The threshold melt temperature response curves of the first and third snowmelt models are identical for both metrics. The Q5 response curves show an initial rising then decreasing limb. The first limb may be due to the reduction of events and locations at which melt can occur allowing larger snowpacks to accumulate releasing more melt later on thus increasing extreme flows and the differences between maximum and minimum snowpack conditions. The decline appears to begin beyond $0.7^0$C which may represent where the difference between air temperature and the threshold becomes so small that snowmelt due to positive-degree air temperature significantly declines. This will reduce the magnitude of melt water release during extreme events and hence the variability of the overall hydrograph series. The Q50 response curve shows a consistent negative trend due to the reduction of potential melt from positive-degree melt. As explained above the difference between positive air temperature and the threshold melt declines as the latter increases thus reducing potential melt. This effect is expected to produce a consistently negative response curve as shown in the Q50, it is unclear why this is not the case for the Q5 curves.

*Snowmelt Model 3* responses to changes in the solar radiation parameter all show a non-linear change where the Q5 is positive whilst Q50 shows a negative trend. Increasing the solar radiation coefficient is expected to produce a positive response in the first metric since it will increase the potential snowmelt amount meaning more is released during each melt event increasing the overall melt hydrograph magnitude and that which is released during extreme events. This increases the rate at which snowpacks decay leading to a reduction in the amount of melt during low melt events hence increasing the variability of the melt hydrograph series. However there is a brief rising limb at the start of the Q50 response curve which contradicts the expected response. It is unclear whether this may represent a physical instability within the model or be an outlier resulting from the sampling strategy. Denser sampling around this area for example assuming a uniform distribution would distinguish if this outlier is a physical instability or a product of the sampling strategy.

Overall the majority of the response curves presented in **Figure 4.2** and **Appendix 1** can be attributed to a realistic physical process. Outliers and instabilities are present and may be the result of narrow parameter ranges, sparse sampling in that area of parameter space or the nature of the output metric used. Further work should consider either denser sampling or undertaking field work to find physical, site-specific explanations of the instabilities and outliers.

#### 4.2.2.6 Sensitivity Assessment: Response Comparison Analysis

The assessment in the previous sub-section was not able to accurately compare the sensitivity of each parameter because of the difference in parameter range magnitude relative to the *base case* value for each parameter. For example the degree-day parameter in *Snowmelt Model 3* is varied between -100% to +66.6% of the *base case* whilst its radiation parameter is varied between -100% to +1566.7%. Therefore it was decided to re-assess parameter sensitivities by using standardised ranges of -50% to +100% relative to the *base case* value for each parameter. Twenty samples were systematically sampled from each range in order to maximise comparability. Each parameter realisation was then run and the same output metrics were calculated and compared to the *base case* run. The resultant response curves for each parameter were plotted on a graph (percentage parameter value change relative to *base case* on the *x axis* and percentage output metric change relative to *base case* on the *y-axis*) for each metric. The range (maximum *y-axis* value minus the minimum *y-axis* value) was then

calculated for each response curve enabling the parameters to be ranked in order of sensitivity (the greatest range being the most sensitive) for each metric. Those which were most sensitive were likely to contribute the most to model uncertainty.

The results of this comparison analysis are shown below in **Figure 4.3**. They show that the temperature lapse rate parameter is the most sensitive for all snowmelt models and for both metrics which is then followed by the degree-day (degree-hour for *Snowmelt Model 3*) parameter. The precipitation lapse rate is the next most sensitive for the first two snowmelt models but it ranks after the solar radiation parameter in *Snowmelt Model 3*. The threshold melt temperature response curve is flat in the first two snowmelt models along with the rain-on-snow parameter in the second. This latter parameter is the least sensitive in the third snowmelt model but shows a slight response unlike its response in the second.

It is realistic for the temperature lapse rate to be the most relatively sensitive parameter since it controls whether accumulation or melt processes are induced at a particular time step and location. Furthermore when a snowpack accumulates the temperature lapse rate impacts upon its vulnerability to melt especially at higher altitudes as a smaller temperature lapse rate is more likely to expose the snowpack to positive temperatures recorded at lower altitudes. Therefore because of the temperature lapse rate's influence over the rest of the snowmelt and accumulation it is the most relatively sensitive parameter.

On the above basis it would also be expected that the precipitation lapse rate would be a relatively sensitive parameter. It controls the rate of precipitation increase with altitude affecting the total amount of precipitation which accumulates in the snowpack and hence the amount that is available for melt. The response range however is less than that of the temperature lapse rate perhaps because rather than controlling which processes occur, it only affects the magnitude of them. Another explanation may be that the precipitation lapse rate is an order of magnitude lower than the temperature lapse rate. This means that the precipitation lapse rate is varied by an order of magnitude lower than the temperature lapse rate in this comparison analysis. However looking at the full range response curves from the two parameters from the previous section, the precipitation

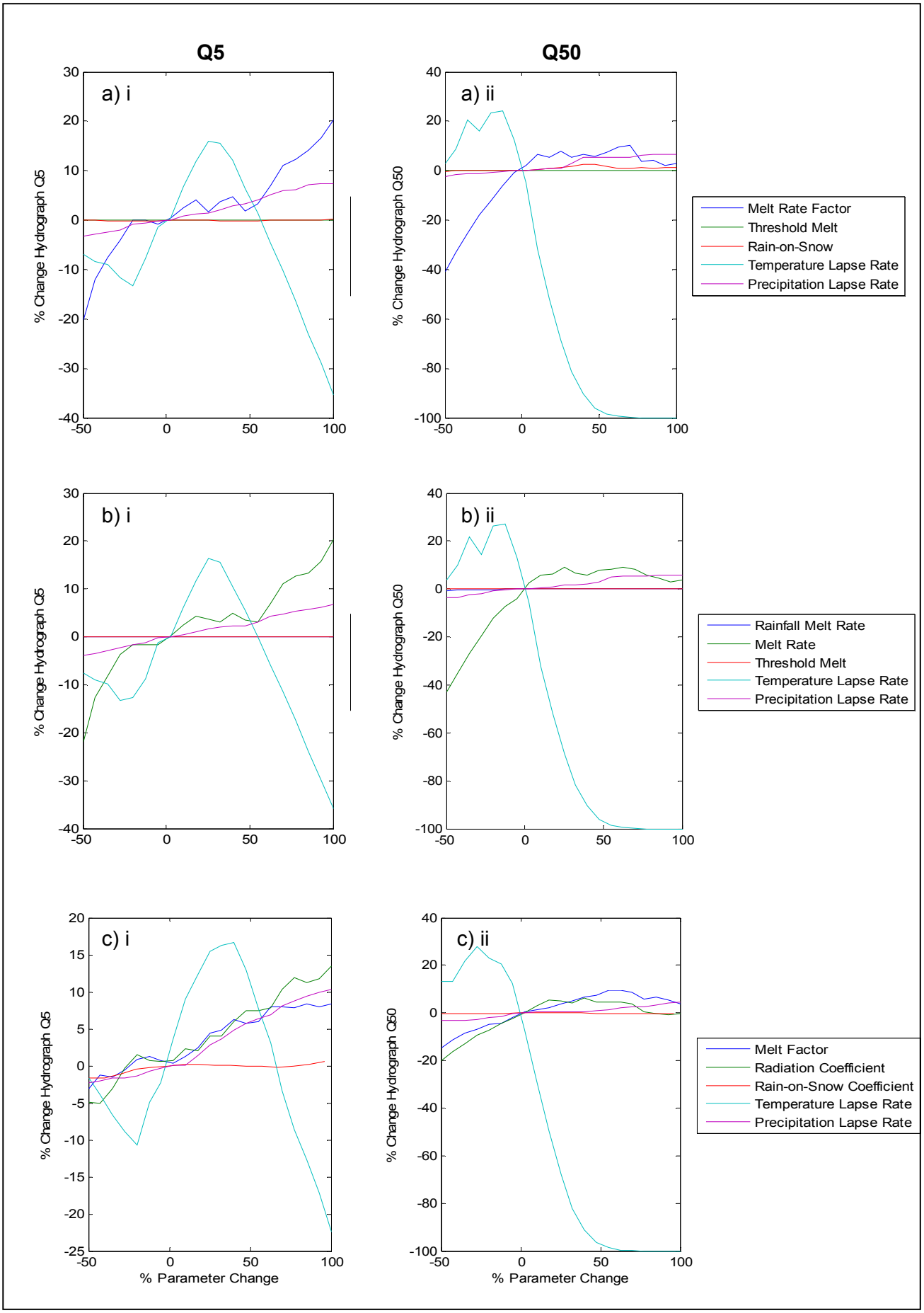


**Figure 4.3** Sensitivity assessment comparison analysis response curves for *Snowmelt Model 1* (a), *2* (b) and *3* (c). (i) refers to the Q5 metric and (ii) is the Q50 metric. The *x-axis* on each graph is percentage change in parameter value from the *base case*. Note: the rain-on-snow parameter in (a) is not discussed in this chapter or subsequently included. The *Melt Factor* parameter is another name for the *Degree-Day* parameter.

lapse rate only has a maximum response range of 18% whilst the temperature lapse rate has a response range of approximately 50%. Even when the parameter variation range is expanded the temperature lapse rate is still the more sensitive of the two. The temperature lapse rate therefore may be the more sensitive of the two because it controls which processes occur rather than solely their magnitude.

The other parameters, all contained within the snowmelt equations, show that the degree-day is the most sensitive, alongside solar radiation melt for *Snowmelt Model 3*, whilst the threshold melt temperature and rain-on-snow melt barely respond. These results are dependent upon how each process in each parameter is represented within the snowmelt equations. The degree-day parameter is of at least one order of magnitude greater than the other parameters meaning it produces some of the greatest potential snowmelt within the equations. Since it produces more melt it would be expected that the results from the equations are most sensitive to changes in this parameter. Unexpectedly the radiation coefficient in the third snowmelt model, which is two orders of magnitude lower, is almost equally sensitive. However in order to convert the amount of solar radiation received by the catchment into a realistic amount of melt a very small parameter value is required. Therefore the process this parameter represents actually produces an equal amount of melt to the positive degree-day process explaining why the two are almost equally sensitive. The rain-on-snow and threshold melt temperatures however are not relatively sensitive perhaps because the melt produced by the processes they represent is not very large. It was not yet possible however, to rule these parameters out from the calibration and uncertainty evaluation due to their apparent insensitivity as they may still have had significant interactive effects with other parameters in the snowmelt model.

#### 4.2.2.7 Sensitivity Assessment: Parameter Interactions

Neither of the previous two OAT sensitivity assessments above were able to reveal the effects of parameter interactions which may have occurred throughout global model space (Jacques *et al.,* 2006; Beven, 2009). OAT strategies may find minimal elementary effects in one parameter however this does not mean its role in output uncertainty is insignificant due to its potentially important interactions with other parameters. Furthermore the previous two strategies did not explore global multidimensional parameter space as fully as other methods. OAT is only able to explore a very small area of the global parameter space (Sulieman *et al.,* 2009). Variance based methods such as Sobol' variance decomposition (Sobol', 2001) are able to account for parameter interactions by identifying

n-dimensional effects throughout a much more extensive global parameter space (Saltelli *et al.,* 2006; Beven, 2009). However they are informed by n-dimensional Monte Carlo sampling which, as explained above, was not economical for this study.

Instead parameter interactions can be assessed qualitatively over a global scale by creating a two-dimensional response contour where an apparently insensitive parameter identified from the previous analyses is simultaneously varied with a parameter with which it is conceptually expected to interact. The shape of the response contour can be used to qualitatively assess if parameter interactions are occurring (Kirkby *et al.,* 1992). Latin Hypercube sampling was used to generate the parameter realisations which were inputted to the model. For each realisation the percentage change for each model output objective function was calculated. A response contour was then created by plotting an *xyz* graph where the *x-axis* and *y-axis* were the percentage changes in the parameter values from the *base case* and the *z-axis* was the percentage change in the output metric. However a problem was found with the Latin Hypercube sampling. If 15 samples were taken from each parameter range the first parameter's first sample was then randomly paired to a sample from the second parameter. In this case the posterior distribution was unknown so each sample in the first parameter had an equal likelihood of being paired with any sample in the second parameter. This was rectified by creating a function which paired each sample within the first parameter to every sample in the second parameter. Therefore if 15 samples were created a total of 225 parameter realisations were generated. It was intended that the results of this analysis would be able to judge if an insensitive parameter identified from the previous two assessments actually could be eliminated from the subsequent calibration and uncertainty evaluation of the hydrological model (Chapter 6).

It was decided to run this assessment firstly between the apparently insensitive threshold melt temperature parameter and the relatively sensitive degree-day parameter for *Snowmelt Model 1*. The two parameters were expected to interact since threshold melt temperature affects the amount of positive degree energy inputted into the degree-day melt equation. High threshold melt temperature values would be expected to interact with low degree-day melt values reducing the overall magnitude of melt water that is produced. If conclusive results were obtained from this initial assessment (**Figure 4.4** below), then it was intended to extend it to other parameters and the other two snowmelt models.

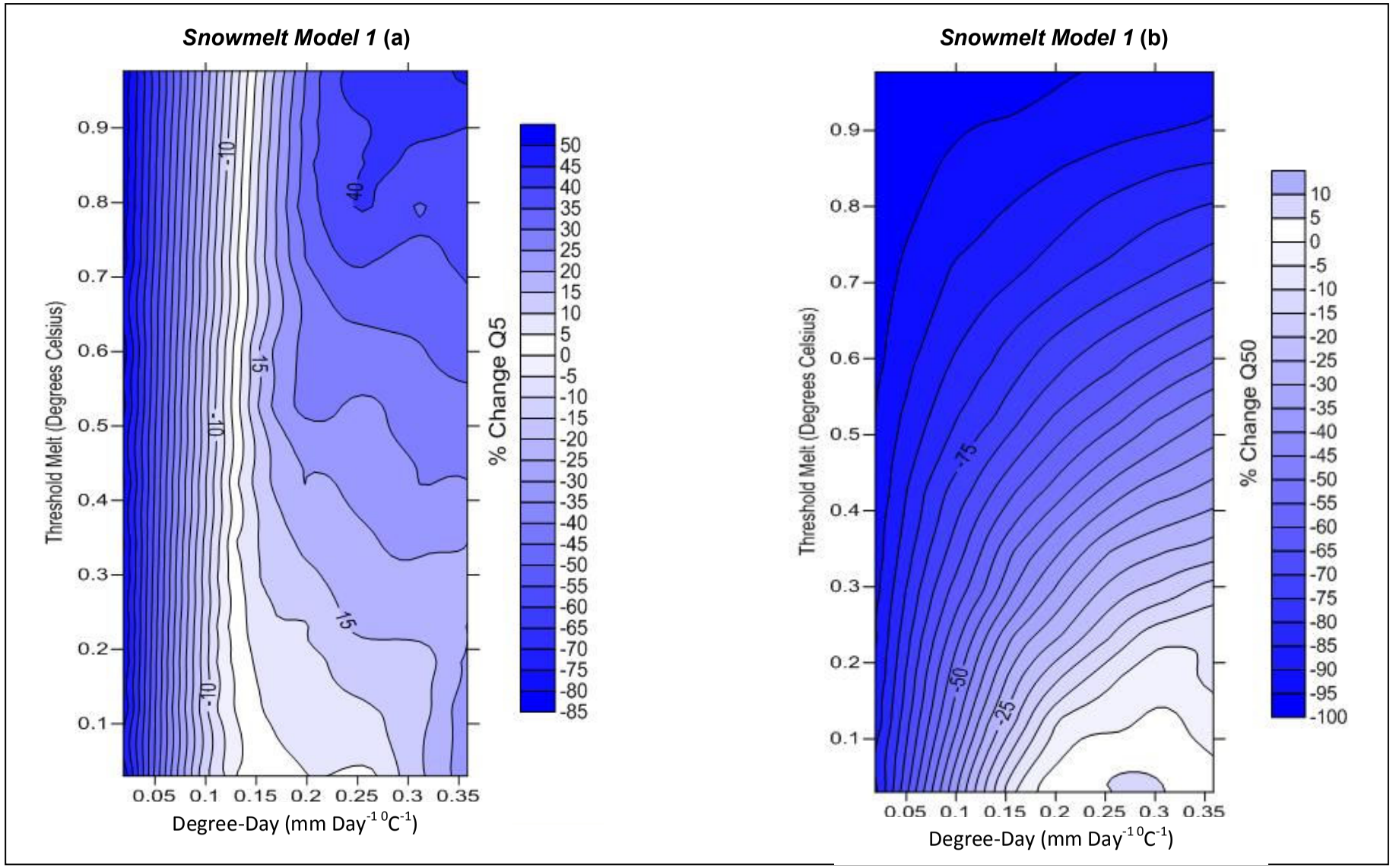


**Figure 4.4** Response surface contours for *Snowmelt Model 1.* (a) is the Q5 metric and (b) is the Q50 metric

The vertical lines in **Figure 4.4** (**a**) demonstrate threshold temperature insensitivity up to a degree-day value of 0.15 mm $day^{-1}$ $^{0}C^{-1}$. Before this, for a given degree-day value, a change in the threshold melt temperature resulted in a minimal change in the Q5 metric. Beyond this point on the *x-axis* the contour plot has an unusual shape where the contours become almost horizontal and unstable. This trend may be caused by the response sensitivity of the degree-day melt parameter becoming flatter as shown by the respective response curve in **Appendix 1**. The horizontal contours mean that changes in the degree-day melt value do not effect changes in the objective function. However when the insensitivity of this parameter combines with that of the other it produces the unusual contour pattern that resulted in this study.

The response contours of the Q50 response surface (**Figure 4.4** (**b**)) show a diagonal pattern which qualitatively indicates interactions between the two parameters (Kirkby *et al.,* 1992). The output metric decreases with higher threshold melt temperatures and low degree-day melt values whilst increasing when the opposite case is true. Interactions may be evident in this objective function and not the others because its values are of a much lower order of magnitude. The Q5 for example is five orders of magnitude greater than the Q50. Smaller analysis values mean that it is easier to detect small trends so interactions are present but may actually be insignificant. However it is difficult to assess how significant these interactions are in comparison to the other elementary and higher-order effects which are present in the model.

It was not possible in the analysis above to ascertain whether an apparently insensitive parameter has significant higher-order interactions with other parameters. The qualitative nature of the analysis meant even though some interactions were found their significance could not be judged.

Quantitative assessment methods such as Analysis of Variance (ANOVA) and Sobol' linear decomposition (Sobol', 2001) are able to judge both elementary and higher-order effects. The former quantifies the difference in mean model responses from samples of each parameter and decomposes it into elementary and secondary-order effects (Tang *et al.,* 2007).

Sobol' linear decomposition meanwhile, uses Monte-Carlo quasi-random sampling to calculate elementary and higher-order effects before comparing each against the total variance to ascertain its relative importance. The elementary effects, $V_i$ of variations in parameter $X_i$ to model, $Y$ are calculated as in Beven (2009):

$$V_i = Vx\left(Ex_{-i}\{Y|X_j\}\right) \quad \text{(Eq. 4.7)}$$

Secondary effects, $V_{i,j}$ with parameter, $x_j$ are then calculated as in Beven (2009):

$$V_{i,j} = Vx_i, x_j\left(Ex_{-ij}\{Y|X_i\}\right) - V_i - V_j \quad \text{(Eq. 4.8)}$$

Where $V_j$ is the elementary sensitivity from parameter, $x_j$. This process could be continued to find the $n^{th}$-order sensitivity however the significance of these effects beyond the secondary-order is often negligible. For example, the ANOVA method only analyses up to the secondary-order. After all the elementary- and secondary-order effects have been calculated they are summarised to find the total model variance, *V(Y)* (Rosero *et al.,* 2010):

$$V(Y) = \sum_i V_i + \sum_i \sum_{j>i} V_{i,j} + \sum_i \sum_{j>i} \sum_{k_x>j} V_{i,j,k_x} + \cdots V1,2,\ldots k_x \quad \text{(Eq. 4.9)}$$

Where, $k_x$ represents additional parameters. Sensitivity indices, *SI* can then be calculated for each parameter's elementary and higher-order effects:

$$SI_i = V_i|V(Y) \quad \text{(Eq. 4.10)}$$

$$SI_{i,j} = V_{i,j}|V(Y) \quad \text{(Eq. 4.11)}$$

$$SI^c_{i,j} = SI_i + SI_j + SI_{i,j} \quad \text{(Eq. 4.12)}$$

Where, $SI^c_{i,j}$ is the total effect of parameters $x_i$ and $x_j$. All of the indices range from 0-1 (Jacques *et al.,* 2006) making it simpler to ascertain their relative significance.

Previous research has shown that the Sobol' linear decomposition provides more robust sensitivity rankings than ANOVA (Tang *et al.,* 2007). However since it is informed by quasi-random Monte-Carlo sampling its computational cost is much higher than the other method. Since this study has no prior knowledge of each parameter's posterior distribution many more runs would have to be undertaken before a representative sample of parameter realisations is achieved. It was decided not to proceed with either method due

to the reduced computational efficiency of the Sobol' method and the lack of robustness in the results of the ANOVA method.

### 4.2.3 Sensitivity Analysis Synthesis

This analysis had the aims of testing the reality of the model output variability to changes in the input parameters and assessing which were the most sensitive. Altering each of the parameters one-at-a-time and assessing the changes in two output metrics showed that all of the resulting trends (**Appendix 1**) could be explained as being physically realistic. Comparing each parameter response curve on the same axis (**Figure 4.3**) showed that at least three parameters in each model were relatively sensitive in comparison to the others. It would be expected that parametric uncertainty would mostly arise from these three and will be assessed in the next chapter. However it was not possible to rule out apparently insensitive parameters from the next stage of analysis as it was not possible to use a method which could quantify each parameter's elementary and higher-order effects relative to the others (**Figure 4.4**).

## 4.3 Conclusions

This chapter has described the construction and verification of a distributed model which can apply three different snowmelt models across a DEM of the study catchment and route the resulting snowmelt and rainfall as runoff to the outlet. Each of the snowmelt models used accounts for a different range of processes from a basic degree-day approach to an improved one that represents positive air temperature, short-wave solar radiation and rain-on-snow. The resulting model was then verified firstly by ensuring that water mass was conserved for each point in the catchment at each time step. Secondly, a sensitivity analysis was undertaken and concluded that the model behaved realistically in response to changes in its input parameters. It also identified sensitive parameters in each snowmelt model but was unable to confidently rule out any as being insensitive. The next chapter will apply this distributed model to analyse the effect climate change upon snowmelt hydrology in the study catchment.

# Chapter 5

# Climate Change and Snowmelt Hydrology

## 5.1 Climate Change Modelling: UKCP09

This chapter outlines how the distributed model developed in Chapter 4 was applied to the Dacre Beck using climate change scenarios in order to assess how snowmelt hydrology is likely to change in the future. Firstly (section 5.1), the methodology of deriving climate change projections for the UK will be reviewed. Then a suitable climate change scenario will be selected and hourly weather series for the catchment under this will be developed. The impact of this scenario upon climatological variables such as temperature, precipitation and snow accumulation will then be assessed (section 5.2) before applying the weather series to the model and analysing the impact upon snowmelt hydrology (section 5.3).

The UK Climate Projections 2009 report (UKCP09 [Murphy *et al.,* 2009]) provides the most recent projections of climate change within the UK applied across a 25x25 km grid for three different thirty-year periods (2010-2039 [2020s], 2040-2069 [2050s] and 2070-2099 [2080s]). It forces the future climate using one of three emissions scenarios, low, medium and high which correspond respectively to the B1, A1B and A1FI scenarios in the IPCC *Special Report on Emissions Scenarios (SRES* (Nakicenovic *et al.,* 2000)). The results from the UKCP09 are presented as probabilistic changes in climate variables. That is, a range of possible changes are presented based on uncertainties in the methodology due to natural variability, incomplete understanding of the climate system and future emissions (Murphy *et al.,* 2009). A Bayesian statistical framework is then used to assign a likelihood to each possible outcome. The results of this process are then presented to the user as with a likelihood frequency assigned to each probabilistic projection for each climate variable.

### 5.1.1 UKCP09 Methodology

A summary of the methodology will be given in this sub-section however a more detailed explanation can be found in section 3.2 (page 49) of the UKCP09 projections report (Murphy *et al.,* 2009). In deriving these probabilistic projections the UKCP09 had to firstly define the possible uncertainty space of the climate model and then assess the likelihood of a sample of points within that space. Uncertainty space was defined firstly according to incomplete representation of the climate system by the HadCM3 global climate model. Key process deficiencies within this model were identified within the ocean, sulphur and carbon cycle modules (Murphy *et al.,* 2009). Sensitive parameters within these modules

were identified and prior likelihood distributions for each were defined. An ensemble of 280 members was then sampled from these distributions. Uncertainties in the model's response to changes in $CO_2$ concentrations were then assessed by running each ensemble member, from the previous step, in the HadSM3 model (which is similar to HadCM3 but computationally less demanding due to its treatment of the ocean as a '*slab*') with double the current $CO_2$ concentration. The number of ensemble members run was insufficient to represent the entirety of the feasible parameter space so a statistical emulator (Rougier 2008) was trained on the results and run for many more ensemble members. This would enable integration over the entire parameter space allowing estimates of historical and future climate variables. The previous step gave uncertainty estimates of *equilibrium climate change* but uncertainties in transient changes over the 21$^{st}$ century were assessed by running a 17 member perturbed physics ensemble sampled from the previous ensemble members. Each ensemble member was inputted to the HadCM3 model and driven by historical changes in greenhouse gas concentrations from 1860 to 2000 and by the A1B SRES scenario from 2000 to 2100. In order to integrate these results over the entire parameter space relationships between the transient and equilibrium (from the previous step) responses were developed using a *timescaling* method (Harris *et al.,* 2006). This method involves normalising the regional climate equilibrium response and then scaling this by the transient response of the global average surface temperature (Harris *et al.,* 2006). Additional uncertainties in earth system processes such as ocean transport and the sulphur cycle were included by re-running the perturbed physics ensemble including parameter cases sampled from the parameters of the respective processes.

Probabilistic projections of equilibrium climate change to doubled $CO_2$ were then estimated within a Bayesian framework which weighted the climate variables across the entire parameter space according to observed values as well as their associated errors. The latter reflects the likelihood that a given parameter case provides a representation of the system processes that is consistent with observations, this discrepancy was due to structural errors. The magnitude of discrepancy was assessed using a multi-climate model ensemble (Randall *et al.,* 2007), where the emulator of the HadSM3 model was used to find the best multivariate fit between it and the multi-climate model ensemble member (which was assumed to represent the real world).

Thus far the UKCP09 methodology had worked at the 300x300 km resolution of the HadCM3 general circulation model (GCM). The probabilistic projections derived above needed downscaling to a finer resolution in order to be useful at the regional scale for which they were intended. A perturbed physics ensemble of 17 regional circulation model (RCM [25x25 km resolution]) variants were produced which sampled uncertainties in the effects of regional scale processes such as mountainous terrain. The parameters in each RCM ensemble corresponded to those in the perturbed physics ensemble of the GCM outlined above. Downscaling was then achieved by developing statistical relationships between changes simulated by the RCM and changes at the nearest GCM point (Wilby and Wigley, 1997; Wilby *et al.,* 1998) for five separate time periods (1950-1979, 1980-2009, 2010-2039, 2040-2069, 2070-2099, Murphy *et al.,* 2009).

The above methodology was able to account for the most significant uncertainties in projecting climate change and assign likelihoods distributed across the parameter space. The next stage was to apply the above Bayesian framework in order to produce the final probabilistic projections for a given SRES scenario. For example, using the A1B emissions scenario a Monte Carlo sample of $10^6$ members of the parameter space is produced using the statistical emulator. This produces climate variables for the observed period and the projection time period under an equilibrium response to doubling $CO_2$. An interim weight for each sample is calculated based on observed values for each climate variable. At this stage, uncertainties in the emulator, observations and model structure have been accounted for. A sub-sample of 25,000 members was then taken from the Monte Carlo sample using the interim weights to ensure a wide range of the parameter range is covered. Time-dependent climate changes for each sub-sample member were found by applying the *timescaling* technique, introduced above, and by forcing a simple climate model from 1860 to 2100 using historical and future forcing agents which are aspects of the climate, such as CO2 concentration, for which changes in these can feed through to change the overall climate. The forcing agents were sampled from the uncertainty ranges from the emulator, *timescaling* error and process representation. Final weights were then calculated for each sub-sample based on emulated values of present-day climate and change indices for surface temperature. A further sub-sample of 10,000 members was taken for each 300x300 km GCM grid square from the 25,000 sub-samples based on the ratio of final weights to interim weights. The climate variables in each grid square for each sub-sample member were then downscaled to the 25x25km RCM grid squares using the statistical relationships derived above.

To demonstrate the UKCP09 projections the above procedure was applied to the area that covered Dacre Beck using the medium emissions forcing scenario. The sampled probabilistic projections for the mean winter temperature and total winter precipitation were then presented as probability density functions {PDFs (**Figure 5.1** [**a**] and [**b**])}. The PDF describes the relative likelihood for a random variable to occur at a point in the *x-axis* space. In this case it shows the likelihood of change (frequency [where a greater value means greater likelihood]) in the given climate variable being that at a given point in the space of possible change values. Interpreting the first graph shows that winters in the

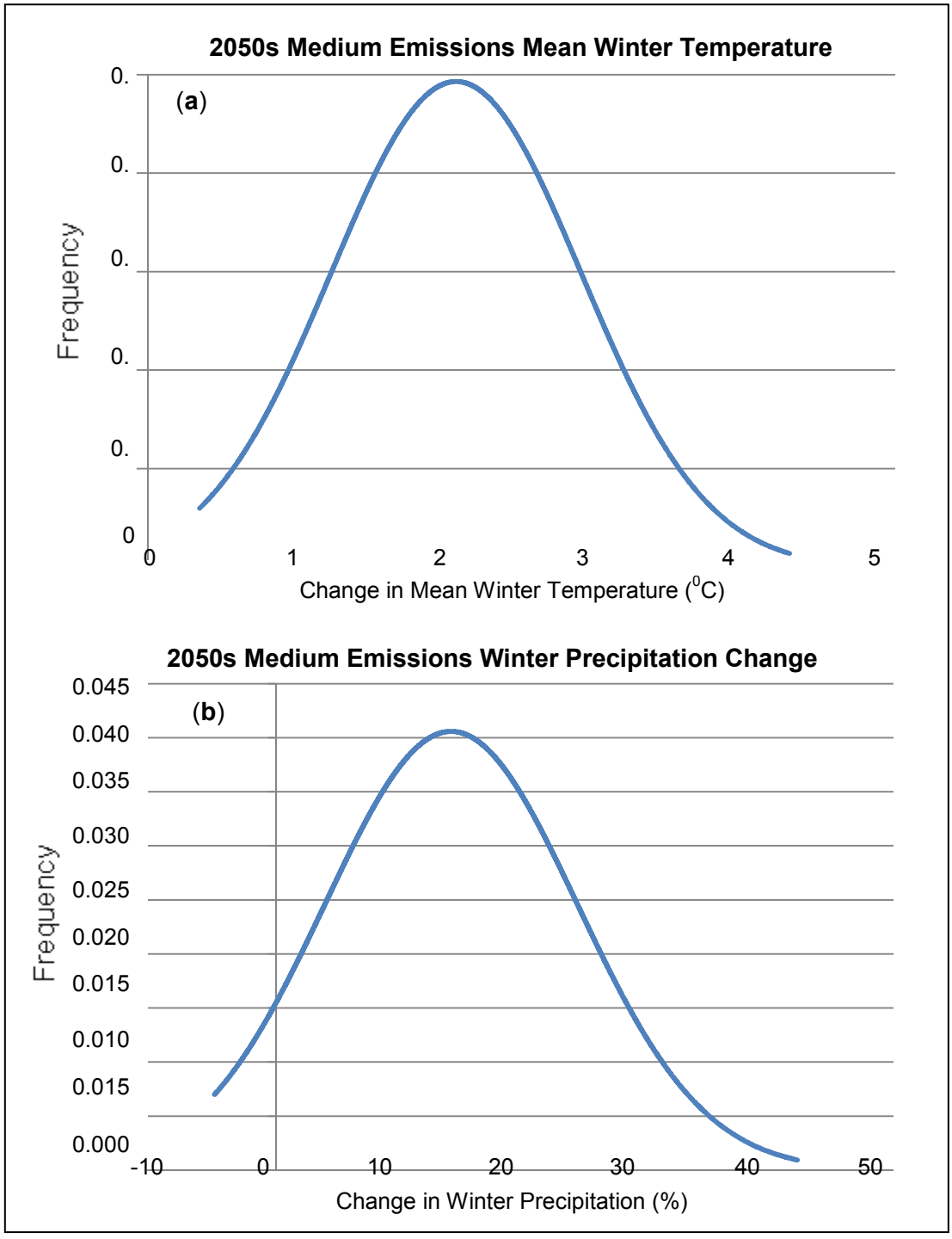


**Figure 5.1** Probabilistic projections from the UKCP09 report (Murphy *et al.,* 2009) for (**a**) mean winter temperature and (**b**) winter precipitation for the 25x25 km RCM grid cell covering Dacre Beck. The probabilistic range is calculated using the method described in

area are likely to become warmer, with the greatest likelihood at 1.9$^0$C warming with increases of 0.3$^0$C and 4.1$^0$C representing the marginal likelihoods. Meanwhile, winter precipitation is most likely to increase by 13% with an increase of 40% and a decrease of -4.5% representing the marginal likelihoods. In terms of snowmelt this could mean more precipitation falling as rain and smaller snowpacks which potentially may increase the winter flow regime variability of Dacre Beck. However, this methodology can only produce projections of climate variables at a minimum of a monthly temporal resolution. Since this project is focused around daily and sub-daily flow variability it is necessary to obtain an understanding of climate change at a finer temporal resolution. Such an understanding can be made possible by using the UKCP09 Weather Generator. This can produce weather series at a daily and hourly resolution and will outlined in the next sub-section.

### 5.1.2 UKCP09 Weather Generator

The weather generator is a stochastic model that generates *synthetic* time series of rainfall, temperature, humidity, potential evapotranspiration and sunshine amount. It is stochastic in that the "*state of the system at one time does not completely determine the state at the next time"* (Jones *et al.,* 2009). The generated time series are *synthetic* because they represent the characteristics of the climate system e.g. mean monthly rainfall, but are not a prediction of the time series that might be observed. In essence, the weather generator is intended to predict changes in the climate system characteristics rather than act as a deterministic forecasting tool of future climate series.

Firstly the weather produces a stochastic time series of rainfall using the Neyman- Scott Rectangular Pulses (NSRP) approach (Cowpertwait *et al.,* 1996a). In this method (**Figure 5.2**) storm origins are placed in the time series at a Poisson rate (Rodriguez-Iturbe *et al.,* 1987). From each storm origin a random number of rain cells are generated (Cowpertwait *et al.,*

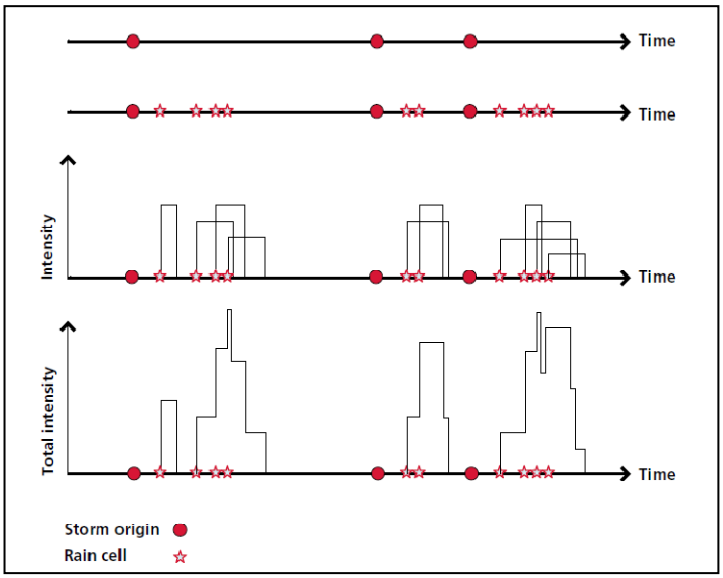


**Figure 5.2** Schematic representation of the NSRP approach. Adapted from Jones (*et al.,* 2009).

1996b). Each cell is independently displaced from the storm origin by distances exponentially distributed. The duration and intensity of each rain cell are exponentially distributed by *two parameters*. At any time step in the series the total intensity is given as the sum of intensities active at that point (Cowpertwait, 1991). This approach has been found to better represent observed characteristics including zero rainfall depth properties than others such as the Bartlett-Lewis model (Velghe *et al.,* 1994; Onof *et al.,* 2000). Each of the above parameters was varied on a monthly basis to allow for transient changes in the rainfall characteristics. The model was calibrated to observed rainfall statistics, mean rainfall rate and proportion of dry days for example, by adjusting each of the above parameters (the parameter affecting the number of rain cells was the average number of cells per storm) in an optimisation routine (Jones *et al.,* 2009). Monthly rainfall statistics were obtained from the 5x5 km gridded dataset of the UK (Perry and Hollis, 2005) for the 1961 to 1990 period. This dataset was generated from rainfall data from 4400 stations using a two-stage multiple regression where each monthly statistic was regressed with geographic factors followed by interpolation of the residuals (Perry and Hollis, 2005). The regression and interpolated surfaces were then added together to obtain the gridded datasets. The optimisation routine sampled the global parameter space, ran the model for each sample and assessed its goodness of fit using an objective function which calculated the differences between the observed and modelled rainfall statistics (Kilsby *et al.,* 2007). Hence a value for each parameter was selected that enabled the model to accurately simulate observed rainfall statistics, yet the processes that each parameter invoked were random allowing the model to generate stochastic rainfall series.

The other climate variables were then generated from the rainfall series using Inter-Variable Relationships (IVRs) which relate rainfall statistics to those of each climate variable (Jones *et al.,* 2009). The IVRs were derived using data from 115 weather stations distributed across the UK for the 1961-1995 period. Seasonal cycles of the mean and standard deviation from the climate variables were removed by subtracting the mean and dividing by the daily standard deviation. Deriving each IVR from rainfall in a conventional regression framework is not possible as rainfall is not always present (i.e. there may be sustained dry periods) yet the other climate variables still need calculating. This issue was solved by deriving each IVR for each of four rainfall transition states: dry day after dry day, wet day after dry day, dry day after wet day and wet day after wet day (Nicks and Harp, 1980). Mean daily temperature, $T_a$ and daily temperature range, $R_i$ IVRs were modelled as first-order autoregressive processes (Jones *et al.,* 2009):

$$T_a = a_1 T_{a-1} + b_1 + e \; ; \; R_i = a_2 R_{i-1} + b_2 + e \qquad \text{(Eq. 5.1)}$$

Where *a* and *b* are the regression coefficients and *e* is the correlation coefficients between $T_a$, $R_i$ and $P_r$ for each month and each rainfall transition state. The remaining variables (relative humidity and sunshine duration) were then determined through regression analyses with rainfall, mean daily temperature and daily temperature range. To ensure that the model accurately represented the climate variables other than rainfall during dry periods the model was fitted to the mean and standard deviation values for each variable for every half month for every rainfall transition state by adjusting the parameters in the regression analyses. It should be noted that stationarity in these IVRs is assumed for projections of future climate series.

All of the weather statistics and IVRs from each of the 115 weather stations were then interpolated onto the 5x5 km rainfall dataset grid using topographic variables so allowing the weather generator generate time series which replicate small-scale (5x5 km) spatial variability. Finally, all the generated weather variables are converted into absolute values using adjusted means (including change factors) and standard deviations. Change factors, *α* are used to force the generated time series by the probabilistic climate change projections from the UKCP09 (see sub-section 5.1.1). They are applied for each month on a multiplicative basis for rainfall statistics and additive for the other climate variables (Jones *et al.,* 2009). So, in the case of the former the change factor, $\acute{\alpha}_c$ would be applied in the following form:

$$P^{Fut} = \alpha_c P^{Obs} \qquad \text{(Eq. 5.2)}$$

Meanwhile an additive change factor is applied in the form (Kilsby *et al.,* 2007):

$$T^{Fut} = T^{Obs} + \alpha_c \qquad \text{(Eq. 5.3)}$$

As mentioned in Chapter 4 it was necessary to run the distributed snowmelt model at an hourly resolution hence the outputs from the UKCP09 weather generator needed to be at this resolution. The UKCP09 developed a methodology which enabled the weather generator to produce weather series at an hourly resolution. Firstly, rainfall was modelled using estimates of hourly observed statistics from 35 stations over the 1976-1995 period. The model could then generate hourly rainfall series using a combination of hourly and daily rainfall statistics, derived from the above methodology. The inclusion of daily

statistics enabled the subsequent parameterisation in the fitting to process to be constrained to physically realistic values (Jones *et al.,* 2009). The other climate variables were then generated by deriving the IVRs at an hourly scale and interpolating to the 5x5 km grid. Checks were then made to ensure that the hourly statistics when aggregated to a daily resolution were equal to those derived directly from daily observations.

Before the weather generator is put to use in this study its limitations must be appreciated, a summary of them will be given here (see Chapter 5 of Jones *et al.,* 2009 for a detailed discussion). Firstly its reliance upon IVRs means that it lacks a physical basis which restricts its accuracy in forecasting extreme events since these events often go beyond the range used to derive the IVRs. Projections of climate change anticipate extreme events to become more frequent in the UK such as convectional thunderstorms or hot dry spells. However, this project focuses upon winter where extreme climate events are not frequently observed and are not expected to change significantly (Murphy *et al.,* 2009) so this limitation should not affect the results of this project. The methodology used to generate hourly data suffers from the assumption of stationarity between daily and hourly statistics. Such stationarity may not apply but no data is available to perturb the relationships. This project will account for this by projecting weather series at a future time period sufficiently close to the control period thus reducing any potential changes in these relationships.

### 5.2 Climate Change Modelling: Dacre Beck 2050s Medium Emissions

In order to begin answering the first research question posed in Chapter 1 (section 1.6) the UKCP09 weather generator was applied to the Dacre Beck. It was intended that the results from this process would show changes in winter climate variables that affect snow accumulation. Therefore it was hoped that this would enable preliminary hypotheses about potential changes in the winter hydrograph to be formulated.

Firstly a future climate period and emissions scenario were selected, climate change would then be assessed according to these. It was decided to assess climate change in the 2050s (2040-2069) as this was sufficiently distant from present conditions making changes easier to detect yet not too distant so that the change factors were subject to high uncertainty. A medium emissions (A1B) scenario was selected as this represents the median emissions estimate within the weather generator, rather than the estimates of the

high and low scenarios. Next, the set of 5x5 km weather generator grid cells which overlay the Dacre Beck catchment were selected and the weather generator was run for 100 randomly selected samples of the input parameters (including the change factors). This produced 100 30-year stochastic simulations of the baseline period and another 100 of the future scenario climate period. In each simulation, each of the 29 continuous winters (December to February) were isolated, then climate statistics which affected snow accumulation and melt were calculated. These statistics included mean winter temperature, the mean winter temperature at the highest altitude (calculated by applying a lapse rate equation to the mean winter temperature), total snow and rain accumulation, total sunshine hours and total direct solar radiation. The mean winter temperature and that at the highest altitude would give an indicator of the likelihood of snowfall during that season. It was expected that trends in temperature would influence trends in snow and rain accumulation. These statistics could then in turn be used to infer possible changes to winter hydrology, for example if rainfall increases then the hydrograph variability may increase (Chapter 1 section 1.4). Finally, by assessing total sunshine hours and direct solar radiation it may be possible to estimate changes in the solar radiation energy flux that is incorporated within the third snowmelt model used in this project (Hock, 1999; Chapter 4 section 4.1).

After each statistic had been calculated for each continuous winter within a stochastic time series the mean of each statistic across the entire time series was calculated. For each statistic, this produced 100 hundred values for the baseline period and 100 hundred for the future scenario period. The future change for each temperature statistic was shown by plotting probability density functions (PDFs) of the baseline and scenario values which would demonstrate if the mean temperature exceeded the $0^0$C threshold in a future climate. PDFs were calculated for each of the 100 values for each statistic for each time period using the mean and standard deviation of each value series. This assigned a likelihood frequency to each value enabling a preliminary assessment of uncertainty within the climate projections. Change in the other statistics was assessed firstly by calculating the percentage difference between the values in the baseline period and those in the scenario. PDFs of the percentage change for each statistic were then calculated and plotted using the same method described above.

### 5.2.1 Projections of Winter Temperature

The graphs below show the weather generator projections of mean winter temperature throughout the whole catchment (**Figure 5.3** (**a**)) and at the highest elevation (**Figure 5.3** (**b**)).

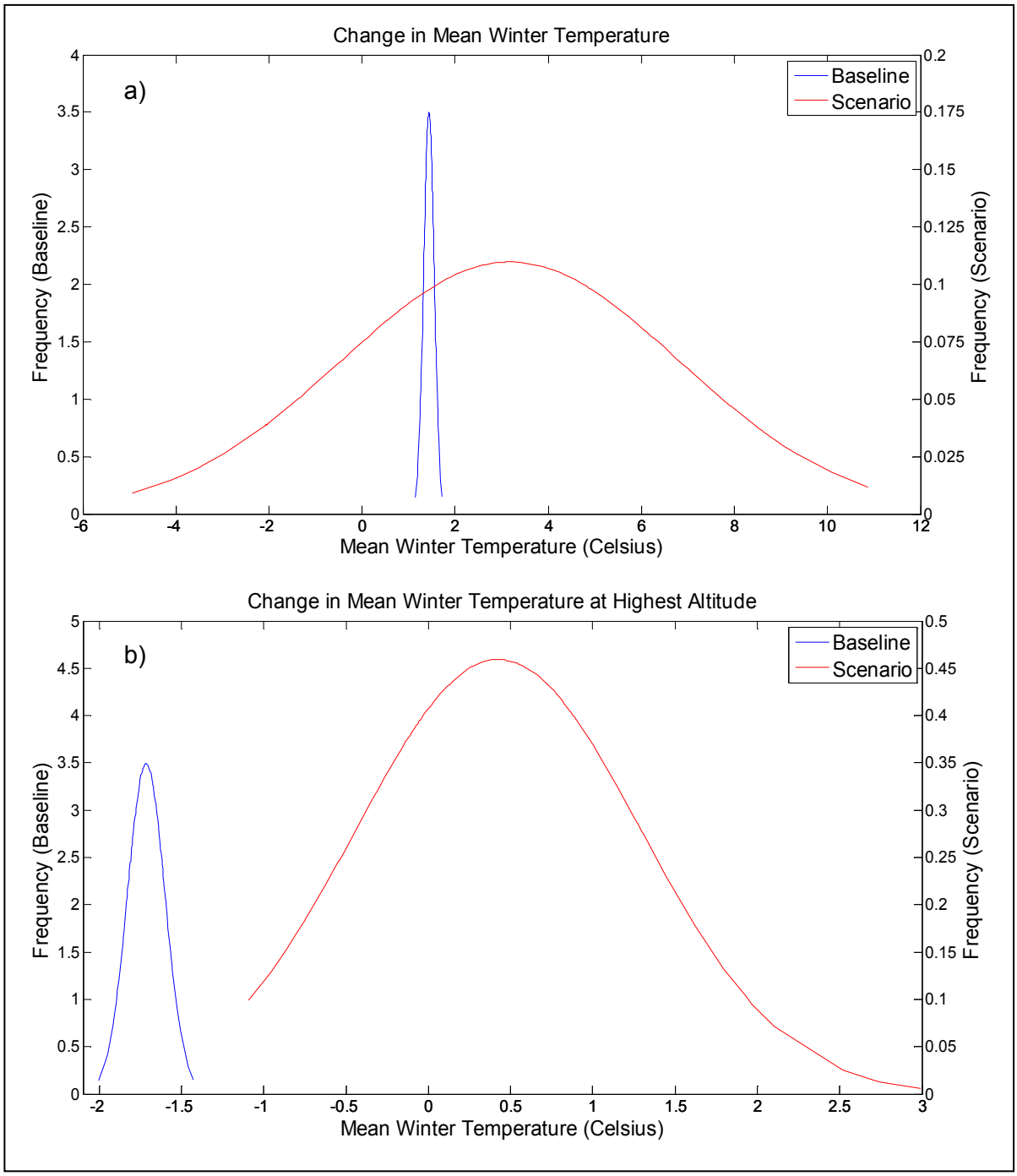


**Figure 5.3** Probabilistic estimates of the mean winter temperature for the baseline (blue) and scenario (red) periods across the whole catchment (**a**) and at the highest elevation (**b**).

Results from the first graph (**a**) showed that mean winter temperatures across the catchment were most likely to increase by 1.7°C however there was a wide spread in uncertainty from a warming of 9.5°C to a cooling of 6.5°C. This spread was caused by the method of calculating the mean catchment temperature whereby at each time step the temperature from the weather generator was firstly spatialised across the catchment using a lapse rate equation. The large elevation range within the catchment (Chapter 2 section 2.2) meant that temperatures at each time step across the catchment were highly variable. Hence when the mean temperature of all the values across the catchment at each time step was calculated it would have been subject to a large amount of elevation-induced variability. Calculating the mean temperature across the whole catchment for every winter season in each time series therefore, would have meant a wider uncertainty spread due to the incorporation of both spatial and temporal variability.

Projections from the second graph (**b**) for the scenario period showed a much narrower uncertainty spread as this assessed temperature change at one point in the catchment hence it was not subject to spatial variability. It showed that the mean winter temperature at the highest elevation (534 m) was most likely to increase from -1.75°C to 0.5°C. Furthermore the majority of the PDF curve lay above 0°C which meant that it was highly likely that a large number of winter days at the highest elevation in Dacre Beck would be above the freezing temperature.

Consequently the above results implied that less snow was likely to accumulate within the catchment including the higher elevations. Therefore it was reasonable to hypothesise that more precipitation would fall as rain which would have consequences for the winter hydrology of the catchment. Changes in snow and rain accumulation were analysed in the next section in order to verify these preliminary conclusions.

### 5.2.2 Projections of Winter Snow and Rain Accumulation

From the above projections in winter temperature (**Figure 5.3** (**a**) and (**b**)) it was anticipated that this would result in a decline in snow accumulation and an increase in rain accumulation. The accumulation of snow and rain was calculated firstly by summarising the amount of each within the catchment at each time step. A point in the catchment was assumed to contain snow fall if its temperature was lower than 0°C and the amount of precipitation falling was greater than 0 mm. Likewise, if precipitation at a point in the

catchment was greater than 0 mm and its temperature was greater than 0°C then rainfall was assumed to occur at that point. This enabled the sum of snowfall and rainfall across the catchment to be calculated at each time step (day). The sum of snow and rain accumulation for each winter within each stochastic time series was then calculated before the mean winter snow and rain accumulation across the time series was calculated. The percentage change in winter snow and rain accumulation were then calculated and plotted on the PDFs shown below (**Figure 5.4**).

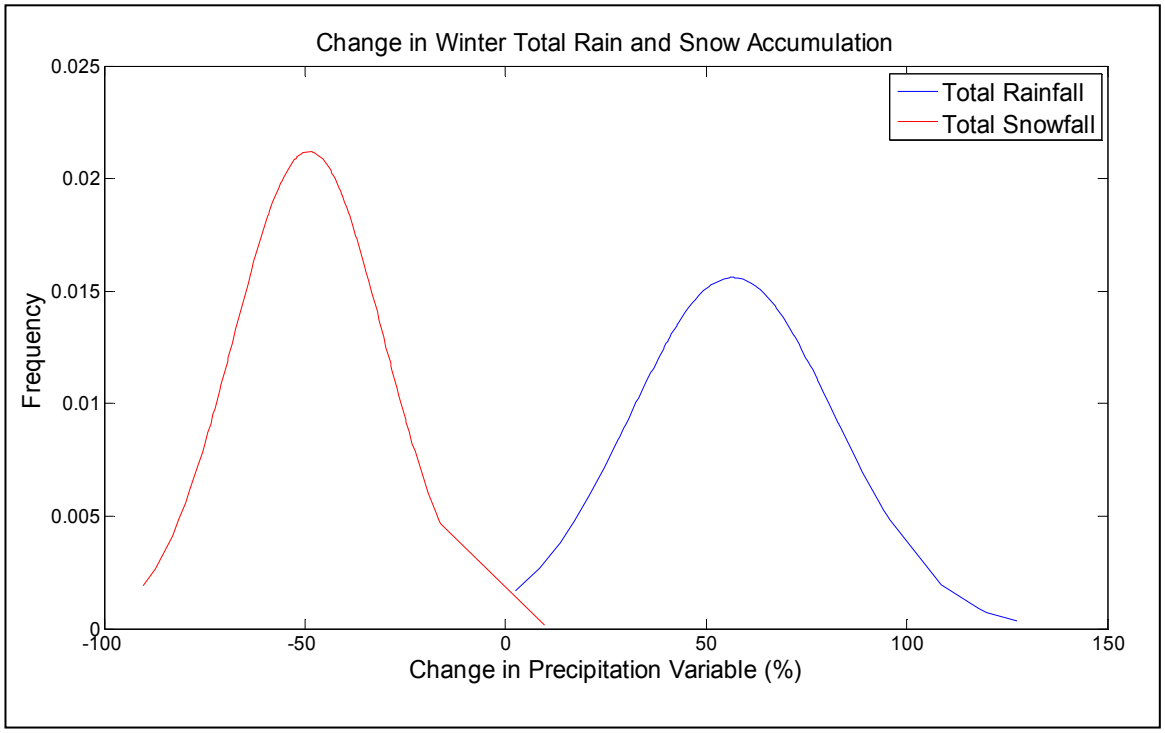


**Figure 5.4** Projections of percentage change in winter snow (red) and rain (blue) accumulation by the 2050s under a medium emissions scenario.

The above projections complimented those in the previous figure as they show that warmer temperatures by the 2050s will be accompanied by a decrease in snow accumulation and an increase in rain accumulation. A 49.5% decrease and a 57.0% increase were the most probable projections of changes in snow and rain accumulation respectively. As was expected, this showed that a decline in snow accumulation would be met with an increase in rain accumulation. The discrepancy between the decline in snow and increase in rain accumulation (the extra 7.5%) was caused by the increase in overall precipitation falling during the winter as forecast in the UKCP09 report (**Figure 5.1** (**b**)). Uncertainty in the amount of precipitation change may also explain why the spread of results in the rain accumulation PDF is greater than in the snow accumulation PDF (**Figure 5.4**). Therefore the results above could be interpreted as suggesting that more precipitation would fall during the winter and that proportionally more of this would fall as rain. It would be expected therefore that if the weather generator had only been perturbed

by changes in the temperature (as opposed to including precipitation perturbation), the decline in snow accumulation would have been matched by an equal increase in rain accumulation. The implications of the above results for the winter hydrology of Dacre Beck were expected to mean an increase in hydrograph variability. The decline in snow accumulation would have meant smaller snowpacks which in turn would have reduced their role in high flow attenuation and low flow supplementation.

### 5.2.3 Projections of Winter Solar Radiation

The weather generator produces daily values of sunshine hours and total direct solar radiation which is important for the solar radiation component contained within the third snowmelt model (Hock, 1999). The sum of total daily sunshine hours and direct solar radiation were calculated for each winter season within a time series and an average value across each time series was calculated. The percentage change for both variables was then calculated, in the same way as snow and rain accumulation before being plotted onto PDFs shown in **Figure 5.5**.

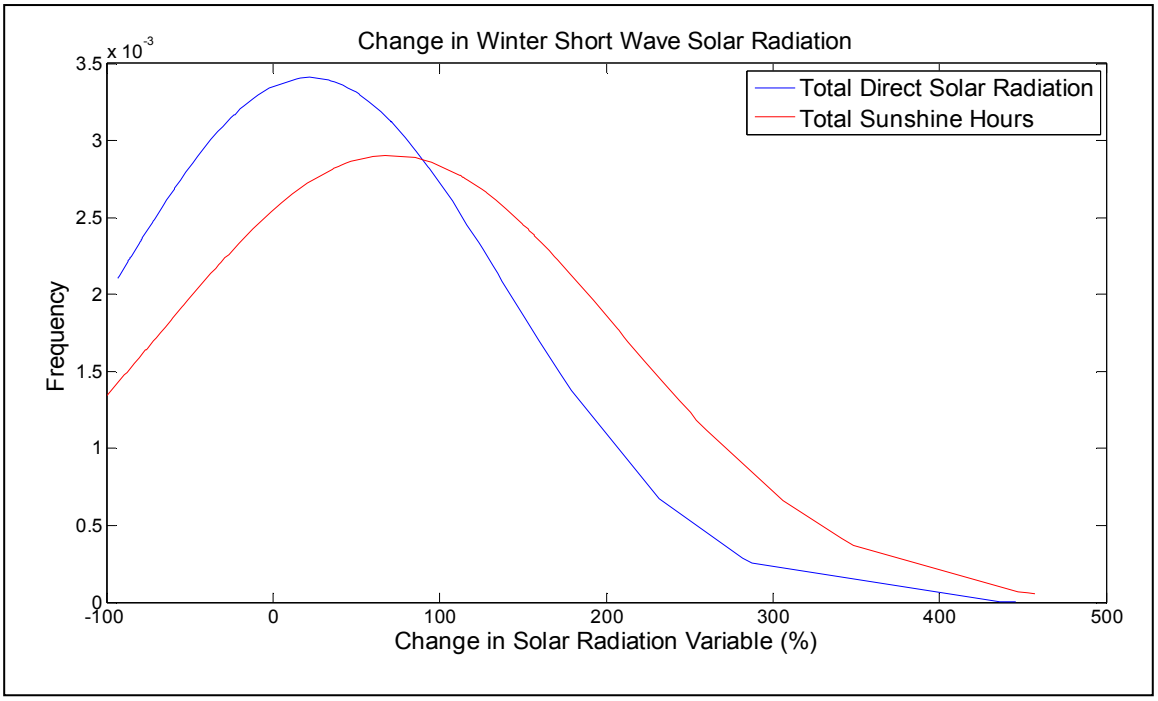


**Figure 5.5** Projections of change in the winter sum of total direct solar radiation (blue) and total sunshine hours (red) for the 2050s period under a medium emissions scenario.

The results (**Figure 5.5**) showed that the winter sum of both total sunshine hours and direct solar radiation were likely to increase by 70% and 20% respectively. This would

mean an increase in the solar radiation energy flux meaning that the smaller snowpacks which accumulate, in accordance with warmer temperatures (**Figure 5.3** (**a**) and (**b**)), would melt more rapidly potentially increasing the variability of the hydrograph. However, the wide spread of results (550% and 500% for sunshine hours and direct solar radiation respectively) meant it was not possible to state a probable change in either variable. For example, the maximum probability frequency for both variables is of an order of magnitude of $x10^{-3}$ (**Figure 5.5**). This wide spread of results could be due to a large amount of uncertainty within the change factors from the UKCP09 used to perturb the climate statistics in the weather generator. Therefore it was not possible to confidently state whether either solar radiation variable would increase or decrease.

### 5.2.4 Dacre Beck Weather Generator Conclusions

The application of the UKCP09 weather generator (Jones *et al.,* 2009) to the Dacre Beck catchment showed that under a medium emissions scenario the mean winter temperature across the catchment will have warmed by approximately 1.7°C by the 2050s. Mean winter temperature at the highest altitude is likely to rise above 0°C which could reduce the number of days during the winter when snow is falling at any point in the catchment. This result was reinforced by the projection of a 49.5% decline in snow accumulation during the winter. In turn, rain accumulation was projected to increase by 57.0% through a combination of warmer temperatures partitioning more precipitation as rain and an overall increase in the amount of winter precipitation. It was not possible to obtain clear projections of the solar radiation flux which was most probably due to large uncertainty in the change factor by which the weather generator perturbed the relevant climate statistics. Overall, these results suggest that the snowmelt hydrology of the Dacre Beck may decline in significance in the future as smaller snowpacks accumulate and more precipitation is partitioned as rain. In order to assess the validity of this conclusion, the next section applied weather series from the weather generator to the distributed snowmelt model developed in the previous chapter.

## 5.3 Application of the Distributed Snowmelt Model

The results from the previous section allowed the formulation of the hypothesis that projected climate change would lead to increased winter hydrograph variability in Dacre Beck by the 2050s. This section aimed to test the validity of this hypothesis by applying the weather series to the distributed snowmelt model and analysing changes in the output

hydrograph. Firstly, the weather generator was run to produce 100 hourly series for the baseline and 2050s scenario periods for the same medium emissions scenario. Each weather series was then applied in turn to each snowmelt equation within the distributed snowmelt model. The snowmelt-only and snowmelt-rainfall hydrographs were extracted from each of the 29 continuous winters within each weather series. From these continuous winter periods the Q5 and Q50 were calculated for both hydrograph types. The percentage change in these statistics between the baseline and scenario periods were then calculated and plotted as PDFs for each snowmelt equation (**Figure 5.6** and **5.7**).

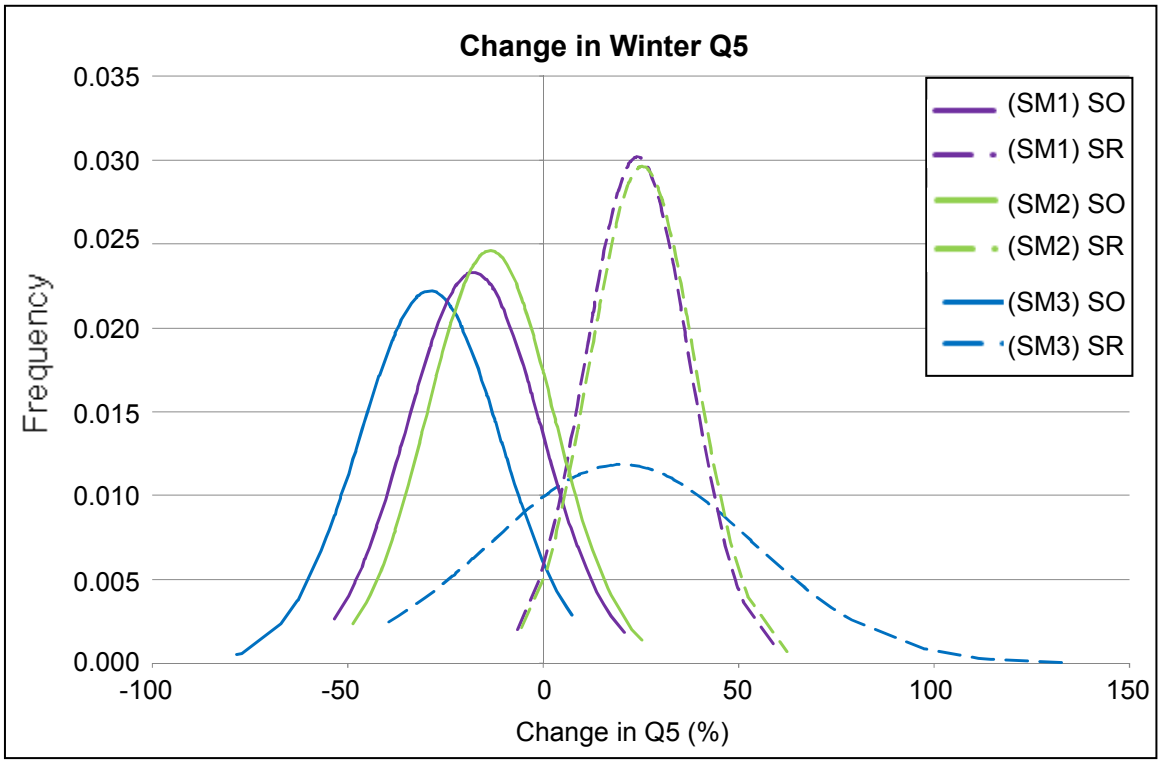


**Figure 5.6** Projections of change in the winter Q5 of Dacre Beck by the 2050s under a medium emissions scenario from the snowmelt-only hydrograph (SO) and snowmelt and rainfall hydrograph (SR) for each of the three snowmelt equations in the distributed snowmelt model (SM1, SM2 and SM3).

The projections from the above figure suggested that high flows derived solely from snowmelt will decrease from between 15% for snowmelt model 2 to 40% for the third snowmelt model. The third snowmelt model projected the greatest decrease because it incorporates more energy fluxes than the other two. It accounts for positive degree air temperature, rain-on-snow melt and clear-sky direct solar radiation all of which are projected to increase by the 2050s (see previous section). For example, total direct solar radiation was projected to increase by 20% (**Figure 5.5**), albeit with a wide uncertainty range, which would mean an increase in the amount of snowmelt produced by the solar radiation flux within the third snowmelt model. The decrease of low probability exceedence snowmelt flows is consistent with the projection of warmer temperature and decreased snow accumulation (**Figure 5.3** and **5.4** respectively) whereby smaller

snowpacks accumulate thus reducing the amount of melt water they can release. It would be reasonable however to expect the increases in the snowmelt energy fluxes, such as positive degree air temperature, to compensate for smaller snowpacks by producing more melt water per time step. For example, if the daily average temperature is projected to increase then more snow will be melted each day. What the above results (**Figure 5.6**) show however, is that the increases in these fluxes are insufficient to compensate for the decrease in snow accumulation.

Results from the combined snowmelt-rainfall hydrographs (**Figure 5.6** (SR)) meanwhile projected an increase in winter Q5 of 30% from all three snowmelt models. This increase could be due to the increase in winter rainfall (**Figure 5.4**) in light of warmer temperatures. When precipitation enters the catchment as rain it immediately begins to route towards the outlet (see Chapter 1), in the distributed snowmelt model it does this as surface runoff. Whereas when it falls as snow it is stored on the hill slope and releases melt water slowly. Therefore if the proportion of rainfall relative to snowfall increases (as projected in **Figure 5.4**) it would be expected that more water will be delivered to the catchment outlet per time step hence high flows would be expected to increase.

Projections from the third snowmelt model of winter Q5 for the combined snowmelt-rainfall hydrograph have a much wider spread of results (-40% to +130%) when compared to the other two snowmelt models (-5% to +65%) and hence a lower probability frequency across the range. This could be because the Q5 values were taken from the hourly hydrograph of the third snowmelt model but from the aggregated daily hydrograph of the other two. Typically, sub-daily hydrographs display greater variability than daily ones, for example in Dacre Beck the peak flow on December 3rd 2006 was 34.7 $m^3s^{-1}$ from a 15 minute hydrograph yet after aggregation to a daily hydrograph the value became 19$m^3s^{-1}$ (see Chapter 2 section 2.4). Therefore the hourly hydrograph from the third snowmelt model would have displayed greater variability than the other two snowmelt models hence the projections of Q5 would also have been subjected to this causing them to be spread across a wider range.

The projections and PDFs of Q5 from the first and second snowmelt models are very similar for the combined snowmelt-rainfall hydrographs and are also reasonably similar in the snowmelt-only hydrographs. This could be due to the relative unimportance of the

inclusion of the rain-on-snow flux in the second model which is the only difference between the two. The parameter governing this flux was found to be relatively insensitive in the sensitivity analysis carried out in the previous chapter (**Figure 4.3** (**b**)). Hence the small difference in results between the two models (**Figure 5.6**) may reinforce the results from the sensitivity analysis. An additional explanation for the similarity is that by including rainfall into the output hydrograph it overrides the differences between the snowmelt models. When the hydrographs were composed solely from snowmelt, subtle differences between each snowmelt model could be observed. However, when rainfall was included these differences became less detectable, the difference in the most probable change in Q5 was 5% between all three models whereas it was 25% when the hydrographs were composed solely from snowmelt. Therefore the similarity in the projections between the first and second snowmelt models are mostly probably the result of a combination of the two explanations outlined above.

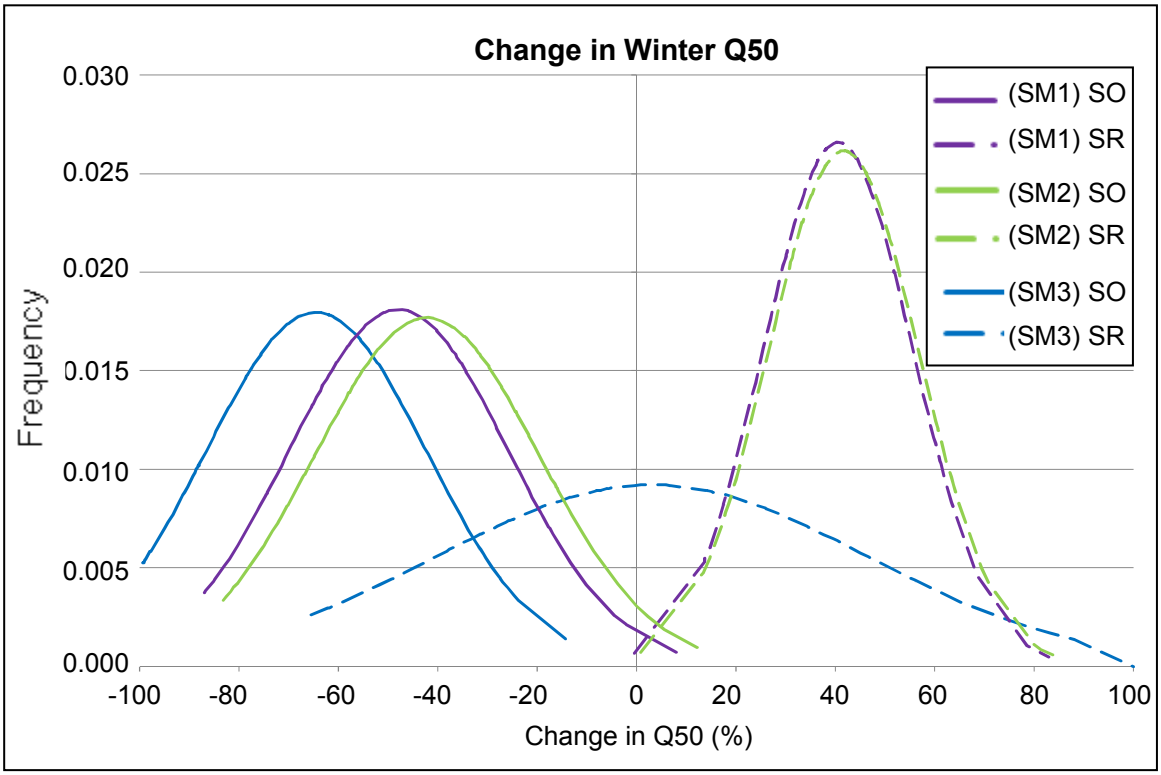


**Figure 5.7** Projections of change in the winter Q50 of Dacre Beck by the 2050s under a medium emissions scenario from the snowmelt-only hydrograph (SO) and snowmelt and rainfall hydrograph (SR) for each of the three snowmelt equations in the distributed snowmelt model (SM1, SM2 and SM3).

The projections of Q50 change (**Figure 5.7**) suggest a decrease in the snowmelt-only component for all three snowmelt models from 40% to 70%. This is consistent with the projection of decreased snow accumulation (**Figure 5.4**) as this will result in smaller snowpacks throughout winter which release smaller amounts of melt water. Therefore the winter snowmelt flow duration curve will consist of lower flows hence the flow at the 50$^{th}$ percentile will decrease. However the projections from the combined snowmelt-rainfall

hydrographs of the first two snowmelt models contradict the expectation that low flows will decrease as they exhibit a most probable increase of 40%. This could be due to the increase in winter precipitation (**Figure 5.1** (**b**)) being coupled with an increase in the number of days of precipitation falling which would mean shorter dry periods so low flows would increase. However, analysis of the weather generator series showed that the number of days of precipitation falling during the winter was not projected to increase (**Figure 5.8**).

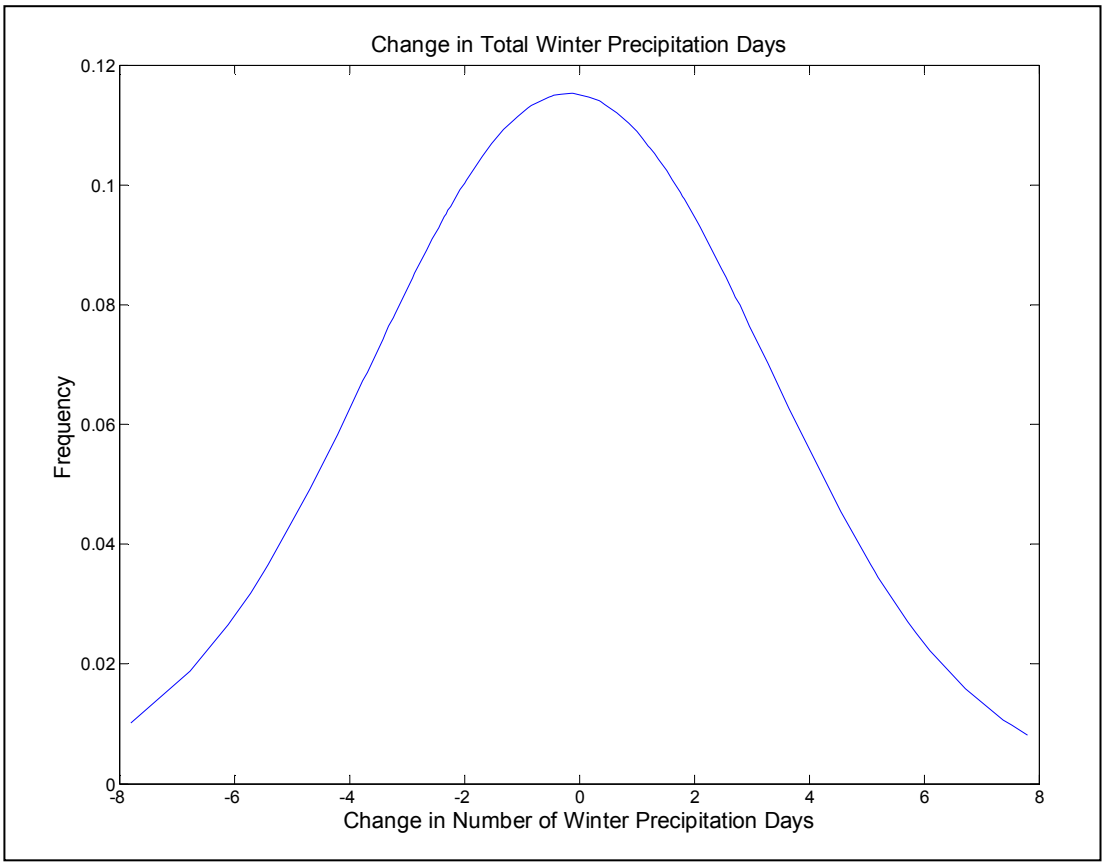


**Figure 5.8** Projections of change in number of winter precipitation days in Dacre Beck by the 2050s under a medium emissions scenario.

This means that if snowmelt release is decreasing and the number of precipitation days is not increasing it would be expected that the Q50 of the combined snowmelt-rainfall hydrograph should decrease by the 2050s. Conceptually, it is possible that because more precipitation is falling the amount of water stored in the soil will increase thus enhancing low flow supplementation with soil water flow. However, since the processes of infiltration and soil water flow are not included within the distributed snowmelt model this does not explain the results found above. Instead it is likely that process deficiencies within the distributed snowmelt model are the cause. As mentioned above, the model does not account for the processes of infiltration and soil water flow as it routes all snowmelt and rainfall to the catchment outlet as surface runoff. This will be problematic during dry

periods when, in reality, any snowmelt or rainfall that does enter the catchment would infiltrate very quickly. The infiltrated water would then be routed to the outlet through soil water flow which is much slower than surface runoff hence during the transit time the discharge at the outlet would continue to decline. In the case of the model however, any snowmelt or rainfall during dry periods is routed as surface runoff which would reach the outlet very quickly in comparison to soil water flow leading to an unrealistically large amount of low flow supplementation. Hence, when more precipitation falls as rain by the 2050s more water reaches the outlet, even during relatively dry periods, thus low flows actually become higher. Interestingly however, the projections from the third snowmelt model show a wide spread of results centred on a change of 0%. As mentioned above, the wide spread of results is due to the hourly time step of this snowmelt model. The hourly time step of this snowmelt model may also explain why the most probable projection of change is almost negligible because at this resolution low rainfall and hence discharge values are very small. Hence, detecting changes in these small values is very difficult and can produce a wide range of results.

Overall, running the distributed snowmelt model using stochastic weather simulations for the baseline and 2050s periods under a future medium emissions scenario showed that the role of snowmelt is likely to decline in its contribution towards both high and low flows. The projected increase in winter rainfall is likely to cause an increase in the magnitude of Q5 flows as well as in Q50 flows. However the poor process representation of the distributed snowmelt model jeopardises the validity of the Q50 results and needs further investigation.

### 5.4 Climate Change Modelling Conclusions

This chapter has shown that projected climate change is likely to see warmer and wetter winters in Dacre Beck by the 2050s under a medium emissions scenario which are likely to cause a reduction in snow accumulation and hence melt water production. Using these projections, the distributed snowmelt model found that winter snowmelt hydrology was likely to decrease. The model however was unable to assess the impacts of changes in snowmelt hydrology upon the winter flow regime due to its poor physical basis. It was decided therefore to incorporate each snowmelt model equation within a physically-based hydrological model and to re-perform the above analysis.

# Chapter 6

# Snowmelt within the Connectivity Runoff Model (CRUM)

## 6.1 Hydrological Model Selection

In Chapter 5 it was argued that there was a need to incorporate each of the snowmelt equations into a physically-based hydrological model in order to improve the process representation involved in the generation of high and low winter flows. Analysis of low flows produced from the distributed snowmelt model (Chapter 5) raised concerns on their validity due to the model treating all snowmelt and rainfall as runoff. Therefore, since the hydrological model developed by this project had poor process representation, it was decided to improve upon an existing physically-based hydrological model by incorporating each of the snowmelt equations. This chapter will firstly outline how a suitable existing hydrological model was chosen before outlining the changes that were made to it in order to enable the incorporation of snowmelt. The final part of this chapter will then calibrate the model output to an observed hydrograph and assess the uncertainty with explicit treatment of uncertainty from each of the snowmelt equations. This chapter therefore intended to create a physically-based hydrological model of Dacre Beck for which the climate change impacts upon winter high and low flows could be assessed using the same methodology as the previous chapter.

There are a large number of hydrological models in existence, such as Topography Model (TopMODEL (Beven and Kirkby, 1979; Quinn *et al.,* 1995; Beven, 1997)), Soil Water Assessment Tool (SWAT (Neitsch *et al.,* 2005; Easton *et al.,* 2008)), Systeme Hydrologique Europeén (SHE (Bathurst, 1986a;b and Abbott *et al.,* 1986a;b), Probability Distributed Model (PDM (Moore and Clarke, 1981; Moore, 2007)) and the Connectivity Runoff Model (CRUM (Reaney *et al.,* 2007; Lane *et al.,* 2009)). In order to select the most suitable, each model was compared according to a set of criteria that reflected the requirements of this project. The criteria included that the model was physically based, that it had simple data requirements and its code structure was easily modified. By assessing each hydrological model using these criteria it was found that the CRUM (CRUM2D v3.1 (for original CRUM see Reaney *et al.,* 2007, for CRUM2D v3.1 see Lane *et al.,* 2009) was ideal for this project. Although it was initially conceptualised for hill-slope event-scale modelling of semi-arid catchments (Reaney *et al.,* 2007) it has been used in the UK at a catchment-scale with successful results. For example, it was applied to the Upper Rye in North Yorkshire to characterise space-time patterns of overland flow connection (Lane *et al.,* 2009). It is a physically based model; its process representation will be described in the next section. It also has minimal data and parameter input requirements with the intention that it could be applied to any UK catchment using national datasets (Lane *et al.,* 2009). In terms of the former, it requires daily rainfall and minimum

and maximum temperature, all three of these are available in Dacre Beck. The CRUM code is structured using an object-oriented approach whereby each process is contained within a module making it easier to modify existing processes and add new ones (Reaney *et al.,* 2007). Before the application and development, CRUM had no treatment of snow accumulation or melt so a new snow module needed to be created in order to incorporate the snowmelt equations.

### 6.2 Connectivity RUnoff Model (CRUM)

CRUM2D v3.1 is a fully-distributed, physically-based, object-oriented model which has been applied to hydrological modelling in the UK (Lane *et al.,* 2009). Two of its founding facets were that it should use minimal input data and parameter sets which are available at any catchment within the UK and that its spatial representation of process description should be explicit (Lane *et al.,* 2009). The latter facet means that the model is fully-distributed (whereby the process equations are applied to each pixel within the DEM) which was originally intended to be useful in land management applications. However in this project the fully-distributed spatial representation of CRUM will allow for spatial variations in snowmelt due to the temperature lapse rate and catchment characteristics which affect solar radiation such as hill slope aspect and gradient. CRUM is physically-based in that the equations used to represent the processes deal explicitly with the physical forces behind the processes as opposed to being empirically derived, such as the temperature-index snowmelt equations. The object-oriented structure of CRUM means that it deals with an object, in this case water, routing it through a series of modules which represent the various physical processes. A brief description of these processes is given below but a more detailed description can be found in Appendix A of Lane *et al.,* (2009).

The process modules are structured into four sections: weather, point hydrological processes, landscape and river channel network (Lane *et al.,* 2009). The weather section uses three variables: rainfall, temperature and solar radiation to drive hydrological processes and vegetation growth for the first two variables respectively. Temperature is also used alongside solar radiation to calculate evapotranspiration rates, the latter is calculated using the same method outlined in Chapter 3 (section 3.2.1). The rainfall is downscaled to the per-minute scale in order for the model to capture the point hydrological processes, such as overland flow, which occur at this temporal resolution. A rainfall generator (based on Mulligan, 1996) is used that: reads daily rain depth, generates individual storm totals using a Monte Carlo model, generates per-minute rainfall intensities

using a Monte Carlo model which uses parameters from the observed data before finally placing the storms at random points in the day (Lane *et al.,* 2009). The per-minute parameterisation is obtained from observed tipping-bucket rain data. Although such data does not exist within Dacre Beck previous testing of CRUM in Dacre Beck found that good results can be achieved if tipping-bucket data from within the North Yorkshire region was used (Pattison, 2010). Temperature data is also downscaled to this resolution using an equation in the weather generator which relates daily minimum and maximum air temperature to the current time of the day (Lane *et al.,* 2009).

The point hydrological processes are calculated for each spatial unit in the landscape. A brief, qualitative description of these processes (**Figure 6.1**) will be given in this section, a more detailed, quantitative description including the conceptual equations is given in Appendix A of Lane *et al.,* (2009). Firstly at each time step, precipitation, *P* enters a point and is divided between interception, *Pi* which falls onto the vegetation canopy store and direct precipitation, *Pd* which bypasses this. The amount of interception is controlled by the vegetation parameters such as gap fraction (which controls the *porosity* of the canopy). The canopy is treated as a non-leaking store which stores water until it overflows whereby water can exit either as evaporation, which is classed as the interception loss *I* or transmission to the surface, *Pt*. The magnitude of evaporation is calculated from the Priestley-Taylor (Priestley and Taylor, 1972) equation of potential evapotranspiration. After the incorporation of snowmelt the sum of *Pd* and *Pt* will be partitioned either into rainfall, *R* or snowfall, *S* depending on whether the temperature is above or below $0^0$C. A description of this incorporation is given in the next section. Currently however, the sum of

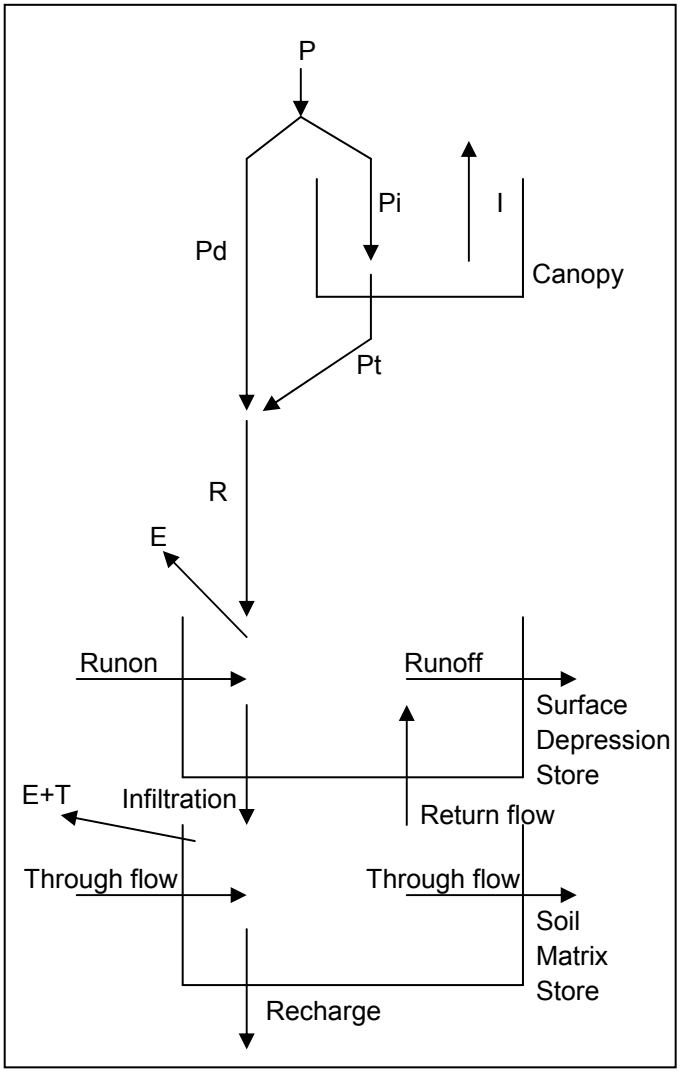


**Figure 6.1** Point and landscape hydrological process representation of CRUM2D v3.1 adapted from Reaney *et al.,* (2007) before incorporation of snowmelt processes. See text for a definition of each term.

*Pd* and *Pt* enters the surface depression store where runon, runoff from the point upslope, is added. The depth of this store is determined from the surface roughness and gradient (Kirkby *et al.,* 2002; Lane *et al.,* 2009). Water in this store can then infiltrate downwards into the soil matrix store, runoff laterally to the next cell or evaporate, *E*. The magnitude of evaporation from the vegetation and soil surface occurs at the potential rate determined from the Priestley-Taylor equation, the evaporation rate from the soil surface is reduced as a function of soil moisture. Infiltration is determined using a simplified equation of the Green and Ampt (1911) equation (Kirkby, 1975; 1985). Runoff is generated either through infiltration excess, saturation excess or return overland flow (Lane *et al.,* 2009). Infiltration excess runoff generation occurs when the rainfall rate is greater than the current infiltration capacity of the soil (Dingman, 1994). Hence in this situation infiltration occurs at the maximum rate and the excess water becomes runoff. Saturation excess runoff generation occurs when the maximum water holding capacity of the soil store is reached as no additional water can enter the soil hence it becomes overland flow (Kirkby, 1978). Return flow is the process of through flow in the soil matrix store exceeding the storage capacity hence the excess overflows into the surface depression store.

Water infiltrating into the soil matrix store is joined by through flow from the upslope cells and it can then exit the cell through transpiration *T,* evaporation *E*, through flow to the downslope cell and runoff generated by return flow. Evaporation and the transpiration are calculated from the Priestley-Taylor equation with the latter being related to the leaf area index of the vegetation, the rooting depth and amount of water available in the soil. Recharge is determined by the hydraulic conductivity at the base of the soil and the bedrock conductivity. Water is assumed to be lost through this process hence CRUM is not suitable for catchments with a significant groundwater component, such as those dominated by Carboniferous Limestone. Dacre Beck is dominated by igneous rocks (Chapter 2 **Figure 2.10**) and although some limestone is present it was not expected to significantly affect the hydrological processes within the catchment. Through- and hence return flow are calculated as part of the landscape processes section explained below.

Landscape processes affect the lateral movement of water from the cell to the next one downslope via the processes of runoff and through flow. In order to model through flow the soil layer is firstly divided into a dynamic layer which is the saturated zone and an overlying unsaturated zone. Through flow in the saturated zone is determined through Darcy's law whilst the flow in the unsaturated zone is considered to be negligible. Runoff

is dealt with as being a combination of laminar, transitional and turbulent flows (Lane *et al.,* 2009) so the Darcy-Weisbach equation is used to calculate its velocity into the next cell. The amount of runoff is divided between all downslope cells using the FD8 multiple flow direction algorithm (Quinn *et al.,* 1991, see Chapter 2 section 2.5.1 for a description).

Flow through the river channel network is modelled using the Muskingham-Cunge approach (Ponce and Lugo, 2001). Each river reach is associated with a landscape cell, at each time step flow enters the cell from overland flow, soil through flow and discharge from an upstream cell if there is a connection. The discharge from the cell is calculated as a function of the discharge at the previous time step and inflow at the current and previous time steps (Lane *et al.,* 2009).

### 6.3 Incorporation of Snowmelt into CRUM

Each of the three snowmelt equations from Chapter 4 (*Eqs. 4.2, 4.3* and *4.4*) were incorporated into the CRUM2D v3.1 structure as shown in **Figure 6.1**. A new class called *CSnow* was created which lay below the canopy class and above the depression store class (**Figure 6.1**), each of the snowmelt equations were added into this new class. This meant that when a water object entered a cell in landscape it would still be subjected firstly to interception. The sum of *Pd* and *Pt* would then be inputted into the snow class as snowfall if the temperature at that landscape cell was lower than the threshold melt temperature thus allowing a snowpack to accumulate. If at the subsequent time step the temperature at that landscape cell was equal to or greater than the threshold melt temperature one of the three snowmelt equations would be applied to the accumulated snowpack within that cell. The resulting melt water would then be added to rainfall in that cell and would enter into the depression store. The variables that were required in the snowmelt equations, including temperature, rainfall and solar radiation were read in from the weather generator class (*CWeatherG*). Each of the parameters for each snowmelt equation were defined in the main parameter input file along with a setting which informed the model of which snowmelt equation to apply.

The temperature lapse rate equation was included into the weather generator class by creating a temperature modification grid which overlaid each landscape cell. Each cell value of the modification grid was calculated by subtracting the elevation of the weather observation station from the elevation of the respective landscape cell and then multiplying this by the temperature lapse rate. The temperature at the landscape cell can then be found by adding the temperature from the weather generator to the respective value from the modification grid. It was not necessary to add a precipitation lapse rate equation into CRUM as it already scaled precipitation depth with altitude using a spatially distributed scaling factor (Lane *et al.,* 2009) obtained from spatial pattern maps such as those found in the Flood Estimation Handbook.

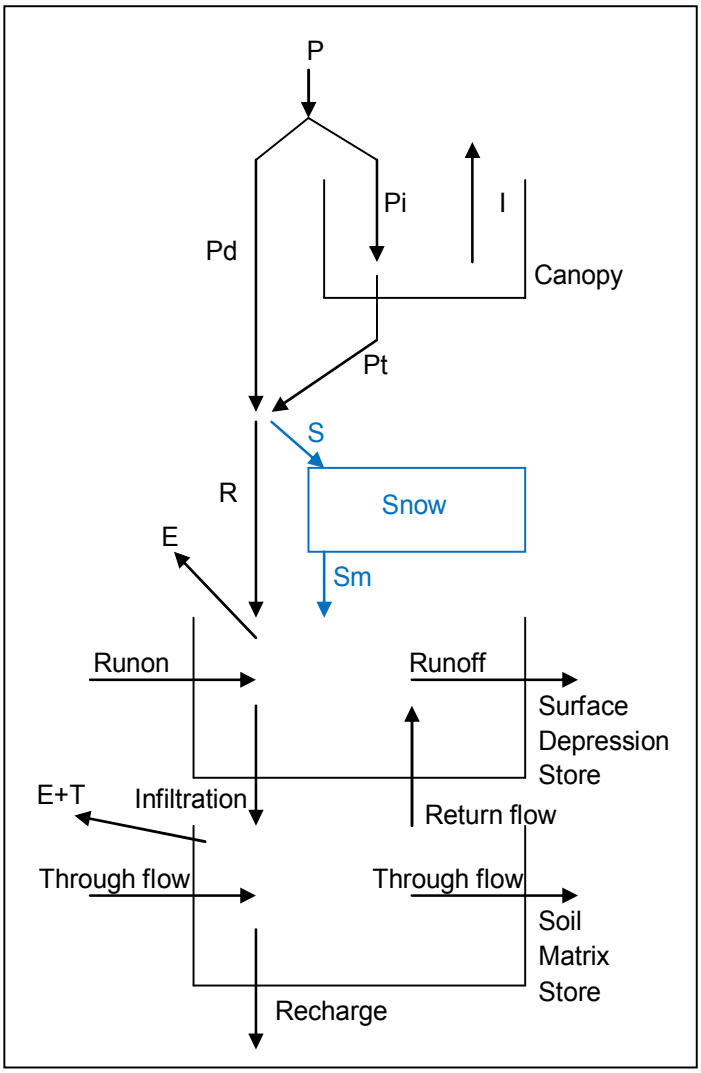


**Figure 6.2** Point and landscape hydrological process representation of CRUM2D v3.1 adapted from Reaney *et al.,* (2007) after incorporation of snowmelt processes (shown in blue). See text for a definition of each term.

The output mass balance of CRUM after the inclusion of these equations was assessed in order to verify that water mass was being conserved. A mass balance equation similar to that in Chapter 4 Eq. 4.5 was already contained within CRUM, using this it was found that CRUM was still successfully conserving mass. The assessment of the sensitivity of the parameters, including those of the snowmelt equations, as part of the calibration and uncertainty assessment process is outlined in the next section.

## 6.4 Calibration, Uncertainty and Sensitivity Assessment

### 6.4.1 Calibration and Optimisation

Calibration is the process of adjusting the model inputs so that its outputs are a reasonably realistic representation of reality (Gupta *et al.,* 1998). The need for the process was borne out of the realisation that no hydrological model is a perfect representation of reality (Beven, 2002). Instead, the processes that are included within a hydrological model are approximations of processes that occur at a finer spatial or temporal scale. In CRUM for example, soil water through flow in the soil profile is approximated by the *kSat* (saturated hydraulic conductivity) parameter. For a model that represents multiple processes, such as CRUM, there will be many parameters. A suitable value for any given parameter that best represents the wide variety of spatial and temporal conditions within the catchment must be chosen in order for the model to produce realistic results. Fieldwork could be undertaken to ascertain a realistic value for each parameter but it would be very difficult to carry this out at the spatial and temporal resolution that was required by the model. Furthermore, fieldwork is unable to deal with interactions between the different parameters as it derives a value for each in relative isolation. The most efficient method of finding suitable values for each parameter is through a computational optimisation routine where all of the model parameters are adjusted simultaneously until the optimal model output has been achieved.

Firstly, in order to assess how good the model is at representing the physical system, it must be run for a calibration period. This is a period of time for which observed input, daily precipitation and minimum and maximum temperature, and output data, river discharge hydrograph are available. The model is then run using the input data in order to produce a modelled output discharge hydrograph which can be compared to the observed discharge hydrograph. The goodness of fit between the observed and modelled hydrographs can be quantified through an objective function which differs from the output metrics used in Chapter 4 (section 4.2.2.4) as it is intended to assess goodness of fit as well as sensitivity.

The calibration period that is used must contain a wide range of catchment conditions in order to maximise the robustness of the analysis. Previous research found that the length of the calibration period was of secondary importance to the information contained within the period (Yapo *et al.,* 1996). Juston *et al.,* (2009) found that a calibration period of between 2 to 3 years contained sufficient information to robustly calibrate a hydrological

model. It was decided to use a calibration period from May 2007 to May 2009 as this would enable the analysis of two continuous winter seasons. The 2008/2009 winter was one of the coldest winters over the period for which the observed hydrograph was available whilst the 2007/2008 winter was relatively mild with 20mm less snowfall (see **Table 2.1** in Chapter 2 section 2.4). It is therefore reasonable that this calibration period represents the range of winter conditions that the hydrological model would have to represent. It should be noted that the model was actually run from January 2007 but the calibration analysis was only started in May 2007, this was to ensure that the model had accurate initial conditions.

There are a number of objective functions available which can quantify the goodness of fit between a modelled and observed hydrograph. The most common of these within hydrological modelling is the efficiency statistic of Nash and Sutcliffe (1970):

$$NS = \frac{F_o - F}{F_o} \quad \text{(Eq. 6.1)}$$

$$F_o = \sum_{i=1}^{n} (q - \bar{q})^2 \quad \text{(Eq. 6.2)}$$

$$F = \sum_{i=1}^{n} (q' - q)^2 \quad \text{(Eq. 6.3)}$$

Where $q$ = observed discharge, $q^-$ = mean observed discharge and $q'$ = modelled discharge. This produces a result ranging from -∞ to +1 where negative values imply the model is of a poorer quality than a random number generator with the same mean as the observed flows and a positive result implies that it is better. This objective function was used in this calibration as it gave a clear indication as to the predictive quality of the model output and has been widely used in previous hydrological modelling studies (Lane *et al.,* 2009). However, because this objective function squared the difference between the observed and modelled discharge values (*Eq. 6.3*) the resulting statistic could be biased towards the prediction of higher flows. Since this project was concerned with both high and low flows another objective function was applied simultaneously. Lane and Richards (2001) suggest the relative mean absolute error (RMAE) as being a suitable objective function for the prediction of low flows:

$$RMAE = \frac{1}{n} \sum_{i=1}^{n} \left( \frac{q - q'}{q} \right) \quad \text{(Eq. 6.4)}$$

Where *n* is the number of predictions in the output time series. Therefore both objective functions were used in a multi-objective calibration procedure (Li *et al.,* 2010). This would ensure that the parameter set which best modelled high and low flows would be found.

Next, the parameters within CRUM that were to be adjusted along with those in the snowmelt equations were chosen. A sensitivity analysis similar to that in Chapter 4 (section 4.2.2) could have been carried out to identify which ones were sensitive and hence which ones should be included within the calibration procedure. Previous work carried out in Dacre Beck found that the parameters listed in **Table 6.1** were the most sensitive and was able to define their feasible ranges (Pattison, 2010).

| Parameter | Minimum | Base Case | Maximum |
|---|---|---|---|
| Saturated Hydraulic Conductivity *(kSat),* [$ms^{-1}$] | $2 \times 10^{-5}$ | $2 \times 10^{-4}$ | $2 \times 10^{-3}$ |
| Hydraulic Conductivity Decay with Depth, (*kDecay*), [$ms^{-1}m^{-1}$] | -1.00 | -3.00 | -7.00 |
| Root Layer Depth, (*rootDepth*), [m] | $5 \times 10^{-4}$ | $5 \times 10^{-2}$ | 0.10 |
| Root Layer Saturated Hydraulic Conductivity, *(rootkSat*), [$ms^{-1}$] | $2 \times 10^{-5}$ | $9 \times 10^{-3}$ | $2 \times 10^{-3}$ |
| Soil Depth Channels, *(SD Chan),* [m] | 0.30 | 1.00 | 1.50 |
| Soil Depth Ridges, (*SD Ridges*), [m] | 0.35 | 0.80 | 1.50 |
| Soil Depth Slopes, (*SD Slopes*), [m] | 0.10 | 0.16 | 1.20 |
| Porosity, [Dimensionless] | 0.05 | 0.20 | 0.80 |

**Table 6.1** The hydrological parameters within CRUM that were included in the calibration process including their feasible ranges.

Automatic optimisation or hill-climbing algorithms were developed in order to find the *optimal* parameter set (Beven, 2002) within the total parameter space (outlined in **Table 6.1**). These techniques operate within pre-defined ranges for each parameter and aim to

find the peak of the response curve for each parameter (**Figure 6.2**). In the idealised example in **Figure 6.2** the hill-climbing technique would start at one of the tails of the response curve. The techniques would then generate a random sample from within the feasible parameter space. The model would then be run with the sampled parameter set and the change in the gradient of the objective function response curve would be assessed. The resulting response gradient informs the technique about where in parameter space to take the next sample in order to climb the response curve. When the peak of the response curve is found the technique has found the best parameter set. In reality the shape of the parameter response curve is not as simple as that in **Figure 6.3** as there may be multiple local optima. Algorithms such as the Shuffled Complex Evolution (SCE (Duan *et al.,* 1992)) have been developed to enable searches in parallel which allows global information about the response surface to be shared (Beven, 2002). However the concept of identifying an optimal parameter set does not provide any assessment of uncertainty within the modelling process as it assumes that only one single parameter set provides a good representation of the system being modelled.

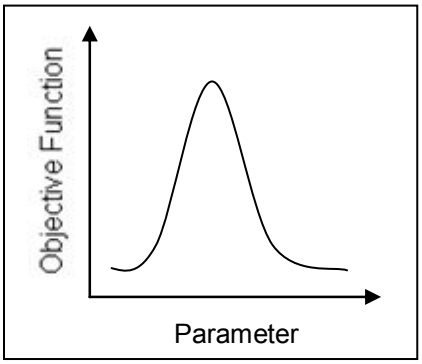


**Figure 6.3** Conceptual response curve for a single model parameter

### 6.4.2 Uncertainty Sources

Within any hydrological modelling study the results will be subjected to errors arising from different sources including input and calibration data errors, structural errors within the model and parametric uncertainty (Beven, 2002; McMillan *et al.,* 2010). Each of these error and uncertainty sources combines to create predictive uncertainty in the model output. In this study, input data errors could arise from errors in the rainfall and temperature gauging. For example because the precipitation gauge is located at a low elevation within the catchment it is possible that it might not record every precipitation event. In catchments with a large elevation range some precipitation events can be confined to the higher elevations. Whilst a precipitation scaling factor is included within CRUM to account for the increase in precipitation with altitude, if the gauge fails to catch a precipitation event then this may propagate through to produce errors in the model output. Errors in the input data could be assessed by including data from neighbouring gauges however these gauges were found to be located at similarly low elevations. Furthermore the network of neighbouring gauges was sparse, the closest precipitation gauge was at Tirril located 4 km outside of the catchment. Therefore the incorporation of additional

gauges would be unable to assess the uncertainty arising from the failure to catch localised precipitation events and was not included in this assessment.

Errors in the calibration data relate to the observed discharge hydrograph series and can arise from the rating curve used to derive the discharge from stage measurements (McMillan *et al.,* 2010) as in Dacre Beck (see Chapter 2 section 2.4). Uncertainties in the rating curve can result from errors in the measurement of stage and discharge, extrapolation of the curve beyond the maximum gauging and cross-section change due to vegetation growth or bed movement (McMillan *et al.,* 2010). It was likely however that the errors associated with each component of the total rating curve error would be small. Errors in stage and discharge measurement can be caused by errors in the equipment however previous research found that these errors were only significant in extreme flows (above 100 $m^3s^{-1}$ (McMillan *et al.,* 2010)) much greater than those in the Dacre Beck discharge record. In addition, the maximum discharge (14 $m^3s^{-1}$) during the calibration period chosen in this analysis did not exceed the maximum gauging value (26 $m^3s^{-1}$). Finally, vegetation growth and channel change were not expected to provide large sources of uncertainty as there was no vegetation in the channel and the cross section at the gauging station only had a very thin layer of sediment overlying the bedrock (see the picture of the gauging station cross-section in Chapter 2 **Figure 2.3**). Furthermore, previous studies which found channel change to be a significant uncertainty source focussed upon large braided channels such as the Wairau River in New Zealand (McMillan *et al.,* 2010). These channels have very different geomorphological characteristics to the comparatively small channel at Dacre Beck. Therefore, uncertainty in the observed discharge data was not analysed as it was expected that, for the reasons explained above, it would not contribute a large amount to total uncertainty in this analysis.

Structural errors arise from the conceptual process representation within a model. These represent the assumptions of the modeller as to the processes that are important within a catchment. However a different model set up by a different modeller is likely to account for different processes that are in line with what they perceive to be important. Both models may yield reasonable representations of reality so the structural errors are the differences between the outputs of the different realistic models. The structural errors of CRUM could be assessed by comparing its output with those of other hydrological models but there was insufficient time to set these up. Instead the structural errors of each snowmelt

equation within CRUM could be assessed by comparing their predicted output whilst holding their parameter values constant.

Finally, parametric uncertainty occurs when multiple parameter sets produce realistic model outputs (Beven and Freer, 2001). The classical optimisation approach aimed to find the best single parameter set whilst rejecting all others. However there is no physical basis for rejecting a feasible parameter set that produces realistic model outputs. Instead, the *optimum* parameter set identified by classical optimisation routines is a product of the hill-climbing technique used. Therefore, when there are multiple parameter sets that produce realistic model outputs the uncertainty arises from how to estimate the physical system from the space of feasible parameter sets (Beven, 2006). This type of uncertainty led to the application of the theory of equifinality (Beven and Freer, 2001) and is one of the principles associated with the Generalised Likelihood Uncertainty Evaluation (GLUE) method discussed in the next section.

### 6.4.3 Uncertainty Assessment

This process aims to attach a probability to the modelled output resulting from a given set of inputs. For example, in order to account for parametric uncertainty a suite of randomly sampled parameter sets, Θ will be generated. Each parameter set, $\theta$ will be inputted into the model producing a time series of output predictions, $q'$ which in this case is discharge. The aim is then to assess the predictive uncertainty associated with this predicted time series by comparing it with observed data, $q$. In this project it was intended to assess parametric uncertainty within Θ and then to compute the banded uncertainty ranges. The parameter sets, $\theta$ which lay within this range would then be used as inputs to run the model with climate change data in the next chapter. The existing methodological approaches used to perform an assessment of modelling uncertainty are discussed below.

The statistical theory of Bayesian inference has been widely used in uncertainty assessments of hydrological modelling. It is an extension of Bayes' theory whereby observations, in this case the discharge series produced by the model, are assigned a probability that a hypothesis may be true. The hypothesis here is that the model with its given inputs such as $\theta$ gives a good representation of the hydrological system in question. Formal application of this theory assigns a probability distribution of predicted (modelled)

flows from a posterior distribution for a given set of inputs, *θ* (Romanowicz *et al.,* 1994). The posterior distribution for a series of predicted discharge time series, *P(θ|Y)* is based upon the prior distribution of inputs, *P(θ)* and a likelihood function, *L(Y|θ)* (Jin *et al.,* 2010)

$$P(\theta|Y) = \frac{L(Y|\theta)P(\theta)}{\int L(Y|\theta)P(\theta)d\theta} \alpha L(Y|\theta)P(\theta) \quad \text{(Eq. 6.5)}$$

A detailed description of how to implement this within hydrological modelling is given by Romanowicz *et al.,* (1994) and Thiemann *et al.,* (2001) but a brief explanation is given below. The prior distribution reflects existing knowledge of the system before the modelling of the catchment has begun. Previous work carried out in similar catchments may allow a prior distribution for an input parameter with a likelihood distribution similar to that in **Figure 6.3** to be created. A suite of parameter sets is then randomly sampled from within the defined space of each parameter according to the prior distribution. The model is then run for each set within the suite, the likelihood function and hence posterior distribution is then calculated for each set before integrating across the entire suite as in *Eq. 6.5*. Concern has been raised that in many cases in hydrological modelling there is insufficient data to define a prior distribution without biasing the resulting posterior distribution (Beven and Young, 2003). Proponents of the methodology however suggest that the prior distribution is not meant to be interpreted literally (Mantovan *et al.,* 2006). Instead, providing that a sufficient number of parameter sets are sampled, the method should be able to converge upon a stationary posterior distribution regardless of any initial bias from the prior distribution.

The likelihood function is calculated from data produced from the hydrological model and combined with an error model to represent the errors arising from the structure and input data. In order to construct the error model the modeller must make prior assumptions about the shape of errors contained within the predicted series. For example Romanowicz *et al.,* (1994) constructed the following error model:

$$\delta_t^* - \eta = \sum_{i=1}^{P} \alpha_i(\delta_{t-i}^* - \mu) + \epsilon_t \quad \text{(Eq. 6.6)}$$

Where *ή, ά$_i$* and *έ$_t$* are parameters for the mean (which was assumed to be constant), autoregressive parameter series and the residual (assumed as normal white-noise error with variance $\sigma^2$). Prior distribution information is required for each of these parameters hence to obtain the marginal posterior distribution for the input parameter set the joint posterior distribution must integrated with the error model parameters (Thiemann *et al.,* 2001). Other studies assume different error models, for example Jin *et al.,* (2010) assume

a simpler error model based solely on $\acute{\varepsilon}_t$, the model residuals, which previous work found worked better for models at a monthly time step (Xu, 2001). In the case of a monthly model the assumptions that the model residual errors: 1) had a mean of zero and constant variance, and 2) were mutually uncorrelated (Xu, 2001) were found to be valid. Hence this error model was appropriate for the study of Jin (*et al.,* 2010) but would not necessarily be applicable to CRUM which operates at much shorter time steps (two minutes to six hours).

Convergence upon the stationary posterior distribution can be achieved through a recursive inference whereby the posterior distribution is continually updated after a suite of runs (Freni and Mannina, 2010). For example a Monte Carlo Markov Chain algorithm (McMillan and Clark, 2009; Jin *et al.,* 2010) starts from an initial parameter set and randomly generates new ones based on the prior distribution. The model is then run using these sets and the posterior distribution is calculated. The next set of parameter sets are then generated from the posterior distribution which is now treated as a prior distribution, the new posterior distribution recursively updates the previous one using Bayesian inference statistics (Thiemann *et al.,* 2001).

So far the paragraphs above have described convergence towards a posterior distribution for the parameter space. Once this has been achieved for both the hydrological and error model parameters the optimal point on the posterior distribution can be used to calculate the predictive uncertainty. Therefore taking the optimal parameter set, the associated predictive uncertainty can be calculated by (Romanowicz *et al.,* 1994):

$$P(\delta_t^* < \delta) = \Phi\left(\frac{\delta - \eta}{\sigma/(1-\alpha_i^2)^{\frac{1}{2}}}\right) \qquad \text{(Eq. 6.7)}$$

Where $\acute{\alpha}_i^2$ is the square of the autoregressive error in the parameter series.

Overconditioning of the information contained within the data is a significant point of contention with the formal Bayesian methodology. For example, in selecting an error model assumptions about the nature of the errors are being made before any information specific to the model application is available. This in turn can potentially affect the final posterior distribution and the subsequent assessment of predictive uncertainty (Beven *et al.,* 2007). Realistically in hydrological modelling studies there is often insufficient data available to reliably inform about the true nature of the errors within a model. The most

problematic assumption is one of stationarity in the errors when, realistically, the errors are likely to be non-stationary (Beven *et al.,* 2007). Uncertainty in the error model however, combined with uncertainty in the structure of the hydrological model, is likely to give rise to equifinality (Freer *et al.,* 1996). Therefore, instead of there being an optimal parameter set there may be multiple feasible sets that provide a good representation of the physical system (Beven and Freer, 2001; Beven, 2006). In response to this realisation the GLUE method (Beven and Binley, 1992) was developed to deal with multiple feasible (behavioural) parameter sets.

The GLUE method was developed in response to the possibility of equifinality within parameter sets (Romanowicz and Beven, 2006). It is intended to be used when there is very little prior information available to the modeller about the nature of errors within the model (Beven and Young, 2003). It a less formal approach to uncertainty analysis as it applies fuzzy averaging procedures to subjectively defined objective functions (Jin *et al.,* 2010), which are in turn transformed into likelihood functions. To implement GLUE a feasible range for each parameter must be specified (Freer *et al.,* 1996) from which a suite of parameter sets can be generated by either random or Latin Hypercube sampling. Next, an objective function that adequately represents the available information content in the observed and modelled data is defined, it is then incorporated into the likelihood function. Finally, an acceptance criterion for the chosen objective function is defined. All parameter sets which exceed it will be treated as behavioural ((are a good representation of the system) **Figure 6.4**) whilst all others will be rejected as being non-behavioural. In this sense the GLUE method uses dotty plots of the parameter space and a predefined criterion to select behavioural parameters, as shown in one-dimensional parameter space in **Figure 6.4**. This differs from the formal Bayesian method whereby a single optimal parameter set is selected by convergence upon the peak of the posterior distribution curve, such as the one-dimensional parameter curve in **Figure 6.3**. Upon identifying the behavioural parameter sets, GLUE then averages across behavioural parameter space by calculating the likelihood function between 0 and 1. The inclusion of all behavioural parameter sets in the averaging procedure allows GLUE to account for larger variance due to a non-additive error model (Romanowicz and Beven, 2006) as opposed to the formal approach which makes specific assumptions about variance from an error model. The averaging approach is an extension of the Hornberger-Spear-Young (HSY) sensitivity analysis (Spear and Hornberger, 1980; Hornberger and Spear, 1981) whereby parametric sensitivity is assessed by comparing the likelihood distributions of behavioural and non-behavioural values. The resulting likelihood distribution presents the modeller with a

possibilistic range of predictive uncertainty as the bounds do not represent a true measure of predictive uncertainty as in the formal approach (Beven and Binley 1992).

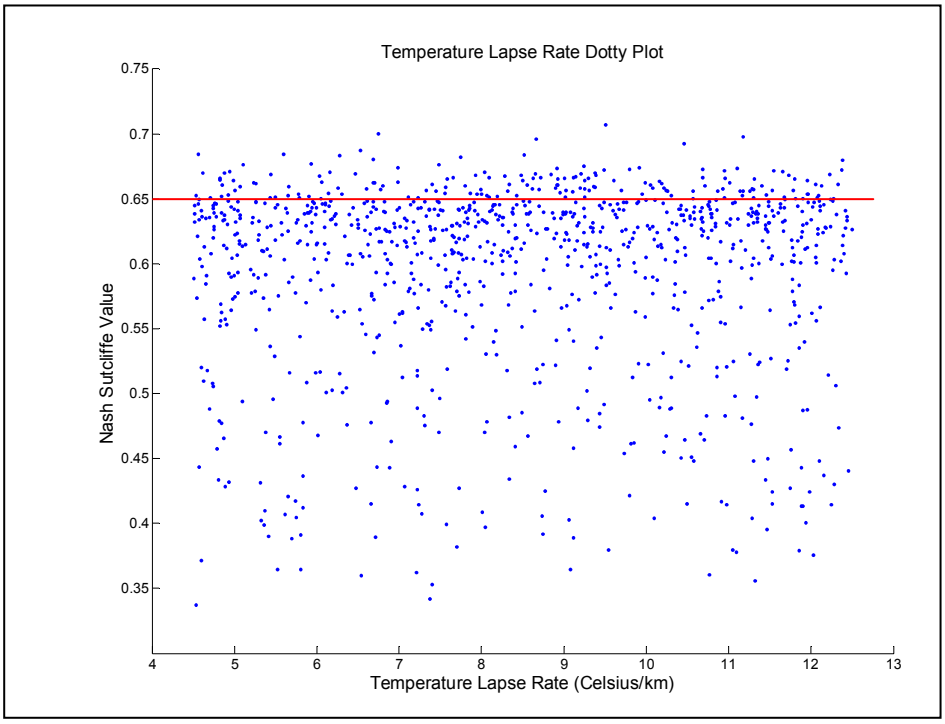


**Figure 6.4** Dotty plot of the temperature lapse rate parameter with a subjectively defined objective function criterion value of 0.65, red line. Each dot represents a single model simulation.

The inclusion of larger variance within the error model by GLUE has been criticised as introducing incoherence into the resulting posterior distribution (Mantovan *et al.,* 2006). It has been argued that by forgoing the formal Bayesian inference approach GLUE has limited learning capabilities resulting in a less well defined posterior distribution (Mantovan *et al.,* 2006). In essence, the criticism is that accounting for a wider variance through subjectively defined objective functions and averaging procedures does not mean GLUE is any more reasonable at defining predictive uncertainty (Gupta *et al.,* 2003; Mantovan *et al.,* 2007).

Therefore, two established methods exist for quantifying predictive uncertainty. The first is a formal approach which requires many prior assumptions about the nature of errors within the model and may possibly lead to over-conditioning of the available information. The second is a less formal averaging approach which requires few formal assumptions instead requiring subjectively defined objective function criteria. The resulting likelihood distribution function from this approach is likely to be much wider and at the risk of being incoherent in that it over-estimates the predictive uncertainty range. In this project the only

prior information available is the feasible range for each parameter. Furthermore the structural errors within CRUM are likely to have a complex structure due to the large number of physical processes it accounts for. To date there has been no work undertaken to assess the nature of the errors within CRUM therefore use of the formal approach in this project would need to make strong assumptions which may not hold true. The decision was taken therefore to assess predictive uncertainty using the GLUE method in light of the lack of prior information. The next section describes how it was implemented in this project.

### 6.4.4 Implementation of the GLUE method

The GLUE method is conventionally used to assess parametric uncertainty but it can also be applied to the assessment of other uncertainty sources including structural and data input (Beven and Binley, 1992). As mentioned in section 6.4.2 it was not possible to assess uncertainty in the boundary condition and calibration data due to a lack of information. It was also not possible to assess structural uncertainty within the CRUM structure as it was not possible to obtain a sufficient number of hydrological models which contained snowmelt or their source codes so that each of the snowmelt models could be added. Instead, it was decided to assess the structural uncertainty of each snowmelt equation that was added into CRUM. This would be achieved by holding the hydrological parameters constant and running the calibration period with each snowmelt equation using their respective *base case* parameter values identified in Chapter 4 **Table 4.1**.

To ensure that the assessment of snowmelt structural uncertainty was realistic, the hydrological parameter set that was used had to be behavioural. This was achieved by undertaking an assessment of parametric uncertainty of the hydrological parameters in **Table 6.1**. It should be noted that the hydrological parameters were varied whilst using the first snowmelt model and holding its parameter values at the *base case.* It was believed that if the behavioural hydrological parameter sets were selected before the inclusion of snowmelt there may be a risk that these sets would no longer remain behavioural after the inclusion of snowmelt.

Conventionally GLUE requires the model to be run with many thousands of parameter samples, for example Romanowicz and Beven (2006) ran TOPMODEL 10,000 times for an evaluation period of three months at a twenty minute resolution. This project however

had a calibration period of two years and the time step of CRUM could range from two minutes to six hours which meant that the duration of each run was never lower than three hours. Consequently it was not possible to take this many samples, especially since further sampling was required later in this uncertainty assessment, so a more efficient sampling strategy was sought. Firstly the mass balance of water components, water flow to channels and water lost to evaporation and recharge, within CRUM were calibrated to the data available in the UK hydrometric register (Marsh and Hannaford, 2008). This register provided a list of summary flow statistics from the gauging stations run by the Centre for Ecology and Hydrology (CEH). Among these statistics is mean annual rainfall and mean annual runoff, the latter being the total amount of water in the river channel. These statistics were used as a measure of the ratio between total water inputted into the catchment as precipitation and the total amount of water exiting the catchment in the channel. Data was not available for the Dacre Beck (as the gauge is operated by the Environment Agency rather than the CEH) so data from the gauge at Pooley Bridge, 1.5 km south-east of the catchment was used instead which gave a precipitation to runoff ratio of 77%. The parameters in CRUM that affected the amount of water lost to evaporation and recharge, *albedo* and *bedrock conductivity* respectively, were adjusted until the modelled rainfall to runoff ratio matched that of the observed data (the final values were 0.25 and $2.5 \times 10^{-9}$ ($ms^{-1}$) respectively).

After the correct mass balance had been achieved a narrower range within the hydrological parameters had to be identified in order to justify taking fewer samples. This was done firstly by creating 20 parameter sets from within the total feasible parameter space and running the model for each of these and assessing the output using both objective functions outlined in section 6.4.1. This provided an estimate of where in the parameter space most of the behavioural runs would be situated. From this, a further 20 parameter sets were generated from within this narrower range. The outputs from these were assessed and it was confirmed that better results were obtained from this narrower range, for example the Nash-Sutcliffe objective function ranged from 0.4 to 0.49 in this range compared to -0.1 to 0.45 from the total range. However, this method slightly contradicted the conventional application of GLUE as it involved convergence towards an optimal point in the parameter space meaning it would ignore potentially behavioural runs outside of this narrower range. However, in doing so this method may actually introduce a preliminary yet subjective form of statistical inference whereby it concentrates the sampling into an area of the parameter space which will have a high density of behavioural runs.

Next, 1000 parameter samples were generated from the narrower ranges outlined in **Table 6.2**. A uniform distribution was assumed for each parameter and the samples were randomly generated using a Mersenne Twister routine (Matsumoto and Nishimura, 1998). The model was run for each parameter sample and behavioural runs were identified as having a Nash-Sutcliffe value greater than 0.65 and an RMAE value between -0.05 and +0.05. Ideally, structural uncertainty would have been assessed by running the *base case* snowmelt equation parameter set with each behavioural hydrological parameter set. Preliminary testing however had shown that the difference between the three snowmelt models was very small so it was decided not to dedicate a large amount of the available computer resources to this assessment. Instead it was decided to run each snowmelt model with one behavioural hydrological parameter set, which was chosen at random and held constant for the subsequent simulations. The uncertainty within the modelled calibration discharge series due to the snowmelt models was then assessed by plotting the minimum and maximum discharge values at each time step. If there was a large amount of structural uncertainty then this range would be large and clearly visible on the graph.

| Parameter | Minimum | Maximum |
|---|---|---|
| Saturated Hydraulic Conductivity *(kSat),* [$ms^{-1}$] | $5 \times 10^{-5}$ | $9 \times 10^{-4}$ |
| Hydraulic Conductivity Decay with Depth, (*kDecay*), [$ms^{-1}m^{-1}$] | -2.00 | -5.00 |
| Root Layer Depth, (*rootDepth*), [m] | $5 \times 10^{-4}$ | 0.07 |
| Root Layer Saturated Hydraulic Conductivity, *(rootkSat*), [$ms^{-1}$] | $5 \times 10^{-4}$ | $9 \times 10^{-3}$ |
| Soil Depth Channels, *(SD Chan),* [m] | 0.75 | 1.20 |
| Soil Depth Ridges, (*SD Ridges*), [m] | 0.50 | 1.20 |
| Soil Depth Slopes, (*SD Slopes*), [m] | 0.08 | 0.80 |
| Porosity, [Dimensionless] | 0.10 | 0.30 |

**Table 6.2** The hydrological parameters within CRUM after the identification of narrower ranges.

By comparing the uncertainty associated with the hydrological parameters and the uncertainty associated with the parameters of each snowmelt model it was possible to assess the parametric uncertainty within CRUM and each snowmelt model. The behavioural hydrological parameter sets identified in the procedure outlined above were used to assess hydrological parametric uncertainty. The single hydrological parameter set mentioned above was used alongside 300 snowmelt parameter sets for each snowmelt model. Fewer samples were taken than when the hydrological parameters were varied because there were only three to four parameters being investigated hence the size of the total parameter space was much smaller. The snowmelt parameter sets were randomly generated from the ranges outlined in column two of **Table 4.1** in Chapter 4. Behavioural sets were identified using the same criteria as above, then for each behavioural set the winter Q5 and Q95 was calculated before a PDF was plotted for each snowmelt model. This would allow for a comparison of the uncertainty associated with the snowmelt parameters, a wide spread of results would indicate a large amount of uncertainty. The Q5 and Q95 from the behavioural parameter sets of the hydrological parameters calculated in the previous paragraph were then added to the respective plots to allow a comparison between uncertainty from the snowmelt and hydrological parameters.

Finally the combined parametric uncertainty of the hydrological and snowmelt parameters was assessed by simultaneously varying both. For each snowmelt model 1000 parameter sets were generated and the Q5 and Q95 were calculated from each behavioural parameter set and plotted as a PDF as above. If the snowmelt models contributed very little towards the total parametric uncertainty the PDFs would be identical. The results from this process could be explained by analysing the sensitivity of the individual snowmelt parameters using the HSY method (Spear and Hornberger, 1980). For each parameter in each snowmelt model the cumulative distributions of the values from the behavioural and non-behavioural runs were calculated. If the two distributions were significantly different then this would indicate that the parameter in question was sensitive. The significance of the difference was assessed using a two-sample Kolmogorov-Smirnov test at a 95% confidence level.

### 6.4.5 Uncertainty Assessment Results: Structural Uncertainty

The results from adjusting hydrological parameters (**Figure 6.5**) show a generally good fit to the observed hydrograph in terms of the timing of the peaks and the decay to lower flows. All the behavioural runs failed to represent the peaks observed in June of the

second year because the soil was too dry. Since this project was interested in the winter hydrograph it was decided to accept this error as it did not affect the winter flow predictions. Winter flows were generally modelled quite well however the peaks were consistently under-estimated. It was hypothesised that this might be due errors within the precipitation data where the gauge may have missed or under-caught precipitation events due to it being at a low elevation in the catchment. Consequently CRUM would have inputted less water into the catchment resulting in lower flows than were actually observed. The spread of uncertainty in the modelled flow was found to be quite small when compared to the uncertainty range calculated in previous applications of CRUM (Lane *et al.,* 2009). This could be because the parameter samples were generated from a much smaller range which constrains the uncertainty in the behavioural runs.

Assessment of structural uncertainty (**Figure 6.6**) found that the uncertainty contributed to the CRUM output from the snowmelt models was very small. The structural uncertainty bounds in the modelled hydrograph were very small and hardly visible in the resulting hydrograph. Plotting a scatter graph of the difference between the three modelled hydrographs at each time step (**Figure 6.7**) showed that the greatest differences were during peak flows in the winter especially the first winter. These differences probably occurred during large snowmelt events which would exacerbate differences between the snowmelt models. The differences may be larger in the first winter because there was more water in the catchment which would have resulted in larger snowpacks thus increasing the differences between the snowmelt models. Modelled discharge in the first winter is higher than the second supporting the idea that more water was in the catchment during this time hence any snowpacks that would have accumulated would have been larger. Overall these results showed that there was structural uncertainty within the snowmelt models but the contribution of this to total uncertainty in the CRUM discharge series was very small.

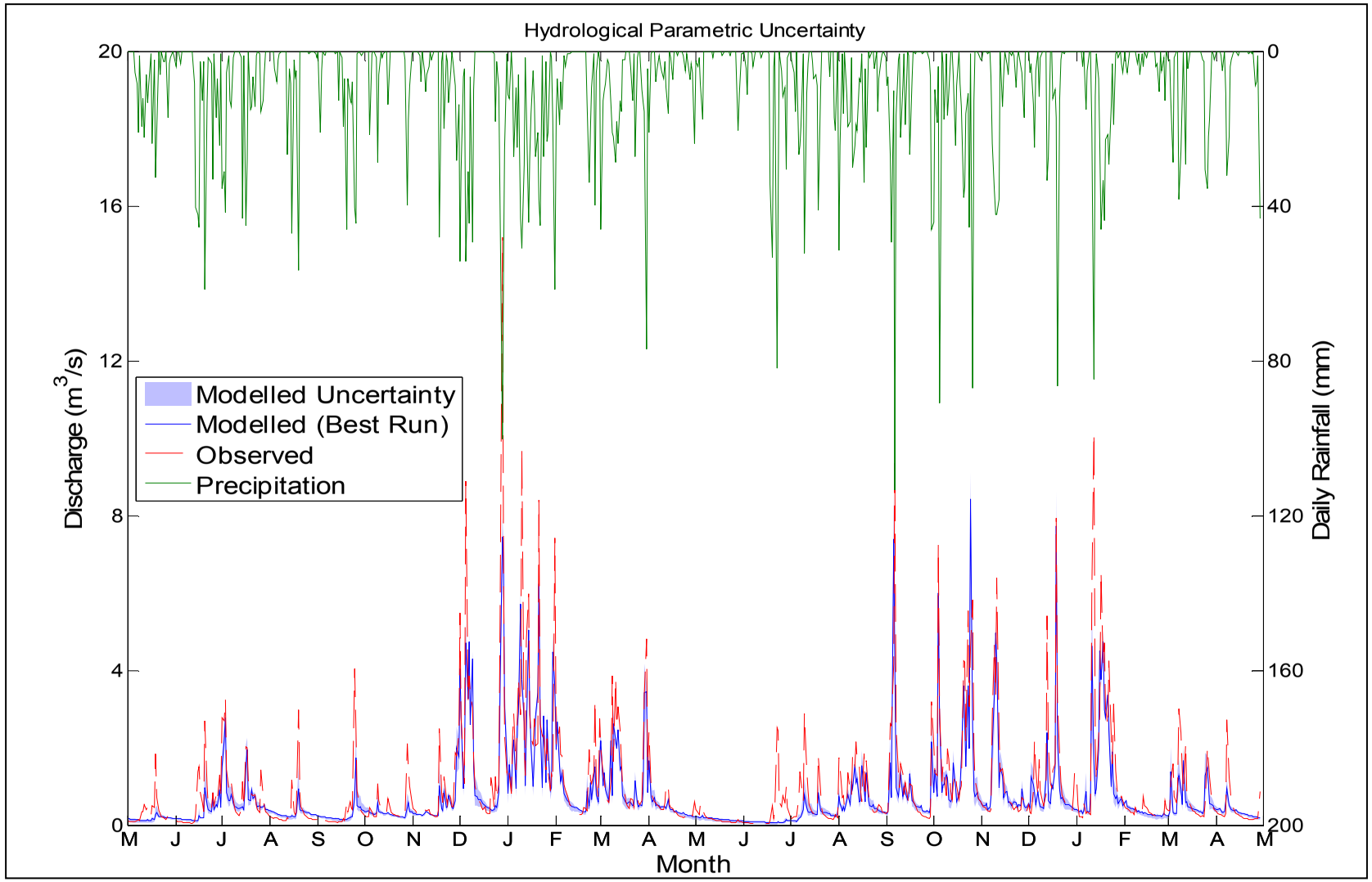


**Figure 6.5** The modelled hydrograph (blue line), used in the structural uncertainty assessment, generated from the initial assessment of hydrological uncertainty plotted with the possibilistic predictive uncertainty bands from all the behavioural runs (shaded blue area) plotted against the observed hydrograph (dashed red line) and observed precipitation (green line).

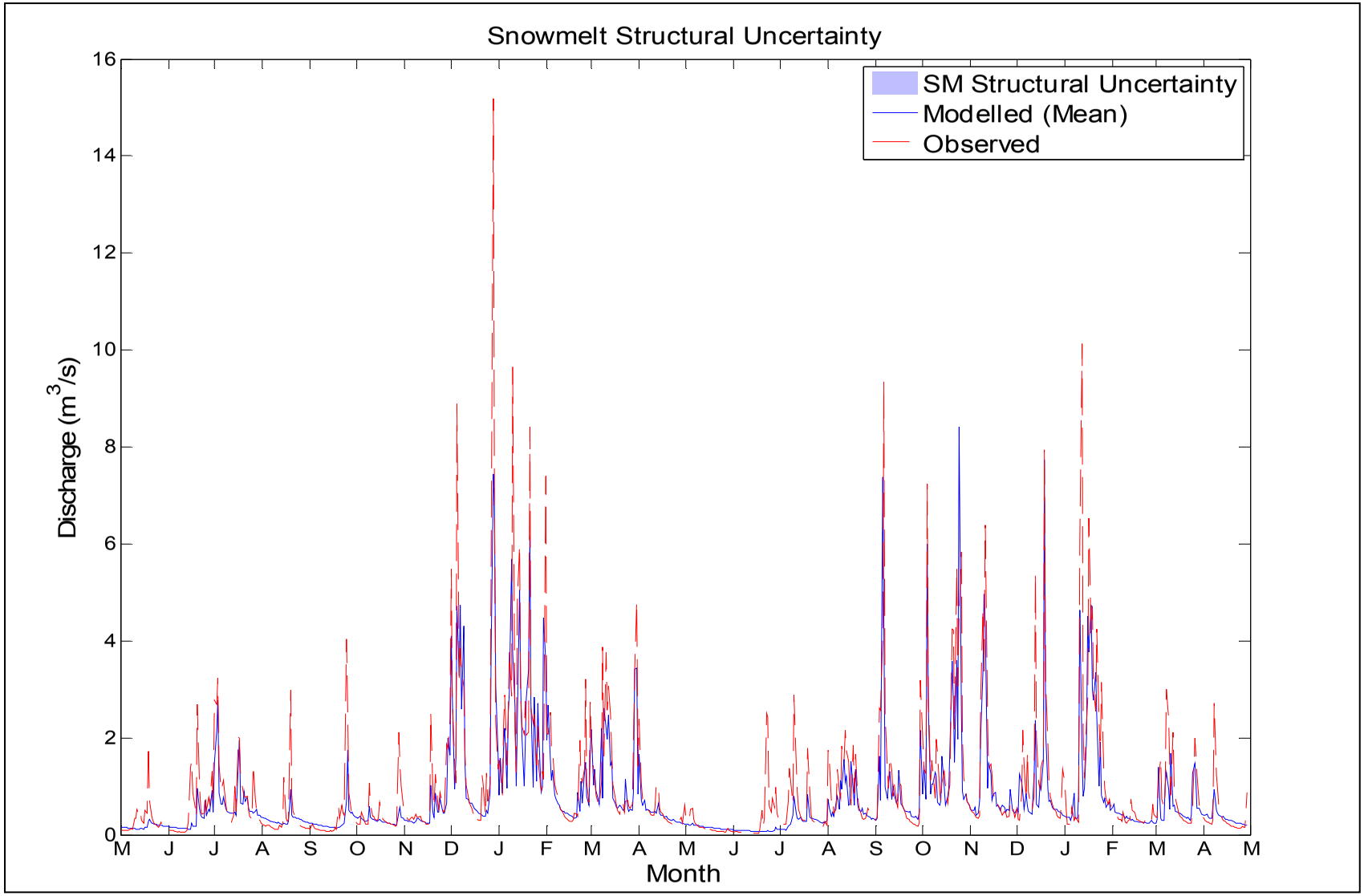


**Figure 6.6** Structural uncertainty from the snowmelt models. At each time step the mean modelled (blue line) and modelled uncertainty (shaded blue) is plotted alongside the observed (dashed red line).

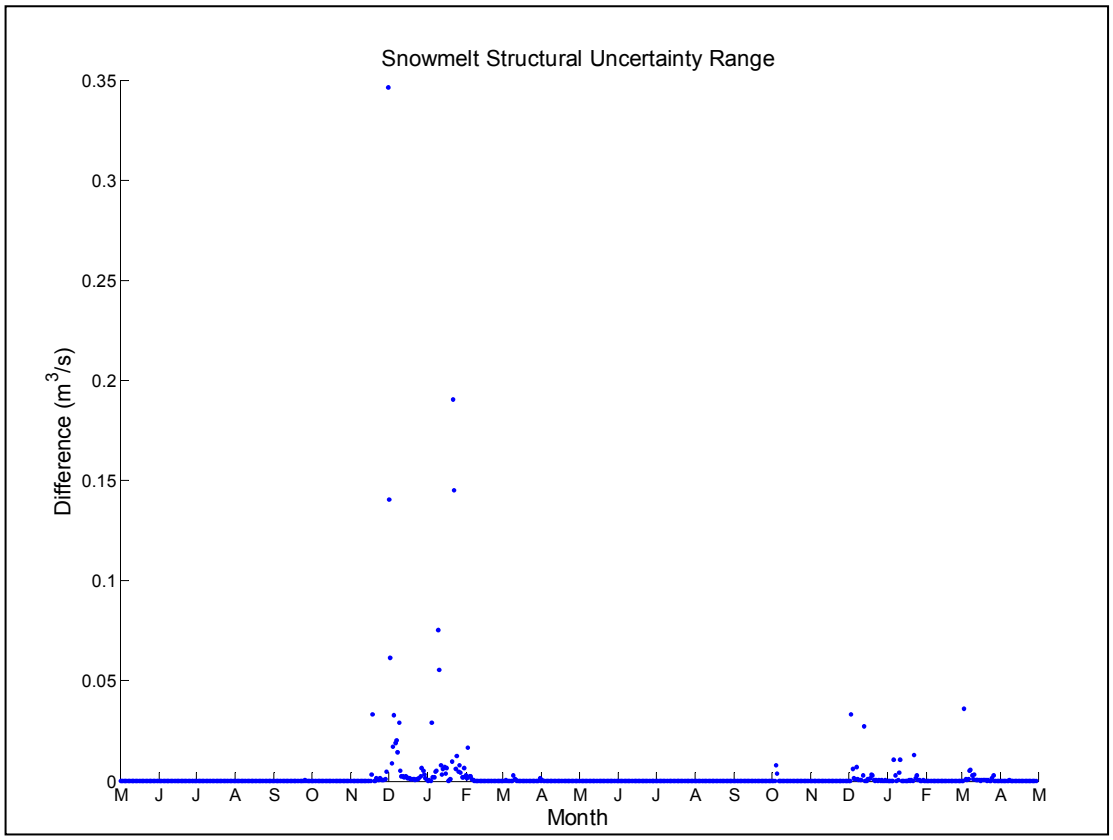


**Figure 6.7** Snowmelt structural uncertainty shown by plotting the differences between the three modelled discharge at each time step.

### 6.4.6 Uncertainty Assessment Results: Parametric Uncertainty

The parametric uncertainty of the snowmelt model parameters was found to be small in comparison to the uncertainty associated with the hydrological parameters contained within CRUM (**Figure 6.8** (**a**) and (**b**)). The spread of winter Q5 resulting from the snowmelt parameters ranged from 3.68 $m^3s^{-1}$ to 3.74 $m^3s^{-1}$ whilst the spread from the hydrological parameters was from 3.47 $m^3s^{-1}$ to 3.85 $m^3s^{-1}$. Meanwhile, for Q95 the range spread from 0.219 $m^3s^{-1}$ to 0.221 $m^3s^{-1}$ for the snowmelt parameters and from 0.165 $m^3s^{-1}$ to 0.254 $m^3s^{-1}$ for the hydrological parameters. The smaller uncertainty range of the snowmelt parameters may be because snowmelt processes only occur intermittently during the winter period in Dacre Beck. Consequently their contribution to discharge is smaller than other hydrological processes that occur throughout the period such as through flow. The Q95 PDF curves are very similar for each snowmelt model but differences in the Q5 curves highlight structural uncertainty. The curves Q5 PDF curves of the first two snowmelt models are very similar as they both treat positive degree air temperature in the same way (Chapter 4, *Eqs. 4.2* and *4.3*). Their similarity may also suggest that the additional rain-on-snow process in the second snowmelt model contributes very little towards the output hydrograph. Conversely, the third snowmelt

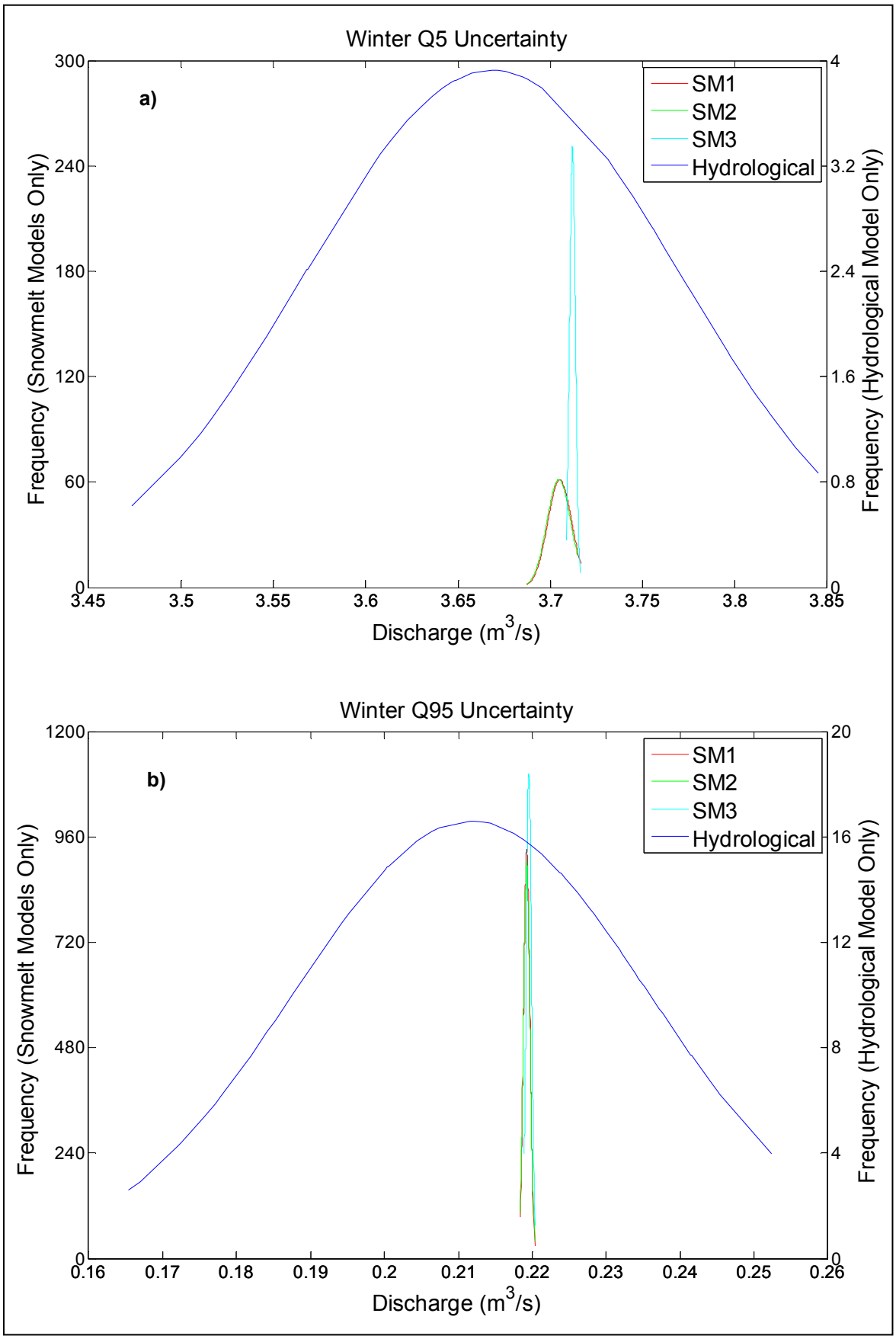


**Figure 6.8** PDF curves of parametric uncertainty arising from the parameters within each snowmelt model (SM1, SM2, and SM3) and the hydrological only parameters for the winter (**a**) Q5 and (**b**) Q95 flows.

model treats positive degree temperature differently and includes a solar radiation process (Chapter 4 *Eq. 4.4*). In dealing with positive air temperature the third snowmelt model divides the degree-hour parameter by the reciprocal of the number of time steps per day which reduces the value to an order of magnitude lower than the other two snowmelt models. As a result this reduces the amount of snowmelt produced by this process and hence the uncertainty range associated with this. If there was a large amount of uncertainty associated with the solar radiation parameter then this would be expected the re-broaden the Q5 PDF of the third snowmelt model. However, because its PDF curve is so narrow it is likely that the uncertainty associated with this parameter is very small. Analysis of the sensitivity of the individual parameters in the next paragraph would be able to confirm whether this was the case.

Simultaneously varying the snowmelt and hydrological parameters, as expected, did not increase the uncertainty range of the Q5 and Q95 flow predictions by a large amount when compared to the uncertainty range from the hydrological parameters alone (**Figure 6.9** (**a**) and (**b**)). For example, the uncertainty range of the Q5 prediction increased from 0.57 $m^3s^{-1}$ to 0.78 $m^3s^{-1}$ after the inclusion of the third snowmelt model. The increase in the uncertainty range was smaller for the first and second snowmelt models which contradicted the results from **Figure 6.8** (**a**). This had suggested that uncertainty from the third snowmelt model was smaller than the other two. The most likely explanation for this is that the wider spread in uncertainty was actually due to uncertainty in the hydrological parameters as new hydrological parameter samples were generated for each snowmelt model. This would suggest that the 1000 parameter samples used to create the hydrological only PDF were not enough to create a stationary uncertainty response curve. The solution therefore, would be to take more samples of the hydrological parameters, evaluate these and then attach the same parameter samples for each snowmelt model and evaluate their combined uncertainty. Using this method would firstly enable a more accurate quantification of the uncertainty range in the hydrological parameters. Then it would be able to evaluate the additional uncertainty contributed by the snowmelt parameters without reflecting additional uncertainty in the hydrological parameters. Results from the Q95 PDF curves (**Figure 6.9** (**b**)) show a similar trend whereby the addition of snowmelt only increased the uncertainty range by a small amount. Snowmelt model one showed a larger uncertainty range than the other two when it would have been expected to have a similar range to the second as in **Figure 6.8** (**b**)). Again this could be due to the same reason that led to the anomalous Q5 PDF curve of the third snowmelt model.

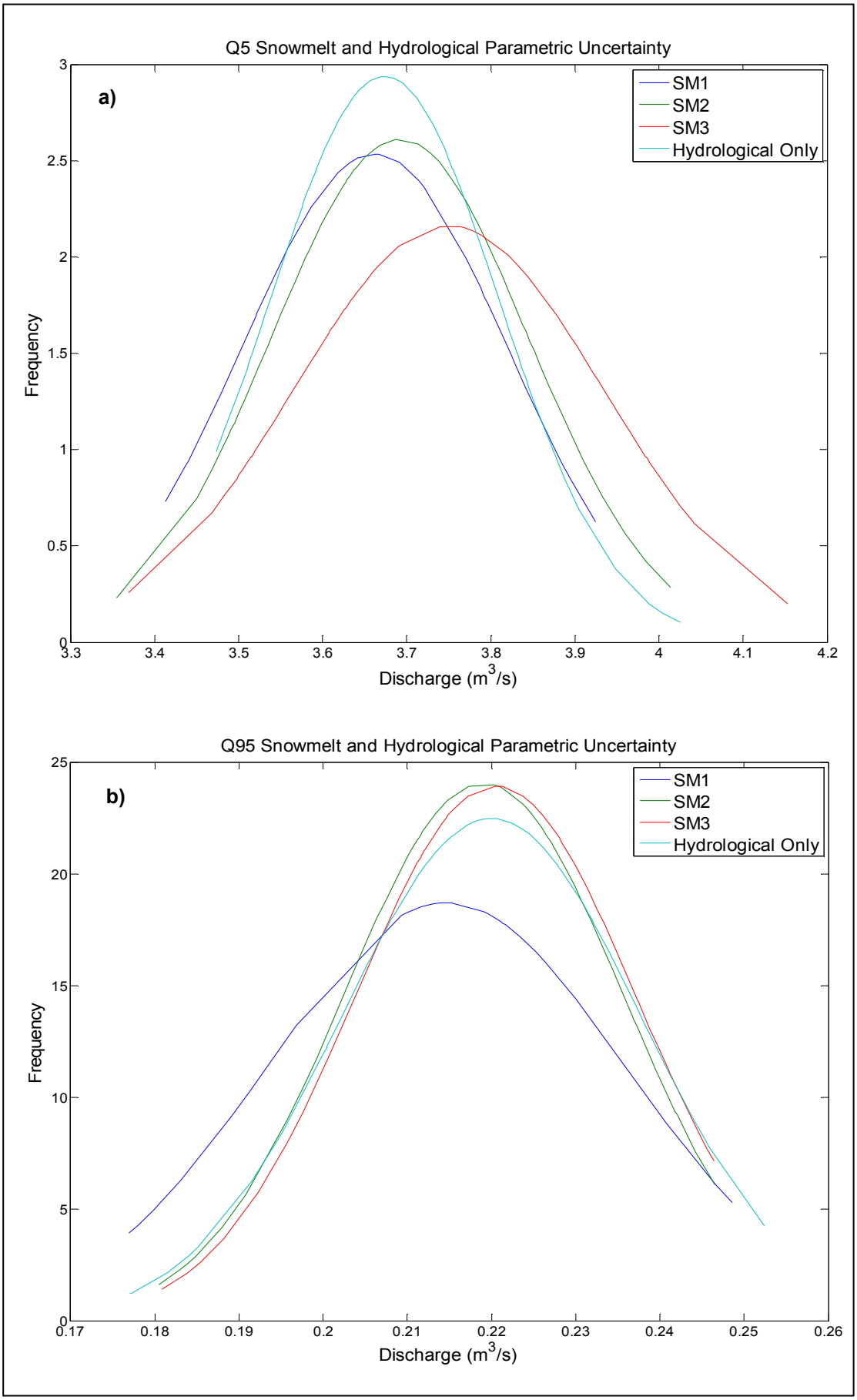


**Figure 6.9** PDFs of parametric uncertainty arising from a combination of the snowmelt and hydrological parameters for each snowmelt model (SM1, SM2 and SM3) and the hydrological parameters only for the winter (**a**) Q5 and (**b**) Q95 flows.

None of the snowmelt model parameters were found to contribute to output sensitivity which explained why the addition of snowmelt added little to the uncertainty range of the winter Q5 and Q95 flow predictions. Instead, the most sensitive parameters were the saturated hydraulic conductivity, slope soil depth and porosity of the soil. The relative sensitivity of each snowmelt parameter to each other largely agreed with the results of the sensitivity analysis in Chapter 4 (**Figure 4.2**). For example, in the first snowmelt model the sensitivity analysis in Chapter 4 found that the temperature lapse rate was the most sensitive of the snowmelt parameters followed by the degree-day parameter and then the threshold melt temperature. The HSY response curves calculated in this chapter reflect these findings (**Figure 6.10**) as the differences in the behavioural and non-behavioural distributions of the temperature lapse rate were slightly greater than the differences in the degree-day parameter. Meanwhile the behavioural and non-behavioural distributions of the threshold melt parameter were very similar reflecting the insensitivity of this parameter and confirming the flat response curve for the same parameter in **Figure 4.2** (**a**[**ii**])).

The sensitivity curves for the parameters of the second snowmelt model (**Figure 6.11**) again largely agree with the results in **Figure 4.2** (**b**). They showed that the temperature lapse rate was the most sensitive and that the threshold melt temperature was the least sensitive. However, unlike the results in the first sensitivity analysis the degree-day parameter was very insensitive whilst the rain-on-snow parameter showed greater sensitivity. This was unexpected as the results from **Figure 6.8** appeared to imply that the rain-on-snow component of the second snowmelt model was fairly unimportant in contributing to output uncertainty. It was expected that the degree-day parameter in the second snowmelt model would have a similar sensitivity to that in the first as they both treat positive air temperature in the same way.

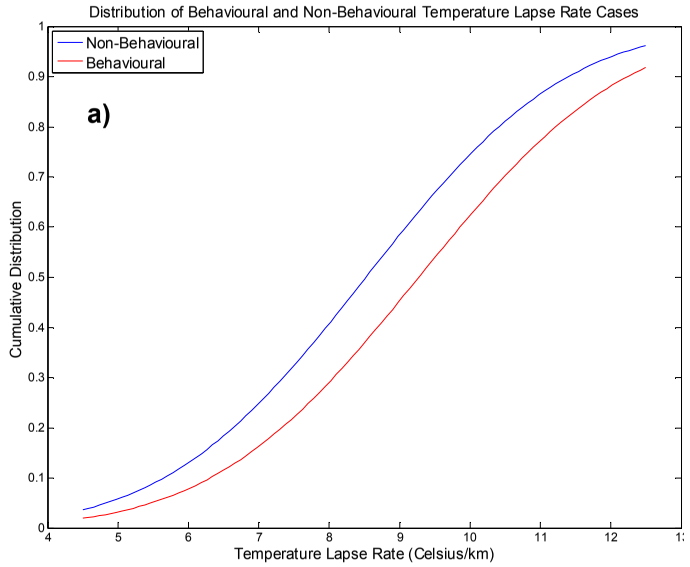


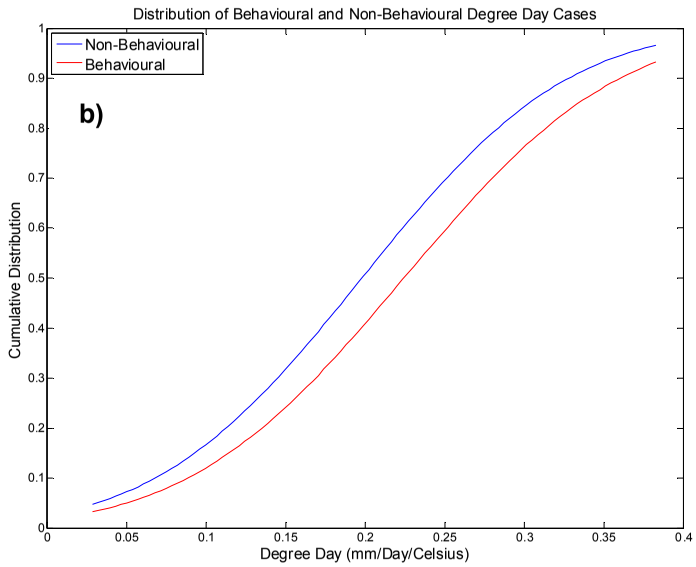


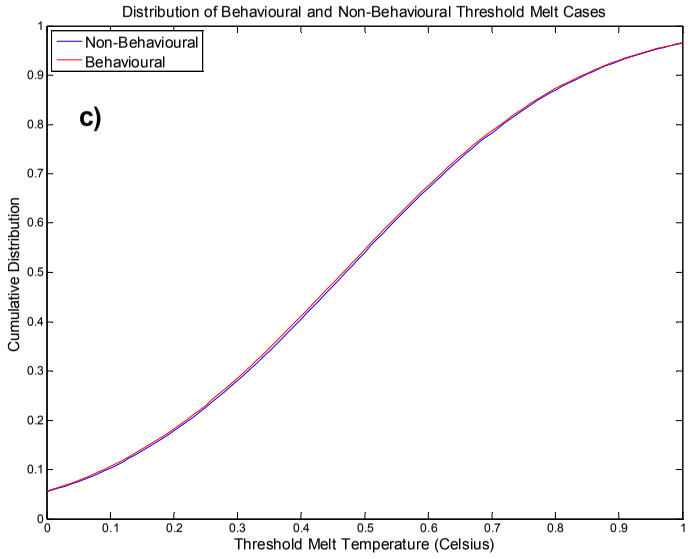


**Figure 6.10** Non-behavioural (blue) and behavioural (red) distribution curves for the (**a**) temperature lapse rate, (**b**) degree-day and (**c**) threshold melt parameters for the first snowmelt model.

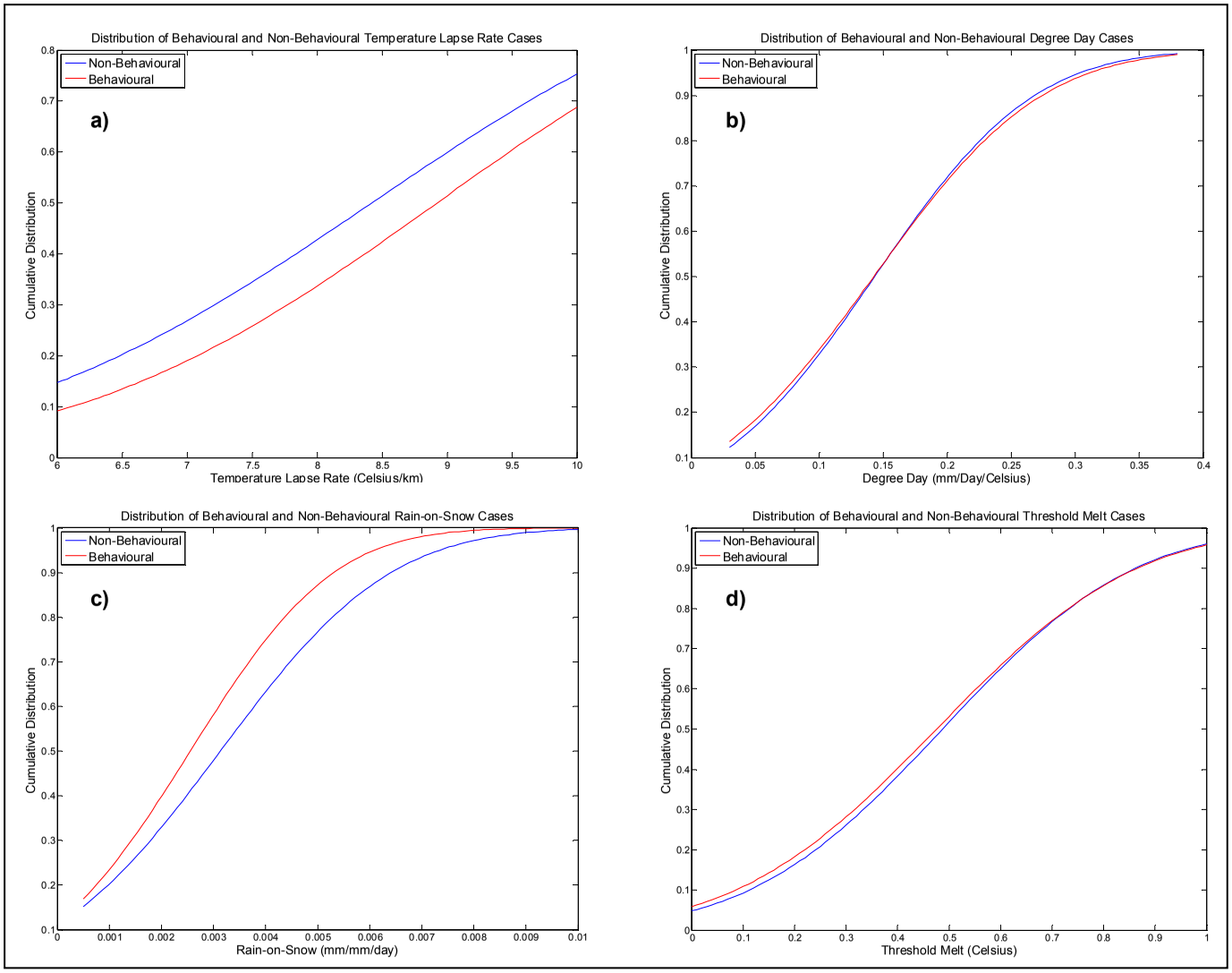


**Figure 6.11** Non-behavioural (blue) and behavioural (red) distribution curves for the (**a**) temperature lapse rate, (**b**) degree-day, (**c**) rain-on-snow and (**d**) threshold melt parameters for the second snowmelt model.

The sensitivity response curves of the third snowmelt model parameters (**Figure 6.12**) were also similar to those of the second snowmelt model (**Figure 6.11**). The temperature lapse rate was the most sensitive parameter followed by rain-on-snow with degree-hour being insensitive. Temperature lapse rate was also found to be the most sensitive in the first sensitivity analysis (Chapter 4 **Figure 4.2** (**c**)). The insensitivity of the degree-day parameter slightly contradicted the findings of the first analysis but can be explained because of the multiplication of the parameter by the reciprocal of the number of time steps per day (Chapter 4 *Eq. 4.4*). The distributed snowmelt model had fewer time steps per day (24) than CRUM (180) so the latter would have multiplied the degree-day parameter by a smaller number resulting in less snowmelt from positive air temperature. Consequently this would reduce the importance of this parameter which would explain the narrower uncertainty band associated with this snowmelt model (**Figure 6.8**). Rain-on-snow was found to be insensitive in the first sensitivity analysis, the result to the contrary in this chapter may also be due to structural differences between the distributed snowmelt model and CRUM. As mentioned above this would have significantly reduced the magnitude of the positive degree snowmelt process but the same downscaling was not applied to the rain-on-snow process which would have favoured the latter. These results highlight a limitation in applying temperature-index snowmelt models on a time step lower than that at which they were derived. Testing was undertaken to establish whether downscaling the parameters to the time step of CRUM solved this problem, for example scaling the degree-day parameter to a per-minute resolution. However this rendered snowmelt all but negligible within CRUM. Furthermore, since the snowmelt coefficients were empirically derived there is no physical justification for downscaling them to a smaller time step as there is no guarantee that the relationships will hold true (see Chapter 8 for a discussion of the limitations of the temperature-index method). **Figure 6.12** (**d**) showed that the solar radiation parameter was insensitive which contradicted the results of the first sensitivity analysis which found it to be joint second-most sensitive. Again this could be the result of temporal downscaling within CRUM as the parameter is added to the degree-day parameter after it has been multiplied by the reciprocal of the number of time steps per day.

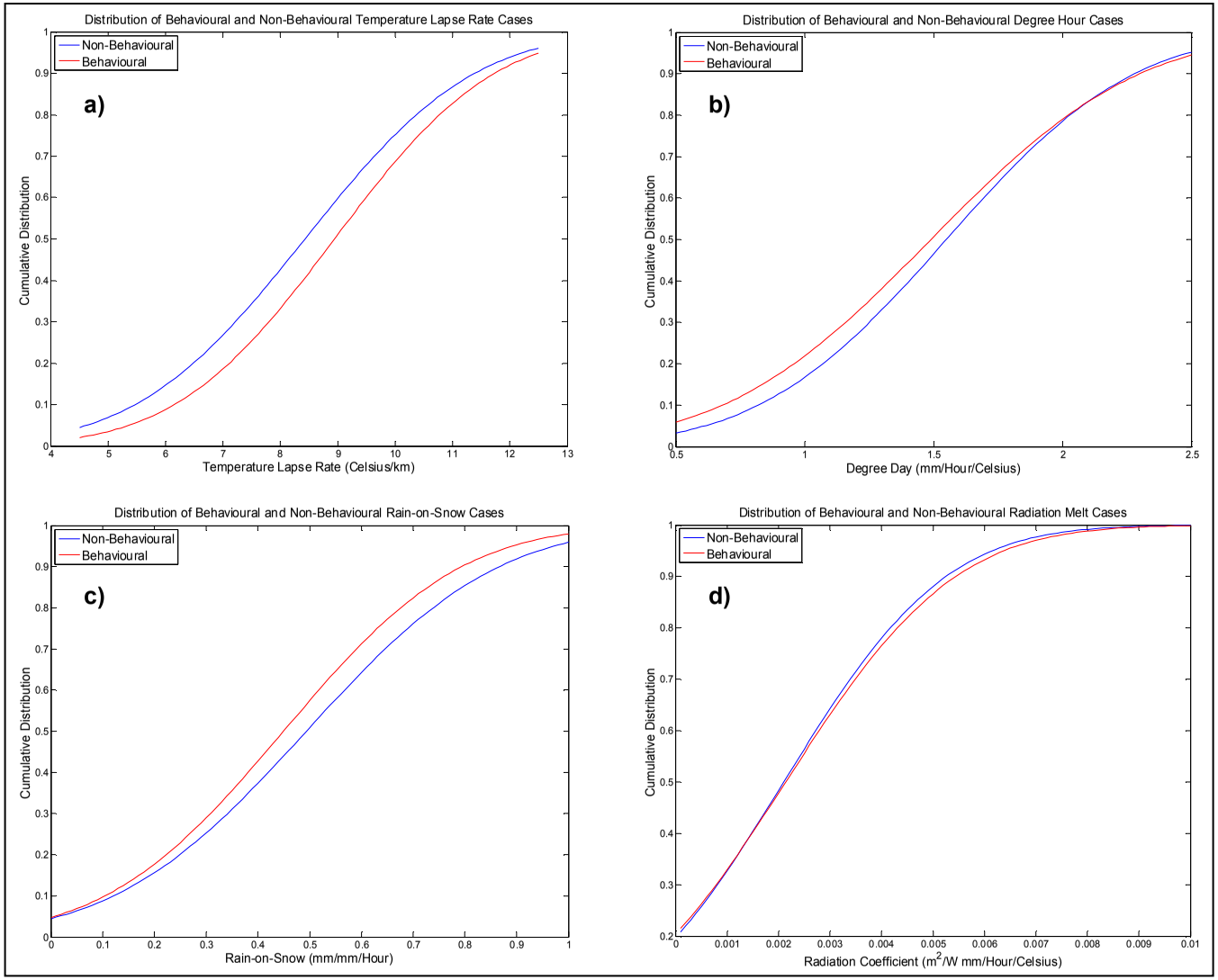


**Figure 6.12** Non-behavioural (blue) and behavioural (red) distribution curves for the (**a**) temperature lapse rate, (**b**) degree-hour, (**c**) rain-on-snow and (**d**) solar radiation parameters for the third snowmelt model.

### 6.4.7 Uncertainty Assessment: Discussions

The aim of this section was to calibrate the parameters of CRUM and each snowmelt model to observed data whilst simultaneously acknowledging uncertainties throughout the modelling process. Uncertainty assessment was carried out using the less formal GLUE method due to the lack of prior information available in Dacre Beck. It was not possible to assess uncertainties in the input and calibration data or the structure of CRUM. Instead, structural and parametric uncertainties in the snowmelt models were calculated before analysing the combined parametric uncertainty of each snowmelt model with the hydrological parameters contained within CRUM. To this end it was found that uncertainties associated with the snowmelt models were small and did not add much additional uncertainty to that which already arose from the hydrological parameters of CRUM. At the same time it was not possible to determine if one snowmelt model performed better than the others as all three produced small improvements in both objective functions. Assessment of the sensitivity of each snowmelt model parameter after inclusion in CRUM yielded results that contradicted those found in the sensitivity analysis of the distributed snowmelt model (Chapter 4). It was hypothesised that these differences may have arisen due to the different temporal structure of CRUM affecting how each component in the snowmelt models was calculated. It is likely that the effects of this would be small, in line with the findings of this uncertainty assessment, but they highlight one of the limitations of using temperature-index snowmelt model beyond the timescale upon which they were derived. Their effect upon the final results of this project must be considered and will be the attention of more discussion later in this report (Chapter 8).

## 6.5 Conclusions

This chapter has improved upon the process representation of the distributed snowmelt model by including each snowmelt model into a physically based hydrological model. CRUM was chosen for its physical basis, minimal data input requirements and its code structure that enabled simple modifications. A new snowmelt module was constructed that enabled CRUM to accumulate snow and then melt it using one of the three snowmelt models. The new code was verified using the built-in mass balance routine which showed that water mass was still being conserved. Next, the snowmelt and hydrological parameters were calibrated to observed data whilst uncertainty in the model output was assessed. This identified a number of behavioural parameter sets from each snowmelt model although issues with temperature-index snowmelt modelling were also highlighted. Overall, the procedure in this chapter has produced a physically-based model capable of

modelling snowmelt hydrology along with an uncertainty framework. These will be used to assess the impacts of climate change on the winter flow regime of Dacre Beck in the next chapter.

# Chapter 7

# Hydrological Modelling of Climate Change Impacts upon Snowmelt Hydrology and the Winter Flow Regime

## 7.1 Selecting the Model Inputs

In the previous chapter snow accumulation and melt were incorporated into CRUM v3.1 (Lane *et al.,* 2009) and a parametric uncertainty range was defined as a result of calibrating the model output to an observed hydrograph (Chapter 6). This chapter uses the hydrological model and its associated uncertainty framework along with the probabilistic projections of climate change (Chapter 5) to forecast changes in the snowmelt hydrology and winter flow regime of Dacre Beck. The results from this analysis will then directly inform the second and third research questions posed at the end of Chapter 1 and the discussion in the next chapter. This chapter firstly describes how the hydrological model inputs were created based upon the uncertainty frameworks of CRUM (Lane *et al.,* 2009) and the UKCP09 Weather Generator (Jones *et al.,* 2009). It then presents and assesses the results obtained from these inputs according to the impacts upon high and low winter flows. The results found that changes in the winter flow were contrary to observed historical trends in upland UK catchments affected by snowmelt (SEPA, 2008). It was difficult however to define the role of snowmelt hydrology in driving the changes in the winter flow regime as the output from the hydrological model did not define the contribution from snowmelt as in the distributed snowmelt model. Therefore further work was carried out to understand the role of snowmelt hydrology.

To model the impacts of projected climate change CRUM had to be run using weather input data derived from the weather generator (Chapter 5) and parameter values from the behavioural parameter sets (Chapter 6). As mentioned in these chapters there is uncertainty associated with the magnitude of climate change and equifinality in the behavioural parameter space. To represent the uncertainty in the magnitude of climate change, 10,000 weather series for the baseline and future scenario periods from the weather generator were used to create PDFs of forecast change for each climate variable. Meanwhile, approximately 60 behavioural parameter sets were identified for each snowmelt model within CRUM which implied there were a total of approximately 180 behavioural parameter sets as no single snowmelt model clearly outperformed the others. Therefore theoretically, to represent uncertainty in the projections of the climate change impacts upon the winter flow regime CRUM should be run for every combination of weather series and behavioural parameter set. This would have meant a total of 3,600,000 simulations. Uncertainty in the results was however, represented in fewer runs by selectively sampling weather files and parameter sets which represented the total probable space of the variable(s) of interest to this project.

Uncertainty in the behavioural parameters sets was represented by sampling three sets from each snowmelt model from a likelihood distribution composed of high and low flow predictions. In this case the variables of interest were the winter Q5 and Q95 as they represented the extreme ends of the flow duration curve and were affected by snowmelt hydrology and hence potentially by climate change (Chapter 1 sections 1.4 and 1.5). Firstly, for each snowmelt model the winter Q5 and Q95 from the calibration period from each behavioural run (Chapter 6 section 6.4.6) was calculated. For each run the cumulative distribution function for the resultant Q5 and Q95 was calculated and added together. Then a new cumulative distribution function was calculated for this combined value series which re-scaled the values between 0 and 1 (**Figure 7.1**). The *x-axis* value which corresponded to the likelihood distribution values of 0.1, 0.5 and 0.9 were then calculated (**Figure 7.1**). The parameter set which lay closest to each value was then selected. These likelihood values were chosen as they represented the extreme prediction cases before the distribution became marginal and a middle case for which the probability of excedence was equal to that of non-excedence. The application of this procedure to each of the snowmelt models meant that nine parameter sets were chosen (**Appendix 2 Table 1**), CRUM would then subsequently be run with each.

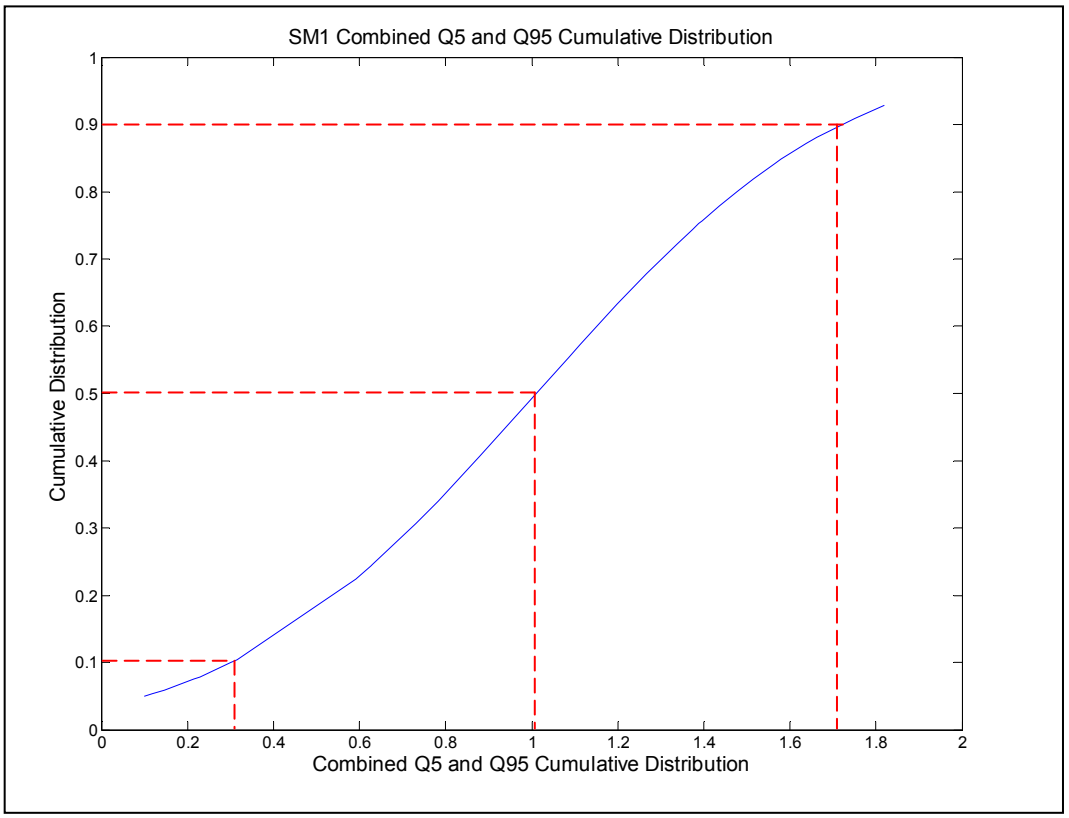


**Figure 7.1** The combined Q5 and Q95 cumulative distribution curve (blue solid line) which was used to sample three behavioural parameter sets from the first snowmelt model at three likelihood values (red dashed lines)

A similar approach was used to sample daily weather series from the weather generator according to the likelihood distribution of mean winter temperature. Temperature was chosen as it represents the mechanism controlling whether precipitation falls as snow or rain (Chapter 1 section 1.1) hence it affects the magnitude of snow accumulation and melt thus impacting the winter flow regime. A separate cumulative distribution of the mean winter temperature was created for the 10,000 baseline series (**Figure 7.2**) and the 10,000 scenario series. For each curve nine *x-axis* values were taken at *y-axis* values of 0.1 to 0.9 in increments of 0.1. The weather series whose mean winter temperature lay closest to each *x-axis* value was then selected. The range of these values, as above, represented the extreme ends of the distribution before it became marginal. Nine values were taken in order to equal the number of sampled hydrological parameter sets so that both uncertainty sources were treated equally.

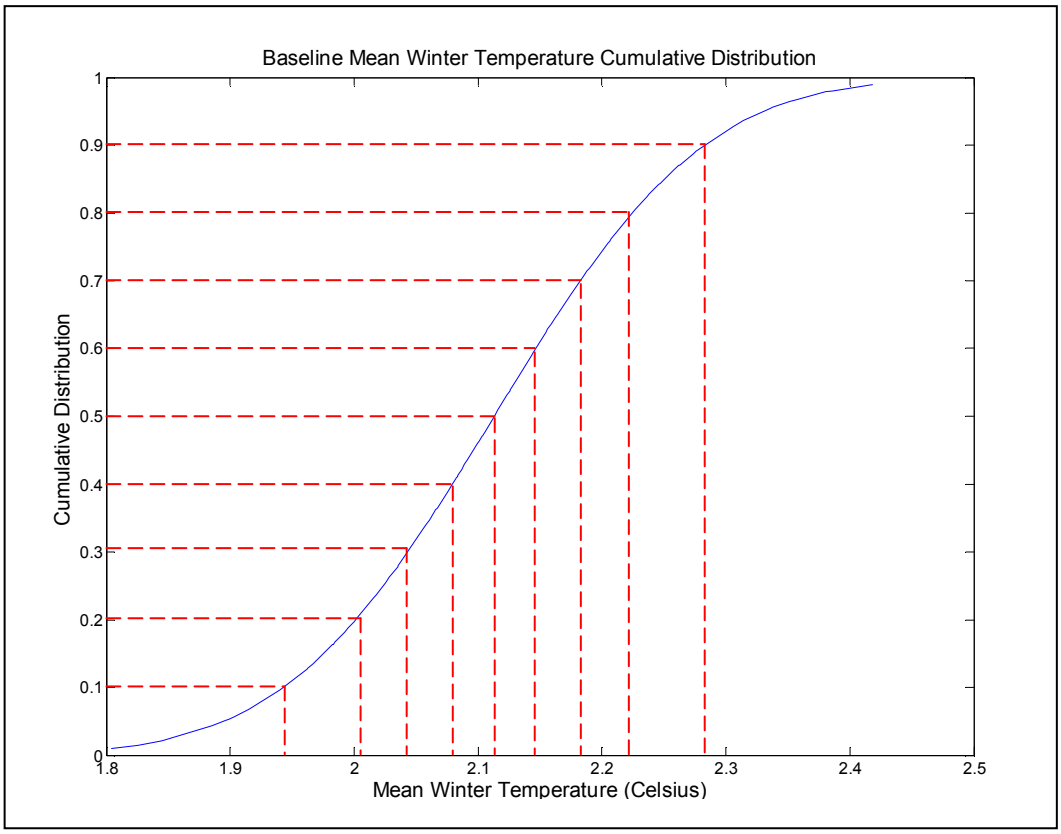


**Figure 7.2** Cumulative distribution of the mean winter temperature from the weather generator baseline series (solid blue line) used to sample nine weather series at nine likelihood values (red dashed lines). The same was repeated for the future scenario weather series.

## 7.2 Methodology

CRUM was run for every combination of the selected weather series and parameter sets - 162 runs. After each run the winter high flows were assessed by calculating the Q5 and number of peak-over-threshold (POT) exceedence events. Both of these statistics recorded high flow events in the winter discharge series, the former was calculated from

the flow duration curve as explained in Chapter 2 (section 2.4 *Eq. 2.1*) and was also used in the analysis of the distributed snowmelt model (Chapters 4 and 5). The latter was computed by counting the number of discharge peaks throughout the entire winter flow series which exceeded a given threshold value (20.73 $m^3s^{-1}$). This value was obtained from the Environment Agency who had applied the Flood Estimation Handbook method (Robson and Reed, 1999) of analysing the observed discharge series and selecting a value which produced five exceedence events per year. The independence of the peaks was verified by using the criterion that two peaks must be separated by at least three times the average time to rise (Bayliss and Jones, 1993). Preliminary investigation of the modelled hydrographs found that the average peak rise time was one day so the independence criterion was set at three days.

Low flows were assessed by calculating the Q95 and 7-day consecutive low flow statistics. The former was calculated in the same way as the Q5 but to represent the other extreme end of the winter flow duration curve. Q95 could be used as opposed to Q50 in Chapters 4 and 5 because CRUM accounts for more hydrological processes producing a more continuous output of water to the outlet. The 7-day low statistic (Novotny and Stefan, 2007) was calculated for each discharge series firstly by calculating the lowest 7-day mean flow for each winter within the series and then calculating the mean value for the entire series.

After all the runs had been analysed there were 81 values for each statistic for the baseline runs and 81 for the future scenario runs. The impacts of climate change were assessed by calculating either the relative change for each statistic for every possible combination of baseline and future climate scenario (6561 possible combinations) and then plotting the results as PDFs.

## 7.3 Climate Change Impacts upon Snowmelt Hydrology and the Winter Flow Regime: Results

The most probable projection of winter Q5 was an increase of 13% (**Figure 7.3**) although projections ranged from -13% to 53% signifying a large uncertainty contribution from the sampled weather generator files and behavioural parameter sets. These projections mirrored those from the distributed snowmelt model when rainfall was included into its calculations (Chapter 5 **Figure 5.6**).

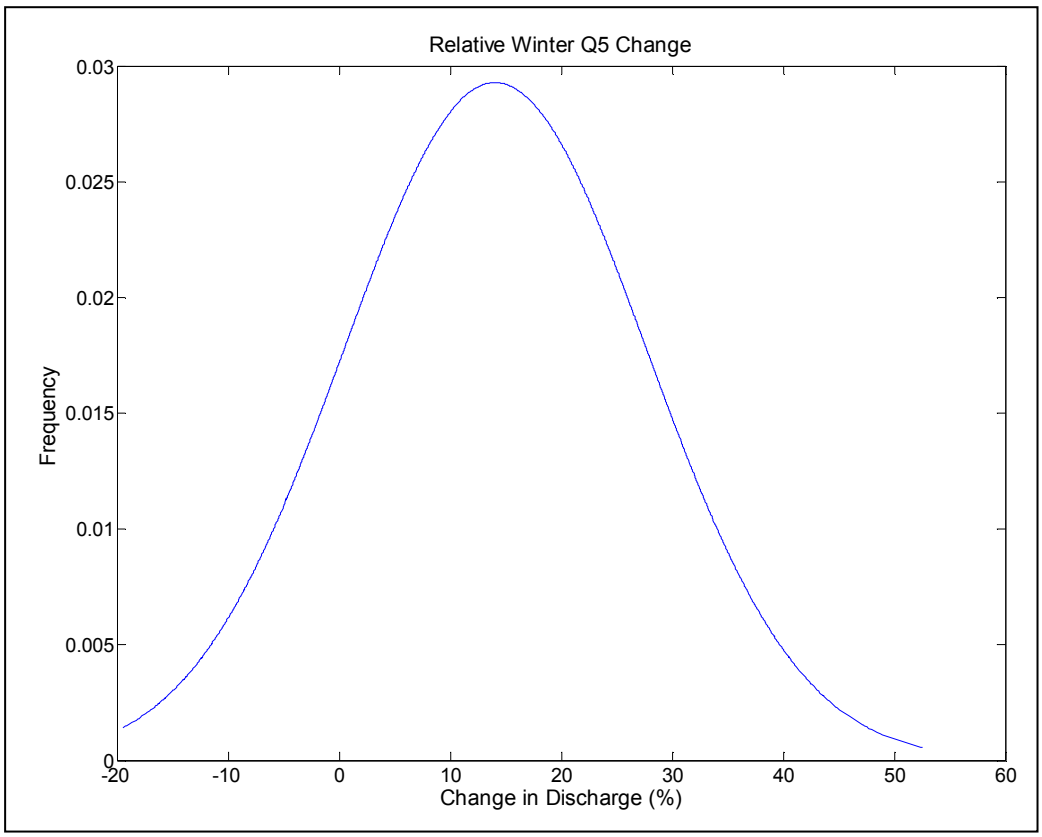


**Figure 7.3** Projections of change in winter Q5 of Dacre Beck under a medium emissions scenario according to uncertainty in the UKCP09 projections and behavioural hydrological parameter sets.

Projections in POT exceedence events however were unclear as the changes appeared to be negligible (**Figure 7.4**(**a**)) with an uncertainty range of ±2 days. These contradicted the above projections in Q5 as they appeared to show that there would be very minimal change in peak flows whereas **Figure 7.3** projections were centred round an increase of 15%. Further investigation of the POT results found that there were only ever a maximum of three exceedence events in any of the discharge series, in half of the series the threshold was never exceeded. In the seven year observed discharge record (Chapter 2 **Figure 2.5**) it was found that only one winter peak flow event exceeded the threshold. Therefore, it was decided to set a lower threshold value which would be exceeded more frequently thus increasing the clarity of future projections. A lower threshold value of 10 $m^3s^{-1}$ was chosen as this was exceeded on average 8 times during the simulation period. The results from this re-analysis projected a most probable increase of two exceedence days within a range of -15 to 18 days (**Figure 7.4**(**b**)). These projections were in line with those of the Q5 (**Figure 7.3**) as they both projected an increase in winter peak flows by the 2050s under a medium emissions scenario.

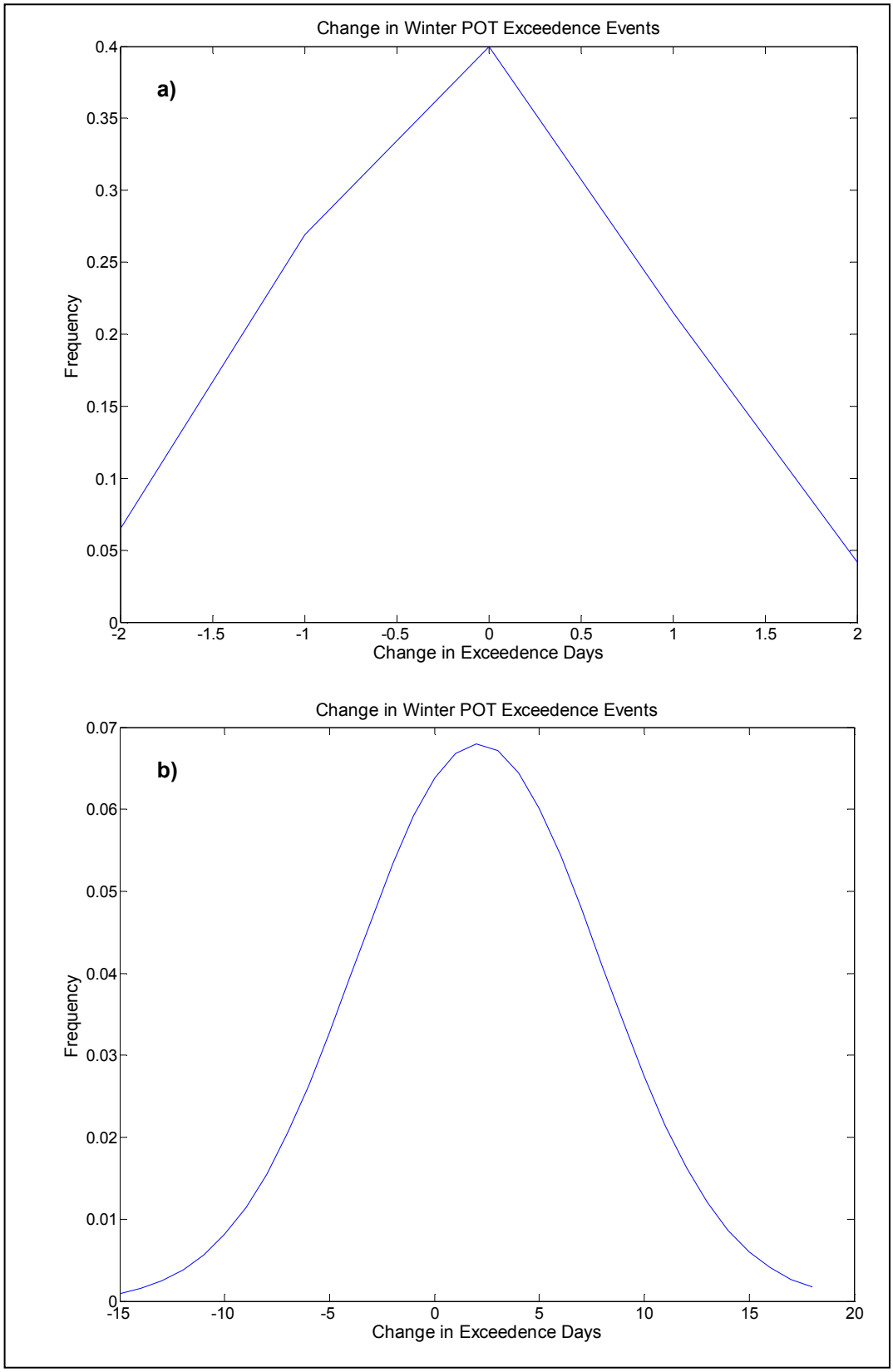


**Figure 7.4** Projections of winter Peak Over Threshold exceedence events (at a daily time step) under a medium emissions scenario according to uncertainty in the UKCP09 projections and behavioural hydrological parameter sets. **a)** Original threshold value (20.73 $m^3s^{-1}$), **b)** revised lower threshold value (10 $m^3s^{-1}$).

Low flows, like high flows, were also projected to increase according to the Q95 and 7-day consecutive low flow statistics. The former projects an increase of 15% in a range of -38% to 100% (**Figure 7.5**), the direction of projection agrees with that of Q50 from the distributed snowmelt model (Chapter 5 **Figure 5.7**). Meanwhile, the projections of the 7-day consecutive low flow agreed with those of the Q95 as they forecast a probable increase of 15% with a range of -30% to 80% (**Figure 7.6**). However, according to previous research these findings contradicted what would be expected as low flows should decrease in light warming temperatures (Chapter 5 **Figure 5.3**) and hence smaller snowpacks (Chapter 5 **Figure 5.4**).

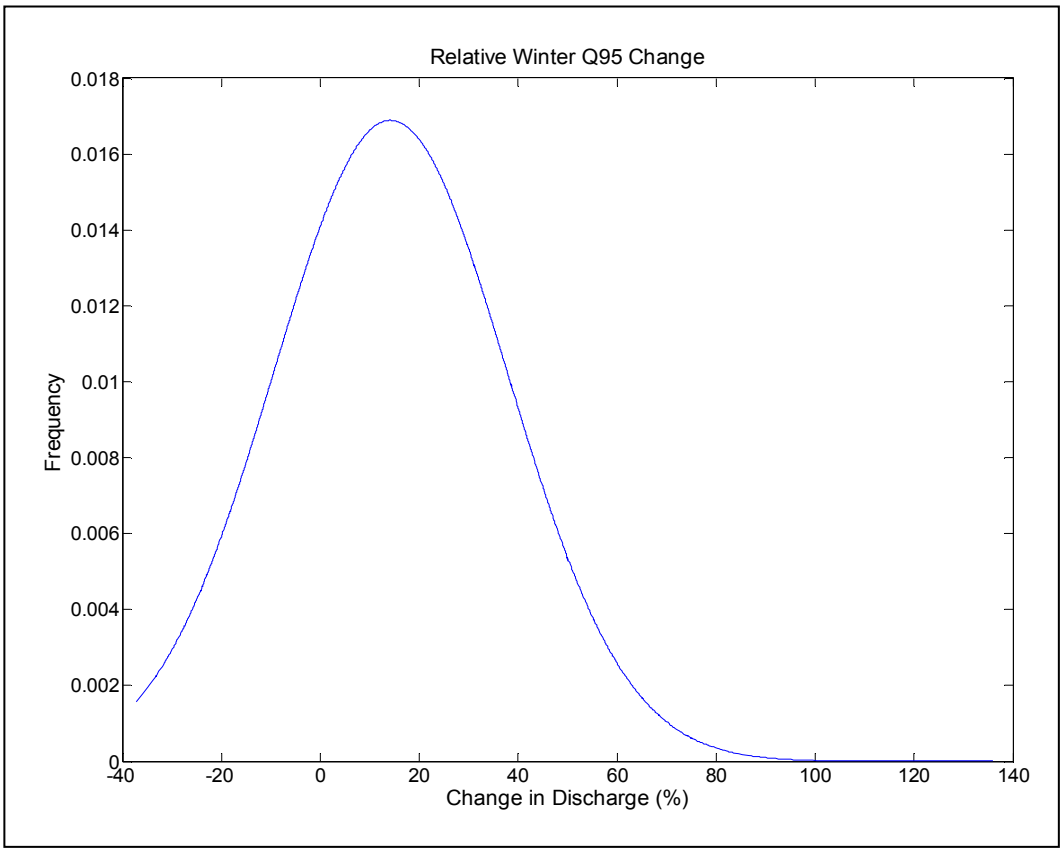


**Figure 7.5** Projections of winter Q95 under a medium emissions scenario according to uncertainty in the UKCP09 projections and behavioural hydrological parameter sets.

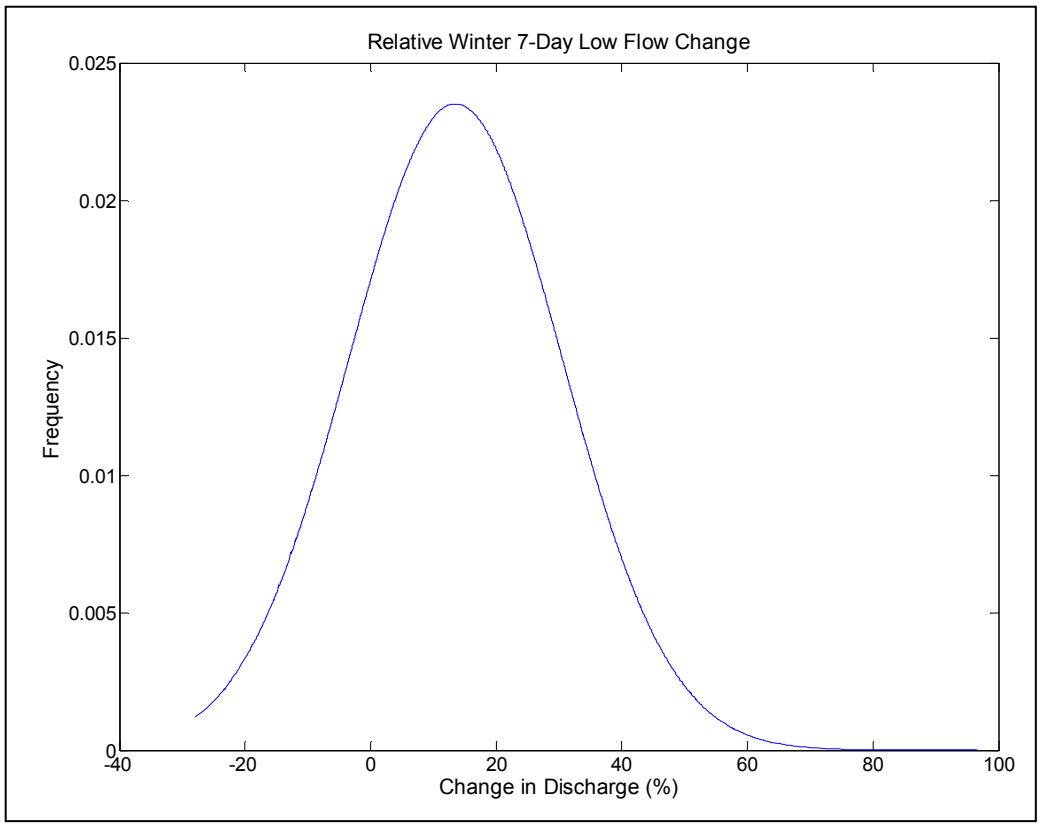


**Figure 7.6 P**rojections of 7 day consecutive low flow under a medium emissions scenario according to uncertainty in the UKCP09 projections and behavioural hydrological parameter sets.

It was expected that the projections of warmer temperatures (Chapter 5 **Figure 5.3**) and reduced snowpack accumulation (Chapter 5 **Figure 5.4**) would have resulted in greater winter hydrograph variability (SEPA, 2008). The results above however, projected that both high and low flows would increase which agreed with the Q5 and Q50 projections from the distributed snowmelt model (Chapter 5 **Figure 5.6** and **5.7**). These unexpected results were explained in Chapter 5 as being the consequence of a combination of changes in temperature and precipitation. It was found that both of these variables were likely to increase by the 2050s which meant that more precipitation would fall as rain, then the amount of rain would be further increased by the greater amount of winter precipitation. Consequently, as was hypothesised in Chapter 1 (section 1.5), the results above and in Chapter 5 showed that the winter flow regime of Dacre Beck would become rainfall dominated as opposed to rainfall-snowmelt. These results however did not demonstrate the changing role of winter snowmelt hydrology of Dacre Beck as the trends were overridden by changes the general catchment hydrology due to changes in rainfall. The results from Chapter 5, when dealing solely with snowmelt, produced results which were closer to showing increased hydrograph variability however the poor process representation of the distributed snowmelt model meant that the results could not be interpreted as being physically meaningful. To demonstrate the change in snowmelt

hydrology CRUM was run with the climate scenarios which were perturbed by changes factors that only affected temperature and not precipitation magnitude.

By assessing the consequences of changes in temperature only it was expected that the results would directly reflect changes in the snowmelt hydrology. For example, increasing the temperature may reduce the number of negative degree-days hence reducing snowpack accumulation thus reducing their attenuating role in the hydrology of the catchment (see Chapter 1 section 1.4). However the UKCP09 weather generator produces daily weather series for variables including temperature based upon stochastically generated precipitation (see Chapter 5 section 5.1.2). Consequently the weather generator could not be used to produce future weather series which only accounted for changes in temperature. Instead, as a form of sensitivity analysis, it was decided to perturb a baseline weather series from the weather generator with a range of different temperature change factors. In doing so, the precipitation variable would be held constant ensuring that any changes in the hydrograph were solely the results of changes

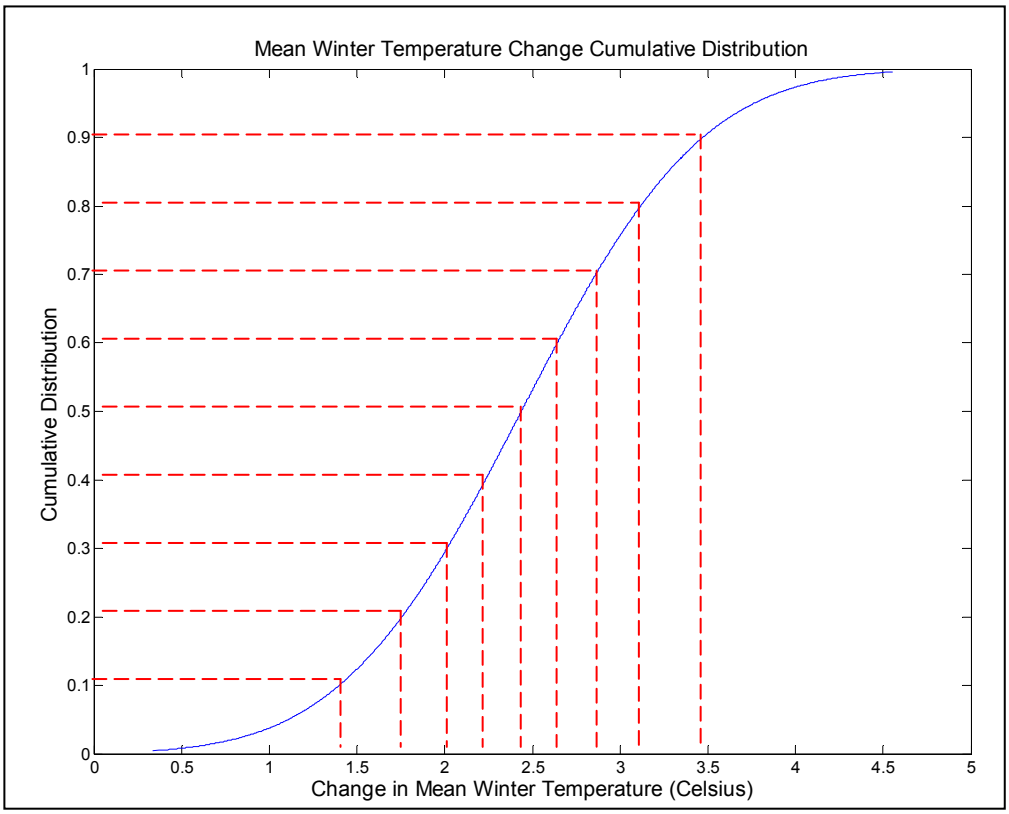


**Figure 7.7** Cumulative distribution of mean winter temperature change (solid blue line) under a 2050s medium emissions scenario produced by the UKCP09 Weather Generator and the nine likelihood values from which the change factors were sampled (red dashed lines).

| | 1 | 2 | 3 | 4 | 5 | 6 | 7 | 8 | 9 |
|---|---|---|---|---|---|---|---|---|---|
| **Change Factor (Celsius)** | 1.40 | 1.75 | 2.05 | 2.25 | 2.45 | 2.70 | 2.90 | 3.15 | 3.45 |

**Table 7.1** Mean winter temperature change factors selected from the cumulative distribution in **Figure 7.7**.

in snow and rain partitioning. A decision was made to perturb the mean winter temperature statistic as this summarised the magnitude of snowpack accumulation and melt over a winter season. Firstly a baseline weather series was selected by choosing the weather series whose mean winter temperature was closest to 0.5 on the likelihood distribution of all baseline weather series (**Figure 7.2**). Next, nine mean winter temperature change factors were chosen by producing a cumulative distribution of the mean winter temperature change PDF in Chapter 5 (**Figure 5.3** (**a**)). The change factors were then selected by reading off the *x-axis* values that corresponded to likelihood values of 0.1 to 0.9 in increments of 0.1 (**Figure 7.7**). The baseline weather series was then perturbed by each change factor (**Table 7.1**) by adding it to each daily minimum and maximum temperature, the UKCP09 also dealt with temperature change factors in an additive manner (Chapter 5 *Eq. 5.3*). Each perturbed weather series was then run for each of the nine behavioural parameter sets and the same flow statistics as above were calculated. These were then compared to the nine sets of flow statistics from the runs of the baseline series which enabled PDFs of change to be calculated for each statistic.

The high flow statistics from this analysis showed a projection of high flow decline by the 2050s. The Q5 showed a probable decrease of 2.5% in a range of -13% to 10% (**Figure 7.8**) whilst POT exceedence events (using the lower threshold values) showed a decrease of 5 days in a range of -10 to -1 days (**Figure 7.9**). These projected decreases were not expected as the temperature perturbation should only affect the partitioning of precipitation between rain and snow (evapo-transpiration would also be affected however it only represents a small part of the total catchment mass balance so changes in its magnitude would not significantly affect the winter flow regime). This was expected to decrease snowpack accumulation and hence their attenuating role so that the winter hydrograph would become more variable. The reason behind these results could be because of a reduction in snowmelt contribution to high flow events. As explained in Chapter 1 (section 1.4), flooding can result when a pulse of melt water coincides with a high rainfall event (Reed and Field, 1992). Therefore, in a warming scenario less snow will

accumulate in a snowpack prior to a high rainfall event meaning that there would be less water in the catchment during the event thus reducing the magnitude of the peak discharge. This possible explanation was explored for the 8th January 2005 peak flow event which coincided with other peaks to result in flooding downstream at Carlisle.

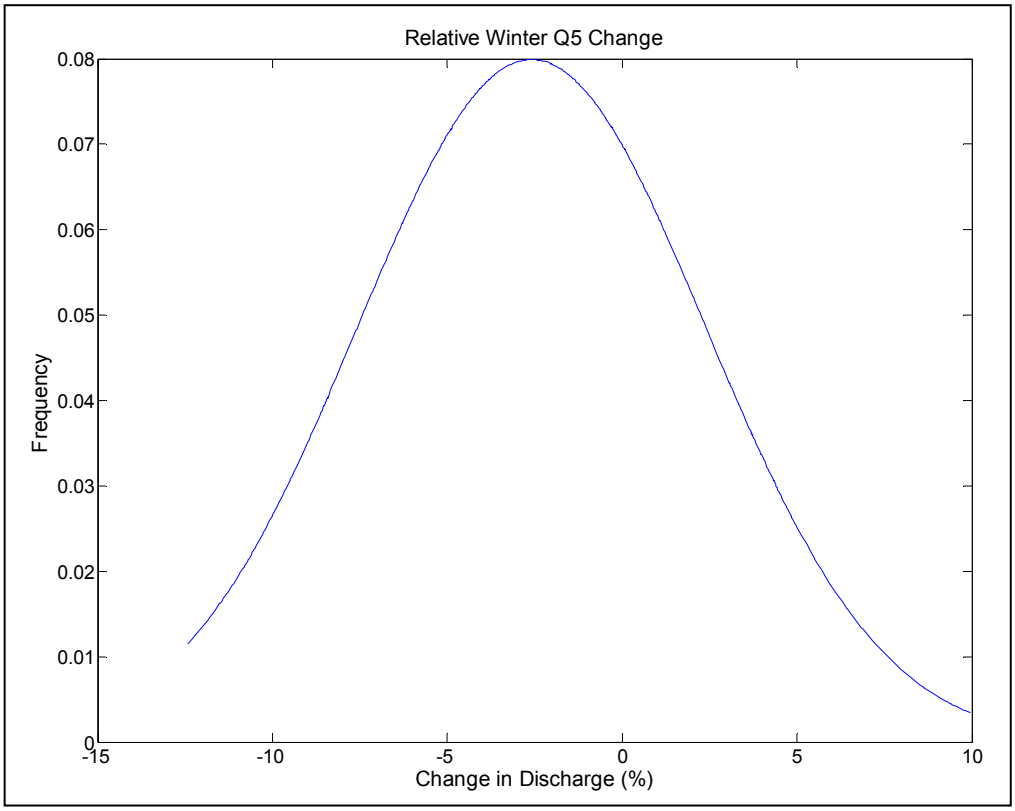


**Figure 7.8** Projections of change in winter Q5 of Dacre Beck using the perturbed temperature change factors.

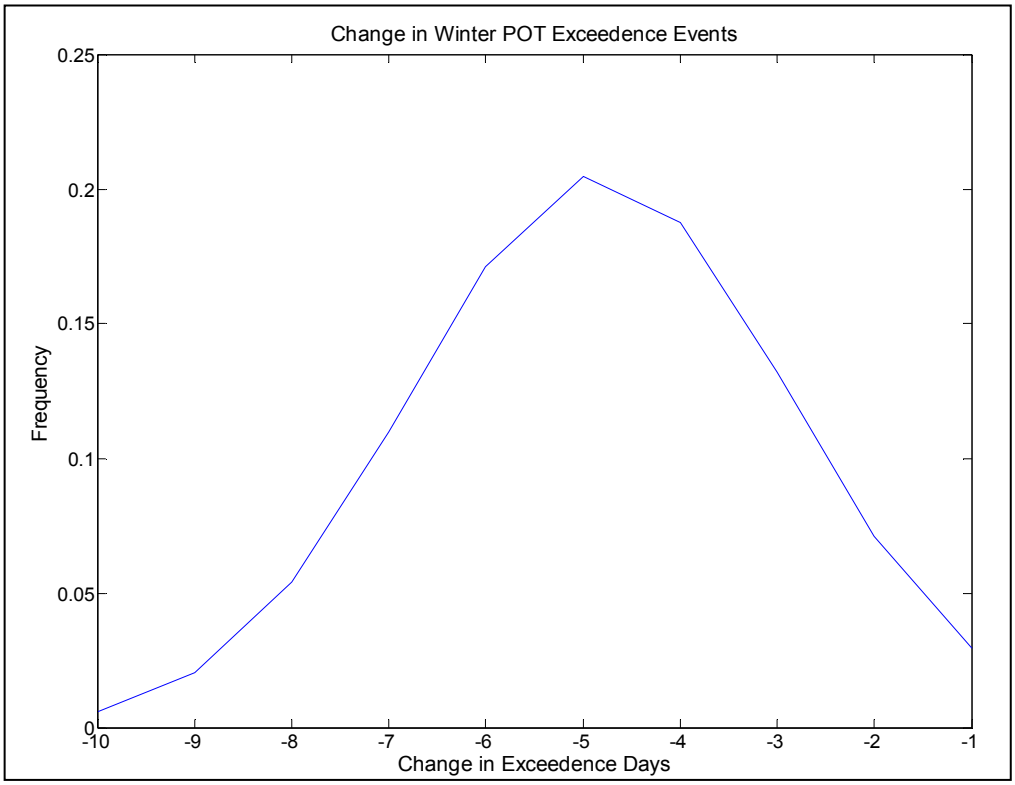


**Figure 7.9** Projections of change in winter peak over threshold exceedence events (of the lower threshold value) of Dacre Beck using the perturbed temperature change factors.

During this event, over 200 mm of rain fell in a period of two days in some parts of the Eden catchment such as Wet Sleddale near Shap (Environment Agency, 2006; Roberts *et al.,* 2009) resulting in a peak flows of 23 $m^3s^{-1}$ at the outlet of Dacre Beck, the highest in the observed discharge record (Chapter 2 **Figure 2.5**). Snowmelt contribution was not explicitly mentioned in the Environment Agency report however it was found by one study to have contributed to peak flows from the some of the upper Eden catchments although Dacre Beck was not mentioned specifically (Watkins and Whyte, 2008). It was decided therefore to use temperature and precipitation observations during this event to investigate the impact of perturbing the temperature upon the peak flow. The observed weather series was perturbed by each temperature change factor before each weather series was run for each behavioural parameter. The peak flow during the event was then calculated from each run and a PDF of peak flow change was calculated (**Figure 7.10**).

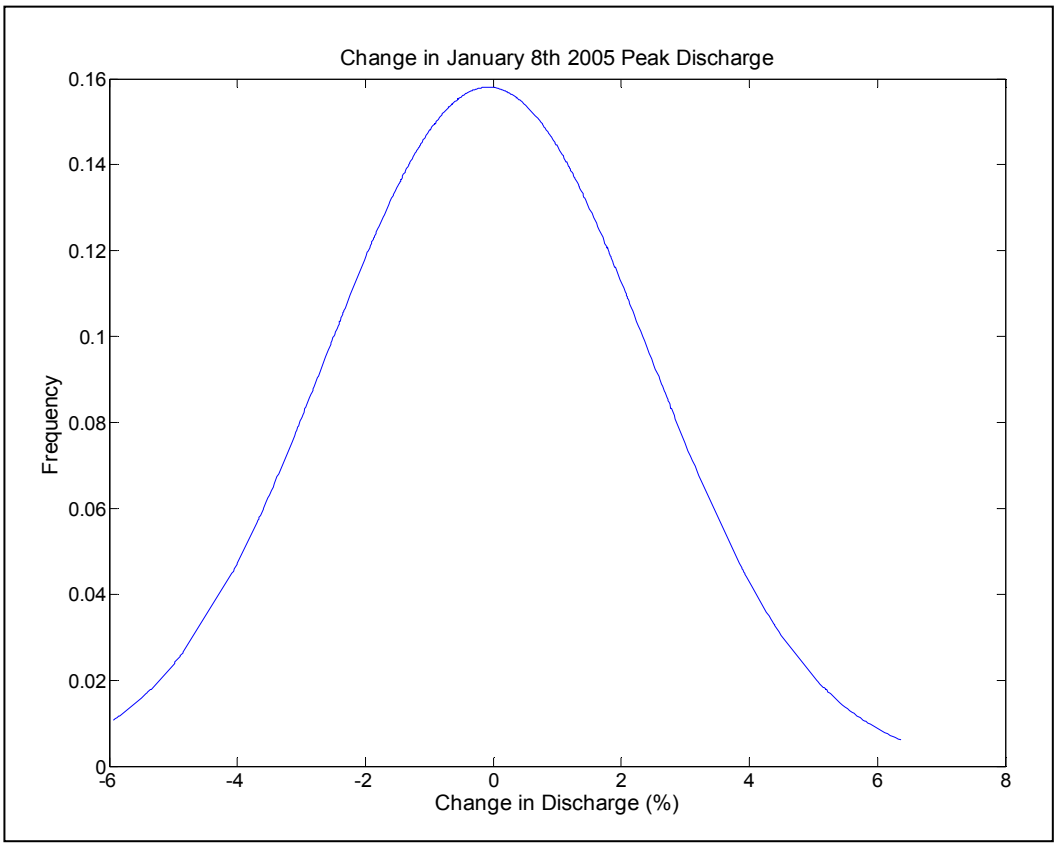


**Figure 7.10** Projections of change in the January 8th 2005 peak discharge using the perturbed temperature change factors.

Projections of the January 8th 2005 peak discharge showed a very minimal change (**Figure 7.10**) which would appear to mean that changes in snowmelt would have a minimal impact on changes in peak discharge. However, it was explained above that there was no previous description of the contribution of snowmelt during this event in Dacre Beck. Therefore, if snowmelt had played a relatively small role during the peak flow event

it would be expected that changes in the snowmelt hydrology would not have had an easily detectable impact upon the peak flow event. To test this CRUM was re-run for a single behavioural parameter set but without the treatment of snowmelt. Peak discharge on January 8th 2005 from the resulting hydrograph was then compared to the peak discharge from the hydrograph produced from the same parameter set but with the inclusion of snowmelt, the difference would highlight the contribution of snowmelt hydrology (Dunn *et al.,* 2001). It was found that there was a very small difference between these two values (0.54%) which meant that snowmelt contribution to the peak discharge during this event was very small. Therefore the above analysis was not able to confirm if the decreasing projection of winter threshold exceedence events (**Figure 7.9**) was due to a reduction in the snowmelt contribution to peak flows.

The analysis of low flows found that there was very little change in the Q95 and 7 day consecutive low flow statistics (**Figure 7.11** and **7.12** respectively). It was expected that perturbing the mean winter temperature would have decreased low flows as the consistent release of melt water would decline. The smaller snowpacks would have meant that flow

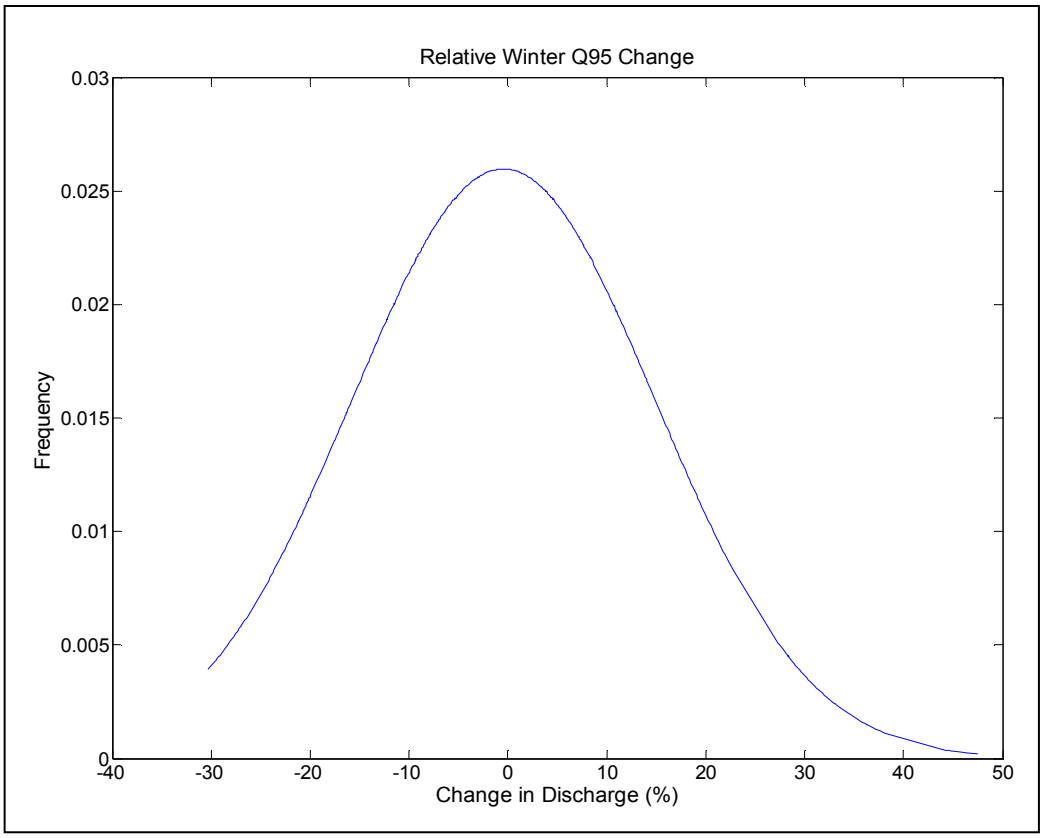


**Figure 7.11** Projections of change in winter Q95 of Dacre Beck using the perturbed temperature change factors.

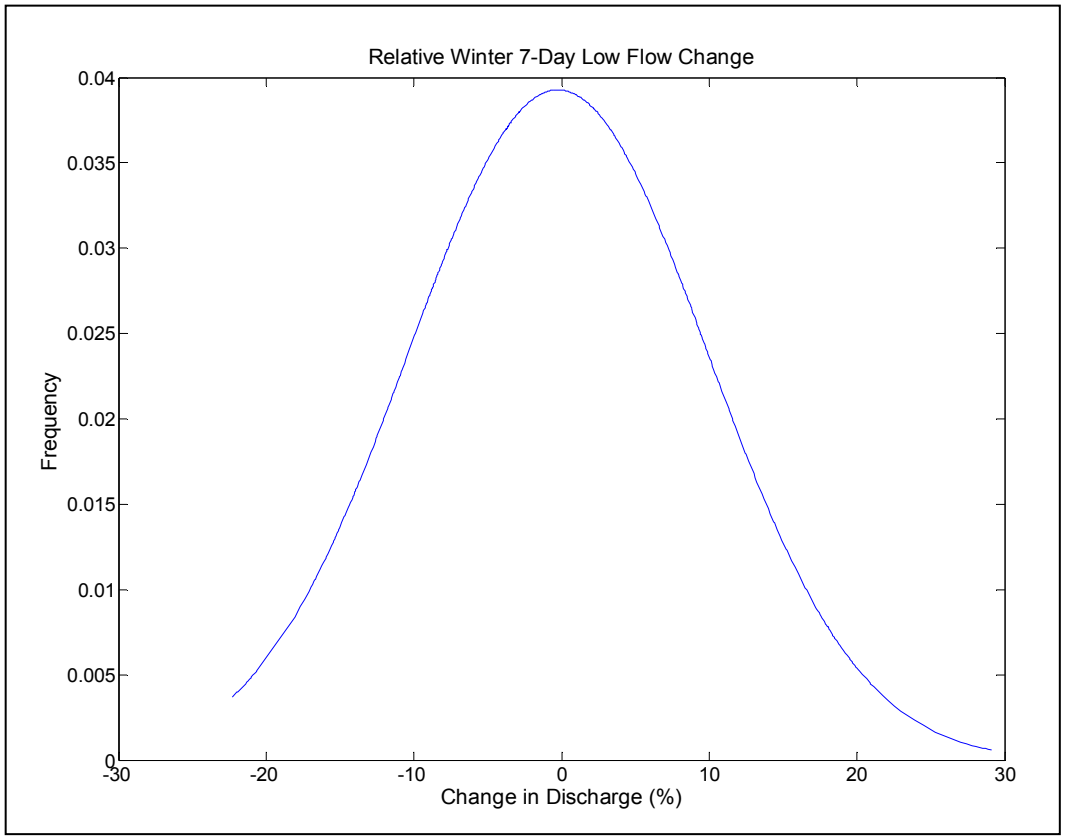


**Figure 7.12** Projections of change in winter 7 day consecutive low flow of Dacre Beck using the perturbed temperature change factors.

supplementation would be dependent upon rainfall whose temporal variability is greater (Chapter 1 section 1.4). Instead, these results may suggest that snowmelt hydrology in Dacre Beck plays a negligible role in low flow supplementation both at present and in the future. The supplementation of low flows from snowpacks is most important when there are prolonged days without precipitation (SEPA, 2008). At present however, during the winter in Dacre Beck the length of periods without precipitation was found not to exceed twelve days. These periods were too short to produce low flows comparable to those in the summer as they were surrounded by periods of high precipitation. This meant that there was sufficient water stored within the soil to supplement the river flow meaning that the contribution of snowmelt was very small by comparison. It was found in Chapter 5 (**Figure 5.8**) that the number of precipitation days was not expected to change. Therefore precipitation-free periods were not likely to increase so soil moisture would still be able to supplement river flows in the future. As a result this meant that changes in snowmelt contribution to supplementation were difficult to detect as the trends would be overridden by soil moisture trends.

## 7.4 Discussions and Conclusions

The results from this chapter showed that the winter flow regime of Dacre Beck by the 2050s under a medium emissions scenario was likely to change due to an expected increase in both high and low flows. These expectations agreed with the projections from the combined snowmelt-rainfall hydrographs of the distributed snowmelt model (Chapter 5) but did not show the expected increase in hydrograph variability (SEPA, 2008). It was hypothesised both in this chapter and Chapter 5 that these results were the consequence of a combination of changes in snowmelt hydrology and rainfall. However because these results were derived from weather series where both temperature and precipitation were perturbed it was difficult to ascertain the role of snowmelt hydrology in these changes. Therefore a decision was made to perturb the weather series by only using temperature change factors so that changes due to snowmelt hydrology were more detectable. Results from this analysis found that high flows were likely to decrease and low flows were likely to see a minimal change. The decrease in high flows agreed with the projections of snowmelt hydrology from Chapter 5 (**Figure 5.6**) but again disagreed with the increase expected from the findings of previous research (SEPA, 2008). The results meant that less water was being routed to the outlet during peak flow events and it was argued that this may have been due to a reduction in the contribution from snowmelt due to the accumulation of smaller snowpacks. Analysis of the 8$^{th}$ January 2005 peak flow was unable to confirm this as it was found that the original event had a minimal contribution from snowmelt. Changes in low flows from this analysis were found to be minimal possibly due to the small role of snowmelt in supplementing flows during the winter. Instead it was hypothesised that the large amount of winter rainfall in Dacre Beck meant that the soil was able to store and subsequently release water which supplemented flows more than snowmelt.

The synthesis above shows that this chapter was able to model future changes in the winter flow regime of the study catchment but was unable to explicitly assess the changing role of snowmelt hydrology. This was because unlike the distributed snowmelt model it did not feature an output hydrograph composed solely from snowmelt. Instead changes in snowmelt hydrology had to be inferred from a separate analysis of the future climate series. Previous studies have attempted to quantify the role of snowmelt in the winter flow regime by running a hydrological model for the same weather series with and without treatment of snowmelt processes (Dunn *et al.,* 2001). This procedure however would require twice the number of model runs which may be problematic when applying a hydrological model within an uncertainty framework. Instead it would be more appropriate

to further improve the hydrological model so that it produced an output hydrograph composed solely from snowmelt. This would improve the analysis of the winter flow regime as it could assess the changing percentage contribution from snowmelt towards high and low flows.

This chapter has outlined how the winter flow regime of Dacre Beck is likely to change by the 2050s under a medium emissions scenario. The results suggested that the role of snowmelt hydrology in these changes may be overridden by changes in winter rain accumulation. Further improvements to the approach in this chapter have been outlined which could be implemented in future studies which would simplify the quantification of the contribution from snowmelt hydrology to the winter flow regime. The next chapter discusses these results and further improvements in greater detail. It will also draw upon the results and discussions from previous chapters to formulate general conclusions in relation to the project's overall research aim.

# Chapter 8

# Discussions and Conclusions

## 8.1 Introduction

This project investigated the impacts of projected climatic change upon the snowmelt hydrology and subsequently the winter flow regime of an upland UK catchment. Previous research had shown that snowmelt hydrology was important in attenuating the extreme high and low flows of the winter flow regime (SEPA, 2008) but that its role was likely to change in future warmer winters (Harrison *et al.,* 2001). However, little of the previous research within the UK had used projections of future winter climate to explicitly assess the impact upon snowmelt hydrology and its impact upon the winter flow regime. Changes in climate were likely to impact upon the processes of snow accumulation and melt and hence affect the winter flow regime. Therefore this project was split into three research questions which assessed changes in snow accumulation, snowmelt hydrology and the resulting impacts upon the winter flow regime. The next section re-iterates how each research question was investigated, outlines the key results from each and provides a discussion of any contentious issues with the methodology or the results before making recommendations for future work.

## 8.2 Research Questions: Key Findings and Discussions

1) *How will snow accumulation change in the future climate in comparison to present conditions?*

Changes in snow accumulation were investigated as it affected how much was available to melt. This accumulation and melt balance would in turn affect the role of snowmelt hydrology within the catchment and the winter flow regime. Present and projected (2050s medium emissions) weather series from the UKCP09 weather generator (Jones *et al.,* 2009) were used to investigate this research question. Snow accumulation was modelled from each weather series by spatialising temperature and precipitation across the study catchment using lapse rate equations for each. Changes in total snow accumulation between the present and future weather series were then assessed from this modelling along with changes in the mean winter temperature across the whole catchment and at the highest altitude as well as changes in total winter rain accumulation.

The results from this analysis found that the total winter snow accumulation was most likely to decrease by 49.5% which is likely to have resulted from the 2°C mean winter temperature increase across the catchment. The mean winter temperature at the highest altitude was found to increase above 0°C. Meanwhile, the magnitude of winter

precipitation falling as rain was projected to increase by 57.0%. A detailed interpretation and discussion of these results is given in the following paragraphs.

The large decline in snowpack accumulation was due to the large temperature increase, in particular the increase of the mean winter temperature above 0°C at the highest elevation. The 0°C temperature was used by the distributed snowmelt model as a threshold to partition precipitation between rain and snow. Presently, winter temperatures at the highest elevations of Dacre Beck were often below this threshold value which enhanced snow accumulation. Projections of future winter temperatures at the highest elevation however, indicated that winter temperatures at the highest elevations in general were likely to be above this threshold value. Hence the more frequent exceedence of this winter threshold temperature resulted in a large decrease in snowpack accumulation within the catchment. The use of a threshold temperature to distinguish between rain and snow is subject to discussion as this empirically represents the physical snow atmospheric snow formation processes. Previous studies have confirmed the validity of this empirical approach for catchments at similar elevations to Dacre Beck (Barry, 1992) in producing realistic results of snow accumulation. The precise value of this threshold temperature is subject to local catchment conditions and was treated as a parameter in this study. However, it was found to be insensitive when included in a sensitivity analysis of the distributed snowmelt model (Chapter 4 section 4.2.2.6) and CRUM (Chapter 6 section 6.4.6) hence it was treated as a fixed parameter. Furthermore this threshold value was used in previous studies of UK snowmelt hydrology (Harrison *et al.,* 2001; Dunn *et al.,* 2001) to produce realistic results of snow accumulation. Therefore the approach used in this study to model snow accumulation was able to produce realistic results for the available climatic data.

The results from this analysis continued from previous observations of present UK snow accumulation decline and confirmed previous modelling of future UK snow accumulation changes (Harrison *et al.,* 2001). It had been observed that mean winter temperatures had warmed by 1°C from 1961 to 2004 (Barnett *et al.,* 2006) which had resulted in reduced snowpack accumulation since this warming raised the freezing elevation (SEPA, 2008). Previous modelling of the future change in snowpack accumulation in Scotland using UKCIP98 projections found a continued reduction especially at elevations of 400 m (Harrison *et al.,* 2001). Therefore the results from this project confirmed that continued warming of winter temperatures was most likely to result in the continued decline in snow

accumulation. The large reduction in snow accumulation may also confirm the previous finding that the greatest sensitivity was at 400 m elevation (Harrison *et al.,* 2001) as the Dacre Beck catchment was situated at this level. Projections of temperature at the highest elevation confirmed that they were most likely to be raised above the threshold value meaning that the freezing level was often higher than the highest elevation thus greatly reducing snow accumulation.

2) *How will changes in climate affect snowmelt hydrology?*

This question was investigated to assess whether the role of snowmelt hydrology would be impacted by the expected reduction in snow accumulation or if the increase in energy fluxes would compensate for the reduced accumulation by releasing more in the initial melting of a snowpack. Changes in snowmelt hydrology were assessed by creating a distributed snowmelt model which used three different temperature-index snowmelt equations. Each of the UKCP09 weather series were then used to drive the model and changes in the Q5 and Q50 snowmelt hydrograph flows were analysed. If changes in the energy fluxes were sufficient to compensate for the reduced accumulation then there would have been a negligible change in both the high and low flows. The results found that high snowmelt-derived flows were likely to decline from between 15% to 40% whilst low snowmelt-derived flows were likely to decrease from between 40% to 70%. These large changes meant that the changes in the energy fluxes were unable to compensate for the large reduction in snow accumulation projected in the first research question.

Projections of smaller accumulated snowpacks, found in the first research question, meant that less snow water equivalent (SWE) was stored on the slopes of the catchment. Therefore during large snowmelt events caused by large temperature increases, for example, less melt water would be produced hence peak snowmelt flows would be smaller. The decrease in high flows shown by these results also meant that the increase in the energy fluxes, such as latent and sensible heat which were related to air temperature, was unable to compensate for the decline in snowpack accumulation. The accumulation of smaller snowpacks also resulted in a reduction in snowmelt derived low flows. This was because warmer temperatures would have reduced the number of days of snow falling thus the frequency of small snowpacks which may have accumulated very infrequently under present conditions would become more frequent. Consequently, the small amount of melt water produced by these small snowpacks would also occur more frequently. On the snowmelt flow duration curve therefore, the low flow presently

associated with the 99$^{th}$ percentile would become associated with the 95$^{th}$ percentile under future conditions.

All three temperature-index equations were applied at an hourly time step within the distributed snowmelt model. This may be contentious for the first and second equations which were derived at a daily resolution as these derivations may not have held at a finer temporal resolution. However, by aggregating the hourly hydrographs to daily values it was found that the results were not vastly dissimilar to those from the third equation (Chapter 5 section 5.3) which was derived at an hourly resolution. Another potential limitation of this analysis was the lack of validation to observed snow accumulation and melt data. It was mentioned above that the method of snow accumulation modelling was the most suitable for this project and that the threshold value was found to be insensitive. This suitability could have been confirmed by comparing predictions of snow accumulation depth for a point in the catchment with observations of snow depth at the same point (Dunn *et al.,* 2001). Observations of snow depth were not available in the catchment, even if they were available it would only validate snow accumulation at a point rather than across the entire catchment. Instead, catchment scale snow accumulation could be validated by comparing results with optical satellite observations of snow cover (such as the $MODIS_{SCA}$ product (Maurer *et al.,* 2003; Roy *et al.,* 2010)). However optical satellite imagery during the UK winter is often obscured by cloud cover making validation very difficult. Therefore there was insufficient data available to this project to ensure the accurate validation of the snow accumulation component of the distributed snowmelt model. Snowmelt production can be validated using lysimeter measurements at the base of a snowpack (Davis *et al.,* 2001). Firstly however, this data was unavailable in the Dacre Beck, but secondly data derived from lysimeters is subject to a large amount of uncertainty due to the development flow fingers because of snowpack heterogeneities (Kattelmann and Dozier, 1999). Therefore it was not possible to directly validate the results of the distributed snowmelt model firstly, because there was insufficient data available within the catchment. Secondly the methods used to validate snow accumulation and melt models are often subject to large uncertainties which may only be able to constrain the models to a broad range of possibilities. In light of this, it is recommended that the results from the distributed snowmelt model are viewed as a sensitivity analysis of snow accumulation and melt processes to changes in climate rather than being taken as physically-meaningful predictions.

The decreasing magnitude of winter snowmelt hydrology under warming temperatures found in this analysis could explain the increase in winter flow regime variability observed in some Scottish catchments during the warming trend from 1961 to 2008 (SEPA, 2008). The results showed that the contribution from snowmelt was likely to decrease and that the amount of rainfall was projected to increase (Chapter 5 **Figure 5.4**) under warmer temperatures. Therefore the winter hydrograph was likely to become composed predominantly from rainfall as opposed to a more equal combination of the two sources. Consequently, the winter hydrograph would be likely to become more variable as the more consistent contribution from snowmelt was likely to decline. Therefore the future decline in snowmelt hydrology was found in this section to impact upon the winter flow regime. However, the winter flow regime would also be affected by changes in precipitation and not just snowmelt hydrology. Hence the full implications of climate change for the winter flow regime of Dacre Beck were also analysed and the results are discussed in below.

3) *What are the implications of changes in climate and snowmelt hydrology for the winter flow regime?*

The third research question aimed to assess the consequences of changes in snow accumulation and melt processes outlined in the previous two research questions upon the winter flow regime. Changes in the winter flow regime of the study catchment were modelled firstly by using the distributed snowmelt model and combining the snowmelt hydrograph with a rainfall hydrograph. However, the results from this were found to have been affected by the limited hydrological process representation of the model. Therefore each of the snowmelt equations were incorporated into an existing physically-based hydrological model (CRUM). Using this improved model, changes in the winter flow regime were assessed by running it with a sample of UKCP09 weather series and analysing the changes in flow statistics that represented high and low flows. It was expected that a reduction in the role of snowmelt hydrology, as forecast by previous research (Arnell and Reynard, 1996), would amplify the high and low flows of the winter flow regime.

The results found that high winter flows were likely to increase; the Q5 was projected to increase by 13% whilst the number of winter peak over threshold events was likely to increase by two days. Low winter flows meanwhile were also projected to increase with both the Q95 and 7-day consecutive likely to increase by 15%. The contribution to these changes from changes in the snowmelt hydrology was investigated by re-running the

model with present weather series perturbed by a range of different future mean winter temperature change factors. The results from this found that changes in the snowmelt hydrology would be responsible for a reduction in high flows and a negligible impact upon low flows. Therefore, changes in the winter flow regime resulting from changes only in snowmelt hydrology were different to those resulting from the original UKCP09 data. It was hypothesised that this might be due to changes in rain accumulation dominating the signal of change in the winter flow regime. These results along with the possible explanations are discussed in greater detail below.

The decreasing role of snowmelt hydrology in future conditions in Dacre Beck as projected in the previous research question was expected to result in greater variability in the winter flow regime. However, when CRUM was run using future projections of both temperature and precipitation the results suggested that both high and low flows were likely to increase. It was expected that these results were the consequence of an increase in the magnitude of future winter precipitation (Chapter 5 **Figure 5.1** (**b**)). This would mean that more water would be inputted into the catchment over the same period of time hence flows across the season were likely to increase. The role of changes in snowmelt hydrology in affecting these projections was investigated by perturbing baseline temperature series with future change factors. It was found that changes in snowmelt hydrology were likely to decrease the magnitude of high flows and have a negligible impact upon low flows. The decrease in winter high flows could have been due to the reduction in snowmelt contribution to peak flows during storm events. Storm events can be accompanied by large temperature increases, 4-6°C during the river Tay January 1993 storm event (Black and Anderson, 1993), meaning that a large amount of snowmelt can combine with large amounts of rainfall to produce high flows. Future warmer temperatures would mean that smaller snowpacks would accumulate, as found in the first research question, thus the contribution of snowmelt during storm events would be reduced. In turn, this would lead to a reduction in the flow magnitude during storm events. An attempt was made to demonstrate this mechanism for the January 2005 storm event but it was found that snowmelt did not play a significant role in the original event. The negligible changes in winter low flows due to changes in snowmelt hydrology meant that snowmelt supplementation of low flows was unimportant both in present and future conditions. Instead supplementation of low flows from soil moisture was likely to be more important than the contribution from snowmelt. However, the impacts of changes in snowmelt hydrology upon the winter flow regime were not present in projections of the winter flow regime when changes in precipitation magnitude were accounted for. As mentioned

above, high and low flows were projected to increase whereas changes in snowmelt hydrology should have resulted in a reduction in the former and a negligible change in the latter. Therefore it was likely that the signals of change in the winter flow regime would be dominated by changes in precipitation magnitude rather than changes in snowmelt hydrology.

The incorporation of each snowmelt equation into CRUM meant they were applied in this study on a per-minute time scale which was beyond the scale at which they were derived. It was found in the application of the distributed snowmelt model that aggregating the resulting hydrographs back to their original temporal resolutions yielded good results. In this application however, it was found that this aggregation was unable to account for the effects of applying the equations at a finer time step. This was particularly evident in the third snowmelt equation where the large number of time steps per day meant the multiplication of its reciprocal with the degree-hour parameter reduced the positive air temperature component relative to the rain-on-snow and solar radiation components (Chapter 6 section 6.4.6). This contradicted the original conceptualisation of this equation which perceived the positive air temperature component to be the most important (Hock, 1999). Rectification of this issue could be achieved by using a physically-based energy balance approach to snowmelt modelling as its equations are independent of the time step on which they are applied. However, as explained in Chapter 3, this modelling approach requires input data that was not available in the catchment. A simplified energy balance model was developed by Walter (*et al.,* 2005) but its simplifications meant it could only be applied at a minimum of a daily resolution. Therefore future development of snowmelt within CRUM should aim to find an approach with a greater physical basis but one whose input data requirements are easily met.

The development of CRUM in this project did not include the creation of a variable that described an output hydrograph composed solely from snowmelt as in the distributed snowmelt model. This meant that changes in the winter flow regime caused by changes in snowmelt were difficult to detect and could only be demonstrated by re-running the model with temperature perturbations. Further development to the CRUM code could be undertaken to produce a snowmelt hydrograph variable which could simplify future analyses.

The projections of increasing high and low winter flows found in this project reaffirmed previous predictions that the role of snowmelt hydrology would decline in warmer temperatures (Arnell and Reynard, 1996). However, they contradicted previous observations that the winter flow regime's variability would increase during warming trends (SEPA, 2008). It was previously thought that the reduction in snowmelt would mean that the winter hydrograph would become predominantly composed from rainfall which was more variable than rainfall. Previous studies however made no observations of changes in the magnitude of precipitation during the warming trends. Hence when projections of precipitation increases were included into the modelling process it was found that both high and low flows during the winter increased due to the greater amount of water in the catchment. Therefore the impacts of changes in snowmelt hydrology upon the winter flow regime were likely to be overridden by changes in precipitation.

However, when the impacts of snowmelt hydrology were treated in isolation the results still did not agree with previous observations. Instead, they projected that high flows would decrease and low flows would see minimal change. These different results could be due to the different role of snowmelt hydrology in Dacre Beck as opposed to the Scottish catchments from which the observed trends in flow variability increases were derived. In the Scottish catchments snowmelt hydrology has been observed to play an attenuating role in the winter flow regime of the catchments (SEPA, 2008). Meanwhile in Dacre Beck, snowmelt hydrology may only play a role in exacerbating high flows during winter storm events otherwise its role in attenuating flows may be much smaller than in the Scottish catchments. This could be explained as being the consequence of the Scottish catchments being colder (Chapter 1 **Figure 1.4**) than Dacre Beck enabling them to accumulate more snow (Chapter 1 **Figure 1.2** (**a**)). As a result these greater snowpacks would exert a greater influence upon the winter flow regime than in Dacre Beck whose snowpacks are only able to play an occasional exacerbating role in winter high flow production. Therefore the consequences of climate change for snowmelt hydrology and hence the winter flow regime of Dacre Beck are likely to be different to the consequences for Scottish catchments. Further work should therefore be undertaken into understanding the different role of snowmelt hydrology upon upland catchments across the UK at present. These results could then in turn be used to understand the varying implications of climate change for the winter flow regime of upland UK catchments.

## 8.3 Recommendations for Future Work

The main difficulty encountered in this project was relating changes in snowmelt hydrology to changes in the winter flow regime. Firstly, the hydrological process representation of the distributed snowmelt model was insufficient to confidently conclude about the role of snowmelt in the winter flow regime. Next, the inclusion of the temperature-index equations into the physically-based hydrological model resulted in the implementation of each equation at a time step much smaller than the time step at which they were derived. This was especially problematic for the third snowmelt equation. Then, since there was no explicit snowmelt output variable in the hydrological model, it was difficult to understand the role of snowmelt hydrology in the winter flow regime. Finally, no attempt was made in this project to directly validate the modelling of either the snow accumulation or melt processes, instead relying on the information in the discharge hydrograph.

It is therefore recommended that future investigations undertake further developments to the physically-based hydrological model by incorporating an energy balance modelling approach to snowmelt which would be more compatible with the time step of the hydrological model than the temperature-index approaches. Then a snowmelt hydrograph variable should be included into the hydrological model making it easier to understand the contribution of snowmelt to the final output hydrograph. Attempts should also be made to validate the snow accumulation process to ensure that this component is behaving realistically. This could be achieved by using a different catchment where measurements of snow depth are available. Snowmelt could also be validated but as explained above the measurements themselves can be subjected to large uncertainties.

## 8.4 Snowmelt Hydrology and its Future Implications for the Winter Flow Regime: Concluding Remarks

A method was developed in this project to assess the contribution of snowmelt hydrology to the winter flow regime in light of projected climate change. The results showed that future forecasts of warmer temperatures are likely to result in smaller snowpacks and a reduction in the role of snowmelt hydrology in the Dacre Beck catchment. The consequences of this for the future winter flow regime in the Dacre Beck catchment were found to be overridden by future changes in the magnitude of winter precipitation. However, different results may emerge for other upland UK catchments due to their unique climatological factors. For example, previous research in Scottish catchments

found a more pronounced signal of snowmelt hydrology in the winter flow regime under present conditions (SEPA, 2008). In the case of Dacre Beck, this project found that projected changes in snowmelt hydrology were of secondary importance to the changes in total winter precipitation in the predicted impact upon the winter flow regime. Applying the same method to other upland UK catchments may however produce different results.

# Appendix 1

## Sensitivity Analysis:

## Snowmelt Model Parameter Response Curves

***Snowmelt Model 1:***

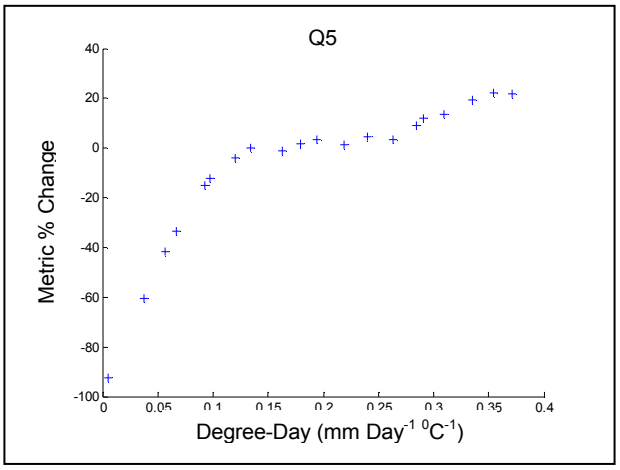


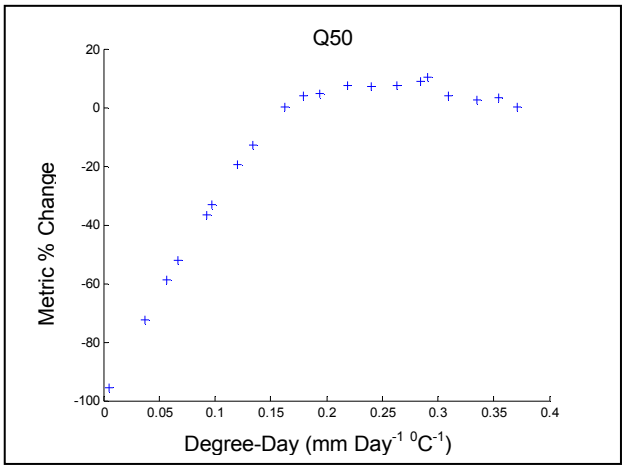


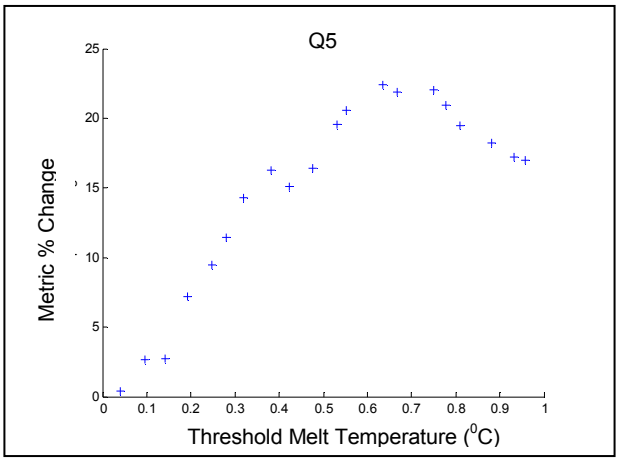


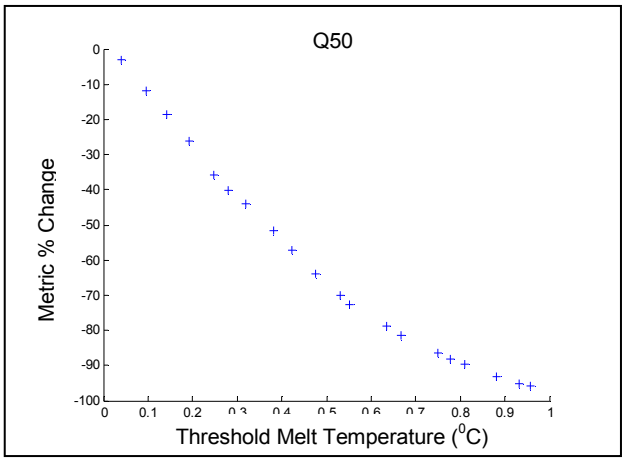


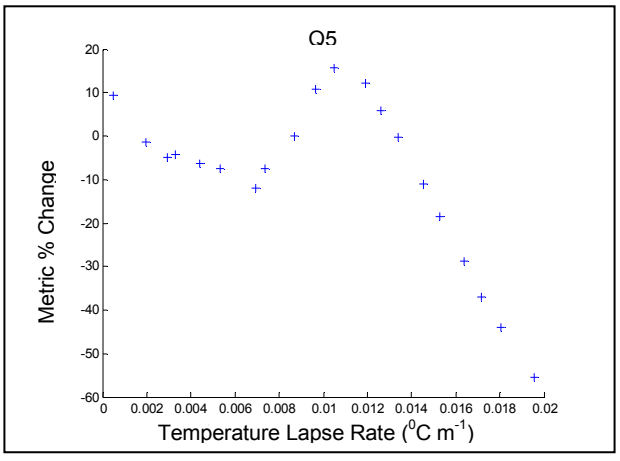


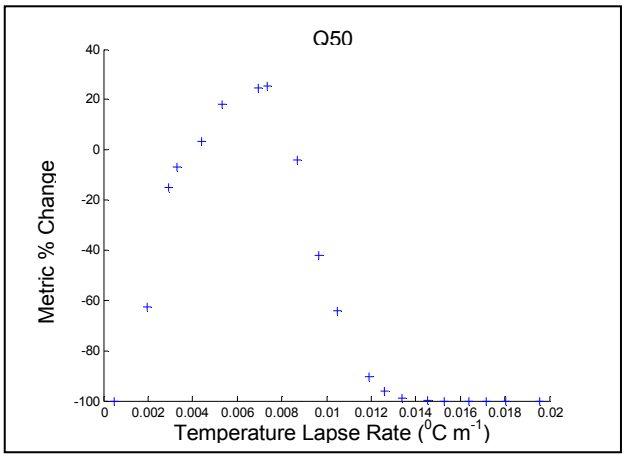


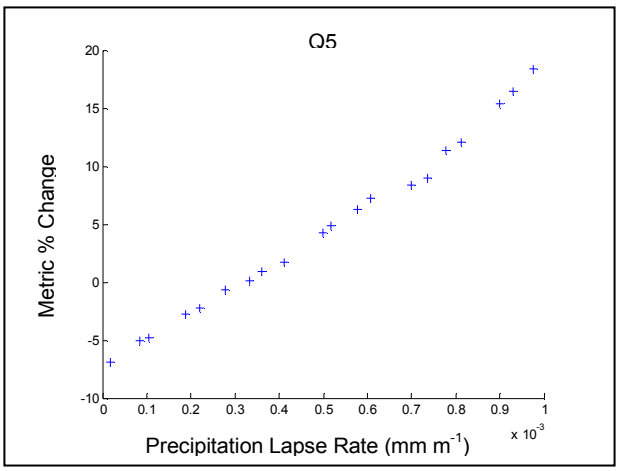


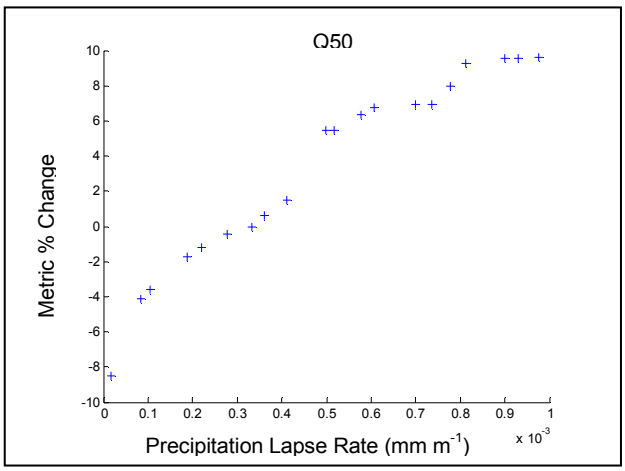

***Snowmelt Model 2:***

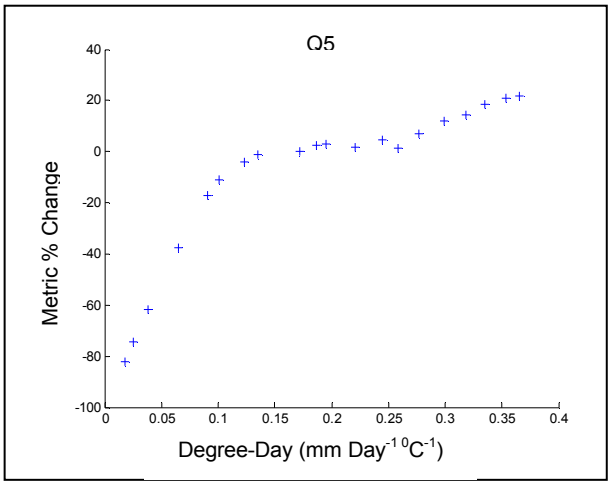


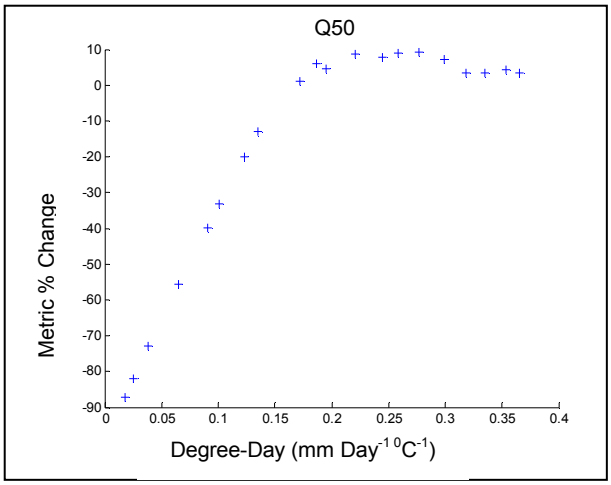


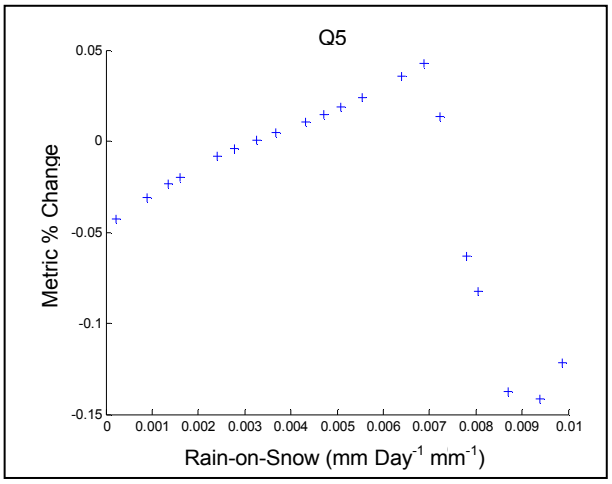


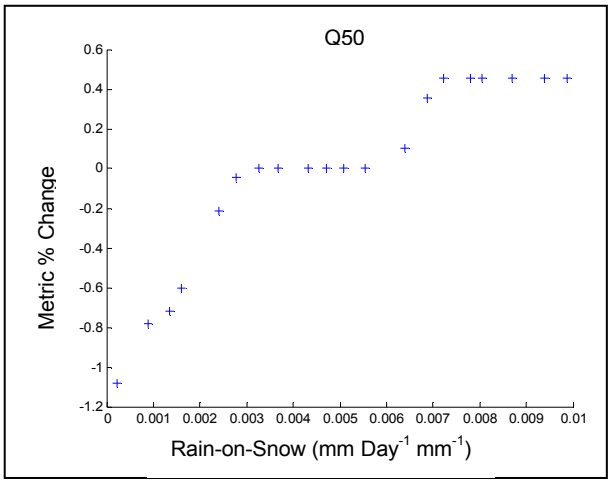


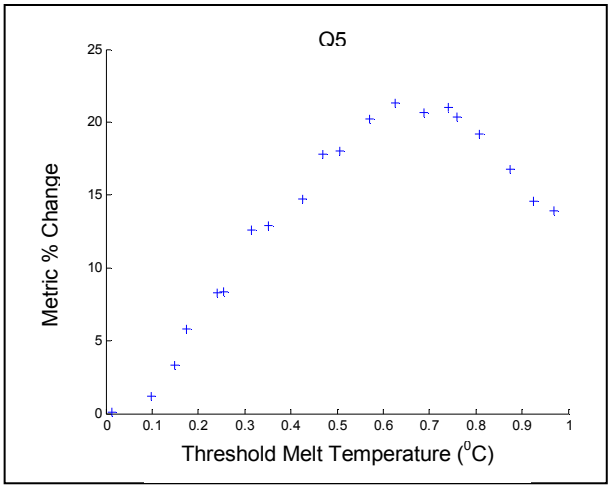


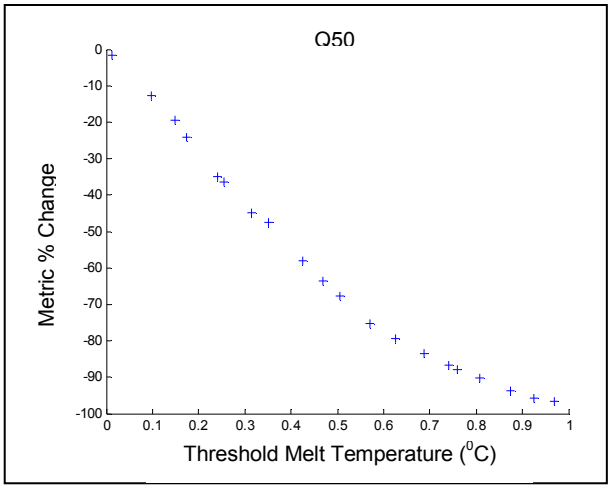

***Snowmelt Model 2 cont.***

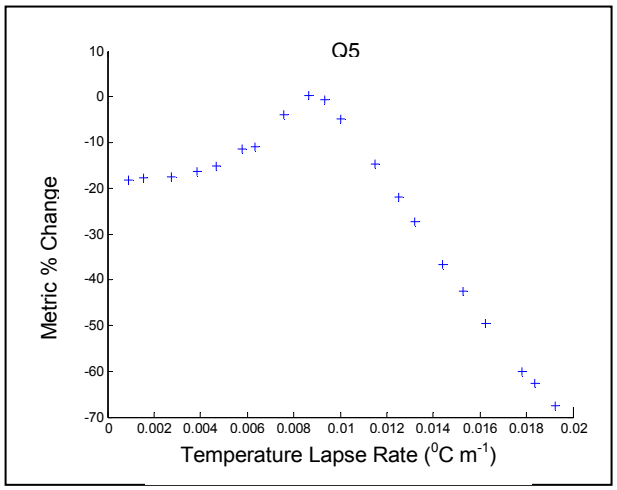


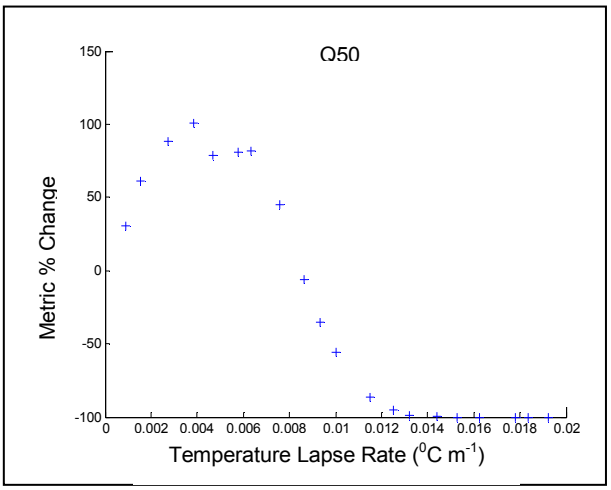


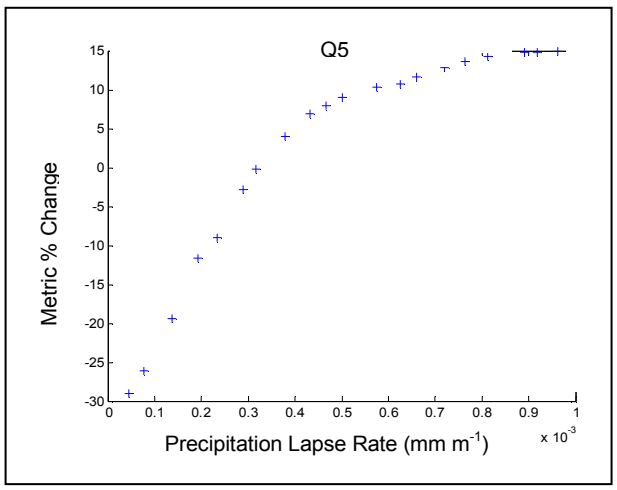


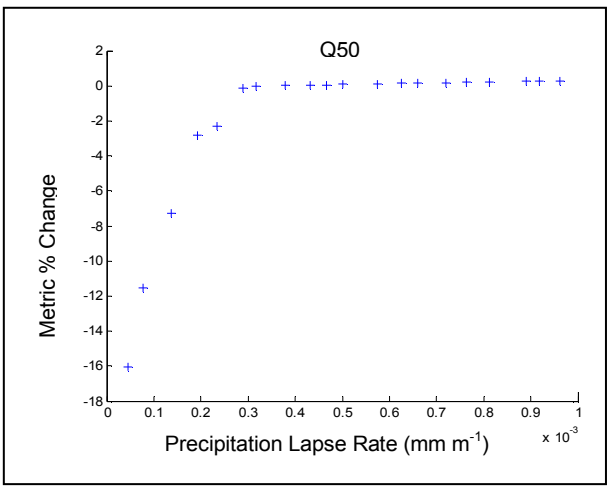

***Snowmelt Model 3:***

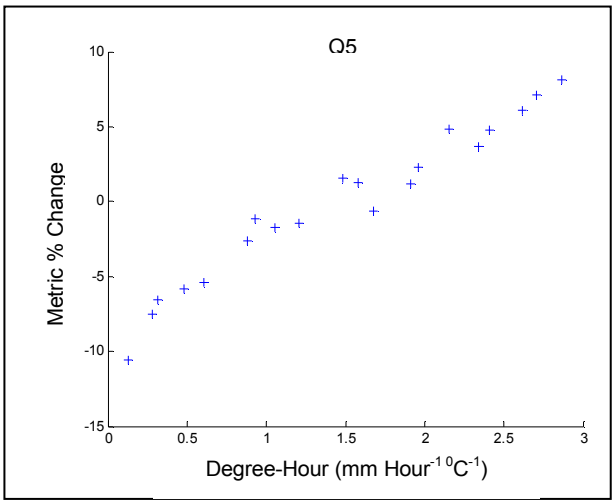


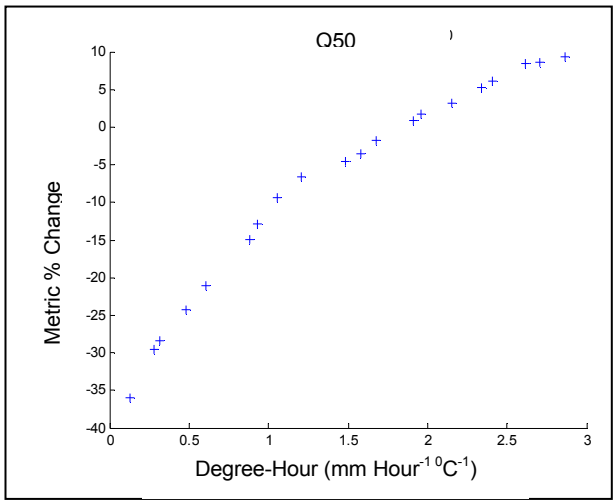


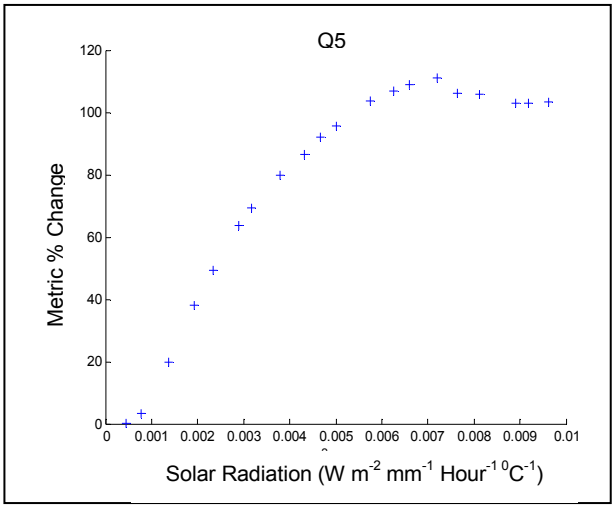


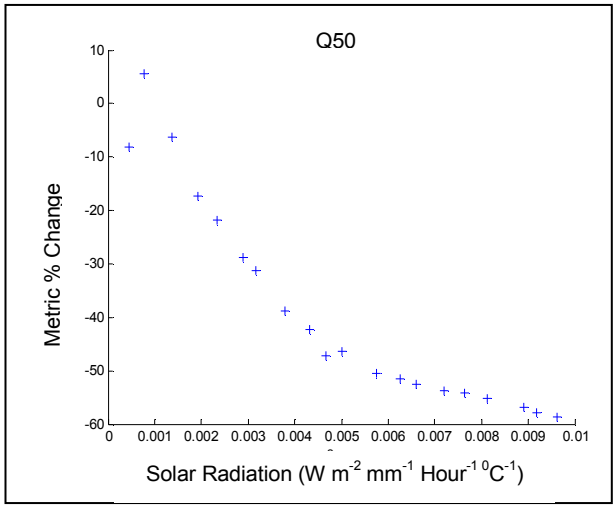


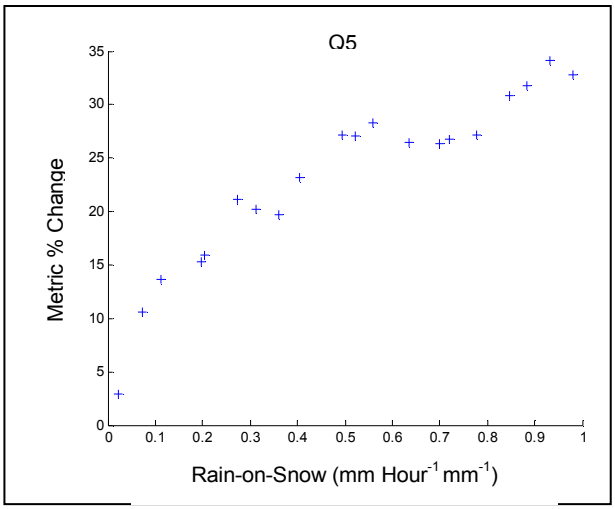


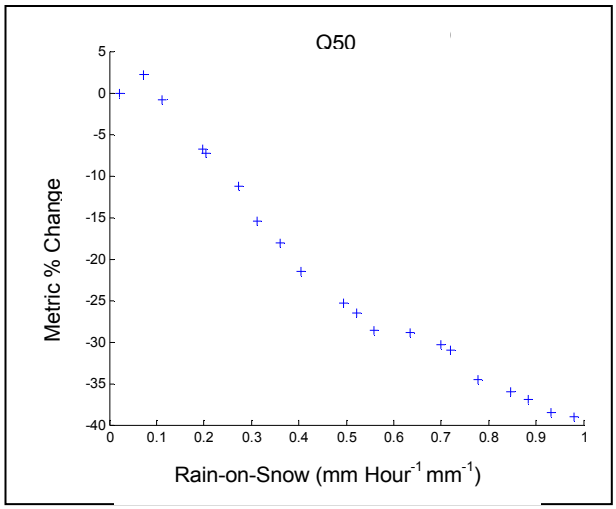

***Snowmelt Model 3 cont.***

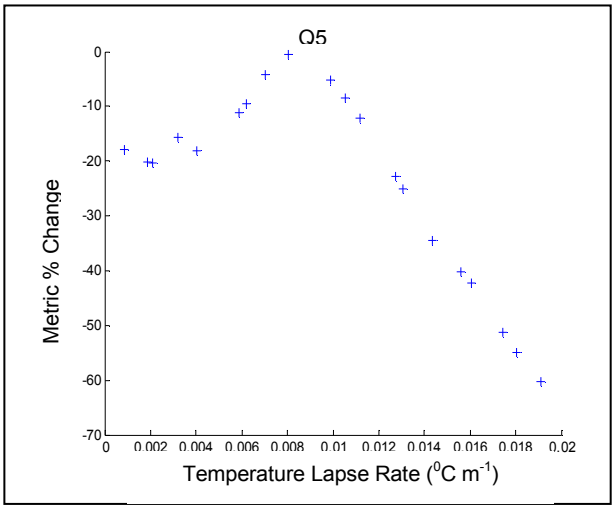


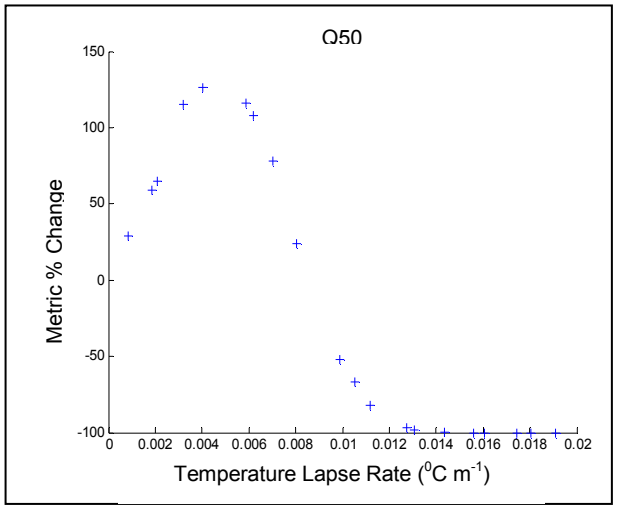


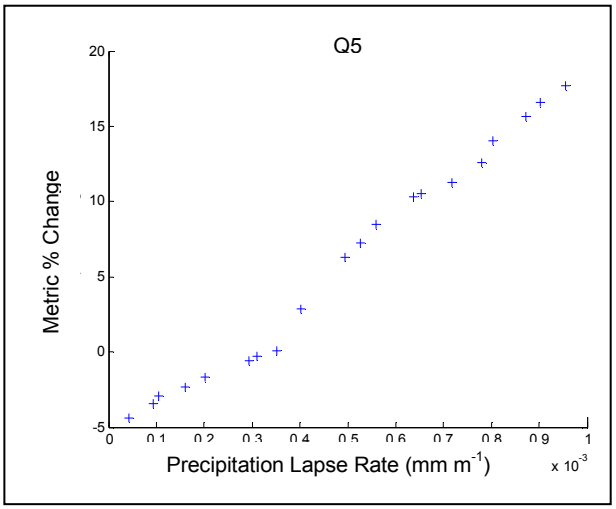


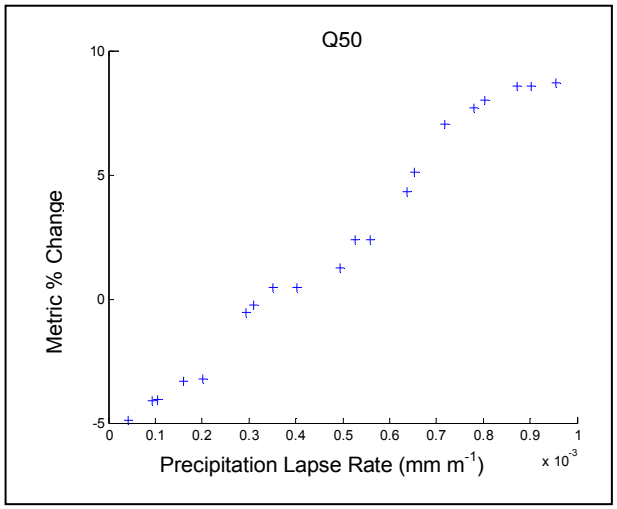

# Appendix 2

# Behavioural Hydrological Parameter Sets

| | 1 | 2 | 3 | 4 | 5 | 6 | 7 | 8 | 9 |
|---|---|---|---|---|---|---|---|---|---|
| **Snowmelt Model** | SM1 | SM1 | SM1 | SM2 | SM2 | SM2 | SM3 | SM3 | SM3 |
| **Temperature Lapse Rate** | 11.319 | 10.565 | 11.246 | 8.0575 | 8.8958 | 8.3150 | 7.1694 | 8.1854 | 4.5282 |
| **Degree-Day/Hour** | 0.032925 | 0.29715 | 0.64958 | 0.04692 | 0.33418 | 0.03134 | 0.52664 | 1.67030 | 1.34750 |
| **Threshold Melt** | 0.50191 | 0.81632 | 0.00509 | 0.21690 | 0.47662 | 0.58930 | N/A | N/A | N/A |
| **Rain-on-Snow** | N/A | N/A | N/A | 0.00047 | 0.00375 | 0.001134 | 0.008797 | 0.6541 | 0.55755 |
| **Solar Radiation** | N/A | N/A | N/A | N/A | N/A | N/A | 0.000483 | 0.001587 | 0.006253 |
| **kSat** | 0.000147 | 0.000435 | 0.000138 | 0.000106 | 0.000177 | 0.000183 | 0.000075 | 0.000179 | 0.000153 |
| **kDecay** | -4.9491 | -4.6042 | -4.4892 | -4.8504 | -3.4205 | -3.3891 | -2.8334 | -3.1093 | -4.6987 |
| **rootDepth** | 0.003356 | 0.001908 | 0.036703 | 0.005473 | 0.003613 | 0.003292 | 0.002107 | 0.008198 | 0.001526 |

**Appendix 2 Table 1** The nine hydrological parameter sets, three for each snowmelt model, used to run CRUM to generate the results in Chapter 7.

| | | | | | | | | | |
|---|---|---|---|---|---|---|---|---|---|
| **rootkSat** | 0.007956 | 0.008953 | 0.000908 | 0.001489 | 0.003378 | 0.001655 | 0.002501 | 0.004576 | 0.003194 |
| **SD Chan** | 0.97934 | 0.88998 | 1.66400 | 0.86945 | 1.11430 | 0.96996 | 0.90194 | 0.82101 | 0.97866 |
| **SD Ridge** | 0.53645 | 0.64130 | 0.62489 | 0.78406 | 0.81306 | 0.88255 | 1.03170 | 1.03585 | 1.11880 |
| **SD Slope** | 0.27536 | 0.14273 | 0.64000 | 0.40543 | 0.53571 | 0.27785 | 0.67085 | 0.63076 | 0.36866 |
| **Porosity** | 0.26448 | 0.19779 | 0.14260 | 0.22866 | 0.12278 | 0.17647 | 0.15586 | 0.11902 | 0.19298 |

**Appendix 2 Table 1 cont.** The nine hydrological parameter sets, three for each snowmelt model, used to run CRUM to generate the results in Chapter 7.

## References


**Abbott MB, Bathurst JC, Cunge JA, O'Connell PE, Rasmussen J.** 1986a. An introduction to the European Hydrological System – Systeme Hydrologique Européen, 'SHE', 1: History and philosophy of a physically-based, distributed modelling system. *Journal of Hydrology* 87: 45-59

**Abbott MB, Bathurst JC, Cunge JA, O'Connell PE, Rasmussen J.** 1986b. An introduction to the European Hydrological System – Systeme Hydrologique Européen, 'SHE', 2: Structure of a physically-based, distributed modelling system. *Journal of Hydrology* 87: 61-77

**Archer DR.** 1981. Severe snowmelt runoff in north-east England and its implications. *Proceedings of the Institution of Civil Engineers, Part 2 – Research & Theory* 71: 1047-1060

**Arnell NW, Reynard NS.** 1996. The effects of climate change due to global warming on river flows in Great Britain. *Journal of Hydrology* 183: 397-424

**Barnett C, Hossell J, Perry M, Procter C, Hughes G.** 2006. *Patterns of climate change across Scotland: Technical Report.* SNIFFER Project CC03, Scotland and Northern Ireland Forum for Environmental Research, Edinburgh: 102pp

**Barry RG.** 1992. *Mountain Weather and Climate 2nd Edition.* Routledge, London

**Bathurst JC.** 1986a. Physically-based, distributed modelling of an upland catchment using the Systeme Hydrologique Européen. *Journal of Hydrology* 87: 79-102

**Bathurst JC.** 1986b. Sensitivity analysis of the Systeme Hydrologique Européen for an upland catchment. *Journal of Hydrology* 87: 103-123

**Bayliss AC, Jones RC.** 1993. *Peaks-over-threshold flood database: Summary statistics and seasonality.* Institute of Hydrology, IH Report No. 121: 68pp

**Bengtsson L.** 1986. *Snowmelt Simulation Models in Relation to Space and Time.* In Morris EM (ed). *Modelling Snowmelt-Induced Processes: Proceedings of the Budapest Symposium.* International Association of Hydrological Sciences, Wallingford. IAHS Publ No. 155.

**Beven KJ.** 1997. TopMODEL: A critique. *Hydrological Processes* 11: 1069-1085

**Beven KJ.** 2002. *Rainfall-Runoff Modelling: The Primer.* Wiley, Chichester

**Beven KJ.** 2006. A manifesto for the equifinality thesis. *Journal of Hydrology* 320: 18-36

**Beven KJ.** 2009. *Environmental Modelling: An Uncertain Future?.* Routledge, Abingdon

**Beven KJ, Kirkby MJ.** 1979. A physically-based variable contributing area model of basin hydrology. *Hydrological Sciences Bulletin* 24(1): 43-69

**Beven KJ, Binley A.** 1992. The future of distributed models: Model calibration and uncertainty prediction. *Hydrological Processes* 6: 279-298

**Beven KJ, Freer J.** 2001. Equifinality, data assimilation, and uncertainty estimation in mechanistic modelling of complex environmental systems using the GLUE methodology. *Journal of Hydrology* 249: 11-29

**Beven KJ, Young P.** 2003. Comment on "Bayesian recursive parameter estimation for hydrologic models" by M. Thiemann, M. Trosset, H. Gupta, and S. Sorooshian. *Water Resources Research* 39(5): 1116

**Beven KJ, Smith P, Freer J.** 2007. Comment on "Hydrological forecasting uncertainty assessment: Incoherence of the GLUE methodology" by Pietro Mantovan and Ezio Todini. *Journal of Hydrology* 338: 315-318

**Birkeland KW, Mock CJ.** 1996. Atmospheric circulation patterns associated with heavy snowfall events, Bridger Bowl, Montana, USA. *Mountain Research and Development* 16 (3): 281-286

**Black AR, Anderson JL.** 1993. The great Tay flood of January 1993. *Hydrological Data*: 25-34

**Campolongo F, Saltelli A, Sørenson T, Tarantola S.** 2000. *Hitchhiker's Guide to Sensitivity Analysis.* In Saltelli A, Scott EM (eds). 2000. *Sensitivity Analysis.* Wiley, Chichester

**Campolongo F, Cariboni J, Saltelli A.** 2007. An effective screening design for sensitivity analysis of large models. *Environmental Modelling and Software* 22(10): 1509-1518

**Carroll DM, Hartrup R, Jarvis RA.** 1979. *Soils of South and West Yorkshire.* Soil Survey Bulletin No.7, The Soil Survey of England and Wales, Harpenden,Norwich

**Cowpertwait PSP.** 1991. Further developments of the Neyman-Scott clustered point process for modelling rainfall. *Water Resources Research* 27(7): 1431-1438

**Cowpertwait PSP, O'Connell PE, Metcalfe AV,Mawdsley JA.** 1996a. Stochastic point process modelling of rainfall. I. Single-site fitting and validation. *Journal of Hydrology* 175: 17-46

**Cowpertwait PSP, O'Connell PE, Metcalfe AV, Mawdsley JA.** 1996b. Stochastic point process modelling of rainfall. II. Regionalisation and disaggregation. *Journal of Hydrology* 175: 47-65Danielson EW, Levin J, Abrams E. 2003. *Meteorology.* McGraw-Hill, London

**Davis RE, Jordan R, Daly S, Koenig G.** 2001. *Validation of Snow Models.* In Anderson MG, Bates PD (eds). *Model Validation: Perspectives in Hydrological Science*: Wiley, Chichester

**Debele B, Srinivasen R, Gosain AK.** 2010. Comparison of process-based and temperature-index snowmelt modelling in SWAT. *Water Resources Management* 24: 1065-1088

**Dingman SL.** 1994. *Physical Hydrology.* Prentice Hall, New Jersey

**Duan Q, Gupta VK, Sorooshian S.** 1992. Effective and efficient global optimisation for conceptual rainfall-runoff models. *Water Resources Research* 28: 1015-1031

**Dunn SM, Langan SJ, Colohan RJE.** 2001. The impact of variable snow pack accumulation on a major Scottish water resource. *The Science of the Total Environment* 265: 181-194

**Easton ZM, Fuka DR, Walter MT, Cowan DM, Schneiderman EM, Steenhuis TS.** 2008. Re-conceptualising the soil and water assessment tool (SWAT) model to predict runoff from variable source areas. *Journal of Hydrology* 348(3-4): 279-291

**Eden Rivers Trust.** 2010. *Results of the Salmonid Fry Electrofishing Surveys and Eden Catchment Overview.* Eden Rivers Trust, Penrith. Accessed on the 24th June 2010 from http://trust.edenriverstrust.org.uk/electrofishing-history.html

**Environment Agency.** 2006. *Cumbria Floods Technical Report: Factual report on meteorology, hydrology and impact of January 2005 flooding in Cumbria.* Report of team consisting of Black and Veatch, Met Office and Environment Agency, Product Code GENW1106BLSF-E-E, November 2006: 168pp

**Etchevers P, Martin E, Brown R, Fierz C, Lejeune Y, Bazile E, Boone A, Dai Y-J, Essery R, Fernandez A, Gusev Y, Jordan R, Koren V, Kowalczyk E, Pyles RD, Schlosser A, Shmakin AB, Smirnova TG, Strasser U, Verseghy D, Yamazaki T, Yang Z-L.** 2002. *SnowMIP, an intercomparison of snow models: first results*. Proceedings of the International Snow Science Workshop, Penticton, BC: 8pp

**Etchevers P, Martin E, Brown R, Fierz C, Lejeune Y, Bazile E, Boone A, Dai Y-J, Essery R, Fernandez A, Gusev Y, Jordan R, Koren V, Kowalczyk E, Nasonava NO, Pyles RD, Schlosser A, Shmakin AB, TG, Strasser U, Verseghy D, Yamazaki T, Yang Z-L.** 2004. Validation of the energy budget of an alpine snowpack simulated by several snow models (SnowMIP project). *Annals of Glaciology* 38: 150-158

**Ferguson RI.** 1984. Magnitude and modelling of snowmelt runoff in the Cairngorm mountains, Scotland. *Hydrological Sciences Journal* 29(1): 49-62

**Ferguson RI.** 1999. Snowmelt runoff models. *Progress in Physical Geography* 23: 205-227

**Fontaine TA, Cruickshank TS, Arnold JG, Hotchkiss RH.** 2002. Development of a snowfall-snowmelt routine for mountainous terrain for the soil water assessment tool (SWAT). *Journal of Hydrology* 262: 209-223

**Freeman TG.** 1991. Calculating catchment area with divergent flow based on a regular grid. *Computers and Geosciences* 17(3): 412-422

**Freer J. Beven KJ, Ambroise B.** 1996. Bayesian estimation of uncertainty in runoff prediction and the value of data: An application of the GLUE approach. *Water Resources Research* 32(7): 2161-2173

**Freeze RA, Cherry JA.** 1979. *Groundwater.* Prentice Hall, London

**Freni G, Mannina G.** 2010. Bayesian approach for uncertainty quantification in water quality modelling: The influence of prior distribution. *Journal of Hydrology* 392: 31-39

**Fu P, Rich PM.** 2002. A geometric solar radiation model with applications in agriculture and forestry. *Computers and Electronics in Agriculture* 37:25-35

**Gray DM, Prowse TD.** 1993. *Snow and Floating Ice.* In Maidment DR (ed). *Handbook of Hydrology.* McGraw-Hill, London

**Green W, Ampt G.** 1911. Studies in soil physics. Part 1. – The flow of air and water through soils. *Journal of Agricultural Science* 4(1): 1-24

**Gupta HV, Sorooshian S, Yapo PO.** 1998. Toward improved calibration of hydrologic models: Multiple and noncommensurable measures of information. *Water Resources Research* 34(4): 751-763

**Gupta HV, Thiemann M, Trosset M, Sorooshian S.** 2003. Reply to comment by K. Beven and P. Young on "Bayesian recursive parameter estimation for hydrologic models". *Water Resources Research* 39(5): 1117

**Gurtz J, Lang H, Verbunt M, Zappa M.** 2005. *The use of hydrological models for the simulation of climate change impacts on mountain hydrology.* In Bugmann HKM, Reasoner MA (eds). *Global Change and Mountain Regions: An Overview of Current Knowledge.* Springer, Dordrecht

**Hamby DM.** 1994. A review of techniques for parameter sensitivity analysis of environmental models. *Environmental Monitoring and Assessment* 32: 135-154

**Harding RJ.** 1986. *Exchanges of energy and mass associated with a melting snowpack.* In Morris EM (ed). *Modelling Snowmelt Induced Processes.* International Association of Hydrological Sciences, Wallingford, IAHS Publ No. 155

**Harris G, Sexton DMH, Booth BBB, Collins M, Murphy JM, Webb MJ.** 2006. Frequency distributions of transient regional climate change from perturbed physics ensembles of general circulation model simulations. *Climate Dynamics* 27: 357-375

**Harrison J, Winterbottom S, Johnson R.** 2001. *Climate Change and Changing Snowfall Patterns in Scotland.* Scottish Executive Central Research Unit; Environment Group Research Programme Research Findings No. 14: 57pp

**Helton JC, Davis FJ.** 2003. Latin Hypercube sampling and the propagation of uncertainty analyses of complex systems. *Reliability Engineering and System Safety* 81: 23-69

**Hock R.** 1999. A distributed temperature-index ice- and snow-melt model including potential direct solar radiation. *Journal of Glaciology* 45(149): 101-111

**Hock R.** 2003. Temperature index melt modelling in mountain areas. *Journal of Hydrology* 282: 104-115

**Hock R.** 2005. Glacier melt: a review of processes and their modelling. *Progress in Physical Geography* 29: 363-391

**Hornberger GM, Spear RC.** 1981. An approach to the preliminary analysis of environmental systems. *Journal of Environmental Management* 12: 7-18

**Hough MN, Hollis D.** 1997. Rare snowmelt estimation in the United Kingdom. *Meteorological Applications* 5: 127-138

**Houghton-Carr H.** 1999. *Flood Estimation Handbook Volume 4: Restatement and Application of the Flood Studies Report Rainfall-Runoff Method.* Institute of Hydrology, Wallingford

**Institution of Civil Engineers.** 1996. *Floods and Reservoir Safety 3rd edition.* The Institution of Civil Engineers, London

**Institute of Hydrology.** 1975. *Flood Studies Report Volume 1: Hydrological Studies.* Institute of Hydrology, Wallingford

**Jackson MC.** 1978a. The influence of snowmelt on flood flows in rivers. *Journal of the Institution of Water Engineers and Scientists* 32: 495-508

**Jackson MC.** 1978b. Snow cover in Great Britain. *Weather* 33: 298-309

**Jacques J, Lavergne C, Devictor N.** 2006. Sensitivity analysis in presence of model uncertainty and correlated inputs. *Reliability Engineering and System Safety* 91: 1126-1134

**Jarvis RA, Bendelow VC, Bradley RI, Carroll DM, Furness RR, Kilgour INL, King SJ.** 1984. *Soils and their use in Northern England.* Soil Survey of England and Wales, Bulletin No. 10, Harpenden, Whitstable

**Jin X, Xu C-Y, Zhang Q, Singh VP.** 2010. Parameter and modelling uncertainty simulated by GLUE and a formal Bayesian method for a conceptual hydrological model. *Journal of Hydrology* 383: 147-155

**Johnson P.** 1966. Flooding from snowmelt. *Civil Engineering and Public Works Review* 61: 747-750

**Johnson P, Archer DR.** 1972. Current research in British snowmelt river flooding. *Bulletin of the International Association of Hydrological Sciences* 17: 443-451

**Jones PD, Kilsby CG, Harpham C, Glenis V, Buton A.** 2009. *UK Climate Projections science report: Projections of future daily climate for the UK from the Weather Generator.* University of Newcastle, UK: 48pp

**de Jong C, Lawler D, Essery R.** 2009. Mountain hydroclimatology and snow seasonality: Perspectives on climate impacts, snow seasonality and hydrological change in mountain environments. *Hydrological Processes* 23(7): 955-961

**Jost G, Moore RD, Weiler M, Gluns DR, Alila Y.** 2009. Use of distributed snow measurements to test and improve a snowmelt model for predicting the effect of a forest clear cutting. *Journal of Hydrology* 376: 94-106

**Juston J, Seibert J, Johansson P-O.** 2009. Temporal sampling strategies and uncertainty in calibrating a conceptual hydrological model for a small boreal catchment. *Hydrological Processes* 23: 3093-3109

**Kattelman RC, Dozier J.** 1999. Observations of snowpack ripening in the Sierra Nevada, California, USA. *Journal of Glaciology* 45(151): 409-416

**Kayastha RB, Ageta Y, Fujita K.** 2005. *Use of Positive Degree-Day Methods for Calculating Snow and Ice Melting and Discharge in Glacierised Basins in the Langtang Valley, Central Nepal.* In de Jong C, Collins D, Ranzi R (eds). *Climate and Hydrology in Mountain Areas.* Wiley, Chichester

**Kilsby CG, Jones PD, Burton A, Ford AC, Fowler HJ, Harpham C, James P, Smith A, Wilby RL.** 2007. A daily weather generator for use in climate change studies. *Environmental Modelling and Software* 22: 1705-1719

**Kirkby MJ.** 1975. *Hydrograph modelling strategies.* In Peel R, Chisholm M, Hagget P (eds). *Progress in Human and Physical Geography*. Heinemann, London

**Kirkby MJ** (ed). 1978. *Hillslope Hydrology.* Wiley, Norwich

**Kirkby MJ.** 1985. *Hillslope Hydrology.* In Anderson MG, Burt TP (eds). *Hydrological Forecasting.* Wiley, Chichester

**Kirkby MJ, Naden PS, Burt TP, Butcher P.** 1992. *Computer Simulation in Physical Geography.* Wiley, Chichester

**Kirkby MJ, Bracken LJ, Reaney SM.** 2002. The influence of land use, soils and topography on the delivery of hillslope runoff to channels in SE Spain. *Earth Surface Processes and Landforms* 27: 1459-1473

**Kingston DG, Hannah DM, Lawler DM, McGregor GR.** 2009. Climate-river flow relationships across montane and lowland environments in northern Europe. *Hydrological Processes* 23 (7): 985-996

**Koivusalo H, Heikinheimo M, Karvonen T.** 2001. Test of a simple two-layer parameterisation to simulate the energy balance and temperature of a snowpack. *Theoretical and Applied Climatology* 70: 65-79

**Kutílek M, Nielsen DR.** 1994. *Soil Hydrology.* Catena, Verlag

**Lane SN, Richards KS.** 2001. *The 'Validation' of Hydrodynamic Models: Some Critical Perspectives.* In Anderson MG, Bates PD (eds). *Model Validation: Perspectives in Hydrological Sciences.* Wiley, Chichester

**Lane SN, Reaney SM, Heathwaite AL.** 2009. Representation of landscape hydrological connectivity using a topographically driven surface flow index. *Water Resources Research* 45: W08423

**Lawler DM.** 1987. *Spatial Variability in the Climate of the Severn Basin: a palaeohydrological perspective.* In Gregory KJ, Lewin J, Thornes JB (eds). *Palaeohydrology in Practice.* Wiley, Chichester

**Li X, Williams MW.** 2008. Snowmelt runoff modelling in an arid mountain watershed, Tarin Basin, China. *Hydrological Processes* 22: 3931-3940

**Li X, Weller DE, Jordan TE.** 2010. Watershed model calibration using multi-objective optimisation and multi-scale averaging. *Journal of Hydrology* 380: 277-288

**López-Moreno JI, Goyette S, Beniston M.** 2009. Impact of climate change on snowpack in the Pyrenees: Horizontal spatial variability and vertical gradients. *Journal of Hydrology* 374: 384-396

**MacDonald MK, Pomeroy JW, Pietroniro A.** 2009. Parameterising redistribution and sublimation of blowing snow for hydrological models: tests in a mountainous subarctic catchment. *Hydrological Processes* 23(18): 2570-2583

**Mantovan P, Todini E.** 2006. Hydrological forecasting uncertainty assessment: Incoherence of the GLUE methodology. *Journal of Hydrology* 330: 369-381

**Mantovan P, Todini E, Martina MLV.** 2007. Reply to comment by Keith Beven, Paul Smith and Jim Freer on "Hydrological forecasting uncertainty assessment: Incoherence of the GLUE methodology". *Journal of Hydrology* 338: 319-324

**Markvart T, Castaner L.** 2003. *Practical Handbook of Photovoltaics: Fundamentals and Applications.* Elsevier, Oxford

**Marsh TJ, Hannaford J** (eds). 2008. *UK Hydrometric Register.* Hydrological data UK series. Centre for Ecology and Hydrology: 210pp

**Martinec J.** 1989. *Hour-to-hour snowmelt rates and Lysimeter outflow during an entire ablation period.* In Colbeck SC (ed). *Snow Cover and Glacier Variations: Proceedings of the Baltimore Symposium.* International Association of Hydrological Sciences, Wallingford. IAHS Publ No. 183

**Matsumoto M, Nishimura T.** 1998. Mersenne twister: a 623-dimensionally equidistributed uniform pseudo-random number generator. *ACM Transactions on Modeling and Computer Simulation* 8(1): 3-30

**Maurer EP, Rhoads JD, Dubayah RO, Lettenmaier DP.** 2003. Evaluation of the snow-covered area data product from MODIS. *Hydrological Processes* 17(1): 59-71

**McIlveen R.** 1992. *Fundamentals of Weather and Climate.* Chapman & Hall, London

**McMillan H, Clark M.** 2009. Rainfall-runoff model calibration using informal likelihood measures within a Markov Chain Monte Carlo sampling scheme. *Water Resources Research* 45: W04418

**McMillan H, Freer J, Pappenberger F, Kreuger T, Clark M.** 2010. Impacts of uncertain river flow data on rainfall-runoff model calibration and discharge predictions. *Hydrological Processes* 24. 1270-1284

**McKay MD, Beckman RJ, Conover WJ.** 1979. A comparison of three methods for selecting values of input variables in the analysis of output from a computer code. *Technometrics* 21(2): 239-245

**Metropolis NM, Ulam S.** 1949. The Monte Carlo Method. *Journal of the American Statistical Association* 44(247): 335-341

**Moore RJ.** 2007. The PDM rainfall-runoff model. *Hydrology and Earth System Sciences* 11(1): 483-499

**Moore RJ, Clarke RT.** 1981. A distribution function approach to rainfall-runoff modelling. *Water Resources Resarch* (17): 1367-1382

**Moore RJ, Bell VA, Austin RM, Harding RJ.** 1999. Methods for snowmelt forecasting in upland Britain. *Hydrology and Earth System Sciences* 3: 233-246

**Morris MD.** 1991. Factorial sampling plans for preliminary computational experiments. *Technometrics* 33(2): 161-174

**Mote PW, Hamlet AF, Salathé E.** 2008. Has spring snowpack declined in the Washington Cascades? *Hydrology and Earth System Sciences* 12: 193-206

**Mulligan M.** 1996. *Modelling the complexity of land surface response to climate variability in Mediterranean environments.* In Anderson M, Brooks S (eds). *Advances in hillslope provesses.* Vol 2, Wiley, Chichester

**Murphy JM, Sexton DMH, Jenkins GJ, Boorman PM, Booth BBB, Brown CC, Clark RT, Collins M, Harris GR, Kendon EJ, Betts RA, Brown SJ, Howard TP, Humphrey KA, McCarthy MP, McDonald RE, Stephens A, Wallace C, Warren R, Wilby R, Wood RA.** 2009. *UK Climate Projections Science Report: Climate Change Projections*. Met Office Hadley Centre, Exeter

**Nakicenovvic N, Alcamo J, Davis G, de Vries B, Fenhann J, Gaffin S, Gregory K, Grübler A, Yong Jung T, Kram T, Lebre la Rovere E, Michaelis L, Mori S, Morita T, Pepper W, Pitcher H, Price L, Riahi K, Roehrl A, Rogner H-H, Sankovski M, Shukla P, Smith S, Swart R, van Rooijen S, Victor N, Dadi Z.** 2000. *Special Report on Emissions Scenarios.* Intergovernmental Panel on Climate Change, Geneva.

**Nash JE, Sutcliffe JV.** 1970. River flow forecasting through conceptual models part 1: A discussion of principles. *Journal of Hydrology* 10(3): 282-290

**National Land Use Database.** 2006. *National Land Use Database: Land Use and Land Cover Classification: Version 4.4.* Office of the Deputy Prime Minister, London. Accessed on 24th June 2010 from http://www.communities.gov.uk/publications/planningandbuilding/nationallanduse

**Neitsch SL, Arnold JG, Kiniry JR, Williams JR.** 2005. *Soil and Water Assessment Tool Theoretical Documentation.* USDA Agricultural Research Service and Texas A&M University: 494pp. Accessed on the 25th August 2010 from: http://swatmodel.tamu.edu/documentation

**Nicks AD, Harp JF.** 1980. Stochastic generation of temperature and solar radiation data. *Journal of Hydrology* 48: 1-17

**Novotny EV, Stefan HG.** 2007. Stream flow in Minnesota: Indicator of climate change. *Journal of Hydrology* 334: 319-333

**O'Callaghan JF, Mark DM.** 1984. The extraction of drainage networks from digital elevation data. *Computer Vision, Graphics, and Image Processing* 28: 323-344

**Onof C, Chandler RE, Kakou A, Northrop P, Wheater HS, Isham V.** 2000. Rainfall modelling using Poisson-cluster processes: a review of developments. *Stochastic Environmental Research and Risk Assessment* 14: 384-411

**Pattison I.** 2010. *Rural Land Management Impacts on Catchment Scale Flood Risk.* Unpublished PhD Thesis, Department of Geography, University of Durham. 454pp

**Pellicciotti F, Brock B, Strasser U, Burlando P, Funk M, Corripio J.** 2005. An enhanced temperature-index glacier melt model including the shortwave radiation balance: development and testing for Haut Glacier d'Arolla, Switzerland. *Journal of Glaciology* 51: 573-587

**Perry M, Hollis D.** 2005. The generation of monthly gridded datasets for a range of climatic variables over the United Kingdom. *International Journal of Climatology* 25: 1041-1054

**Pomeroy JW, Gray DM, Shook KR, Toth B, Essery RLH, Pietroniro A, Hedstrom N.** 1998. An evaluation of snow accumulation and ablation processes for land surface modelling. *Hydrological Processes* 12: 2339-2367

**Ponce V, Lugo A.** 2001. Modelling looped ratings in Muskingham-Cunge routing. *Journal of Hydrologic Engineering* 6: 119-124

**Priestley CHB, Taylor RJ.** 1972. On the assessment of surface heat flux and evaporation using large-scale parameters. *Monthly Weather Review* 100: 81-92

**Quinn P, Beven K, Chevallier P, Planchon O.** 1991. The prediction of hillslope flow paths for distributed hydrological modelling using digital terrain models. *Hydrological Processes* 5: 59-79

**Quinn PF, Beven KJ, Lamb R.** 1995. The ln(ά/tanβ) index: How to calculate it and how to use it within the TOPMODEL framework. *Hydrological Processes* 9: 161-182

**Randall DA, Wood RA, Bony S, Colman R, Fichefet T, Fyfe J, Kattsov V, Pitman A, Shukla J, Srinivasen J, Stouffer RJ, Surni A, Taylor KE.** 2007. *Climate Models and Their Evaluation.* In Solomon S, Qin D, Manning M, Chen Z, Marquis M, Averyt KB, Tignor M, Miller HL (eds). *Climate Change 2007: The Physical Science Basis. Contribution of Working Group I to the Fourth Assessment Report of the Intergovernmental Panel on Climate Change.* Cambridge University Press, Cambridge, UK: 74pp

**Rawls WJ, Ahuja LR, Brakensiek DL, Shirmohammadi A.** 1993. *Infiltration and Soil Water Movement.* In Maidment DR (ed). *Handbook of Hydrology.* McGraw-Hill, London

**Reaney SM, Bracken LJ, Kirkby MJ.** 2007. Use of the Connectivity of runoff Model (CRUM) to investigate the influence of storm characteristics on runoff generation and connectivity in semi-arid areas. *Hydrological Processes* 21: 894-906

**Reed DW, Field EK.** 1992. *Reservoir flood estimation: another look*. Institute of Hydrology, Report No. 114, Wallingford: 94pp

**Roberts NM, Cole SJ, Forbes RM, Moore RJ, Boswell D.** 2009. Use of high-resolution NWP rainfall and river flow forecasts for advance warning of the Carlisle flood, north-west England. *Meteorological Applications* 16: 23-34

**Robson A, Reed D.** 1999. *Flood Estimation Handbook. Volume 3. Statistical Procedures for Flood Frequency Estimation.* Institute of Hydrology: Wallingford

**Rodriguez-Iturbe I, Cox DR, Isham V.** 1987. Some models for rainfall based stochastic point processes. *Proceedings of the Royal Society of London A* 410: 269-288

**Romanowicz RJ, Beven KJ, Tawn JA.** 1994. *Evaluation of Predictive Uncertainty in Nonlinear Hydrological Models Using a Bayesian Approach.* In Barnett V, Turkman KF (eds). *Statistics for the Environment 2: Water Related Issues.* Wiley, Chichester

**Romanowicz RJ, Beven KJ.** 2006. Comments on generalised likelihood uncertainty estimation. *Reliability Engineering and System Safety* 91: 1315:1321

**Rosero E, Yang Z-L, Wagener T, Gulden LE, Yatheendradas S, Niu G-Y.** 2010. Quantifying parameter sensitivity, interaction, and transferability in hydrologically enhanced versions of the Noah land surface model over transition zones during the warm season. *Water Resources Research* 115: D03106

**Rougier J.** 2008. Efficient emulators for multivariate deterministic functions. *Journal of Computational and Graphical Statistics* 17(4): 827-843

**Roy A, Royer A, Turcotte R.** 2010. Improvement of springtime streamflow simulations in a boreal environment by incorporating snow-covered area derived from remote sensing data. *Journal of Hydrology* 390: 35-44

**Saltelli A.** 2000. *What is Sensitivity Analysis?.* In Saltelli A, Chan K, Scott EM (eds). *Sensitivity Analysis.* Wiley, Chichester

**Saltelli A, Ratto M, Tarantola S, Campolongo F.** 2006. Sensitivity analysis practices: Strategies for model-based inference. *Reliability Engineering and System Safety* 91: 1109-1125

**Scottish Environment Protection Agency.** 2008. *Changes in river flow variability in snow influenced catchments in Scotland*, Scottish Environment Protection Agency, Stirling: 7pp

**Singh P, Singh VP.** 2001. *Snow and Glacier Hydrology.* Kluwer, Dordrecht

**Smith L, Wheatcraft SW.** 1993. *Groundwater Flow.* In Maidment DR (ed). *Handbook of Hydrology.* McGraw-Hill, London

**Sobol' IM.** 2001. Global sensitivity indices for nonlinear mathematical models and their Monte Carlo estimates. *Mathematics and Computers in Simulation* 55: 271-280

**Soulsby C, Helliwell RC, Ferrier RC, Jenkins A, Harriman R.** 1997. Seasonal snowpack influence on the hydrology of a sub-arctic catchment in Scotland. *Journal of Hydrology* 192: 17-32

**Spear RC, Hornberger GM.** 1980. Eutrophication in Peel Inlet – II. Identification of initial uncertainties via generalised sensitivity analysis. *Water Research* 14: 43-49

**Sulieman H, Kucuk I, McLellan PJ.** 2009. Parametric sensitivity: A case study comparison. *Computational Statistics and Data Analysis* 53(7): 2640-2652

**Suzuki K, Ohta T, Kojima A, Hashimoto T.** 1999. Variations in snowmelt energy and energy balance characteristics with larch forest density on Mt Iwate, Japan: Observations and energy balance analyses. *Hydrological Processes* 13: 2675-2688

**Tang Y, Reed P, Wagener T, van Werkhoven K.** 2007. Comparing sensitivity analysis methods to advance lumped watershed model identification and evaluation. *Hydrology and Earth System Sciences* 11: 793-817

**Thiemann M, Trosset M, Gupta HV, Sorooshian S.** 2001. Bayesian recursive parameter estimation for hydrologic models. *Water Resources Research* 37(10): 2521-2535

**Trucano TG, Swiler LP, Igusa T, Oberkampf WL, Pilch M.** 2006. Calibration, validation, and sensitivity analysis: What's what. *Reliability Engineering and System Safety* 91: 1331-1357

**United States Army Corps of Engineers.** 1956. *Summary Report of the Snow Investigations: Snow Hydrology.* North Pacific Division, Corps of Engineers, US Army, Portland, Oregon. Accessed on 25th July 2010 from: http://www.crrel.usace.army.mil/icejams/reports/1956-snow_hydrology_report.html

**United States Army Corps of Engineers.** 1998. *Engineering and Design: Runoff from Snowmelt.* Department of the Army, US Army Corps of Engineers, Washington DC: Engineer Manual 1110-2-1406: 142pp

**United States Soil Conservation Service.** 1986. *Urban Hydrology for Small Watersheds.* United States Department of Agriculture, Technical Release 55. Accessed on 24th June 2010 from http://www.cpesc.org/reference/tr55.pdf

**van Griensven A.** 2005. *Sensitivity, auto-calibration, uncertainty and model evaluation in SWAT 2005.* Unpublished SWAT documentation accessed on 10th May 2010 from: http://swatmodel.tamu.edu/publications/calibrationvalidation-publications

**Velghe T, Troch PA, de Troch FP, van de Velde J.** 1994. Evaluation of cluster-based rectangular pulses point process models for rainfall. *Water Resources Research* 30(10): 2847-2857

**von Neumann J, Ulam SM.** 1945. Random ergodic theorems. *Bulletin of the American Mathematical Society*: Abstract 51-9-165

**Wainwright J, Mulligan M.** 2004. *Environmental Modelling: Finding Simplicity in Complexity.* Wiley, Chichester

**Walter MT, Brooks ES, McCool DK, King LG, Molnau M, Boll J.** 2005. Process-based snowmelt modelling: does it require more input data than temperature-index modelling? *Journal of Hydrology* 300: 65-75

**Ward RC, Robinson M.** 2000. *Principles of Hydrology 4th Edition.* McGraw-Hill, London

**Watkins S, Whyte I.** 2008. Extreme flood events in upland catchments in Cumbria since 1600: the evidence of historical records. *North West Geography* 8(1): 33-41

**Wilby RL, Wigley TML.** 1997. Downscaling general circulation model output: a review of methods and limitations. *Progress in Physical Geography* 21(4): 530-548

**Wilby RL, Wigley TML, Conway D, Jones PD, Hewitson BC, Main J, Wilks DS.** 1998. Statistical downscaling of general circulation model output: a comparison of methods. *Water Resources Research* 34(11): 2995-3008

**Whitehead PG, Wade AJ, Butterfield D.** 2009. Potential impacts of climate change on water quality and ecology in six UK rivers. *Hydrology Research* 40(2-3): 113-122

**Xu C-Y.** 2001. Statistical analysis of parameters and residuals of a conceptual water balance model – methodology and case study. *Water Resources Management* 15: 75-92

**Yapo P, Gupta HV, Sorooshian S.** 1996. Calibration of conceptual rainfall-runoff models: Sensitivity to calibration data. *Journal of Hydrology* 181: 23-48

**Zeinivand H, de Smedt F.** 2009. Hydrological modelling of snow accumulation and melting on river basin scale. *Water Resources Management* 23: 2271-2287